A BIOSYNTHETIC APPROACH TO UNDERSTANDING THE ASSEMBLY OF CU_A CENTERS

BY

TIFFANY DIANE WILSON

DISSERTATION

Submitted in partial fulfillment of the requirements
for the degree of Doctor of Philosophy in Chemistry
in the Graduate College of the
University of Illinois at Urbana-Champaign, 2012

Urbana, Illinois

Doctoral Committee:

Professor Yi Lu, Chair
Professor Robert B. Gennis
Professor Andrew Gewirth
Professor Patricia A. Shapley

Abstract

Electron transfer plays a critical role in countless biological processes. Metalloproteins containing copper or iron carry out electron transfer throughout all domains of life. Cu_A is a unique dinuclear, mixed-valence and valence delocalized copper center, which catalyzes remarkably efficient electron transfer under the low driving forces experienced at the termini of electron transport chains. Historically, Cu_A centers have been difficult to study, due to their occurrence in large enzyme complexes that are embedded in membranes and/or the presence of other metallocofactors in the same enzyme. For these reasons, soluble proteins containing only the Cu_A cofactor were created, either by truncating helices that anchored the Cu_A domain to a membrane, or by engineering the Cu_A center into another protein.

The strategy of engineering Cu_A centers into another protein falls under the umbrella of the biosynthetic approach to metalloenzyme studies. In the biosynthetic approach to metalloenzyme studies, the protein is considered to be a large ligand to the metal center, which is customizable to the needs of that center. The biosynthetic approach offers many distinctive benefits in the study of native metal centers over the complementary approach of studying these centers in their native enzymes. These benefits include simpler protein systems, which are easy to express and purify in high yield and are free of other metal cofactors, and the ability to substitute non-native metals into the site.

A biosynthetic model of Cu_A centers was previously designed into a mononuclear copper enzyme called azurin (Az). In this model, the Cu_A center was engineered into the same location of the protein as the original copper center, by replacement of a single loop containing a majority of the copper ligands. The resulting Cu_AAz construct binds copper in a copper site that is very similar to native Cu_A centers, as evidenced by many spectroscopic and structural studies. The ease of purification, amenability to mutagenesis, and stability in solution of Cu_AAz has resulted in many important insights into the properties of native Cu_A centers, such as a direct demonstration of the greater electron efficiency of Cu_A centers compared to mononuclear type 1 (T1) copper electron transfer sites.

Some unresolved questions about native Cu_A enzymes are how these centers acquire copper ions and by what mechanism are these copper ions assembled into a functional Cu_A unit. Copper ions are tightly regulated in living systems, due to their capacity to generate hydroxyl radicals and their superior affinity for the ligand sets of other metals. Proteins, called copper

chaperones, carry and deliver copper ions to their biological targets. One such copper chaperone, named Sco, has been proposed to deliver copper to the Cu_A center of cytochrome *c* oxidase. Sco binds both Cu(I) and Cu(II), supporting a copper chaperone function. However, such a function has yet to be confirmed for Sco proteins, and other redox regulatory functions have been offered as alternatives. Thus, the source of copper ions and the mechanism of their incorporation into Cu_A centers remains a mystery.

Studies of *in vitro* Cu(II) incorporation into the biosynthetic Cu_A site of Cu_AAz have yielded some of the first reported mechanisms for Cu_A assembly. A previous study of Cu(II) incorporation into Cu_AAz under excess copper conditions showed the formation of a single T2 copper intermediate, which then converted directly to Cu_A. As reducing equivalents were required, but not supplied, to form the [Cu(1.5)···Cu(1.5)] resting state of Cu_A, reduction of Cu(II) to Cu(I) by formation of a disulfide between the Cu_A Cys thiols was proposed. Increased Cu_A formation with the addition of exogenous reductant or Cu(I) supported this hypothesis.

In this dissertation, a detailed mechanistic study of Cu(II) incorporation into Cu_AAz is described, in which the unmediated assembly of the Cu_A center is followed by pH- and oxygen-dependent standard and stopped-flow UV-Vis absorbance spectroscopy, as well as freeze-quench and standard EPR spectroscopy. Analysis of mutant Cu_AAz proteins, in which various of the copper-binding ligands were removed or perturbed, provided information about the ligand sets of the intermediates that formed during assembly of the Cu_A center.

Under sub-equivalent copper concentrations, it is discovered that copper incorporation into the Cu_A center proceeds through two pathways. First, a type 2 (T2) copper capture complex forms, analogous to the sole intermediate observed in the previous study of Cu_A formation in Cu_AAz. In this study, it was discovered that this T2 copper capture complex formed between copper ions from bulk solution and Cys116 of the Cu_A site. This T2 copper intermediate then displayed two types of reactivity. In one, it reacted through a bimolecular pathway, involving the formation of Cu(I), to generate Cu_A, in an analogous pathway to that observed previously. In the other pathway, which had not been reported before, the T2 copper intermediate structurally rearranged to another intermediate, with unusual spectroscopic properties, called I_X. Comparison to documented copper-thiolate complexes led us to propose that I_X is a copper dithiolate complex, formed with both of the Cu_A Cys residues. I_X then seemingly converted to a T1 copper complex. This T1 copper intermediate displayed ligation by Cys 112, as revealed through UV-

Vis and EPR spectral characterizations. Spin quantification by EPR spectroscopy revealed that I_X reacts to generate Cu(I) in the system. Oxygen-dependent stopped-flow UV-Vis absorbance spectroscopy showed that the formation of the T1 copper intermediate was dependent on oxygen, from which it was suggested that the T1 copper intermediate is a one-electron oxidation product of a Cu(I) species, generated by decay of I_X. Finally, the T1 copper intermediate slowly converted to Cu_A, by reaction with Cu(I) in solution. The formation of these intermediates was also influenced by pH, with lower pH resulting in faster kinetics and less accumulation of the intermediates.

This mechanism provides a picture of unmediated Cu(II) incorporation into a Cu_A center. The overall yield of this complex process was only ~30% of total expected yield, which was attributed to oxidation of the thiols of the Cu_A center to disulfide, coupled to the generation of Cu(I). Thus, while unmediated assembly of Cu_A centers from Cu(II) ions does result in fully-formed Cu_A sites, the efficiency of this metalation method is low. Nature, however, has evolved proteins for the sole purpose of maintaining a thiol-pair/disulfide in the correct oxidation state, called thioredoxins. Therefore, while metalation of Cu_A through Cu(I) or a mixture of Cu(I) and Cu(II) may be more efficient, metalation of Cu_A through Cu(II) and thioredoxin presents a practical scenario.

Another biosynthetic take on the problem of Cu_A assembly is to try to understand how protein-mediated metalation of this center may occur. Toward this goal, a mutant of Az, H46C/C112H, which binds Cu(II) in a site very similar to a Sco variant, has been characterized. Importantly, while it has been demonstrated that the Cu(II) site of Sco is essential for its function in C*c*O maturation, no Cu(II)-bound Sco structure has been obtained. Despite only exchanging the positions of two copper-binding residues of the original T1 copper site, H46C/C112H Az forms a T2 copper center. The T2 copper center of this mutant exhibits pH- and time-dependent changes, which were investigated by UV-Vis and EPR spectroscopies. At pH 9, the UV-Vis and EPR spectra of this Az variant are nearly identical to those of a Sco mutant, C45A. Conditions where H46C/C112H Az forms crystals have been found, and a diffracted crystal structure is under refinement. Structural characterization of a Sco-like center in Az could provide the first such structure of a Sco-like Cu(II) center. Future designs of this Az mutant will incorporate all of the features of native Sco, which could both lead to a full structural description of these types of sites, as well as yield functional insight into Sco proteins.

To my dear mother, who has nurtured my curiosity throughout my life, instilled in me a marvel of nature, and taught me wrong from right.

ACKNOWLEDGMENTS

Many people have helped me throughout my doctoral studies, in a number of ways. First of all, I would really like to thank my advisor Yi Lu, for supporting me over these years and believing in me, even when I did not believe in myself. I would also like to thank my committee members, Robert Gennis, whose patient thoughtfulness encourages open discussion, Andrew Gewirth, who took time out of his busy schedule as Director of the School of Chemical Sciences to serve on my committee, and Patricia Shapley, who provides such a wonderful model of a successful woman in chemistry academe.

I would also like to thank my fellow coworkers in the Lu Lab, who have been very supportive and patient over the years. I would especially like to express my gratitude to Masha Savelieff, who took me under her wing of mentorship, and taught and supported me during my first couple of years. I would also like to thank Dewain Garner, Natasha Yeung, Nathan Sieracki, Kyle Miner, Yang Yu, Igor Petrik, Shiliang Tian, Saumen Chakraborty, Arnab Mukherjee, and Zhou Dai for their various forms of technical, intellectual, and personal collaborations and support. I would like to give Nicholas Marshall special mention, for the enormous support he has given me, both in terms of research and in friendship and comradery. Additionally, I would like to thank Robert Gennis and Wilfred van der Donk for the use of their stopped-flow and freeze quench instruments, respectively.

I would like to express great gratitude to NSF, for financial support, and the UIUC Chemistry Department for additional fellowships.

Finally, I thank my husband, Tyler Wilson, for being the rock on which I stood every day. I could never have done this without him. We built so many lasting memories during this time, which has only deepened our love and friendship. I also want to thank my family, who have been supportive of me, despite the distance between us, and kept me grounded.

TABLE OF CONTENTS

CHAPTER 1: GENERAL INTRODUCTION – THE BIOSYNTHETIC APPROACH TO THE STUDY OF CU_A CENTERS

Electron transfer is a process of universal importance to living organisms, as the chemical transformations from which such organisms draw energy require a dependable and rapid supply of electrons. The ability of several transition metals to achieve multiple stable oxidation states has made them a natural choice for accomplishing this task. In addition to the accessibility of multiple stable oxidation states, the redox properties of transition metals can be fine-tuned through changes in their coordination environments. Accordingly, nature has selected proteins containing metal centers, assigned with the sole function of passing electron(s) from a source to a target, acting as a biological wire. Out of so many transition metals, the only ones that nature has chosen to use for biological electron transfer are copper and iron.[1] Such a narrow selection is guided by the suitability of available redox potentials for the most stable oxidation states of these metals, as well as their abundance and solubility during the evolution of early organisms.[2,3]

The superficially simple action of passing an electron from source to target is brought into perspective after a careful examination of the conditions under which such electron transfer is achieved in biological systems. Humans have found ways to work pure metals into long, thin cylinders to perform the task of electron transfer, in which the conduction of an electron or hole over large distances is very facile. However, biological electron transfer occurs across distances > 10 Å through polypeptide frameworks, which are built from covalently-bonded carbon, oxygen, nitrogen and sulfur. Theoretical calculations show that electron tunneling through this protein scaffold is expected to fall off exponentially as the distance increases.[1] Yet, the electron transfer across these often large distances takes place rapidly (self-exchange rate of ~ 10^4–10^6 M^{-1} s^{-1} in one example).[4] Thus, nature has honed in on a special formula for facilitating the deceptively simple task of passing an electron from source to target, many secrets of which are locked away in the metal centers of electron transfer proteins.

Through decades of research from many different fields, our understanding of these properties of electron transfer proteins, which enable such facile electron transfer over large distances, has made great strides. The focal point of this dissertation is one such electron transfer center, called Cu_A, and in particular, how this center is formed, considering that its components readily undergo a well-known side reaction to form a deactivated mixture. The study of Cu_A, and

especially of the assembly of Cu_A, has been greatly facilitated by a biosynthetic model of Cu_A in the protein azurin. In this chapter, the extraordinary properties of the Cu_A center, its native context, its biosynthetic model in azurin, and the current understanding of its *in vivo* assembly are reviewed. First, however, the biosynthetic approach to the study of metalloenzymes is briefly introduced.

1.1. The Biosynthetic Approach to Metalloenzyme Studies

Metalloenzymes catalyze numerous important processes in biological systems, from the challenging chemistry of oxygen reduction,[5] water oxidation,[6] and methane oxidation,[7] to deceptively simple electron transfer reactions (including those catalyzed by T1 copper and Cu_A centers).[1] It has recently been estimated that over half of the entire proteome consists of metalloproteins.[8] To duplicate these amazing functions, for example, in alternative energy applications, as well as to treat diseases caused by their malfunction, it is desirable to both understand these metalloproteins and to construct similar catalytic centers. In order to study metalloprotein functions, there are two strategies that can be applied (Fig. 1.1): a "top-down" approach, in which the native metalloproteins are subjected to mutagenesis, and the perturbation to their structure and/or function are measured (Fig. 1.1A), and a "bottom-up" approach, in which a model containing the basic components of the native metal centers is built (Fig. 1.1B). While these two approaches are complementary, the "bottom-up" approach has several advantages over the traditional "top-down" approach. One advantage is that the minimum features needed for function can be identified. Another advantage is that the systems designed by the "bottom-up" approach are often simpler than the native systems, allowing deconvolution of their properties from other factors in the native environment, such as other metal centers.

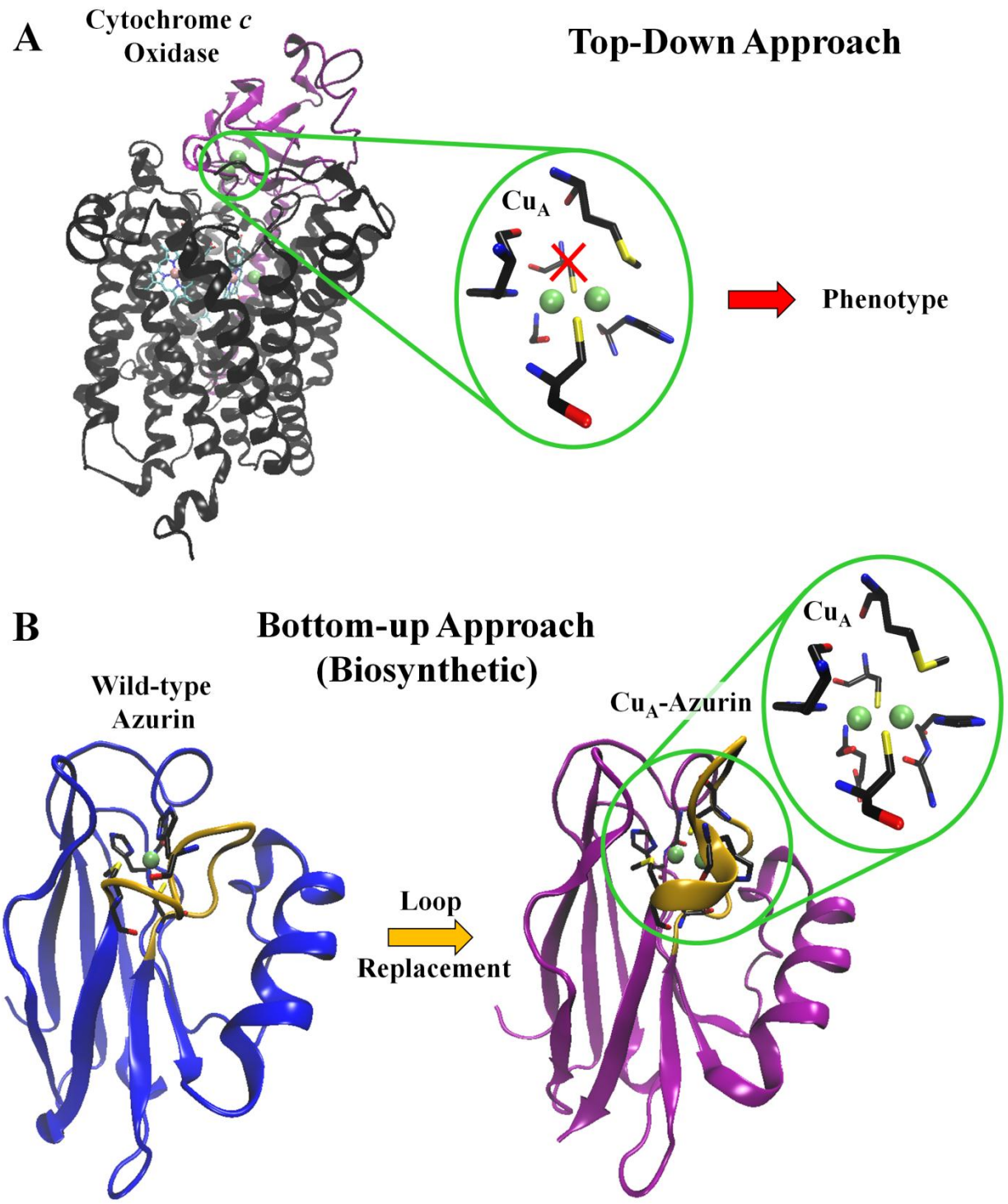

Fig. 1.1. Contrasting examples between the complementary top-down (A) and bottom-up (B) approaches to studying metal centers in biological systems. In the top-down approach (A), a native metal center is perturbed, usually by site-directed mutagenesis, such as mutation of one bridging Cys in Cu_A of C*c*O, and the resulting changes to the system are measured. Measurements of the perturbation to the Cu_A of C*c*O must be performed on the membrane-bound

enzyme complex, in the presence of the other metallocofactors (two hemes and a copper site). In the biosynthetic take on the bottom-up approach (B), a minimal model of the metal center is constructed in a protein free of other metallocofactors. In this example, the ligand loop of the T1 copper protein azurin was replaced with the corresponding ligand loop of a Cu_A center from a native C*c*O, and the resulting Cu_A-azurin biosynthetic model bound copper in a site very similar to those of native Cu_A enzymes. The minimal model here, then, is built from one His ligand of the original T1 copper center and the ligand loop from a native Cu_A, as the sequence identity between the other portions of azurin and the native Cu_A subunit are low. PDB IDs: (A) 1XME, (B) 4AZU (wild type Az), 1CC3 (Cu_AAz).

Traditionally, the only realistic option for using the "bottom-up" approach to model metalloenzyme centers was to synthesize small molecule analogs of these sites. While there have been some great successes using this approach,[9] small molecules can only mimic the protein environment to a certain extent. In particular, the secondary coordination sphere of metal centers in proteins has been demonstrated in a number of cases to be very important for their functions.[10-38] Synthesizing large enough ligand scaffolds to incorporate these secondary coordination sphere interactions, let alone controlling them, is difficult at best. Nevertheless, synthetic chemists have undertaken the incorporation of these secondary coordination sphere effects,[39-43] and in so doing, highlighted how important they are.

With the advent of modern molecular biology techniques, the option of creating "bottom-up" models (Fig. 1.1B) of metalloproteins in protein scaffolds became more feasible. This method of modeling native metal centers has recently been thoroughly reviewed,[44-48] and will only be briefly summarized here. In this approach, the protein can be simplistically regarded as a very large ligand to the metal, and thus, instead of a synthetic model, the resulting construct is a biosynthetic model. Practically speaking, however, the biosynthetic "ligand" for the target metal center must be carefully chosen to reflect the requirements of this center. Ideally, one would be able to choose a sequence of amino acids that would fold and chelate the metal in the desired fashion. This take on biosynthetic modeling is called "de novo design," from the literal Latin translation of "from the beginning."[8,49-54] While it represents the ideal for generating a biosynthetic model, and a number of groups have made great progress in this field,[8,49-55] our current understanding of how polypeptides fold into three-dimensions from a primary sequence of amino acids limits the implementation of this method.

Instead, we can take advantage of Nature's selection of well-folded, stable proteins, as well as the ever increasing volume of 3D structures available for proteins, and set certain criteria for a biosynthetic ligand. These criteria can range from very basic, like an unoccupied space for the metal to fill, to quite complex, such as subtle orientations of potential amino acid ligands, to optimize overlap with the metal's valence orbitals. Computational methods can greatly simplify the process of choosing a biosynthetic ligand, but have generally lacked the required sophistication, particularly in handling transition metals and their preferred ligand geometries. Once a protein scaffold has been chosen, molecular dynamics (MD) of the conceptualized design, with its various amino acid mutations, can provide some indication of how successful the design will be. However, MD computational results must be interpreted cautiously, as this type of energy minimization only considers electrostatic and steric effects. Thus, a drawback of using the biosynthetic approach to metalloprotein modeling is that designing the model systems is often quite challenging. On the flipside, once a successful design has been achieved, incorporating subtler features, such as hydrogen bonding to metal ligands, is much more feasible than in small molecules. Moreover, the model attained through the biosynthetic approach, as opposed to the synthetic approach, is closer to native metalloenzymes in several other ways, such as the immediate dielectric around the metal ion, the water solubility of the overall complex, and the types of functional groups available to interact with the metal ion.

A number of native metal centers have been successfully modeled by the biosynthetic approach.[44-48] These successful biosynthetic models have provided insights that would be difficult or impossible to obtain from the native equivalent. For example, biosynthetic models are typically purified in the metal-free form, allowing substitution of other metal ions to probe the importance of the metal identity and/or charge, whereas this is often not possible in native metalloproteins. As the computational methods for designing biosynthetic models of metalloenzymes improve, we look forward to the development of a greater number of biosynthetic models from which to gain deeper understanding of native metal centers.

1.2. Cu_A Centers Are Specialized Electron Gateways to Respiration

1.2.1. Structure of Cu_A: a Mixed Valence, Valence Delocalized Dinuclear Copper Center

To understand the key features that enable the efficient, long-distance electron transfer carried out by biological electron transfer centers, an intimate knowledge of their structures is of utmost importance. In the case of Cu_A, there are now several three-dimensional structures which reveal the protein fold and coordination geometry of these sites.[56-64] The Cu_A center is always found in cupredoxin folds, which display a Greek-key β-barrel fold (Fig. 1.2A).[35,56-66] The core of the Cu_A site consists of two copper ions bridged by two Cys thiolate ligands (Fig. 1.2B). [35,56-68] The copper-copper separation is small (2.35 – 2.64 Å), reflecting a direct Cu–Cu bond, the first metal-metal bond discovered in biological systems.[67] Together, the copper ions and Cys thiolate ligands form a rigid diamond core, to which many of the unique properties of Cu_A have been ascribed.[66,69] In addition to the two thiolate ligands per copper, from the bridging cysteines, each copper is coordinated equatorially by a His δ-N imidizolyl, creating an overall trigonal coordination environment for each copper. One weak axial ligand completes a distorted tetrahedral geometry for each copper ion, a Met thioether for one, and a backbone carbonyl for the other (Fig. 1.2B).

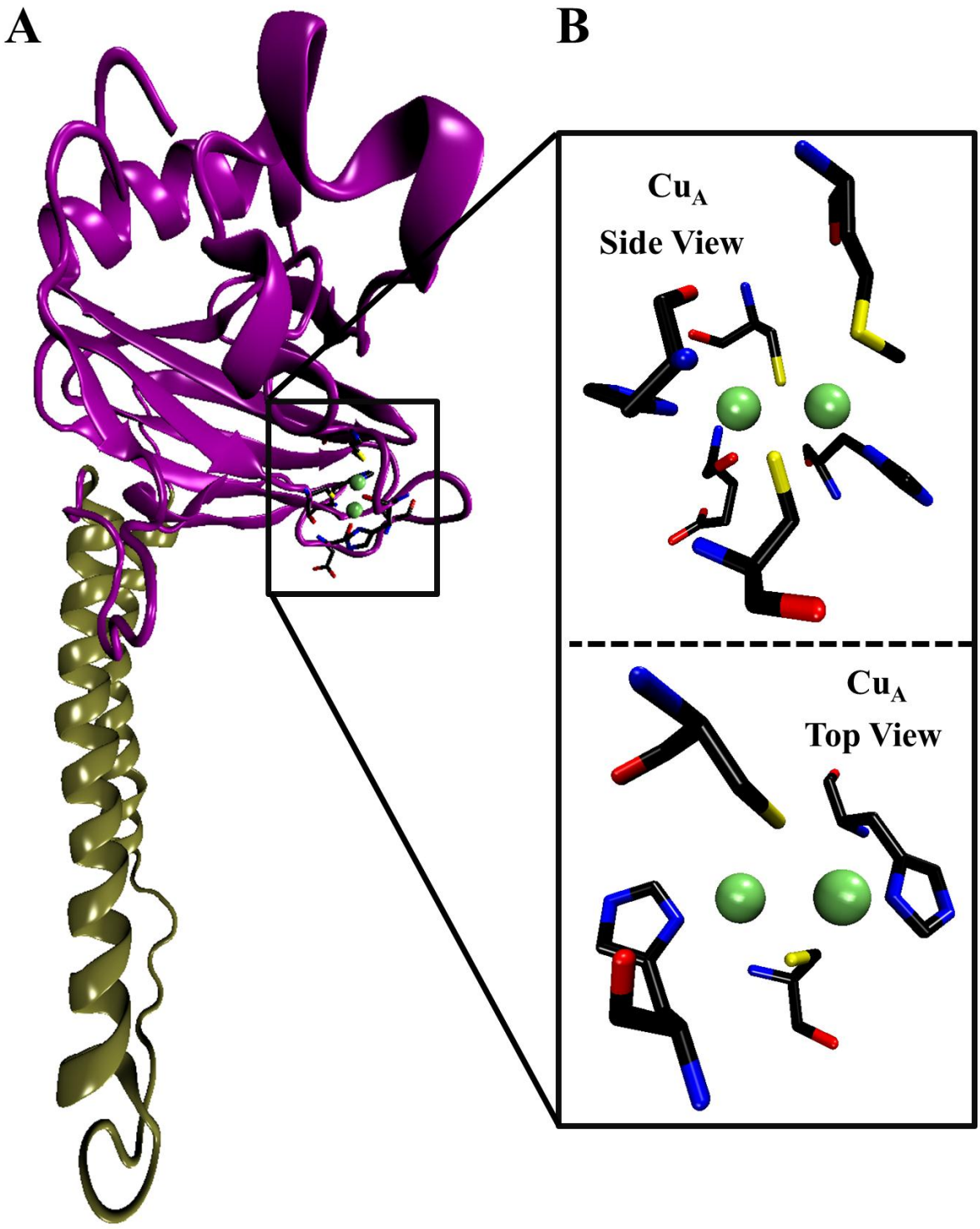

Fig. 1.2. Structure of (A) the Cu_A subunit from *Paracoccus denitrificans* C*c*O and (B) the Cu_A center of this subunit (PDB ID 3HB3). (A) The Greek-key β-barrel, cupredoxin domain of the Cu_A subunit is shown in purple, whereas the transmembrane helices that anchor this domain to the cytoplasmic membrane are shown in tan. (B) Zoomed-in view of the Cu_A center, showing a side view (upper) and top view (lower) of the site. The axial ligands are removed from the top

view for clarity. The copper ions are shown as green spheres. Amino acid coloring scheme: carbon is black, oxygen is red, nitrogen is blue, and sulfur is yellow.

The rigid diamond core structure of Cu_A is responsible for some unique properties of this center.[66,69] One very prominent property is a mixed valence, valence-delocalized resting state. While the resting state of the center is formally [Cu(II)–Cu(I)], the 19th d-electron is completely delocalized across the two copper ions, resulting in a [Cu(1.5)···Cu(1.5)] oxidation state.[69-75] As discussed later, this paramagnetic, valence delocalized resting state provides characteristic spectroscopic handles and confers functional advantages to the Cu_A center.

1.2.2. Occurrence of Cu_A Centers and the Associated Difficulties in Studying Them

Cu_A centers are found only in a handful of enzymes, which are always located at or near the terminus of an electron transport chain.[57,76-84] To date, only four types of enzymes are known to contain Cu_A: 1) cytochrome *c* oxidases (C*c*Os), at the terminus of the aerobic respiration chain,[5,56,57,85-87] 2) nitrous oxide reductases (N_2ORs), at the terminus of an anaerobic respiration chain,[62,63,88] 3) a nitric oxide reductase (NOR), near the terminus of the same anaerobic respiration chain,[89,90] and 4) SoxH, a subunit of a terminal oxidase, SoxM, in the organism *Sulfolobus acidocaldarius*.[91,92] Together, these enzymes constitute members of an important group, as anaerobic and aerobic respiration provide the means for living organisms to convert nutrient sources into stored energy. Moreover, in the case of NOR and N_2OR, these enzymes contribute to the global denitrification cycle, which is important in preventing the accumulation of the potent greenhouse gas, N_2O.[88] In all of these enzymes, Cu_A serves as the electron entry point, passing electrons from a substrate either directly to the catalytic metal center or first through another electron transfer center housed in the same enzyme, such as a low-spin heme *a* in C*c*Os.

After the discovery of Cu_A, scientists wondered at the existence of this center in nature, as another copper-based electron transfer site, called type 1 (T1) or blue copper, had been known to occur in nature and thoroughly investigated.[1,23,34,35,65,93-95] Indeed, T1 copper centers catalyze electron transfer between a large variety of donors and acceptors, correspondingly achieving a broad range of reduction potentials. In view of the apparent malleability of the T1 copper center to suit the requirements of a given situation, the selection pressure that resulted in Cu_A centers was enigmatic. These mystifying origins of Cu_A as well as its vital position at the end of electron

transport chains established a large drive for studies aimed at understanding this center. However, the authors of these studies had to overcome some inherent problems presented by the systems in which Cu_A occurs: the presence of other metallocofactors,[5,88,89,91] which convolute spectroscopic features, and in many cases, the localization of the enzyme to a membrane,[5,89,91] which requires tedious and low-yielding purification procedures.

In N_2OR, the catalytic center is a tetranuclear copper center, called Cu_Z.[88] Thus, in all Cu_Z oxidation states involving Cu(II), this center displays interfering spectroscopic signals with those of Cu_A. C*c*O and SoxM, on the other hand, contain two heme cofactors, as well as another copper center, called Cu_B.[5,91] The heme cofactors always interfere with many of the UV-Vis absorption signals of Cu_A, while the other copper center has commingling signals in electron paramagnetic resonance (EPR) spectroscopy and X-ray absorption spectroscopy (XAS) with Cu_A. NOR also houses two heme cofactors, as well as a non-heme iron center.[89] Again, these heme cofactors always absorb strongly in the visible part of the electromagnetic spectrum, masking the signature of Cu_A. For all of the three enzymes, C*c*O, SoxMH, and NOR, localization to a cellular membrane increases the difficulty of purifying and studying the intact enzyme complex.[5,89,91] All factors considered, studying the Cu_A center in its native context is not a trivial undertaking and may not provide the isolated spectroscopic characteristics of Cu_A.

1.2.3. Design and Isolation of Soluble Cu_A Proteins Free of Other Metallocofactors

The problems associated with studying Cu_A centers in their native enzyme complexes instigated researchers to develop soluble proteins containing Cu_A only, i.e. without any other metallocofactors. Two routes were taken to obtain such soluble Cu_A proteins. In one route, the native Cu_A-containing subunits were modified, such that the transmembrane helices that anchor them to the membrane were truncated, resulting in soluble Cu_A domains.[60,91,96-104] In the second route, Cu_A centers were engineered into suitable scaffold proteins, by introduction of the Cu_A ligand set.[105-108]

Several soluble Cu_A proteins from truncated native subunits have been made. Soluble Cu_A domains now exist for the C*c*Os from *Bacillus subtilis*,[97] *Paracoccus denitrificans*,[96,98,99,103] *Paracoccus versutus*,[102] *Synechocystis* PCC 6803,[104] and *Thermus thermophilus*,[60,100,101,103] and for SoxH from *S. acidocaldarius*.[91] Spectroscopic studies of these soluble Cu_A domains have yielded consistent results, and the measured reduction potentials of these constructs have also

agreed amongst each other.[60,91,96-100,102-104,109-111] Of these soluble Cu_A domains, an X-ray crystal structure has been obtained only for the protein isolated from *T. thermophilus*.[60] Useful insights into the structure and function of Cu_A centers have been gleaned from these soluble Cu_A truncates. However, these Cu_A model systems can present other difficulties, as they often suffer from poor stability, due to the loss of stabilizing interactions with other portions of the native enzyme complex.[91,96,101]

Engineering the Cu_A cofactor into a suitable protein, the second approach to obtaining a soluble Cu_A for further studies, has been accomplished by a handful of research groups.[105-108] It was first achieved in a copper-less quinol oxidase, which possessed a domain, CyoA, with a similar Greek-key β-barrel fold to Cu_A domains but free of any metal cofactors.[105] Through sequence overlays with native Cu_A domains, the authors of this study determined suitable amino acid positions in which to introduce the ligand set of Cu_A, and performed the corresponding mutagenesis. The resulting Cu_A-CyoA construct bound two copper ions in a site that was similar to Cu_A, as judged by UV-Vis and EPR spectroscopy, but bound other copper species as well. Not long after the pioneering report of this engineered Cu_A in CyoA, two other engineered Cu_A proteins were independently developed.[106,107] Both designs utilized T1 copper proteins as the scaffold, which occupy similar Greek-key β-barrel folds to those of Cu_A domains. The two designs were also both founded on the recognition that the majority of the copper binding residues for both the T1 copper and Cu_A centers resided in a single loop between the 7th and 8th strand of the β-barrel. In fact, the ligand that was not positioned in this loop, a His, was also present as a ligand to the T1 copper site. Therefore, each of the research groups chose a Cu_A loop sequence and used it to replace the corresponding loop of the T1 copper protein scaffold. In one case, that loop sequence was the same one used to create the Cu_A-CyoA construct, and the chosen T1 copper protein was amicyanin, giving Cu_AAmi.[106] The loop sequence from *Paracoccus denitrificans* C*c*O and the T1 copper protein, azurin, were used to build the other construct, yielding Cu_AAz (Fig. 1.1B).[107] Both Cu_A model proteins bound copper in a site similar to native Cu_A, as judged by UV-Vis and EPR spectroscopies. The Cu_AAz model went on to yield many interesting insights into Cu_A centers, as will be discussed further below.

1.2.4. Spectroscopy of Cu_A Centers: the Basis for Formulation of Their Electronic Structures

The presence of a paramagnetic oxidation state and cysteine thiolates as ligands in the Cu_A center provides a wealth of spectroscopic information about these sites, which in turn reports on their electronic structures. In the [Cu(1.5)···Cu(1.5)] resting state, Cu_A centers display two $S_{Cys} \rightarrow$ Cu ligand-to-metal charge transfer (LMCT) bands at ~ 480 and 530 nm, with ε ~ 3000-4000 M^{-1} cm^{-1}, in their visible absorption spectra (Fig. 1.3A).[60,63,91,93,96,97,101,102,104,112,113] Additionally, in the near IR region of their absorption spectra, Cu_A centers feature a broad band centered at ~ 760-800 nm with ε ~ 2000 M^{-1} cm^{-1}, which arises from a Cu-Cu $\psi \rightarrow \psi^*$ transition between Cu-Cu bonding and antibonding orbitals.[72] Thus, this feature is a direct consequence of the unique valence-delocalized, Cu-Cu bonding interaction of Cu_A.[69]

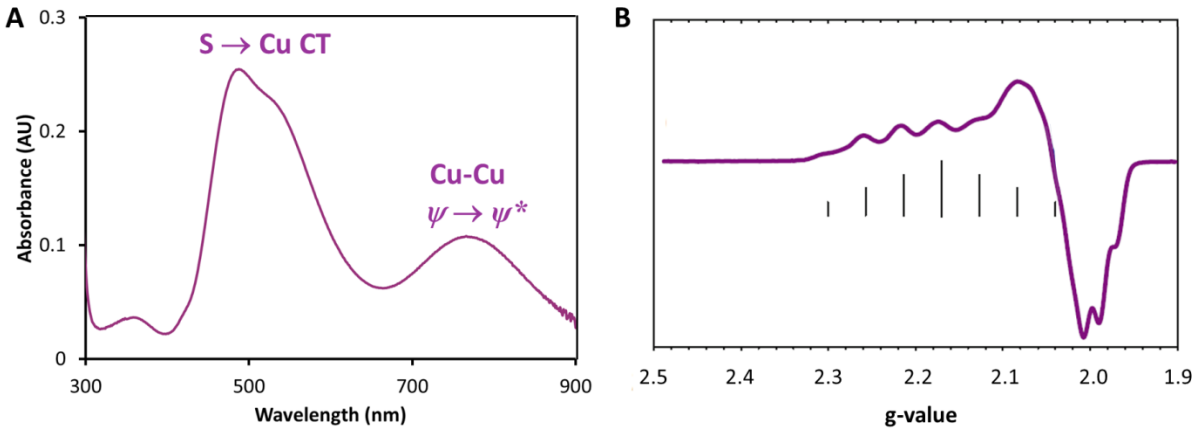

Fig. 1.3. (A) Representative electronic absorption spectrum of a Cu_A center, where the S → Cu charge transfer and Cu-Cu $\psi \rightarrow \psi^*$ are indicated. (B) Representative EPR spectrum of a Cu_A center, displaying a 7-line hyperfine pattern due to complete delocalization of the 19th d-electron across both copper ions (adapted from ref 66). Both spectra were collected in the biosynthetic Cu_A model, Cu_AAz.

Similarly to its electronic absorption spectrum, the EPR spectrum of Cu_A reflects the unique valence-delocalized electronic structure of this site in the resting state, as demonstrated by a 7-line hyperfine splitting pattern (Fig. 1.3B).[74,114,115] Mononuclear copper centers display a 4-line hyperfine splitting pattern, due to the interaction of the unpaired electron with the I=3/2 nuclear spin of the copper ion, according to the formula 2I + 1.[34,35,65] Distribution of the unpaired electron of Cu_A in its resting state across two I=3/2 copper nuclei gives a 7-line hyperfine pattern (2×2I + 1). This 7-line hyperfine pattern was, in fact, one of the first confirmations that Cu_A was a mixed-valence, valence-delocalized center. Another feature of the EPR spectrum, the magnitude of the hyperfine splitting in the parallel region of the spectrum ($A_{\parallel}$), reflects high

covalency between the copper ions and Cys thiolate ligands, as $A_{\parallel}$ is small (~30-40 × 10^{-4} cm^{-1})[71,96,97,101,112,116] in Cu_A compared to standard copper complexes (~130-180 × 10^{-4} cm^{-1}).[65]

A combination of electronic absorption, EPR, and other spectroscopic studies, along with computational studies, has facilitated understanding of the Cu_A center and resulted in a detailed electronic structural description of this site. Before crystal structures of C*c*O became available and small soluble proteins containing only the Cu_A center were developed, MCD studies provided the best picture of the Cu_A site, one that resembled the experimentally determined X-ray structure, containing the dinuclear core with bridging cysteines.[71,72,98,117-122] In a later study, where synthetic and biosynthetic Cu_A models were compared to a native Cu_A center, MCD was one of a suite of experiments that resulted in a full electronic structural description of the Cu_A center.[72] Resonance Raman (rR) also provided an important handle in developing the electronic structural description of Cu_A in this study, as it revealed transitions corresponding to the vibrational modes of the diamond core.[72,123-127] X-ray absorption spectroscopy of Cu_A centers produced the first evidence that this center contained a direct Cu-Cu bond.[67,68,128-131] While the site proposed on the basis of EXAFS was not completely correct, the Cu-Cu distance was very close to that measured later in the crystal structure.[67,68] Importantly, EXAFS measurements in the reduced and oxidized states of the Cu_A center showed that there were very minimal changes to the site in switching between these states.[130] S K-edge XAS has provided a measure of the covalency of the Cu–S interaction in Cu_A.[132,133] A combination of EPR, ENDOR and computational studies led to a detailed molecular orbital description of Cu_A in N_2OR.[74] A couple of years later, a combined electronic absorption, CD, MCD, and rR spectroscopic and computational study of synthetic and biosynthetic Cu_A models and a soluble C*c*O Cu_A domain led to a molecular orbital description of Cu_A in C*c*O.[72]

1.2.5. Key Characteristics of Cu_A that Facilitate Rapid Electron Transfer under Low Driving Forces

Elucidation of the characteristics of Cu_A that enable it to transfer electrons rapidly across large distances and under the low driving forces (~50 mV) experienced at the termini of electron transport chains has been a gradual process, drawing from many different areas of research. Detailed studies of the closest biological electron transfer center, T1 copper (Fig. 1.4), have been of paramount importance to this process, as T1 copper centers are simpler than Cu_A. Moreover,

T1 copper centers are highly analogous to the individual copper ions in the Cu_A center, in terms of similarity in geometry and ligand set, such that Cu_A can be thought of as two T1 copper centers linked together.

The T1 copper site consists of a single copper ion, coordinated in a trigonal fashion by two His δ-N imidizolyls and a Cys thiolate, typically with one or two weaker axial ligands (Fig. 1.4B).[23,34] One of these weaker axial ligands is usually a Met thioether, whereas the other, when present, is a backbone carbonyl. Thus, T1 copper centers can have overall distorted trigonal planar, tetrahedral, or trigonal bipyramidal geometries, depending on whether the weak axial ligand(s) are present. As in the case of Cu_A, their paramagnetic Cu(II) oxidation state and Cys thiolate coordination result in a rich variety of spectroscopic handles for T1 copper centers, including an intense ($\varepsilon \sim 2000\text{-}6000\ M^{-1}\ cm^{-1}$) S $\rightarrow$ Cu CT band at ~600 nm in the electronic absorption spectrum, and a 4-line hyperfine splitting pattern in the EPR spectrum with narrow splittings ($A_{\parallel} \sim 40\text{-}60 \times 10^{-4}\ cm^{-1}$).[34,35,65] These spectral features of T1 copper proteins were quite novel at the time that these centers were being investigated for the first time.[23] In particular, the ~600 nm absorption of these centers imparts a bright blue hue to solutions of their proteins, and the reduction potential of T1 copper sites are much higher than standard aqueous copper complexes. Jointly, these features of T1 copper centers stimulated intensive study of these centers and debate about what properties of the centers imparted them with these unique features, which spanned several decades.[23] From this work, primarily two features of T1 copper centers were credited with bestowing them their rapid electron transfer capabilities: their unusual geometry and highly covalent Cu–S bond.

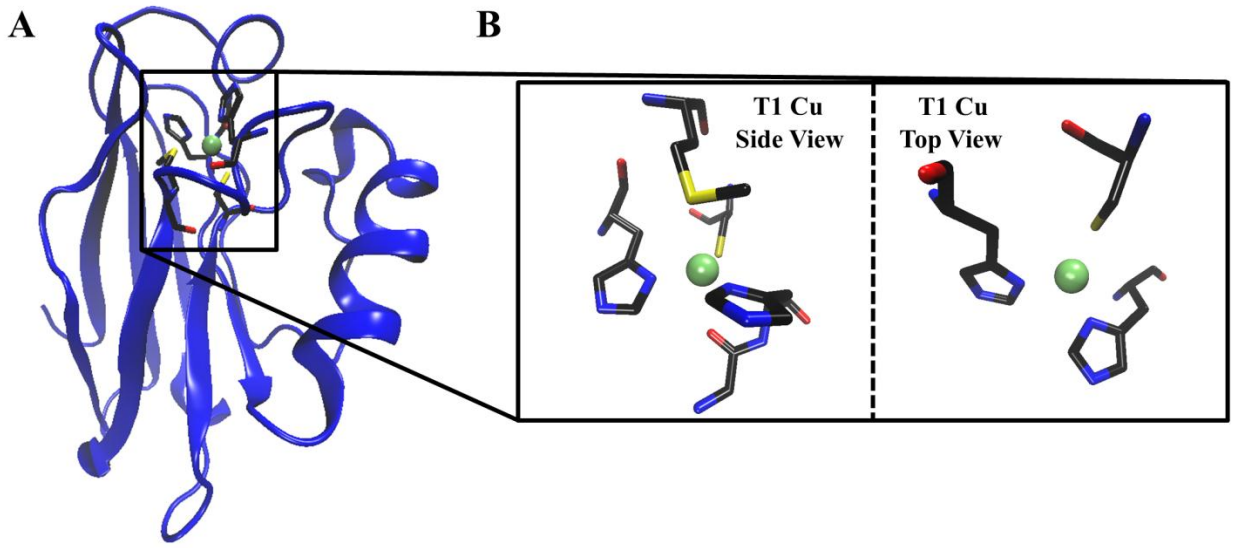

Fig. 1.4. (A) Structure of the T1 copper protein azurin (Az) and (B) its T1 copper center (PDB ID 4AZU). (A) Az exhibits the same Greek-key β-barrel, cupredoxin fold that Cu_A domains adopt. (B) The T1 copper center is shown both from a side view (left) and top view (right). The axial ligands are omitted in the top view for clarity. The residues shown in the top view also correspond to the minimal ligand set required to form a T1 copper center. Copper ions are shown as green spheres. Amino acid coloring scheme: carbon is black, oxygen is red, nitrogen is blue, and sulfur is yellow.

With the advent of widespread biomacromolecular crystallography, several crystal structures of T1 copper proteins in both the reduced and oxidized states were obtained (see [23], and references therein. These structures revealed two important facts. First was the unusual geometry of T1 copper centers, relative to their aqueous, unconstrained counterparts. Whereas the geometries of T1 copper centers fall into the classification of trigonal (i.e. distorted trigonal planar, tetrahedral, or trigonal bipyramidal), the geometries of unconstrained Cu(II) complexes are typically tetragonal, such as square planar, square pyramidal, and octahedral. By comparison, unconstrained Cu(I) complexes typically display trigonal geometries, like T1 copper centers. The other important feature revealed by crystallization of T1 copper proteins in both oxidation states was a very small change in the geometry of the center upon reduction/oxidation, implying a low reorganization energy for these centers. Measurements have confirmed the low reorganization energy for T1 copper centers, giving values of 0.7-1.2 eV.[134-136] A low reorganization energy greatly facilitates rapid electron transfer. From theoretical work, it has been shown that Cu(II) ions placed in the typical geometry of reduced copper complexes (i.e. trigonal geometries) must undergo a Jahn-Teller distortion to relieve orbital degeneracy, giving the final tetragonal

geometry.[34] In the constrained and low symmetry environment of T1 copper proteins, this Jahn-Teller distortion is avoided, thus permitting the Cu(I) and Cu(II) oxidation states to adopt similar trigonal geometries and consequently lowering the reorganization energy.

The other major feature of T1 copper centers which facilitates rapid electron transfer is a highly covalent copper-thiolate bond. S K-edge X-ray absorption spectroscopy has quantified this covalency at ~40% S-character in the HOMO,[137] much higher than most copper-ligand interactions.[34] High covalency in a metal-ligand bond is expected to substantially increase donor-acceptor coupling. Donor-acceptor coupling is, in turn, directly proportional to electron transfer rate. Moreover, anisotropy in the covalency of a ligand set provides directionality to the electron transfer event. Solomon and coworkers demonstrated that, in one T1 copper protein, plastocyanin, the anisotropic covalency of the Cu-S_{Cys} bond accelerated electron transfer ~1500 fold (calculated purely from distance) through a pathway containing this Cu-S_{Cys} bond, compared to a shorter pathway to the site through one of the His ligands.[138] Thus, the anisotropic covalency provided by the copper-thiolate bond of T1 copper centers plays a large role in the ability of these centers to transfer electrons rapidly.

Since the Cu_A center can be thought of as two T1 copper centers joined together, both of the features considered to bestow T1 copper centers with their rapid electron transfer abilities are in effect for Cu_A centers as well. Each of the copper ions in Cu_A adopts a distorted tetrahedral geometry, like many T1 copper centers, thus lowering the reorganization energy of this site relative to unconstrained copper complexes (see above). Likewise, Cu_A has highly covalent Cu–S bonds, 46% S character in the HOMO as obtained from calculations correlated to spectroscopic data.[71] However, in addition to these features shared with T1 copper centers, Cu_A has functional advantages that result from its mixed valence, valence delocalized resting state.[66,69] One such advantage manifests itself in a lower reorganization energy for Cu_A as compared to T1 copper centers.[139] This enhanced decrease of the reorganization energy in Cu_A arises due to the distribution of the geometrical adjustments accompanied by change in oxidation state across twice the number of copper-ligand bonds, resulting in half the change in bond lengths as observed for T1 copper centers. Since the reorganization energy is proportional to the square of the change in bond lengths, the decreased changes in bond lengths for Cu_A results in half the reorganization energy for the Cu_A center compared to T1 copper centers.[69] Another functional advantage is the resistance that the strong, direct valence-delocalized interaction

between the copper ions provides to the Cu_A center against perturbing forces (see below). For example, the Cu_A center can remain valence delocalized even with the loss of an equatorial His ligand.[140] Thus, in addition to the functional advantages enjoyed by T1 copper centers in rapid electron transfer, Cu_A has even greater functional advantage due to its valence delocalized resting state. In light of this knowledge, the selection pressure that resulted in Cu_A centers becomes apparent, as its greater efficiency relative to T1 copper centers gives it an immense advantage under the low driving forces experienced at the end of electron transport chains.

1.2.6. Contributions of the Biosynthetic Cu_A Model Cu_AAz to the Current Understanding of Cu_A Centers

The biosynthetic Cu_A model in azurin (Cu_AAz, see above) has provided a number of useful insights into native Cu_A centers.[59,66,72,84,107,126,131,132,139-158] First of all, several spectroscopic studies, as well as a crystal structure, have established that the Cu_A in Cu_AAz is a good model of native Cu_A centers.[59,72,107,126,132,142,149] The S $\rightarrow$ Cu CT bands of Cu_AAz are positioned at 485 nm ($\varepsilon \sim 3700\ M^{-1}\ cm^{-1}$) and 530 nm ($\varepsilon \sim 3400\ M^{-1}\ cm^{-1}$),[142] compared to 480-485 nm and 530-540 nm for native Cu_A centers. At lower energy, the Cu-Cu $\psi \rightarrow \psi^*$ transition of Cu_AAz is positioned at 760-800 nm ($\varepsilon \sim 2000\ M^{-1}\ cm^{-1}$),[142,154] giving a clear indication that the mixed-valence, valence-delocalized resting state of native Cu_A centers is reproduced in Cu_AAz. Cu_A in Cu_AAz also displays a 7-line hyperfine pattern in its EPR spectrum,[142] further confirming the valence delocalization of the oxidized form of Cu_A. Along with another biosynthetic model, Cu_AAmi, a soluble Cu_A domain from C*c*O and a synthetic mixed-valence Cu_A model, Cu_AAz contributed to the development of a detailed description of the electronic structure of Cu_A, based upon the results from a variety of spectroscopic methods.[72] The composition, geometry, and bond lengths from the crystal structure of Cu_AAz also reveal close structural mimicry of native Cu_A centers (Fig. 1.5), with minor perturbations to the Cu–Cu bond length (slightly shorter in Cu_AAz), planarity of the $His_2Cys_2Cu_2$ unit (more planar in Cu_AAz), Cu-Met distance (longer in Cu_AAz), and Cu-carbonyl distance (to backbone carbonyl of residue 114, which is shorter in Cu_AAz).[59] The reduction potential measured for the Cu_A center in Cu_AAz also compares favorably with those of native Cu_A centers.[153] Thus, studies of this biosynthetic Cu_A model in Az should translate well to native Cu_A systems.

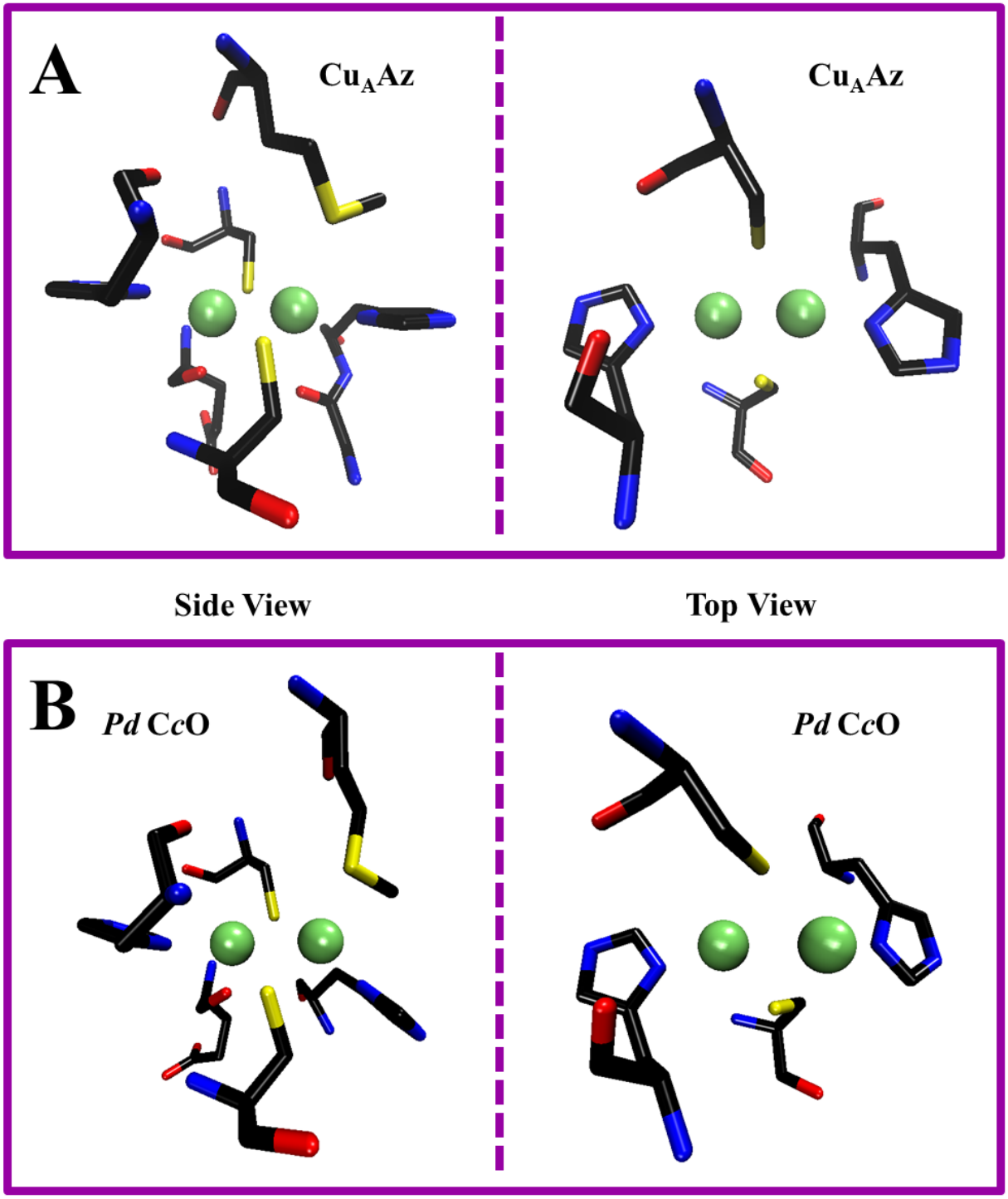

Fig. 1.5. Comparison between the Cu_A centers of (A) the biosynthetic model, Cu_AAz (PDB ID 1CC3) and (B) the native Cu_A from the C*c*O of *Paracoccus dentirificans* (PDB ID 3HB3), showing both a side view (left) and top view (right) of the centers. Axial ligands are omitted from the top view for clarity. Cu_A in Cu_AAz reproduces the key features of native Cu_A centers, such as a rigid diamond core with a direct Cu-Cu bond. In fact, the entire ligand set of native Cu_A centers is reproduced. Small differences are observed in the Cu-Cu bond length (~0.1 Å shorter

in Cu_AAz), in the angle of the His imidazole rings with respect to the plane of the diamond core, in the Cu-Met distance (~0.5 Å longer in Cu_AAz), and in the Cu-O_{CO} distance (~0.6 Å longer in Cu_AAz). Copper ions are shown as green spheres. Amino acid coloring scheme: carbon is black, oxygen is red, nitrogen is blue, and sulfur is yellow.

One advantage of biosynthetic models of native metalloproteins is that these proteins are typically expressed in the metal-free form, allowing substitution of the native metal with other metals. Early studies of the Cu_AAz model probed the preference of the Cu_A center for a specific overall charge.[141,146] Titration of a variety of metals, including Hg(II), Ag(I), Cu(I), Cd(II), Au(I), and Co(II), to metal-free Cu_AAz demonstrated that the Cu_A center of this protein preferred soft metals and an overall +3 charge. This preference for an overall +3 charge may play a part in stabilizing the [Cu(1.5)···Cu(1.5)] resting state of Cu_A centers.

Mutagenesis studies of Cu_AAz have revealed the importance of the rigid diamond core of Cu_A in maintaining the integrity of this center (Fig. 1.6).[140,144,145,148,154,155,157] While it has been demonstrated that mutating the axial Met position in T1 copper centers adjusts the reduction potential of these sites across a ~ 200 mV range,[159] at a similar Cu-Met distance, equivalent mutations in Cu_AAz had very little effect on the reduction potential of its Cu_A center.[155] One explanation for this difference in the role played by the axial Met ligand, between T1 copper and Cu_A in azurin, is that the rigid diamond core of Cu_A renders it far more resistant to perturbations from the axial position. However, a subsequent report of similar axial Met mutations in a soluble Cu_A domain from *Thermus thermophilus* (*Tt*) C*c*O showed ~ 200 mV of change in reduction potential with variation of this axial ligand.[111] This divergence in behavior between the *Tt* Cu_A domain and Cu_AAz was attributed to the difference in Cu-Met distances in these two systems (Fig. 1.7). In the *Tt* Cu_A domain, the Cu-Met distance is 2.47 Å, while in Cu_AAz, this distance is ~ 3.07 Å (average of two molecules in the asymmetric unit). The shorter Cu-Met distance in the *Tt* Cu_A domain may result in a stronger influence of this position on the reduction potential of the Cu_A site. This explanation is not consistent, though, with the difference between the axial Met tuning in T1 copper and Cu_AAz, as in this case, the Cu-Met distances are very similar (3.07 vs. 3.15 Å), yet the axial Met position exerts very dissimilar levels of influence on these two centers (Fig. 1.7). Another explanation is that the Cu–Cu bond length is also shorter in Cu_AAz (~ 2.39 Å) than in the *Tt* Cu_A domain (2.51 Å), which should make diamond core of Cu_AAz stronger (Fig. 1.7). A stronger diamond core would render the Cu_A center in Cu_AAz more resistant to

perturbation from the axial position, which is more consistent with the difference in axial ligand effects between the T1 copper and Cu_A center in azurin.

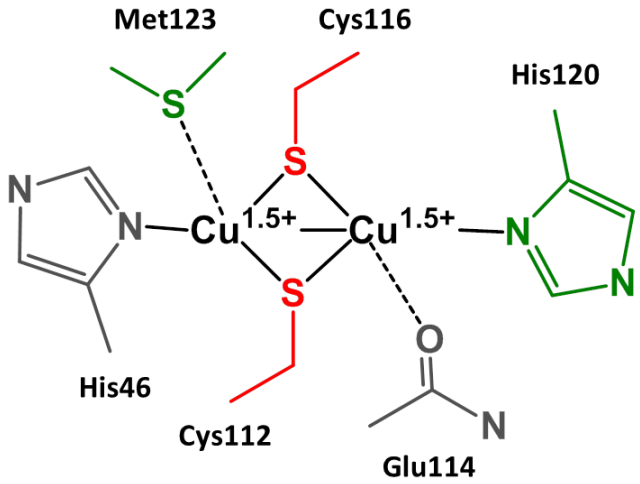

Fig. 1.6. Structure of Cu_A site, showing how tolerant each sidechain ligand is to mutation, based upon studies in the biosynthetic Cu_A model, Cu_AAz. Green color indicates that the position is highly tolerant to mutation or loss, resulting in a Cu_A center that is still valence delocalized. Red color indicates that mutation of these positions results in massive perturbation to the center, such that it no longer forms a Cu_A center. Grey color indicates that the tolerance of these positions to mutation/change is largely unexplored.

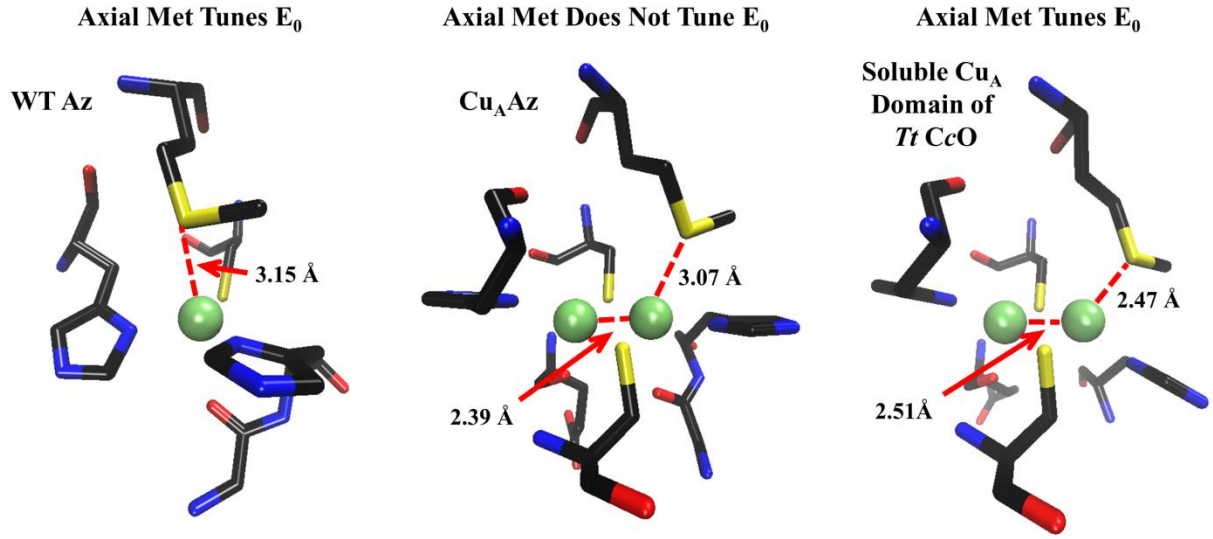

Fig. 1.7. T1 copper center of wild type (WT) Az (left, PDB ID 4AZU), Cu_A center of Cu_AAz (center, PDB ID 1CC3), and Cu_A center of the soluble Cu_A domain from *Thermus thermophilus* C*c*O (right, PDB ID 2CUA), where the Cu-Met and Cu-Cu distances are indicated. Although WT Az and Cu_AAz have similar Cu-Met distances, the axial Met position tunes the reduction potential (E_0) of the T1 copper site in WT Az over a ~200 mV range, but has very little effect on

the E_0 of Cu_A site in Cu_AAz. Conversely, the axial Met position does tune the reduction potential in the Cu_A site of *Tt* C*c*O. This difference between Cu_AAz and *Tt* C*c*O could be attributed to a shorter Cu-Met distance in *Tt* C*c*O. However, this is not consistent with the difference in axial Met tuning observed between WT Az and Cu_AAz, despite their similar Cu-Met distances. An alternative explanation is that the stronger Cu-Cu interaction in Cu_AAz renders its Cu_A center more immune to perturbations from the axial Met position than the Cu_A center in *Tt* C*c*O. Copper ions are shown as green spheres. Amino acid coloring scheme: carbon is black, oxygen is red, nitrogen is blue, and sulfur is yellow.

More surprising than the minor effect of axial Met on the properties of Cu_A in Cu_AAz is that mutation of one of the equatorial His ligands (His120), at 2.16 Å from one Cu ion, to other amino acids (Ala, Asp, Gly Asn) results in a Cu_A center that is still valence delocalized.[140,144,145,148,154,157] Initially, this fact was obscured by a 4-line hyperfine splitting pattern in the EPR spectrum of these H120X mutants, which suggested that the 19th d-electron had become localized to one copper ion. However, an ENDOR study of two His120 mutants indicated that these mutants were still valence delocalized.[148] An extensive spectroscopic and computational study by Solomon and coworkers showed that the apparent localization of the 19th d-electron was due to a 1% mixing of the 4s orbital from one copper ion into the ground state.[140] Thus, the rigid diamond core of Cu_A preserves its valence delocalized ground state even with the loss of a close His ligand and the associated symmetry.

As expected, however, mutations to the rigid diamond core itself, i.e. either bridging Cys, to other residues causes large changes to the Cu_A center in azurin.[84,156] When Cys112 is mutated to Ser, the resulting construct binds two coppers, but in distinct Type 2 (T2) copper centers.[156] T2 copper centers adopt tetragonal geometries, the typical geometries of small molecule Cu(II) complexes, and display different spectroscopic parameters, relative to T1 copper and Cu_A centers.[23,65,160] When thiolate coordination is present, T2 copper centers exhibit an intense S $\rightarrow$ Cu CT band at 360-400 nm, and all T2 copper centers display large parallel hyperfine splittings in their EPR spectra, ~130-180 $\times$ 10^{-4} cm^{-1}.[65] At least one of the coppers in the Cys112Ser mutant binds to the remaining Cys116, as an intense ~390 nm S $\rightarrow$ Cu CT band is present in the UV-Vis spectrum of this mutant.[156] Conversely, when Cys116 is mutated to Ser, a single copper ion binds to the remaining Cys112, in a T1 copper center, as evidenced by an S $\rightarrow$ Cu CT band at 623 nm in its UV-Vis absorbance spectrum and the small parallel hyperfine splittings in its EPR spectrum.[156] To probe whether loss of the Cu_A center in these mutants was due to the introduced asymmetry between the bridging ligands, a double Cys to Ser mutant was studied.[84]

This mutant bound a single copper ion in a T2 copper center at low pH. As the pK_a of Ser alcohol groups is much higher than that of Cys thiols, the ability of this double Cys to Ser mutant to bind copper at high pH was explored. Higher pH did promote the binding of two copper ions, but rather than a dinuclear copper center, EPR revealed that the two copper ions were bound in two distinct T2 copper sites. These studies suggest that the rigid diamond core of Cu_A relies on a foundation of bridging thiolates.

In C*c*O, it has been proposed that some sort of on-off switch is needed to regulate the proton-pumping function of this enzyme, to prevent excessive build-up of protons on one side of the membrane. While both the electron transfer heme *a* and catalytic heme-Cu_B centers have been proposed to fulfill this function, discovery of a pH-dependent alteration in the Cu_A center of Cu_AAz suggested that the Cu_A may serve in this role.[154] Upon lowering the pH of a solution of Cu_AAz from 6.8 to 4.1, the S $\rightarrow$ Cu CT bands increase slightly, while the Cu-Cu $\psi \rightarrow \psi^*$ band centered at ~760 nm red-shifts to ~800 nm. Through mutational studies, this pH-dependent behavior was attributed to protonation/deprotonation of one of the equatorial His residues, His120.[154] It was also found that this change in the Cu_A center is accompanied by a ~70 mV increase in the reduction potential of this center. Under the low driving forces at the end of the aerobic respiratory electron transport chain, this ~70 mV increase in the reduction potential is enough to make electron transfer from Cu_A energetically unfavorable, which could shut down the proton-pumping activity of C*c*O. Accordingly, it was suggested that, as enough protons accumulate on the outside of the membrane, His120 becomes protonated, raising the reduction potential of the Cu_A and stopping proton pumping, until the pH on the outside of the membrane reaches a value where His120 can once again be deprotonated (Fig. 1.8). As an ~ 2000-fold decrease in the rate of electron transfer from Cu_A to heme *a* is observed for the C*c*O from *Rhodobacter sphaeroides* upon transition to low pH,[161,162] this proposed switching function of Cu_A has support from a native C*c*O.

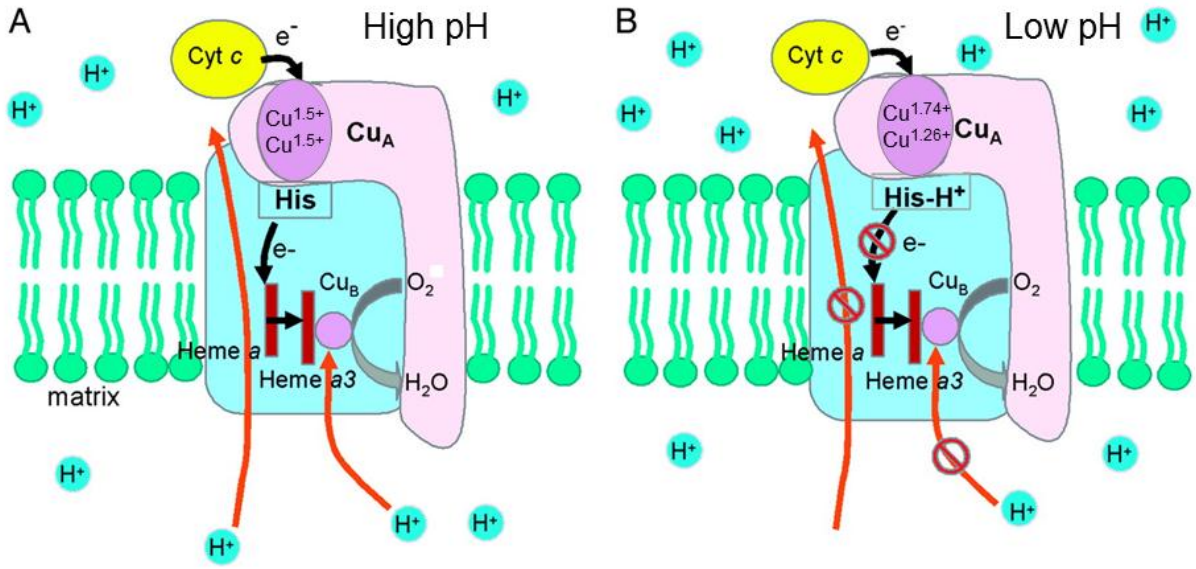

Fig. 1.8. Schematic depiction of possible proton-pumping gateway function of Cu_A in C*c*O. (A) Under high pH conditions, i.e. when few protons have been pumped across the membrane, the Cu_A center is completely valence delocalized, with a reduction potential that enables efficient electron transfer under the operational driving forces. (B) When enough protons have been pumped across the membrane, the Cu_A center becomes 16% less delocalized, and its reduction potential increases by ~70-90 mV, decreasing the efficiency of electron transfer. Solomon and coworkers additionally have found that a conformational change upon transition to low pH shifts the relative positions of two amino acids in one of the electron transfer pathways, which is expected to decrease the electron transfer efficiency by ~30-fold. Figure adapted from ref. 154.

The low pH form of Cu_A found in this study of the pH-dependent changes in Cu_A also corresponds to the previously investigated His120Ala mutant of Cu_AAz. When Solomon and coworkers characterized His120Ala Cu_AAz, they also investigated the low pH form of original Cu_AAz, and showed that, like His120Ala Cu_AAz, the low pH form of Cu_AAz is still valence delocalized, despite a 4-line pattern in its EPR spectrum.[140] In this study, the authors also considered what factors contribute to the ~2000-fold decrease of the electron transfer rate between Cu_A and heme *a* in *R. sphaeroides*. In a DFT calculated structure of the low pH form, a conformational change was found to affect the separation between two residues, where a through-space jump occurs in one of the two electron transfer pathways. This small increase in distance at this electron transfer juncture would result in a ~30-fold decrease in the electron transfer rate. When combined with the known changes to the reorganization energy and reduction potential, as well as the loss of one of the two electron transfer pathways, which occurs through the His corresponding to position 120 in Cu_AAz, Solomon and coworkers were able to

account for ~660-fold of the decrease in electron transfer observed in *R. sphaeroides* C*c*O. However, it is still unknown what factor(s) gives rise to the other ~3-fold decrease in the electron transfer.

Possibly the most significant contribution of the biosynthetic Cu_AAz model to the understanding of Cu_A centers came from measurement of its electron transfer rate.[139] Azurin natively contains a T1 copper center in the same location as the designed Cu_A center of the biosynthetic model. The experiment consisted of measuring the electron transfer rate from a radiolytically reduced disulfide to both the T1 copper and Cu_A centers in the azurin scaffold. The efficiency of the electron transfer by these two centers could be directly compared, as the pathway of electron transfer through the protein, solvent exposure, and other factors were essentially identical. From these studies, it was discovered that the Cu_A center transferred electrons more efficiently, despite a lower driving force. This greater electron transfer efficiency was attributed to the lower reorganization energy of the Cu_A center, which is calculated to be half that of the T1 copper center.

Finally, the biosynthetic Cu_AAz model has provided an excellent system for the study of Cu_A assembly,[143,158] as it is amenable to a wide range of spectroscopic probes and is stable over a broad range of concentrations (up to greater than 5 mM). This subject is the focal point of this thesis, and thus, will be discussed in much greater detail in later chapters.

1.3. A Cu_A Conundrum: Combination of Redox Active Ligands with Redox Active Metal Ions

Copper ions exist as cofactors in a large variety of enzymes across all domains of life, [163-165] playing key roles in important physiological functions, such as aerobic[5] and anaerobic[88,89,91] respiration, super oxide dismutation,[166] iron homeostasis,[167] synthesis of neurotransmitters,[168] and others. The ability of copper to cycle between the Cu(II) and Cu(I) oxidation states is essential to these functions. Whereas enzymes harness the power of this redox cycle, copper outside of a protected protein environment can perform Fenton and Haber-Weiss chemistry, generating hydroxyl radicals that are capable of damaging all types of biomacromolecules.[169] Accordingly, mechanisms to regulate free copper levels in the cell have evolved, and are so efficient that free copper in the cell is estimated to be at the attomolar level.[170-174] Thus, in order for copper enzymes to acquire their cofactor, mechanisms to specifically deliver copper to these proteins are also required. In the 1990s, one such mechanism was discovered in a new class of

proteins, called copper metallochaperones. [170-175] Since the discovery of this protein class, a number of its members have been characterized, including a putative chaperone to the Cu_A center of C*c*Os, called Sco.[176] Before discussing this putative chaperone, however, let us consider the challenges peculiar to Cu_A assembly.

1.3.1. Challenges of Cu_A Assembly

As synthetic chemists who have designed small molecule mimics of T1 copper or Cu_A centers are well aware (see 177 and references therein), Cu(II) catalyzes the formation of disulfide bonds from free thiols in a facile manner. This reaction has been known for several decades now, and has been studied in detail.[178-180] Due to this Cu(II) catalyzed oxidation of free thiols to disulfide, the requirement for Cu(II) in the resting state of Cu_A centers is potentially problematic for the correct assembly of these sites (Scheme 1.1), as a disulfide bond between the bridging Cys residues would destroy the most important components of the ligand set (see above). Thus, an assembly cofactor(s) to the Cu_A center must either avoid this potential reactivity, by loading the center with Cu(I) or a carefully controlled mixture of Cu(I) and Cu(II), or recover disulfide inactivated sites, by reducing the disulfide bond (Scheme 1.1). The physiologically relevant oxidation state of copper during formation of the Cu_A center is currently not known.

Scheme 1.1. Potential problems and unknowns in the metalation of Cu_A centers.

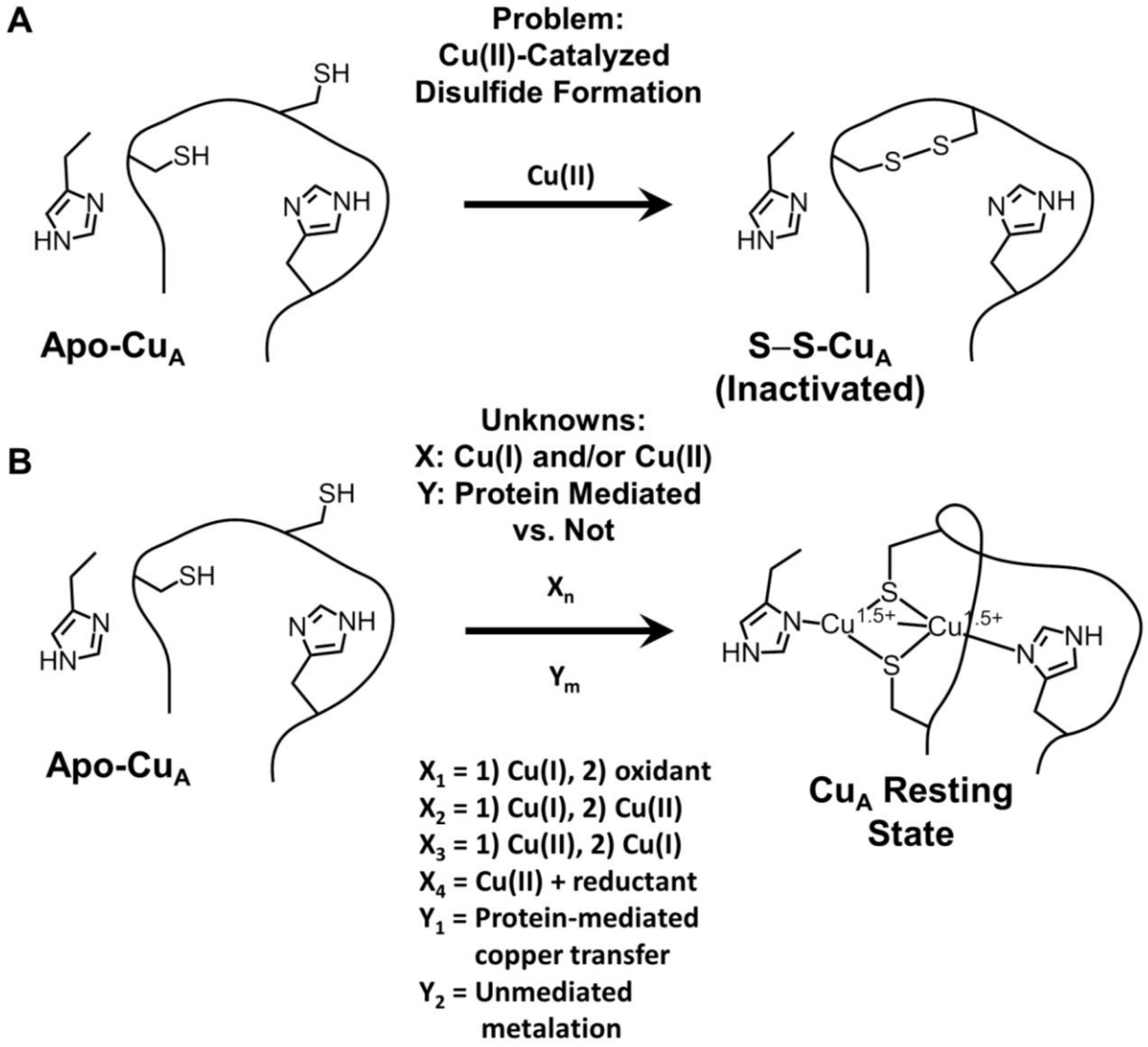

In Chapters 2 and 3 of this dissertation, *in vitro* investigations of the Cu(II)-driven assembly of the Cu_A center in the biosynthetic Cu_AAz are described.[158] It was discovered through these investigations that copper incorporation from addition of a sub-equivalent amount of Cu(II) to apo-Cu_AAz is a complex, multistep process. These studies culminated in a unified mechanism of copper incorporation into the Cu_A site of Cu_AAz. This mechanism may be relevant to N_2OR and prokaryotic C*c*Os, as the Cu_A centers of these enzymes are exposed either to the periplasm or extracellular space, where the +2 oxidation state of copper is stable.[56,181-183] Additionally, this mechanism provides a measure of the feasibility of unmediated assembly of Cu_A centers *in vivo*.

1.3.2. The Uncertain Function of Sco Proteins

As mentioned above, Sco proteins have been proposed to function as a copper chaperone to the Cu_A of C*c*O.[176] Sco was first recognized as a gene product indispensable for production of the subunit housing Cu_A in C*c*O from yeast.[184] Subsequently, it was discovered that Sco genes were associated with C*c*O maturation cassettes across many organisms, both prokaryotic and eukaryotic.[176] The idea that Sco functioned as a copper chaperone to Cu_A arose from a study in yeast that showed overexpression of Sco could rescue a respiratory deficiency caused by knockout of the upstream copper chaperone, Cox17.[185] Many of the following studies were designed and interpreted in terms of this hypothesis.[176] In support of this copper chaperone role for Sco, this protein binds copper tightly, through a CXXXCP motif and a distant His, which swings into proximity to bind copper.[186-190] NMR and X-ray crystal structures, however, revealed that Sco proteins adopt thioredoxin/peroxiredoxin folds, which suggested that this protein may have a redox regulatory role.[191-194] A number of roles have now been proposed for Sco proteins, and these proteins also occur in prokaryotes that do not contain a C*c*O.[176] Therefore, currently it is unknown whether Sco is a copper chaperone to the Cu_A center of C*c*O, as delivery of copper from Sco to the Cu_A center has not been demonstrated directly. Intriguingly, Sco binds both Cu(II) and Cu(I) stably, and the Cu(II) state has been shown to be essential for its function in *Bacillus subtilis*.[187,190,195,196] It is tempting, therefore, to envision delivery of both Cu(II) and Cu(I) ions from Sco to the Cu_A center, to form its mixed valence resting state.

Given the proposed copper chaperone role for Sco proteins to Cu_A in C*c*O, a gene for a Sco in an organism containing N_2OR was knocked out, to discover whether Cu_A assembly was dependent on its expression.[197] Cu_A was metalated despite this gene knock out. The authors of the study proposed that either a Sco paralogue was present in this organism, which rescued the function of the lost Sco protein, or Cu_A assembly in N_2OR was unmediated. The latter proposal was made on the basis of Cu_A formation proceeding spontaneously *in vitro* upon copper addition to the metal-free protein. However, the mechanism of Cu_A assembly in N_2OR, like that in C*c*O, is still unknown.

Progress toward a biosynthetic model in azurin of the Cu(II)-binding site in Sco proteins is described in Chapter 4 of this dissertation. A mutant of azurin is characterized, and shown to exhibit spectroscopic parameters very similar to those of a Sco mutant. This azurin mutant

represents the first step in design of a full structural mimic of Sco Cu(II)-binding sites. Such a mimic may provide important structural information about these Cu(II)-binding sites, that is presently unavailable. Moreover, a full structural mimic of Sco Cu(II)-binding sites would allow characterization of the properties of this center in a different protein fold, allowing deconvolution of the influence of the center and the fold on the function of Sco proteins.

CHAPTER 2: DETERMINATION OF A GENERAL *IN VITRO* ASSEMBLY MECHANISM FOR A CU_A IN AZURIN THROUGH UV-VIS KINETICS[†]

Abstract

Cu_A centers catalyze rapid electron transfer in crucial positions, at the end of electron transport chains, across all domains of life. The features of the Cu_A center which enable it to transfer electrons so efficiently also present challenges to its assembly, as it requires a mixture of Cu(II) and Cu(I) in its resting state and the empty site is capable of being deactivated, through formation of a disulfide. The *in vivo* mechanism of Cu_A assembly is currently poorly understood. In this study, the *in vitro* assembly of Cu_A from Cu(II) alone in a biosynthetic Cu_A model, Cu_AAz, was investigated. Monitoring the reaction that ensues from a sub-equivalent copper addition at pH 6 by stopped-flow and standard UV-Vis absorption spectroscopy reveals a new pathway to Cu_A formation, which proceeds through three mononuclear copper intermediates. Global analysis of these kinetic data allows formulation of a mechanism for Cu_A assembly under these conditions. First, a type 2 (T2) copper capture complex rapidly forms, which then reacts, either to form a Cu_A center directly or to form another intermediate, called I_X. I_X has unusual UV-Vis absorption features for copper centers in proteins, that were best accounted for by a copper-dithiolate complex. I_X then formed a type 1 (T1) copper intermediate, which gradually reacted to form the final Cu_A center. The observation of both T2 and T1 copper intermediates in the Cu_A ligand set of Cu_AAz confirm an evolutionary relationship proposed for these centers.

2.1. Introduction

Cupredoxins are a major class of redox and electron transfer (ET) copper proteins that play important roles in diverse biological functions, ranging from photosynthesis to respiration.[1,23,34,35,65,93-95] All of them share the same core protein scaffold, called a Greek key β barrel (Fig. 2.1A).[35,65] In addition, the copper binding sites of all cupredoxins reside in the same location in the protein and share many common amino acid residues in their primary coordination spheres (Fig. 2.1B). Cysteine thiolate(s), one of the coordinating residue side chains, imparts intense (ε~2,000-6,000 $M^{-1}cm^{-1}$) colors to these proteins. One of the types of

[†] The work presented in this chapter is published under the following citation, and is reproduced here with permission from ACS Publications: Wilson, T. D.; Savelieff, M. G.; Nilges, M. J.; Marshall, N. M.; Lu, Y. *J. Am. Chem. Soc.* **2011**, *133*, 20778.

copper sites is purple Cu_A, which is geometrically distinct from other copper sites, as it forms a rigid diamond core, with two directly-bonded coppers bridged by two cysteine (Cys) thiolates.[56,57,62,63,67,68,126] Each copper additionally interacts with an equatorial histidine (His) imidazolyl, as well as a weak axial methionine (Met) at one copper and backbone carbonyl oxygen at the other (Fig. 2.1B). In its oxidized resting state, the Cu_A site is mixed valent, with the free electron fully delocalized across the two coppers, giving [Cu(1.5)···Cu(1.5)].[67,70-75,109,198-200] In contrast, mononuclear type 1 (T1) blue copper centers possess a single, strong thiolate ligation from a cysteine, as well as two histidine imidazolyl ligands, completing a nearly trigonal coordination environment around the copper ion, with a fourth ligand (usually methionine) providing weak axial distortion (Fig. 2.1B).[23,201] The type 2 (T2) red copper site exhibits an approximately square pyramidal coordination environment, where the copper ion rests in a plane defined by the Cys thiolate, two imidazolyl nitrogens from His residues, and an exogenous water.[202] Oxygen coordination from the carboxylate of a glutamic acid (Glu) occupies the vertex of the square pyramid (Fig. 2.1B). While the makeup of the primary coordination sphere is similar among the T1 Cu, T2 Cu and Cu_A sites, their differing geometries give rise to different colors, unique spectral properties and varied functions.[34,66,201]

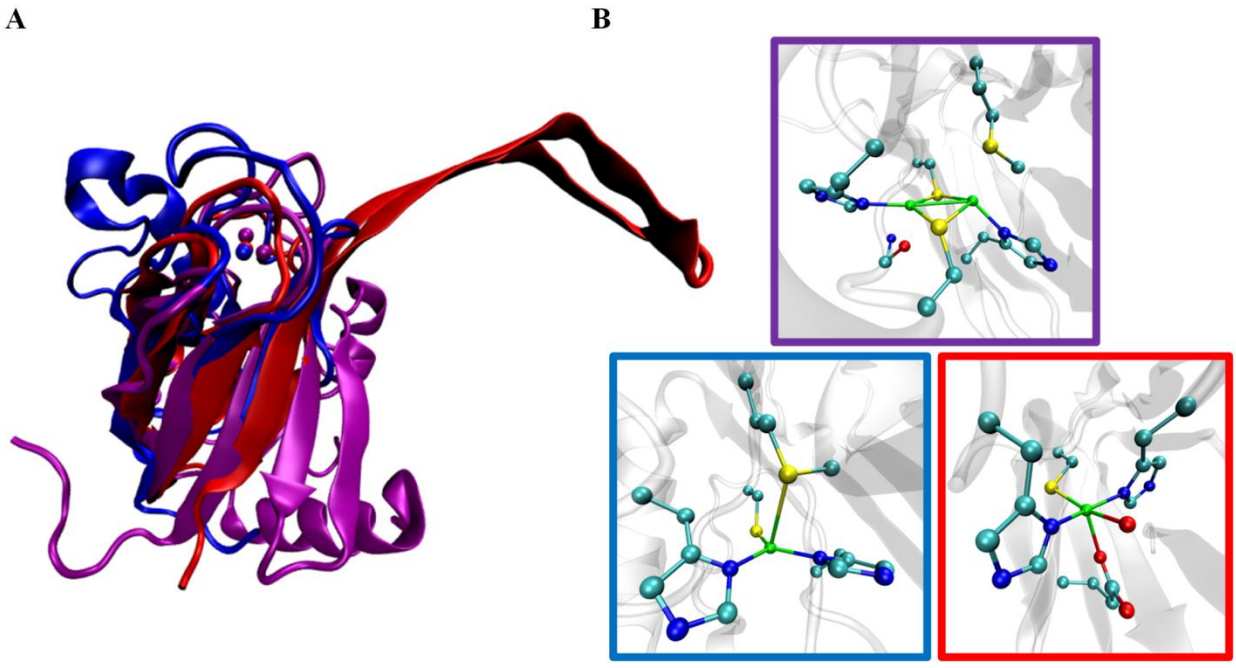

Fig. 2.1. (A) Overlay of the Greek-key β-barrel cupredoxin domains containing Cu_A (purple, *Paracoccus denitrificans* CcO, PDB ID code 3HB3), T1 blue Cu (blue, *Pseudomonas*

aeruginosa azurin, PDB ID code 1AZU), and T2 red Cu (red, *Nitrosomonas europaea* nitrosocyanin, PDB ID code 1IBY), where copper ions are shown as VDW spheres in the same colors as the corresponding protein backbone. (B) Zoom in of associated active-site structures, with Cu_A shown in a purple box, T1 copper in a blue box and T2 copper in a red box. The copper sites are shown in ball-and-stick representation, and colors are assigned as follows: cyan for C, blue for N, red for O, yellow for S, and green for Cu. Figures were rendered using VMD software, and structural overlay performed in the MultiSeq extension of the VMD software.[203,204]

While the dinuclear Cu_A site is different from the mononuclear T1 blue and T2 red Cu centers, phylogenetic analysis has suggested that all three metal ion centers are evolutionarily linked.[205,206,207] However, experimental evidence to support the link is lacking. Recently, we reported the observation of all three types of copper sites—purple Cu_A, T1 blue and T2 red Cu—in the native, Cu_A-containing nitrous oxide reductase (N_2OR), upon the addition of $CuSO_4$ to the apoprotein.[207] The T1 blue and T2 red Cu sites appeared as intermediates on the path to final Cu_A formation, and the process was found to be pH dependent, with more T2 red and T1 blue Cu site accumulation at higher pH. This study constituted the first experimental evidence for the previously proposed evolutionary link between these types of cupredoxins by showing that all three sites are inherently built into the Cu_A site. Despite this report, a question still remains as to whether what was observed in N_2OR is a general feature of other cupredoxins containing Cu_A, as N_2OR contains a tetranuclear Cu_Z center that could contribute to the kinetics of Cu_A formation.

Cu_A performs its electron transfer function with great efficiency, and yet it is utilized very selectively in nature, only at or near the termini of electron transport chains (see Chapter 1).[66,76-83] To date, Cu_A has only been found in cytochrome *c* oxidases (C*c*Os),[208] a nitric oxide reductase (NOR),[89,90] nitrous oxide reductases (N_2ORs)[183] and in a terminal oxidase from *Sulfolobus acidocaldarius* (SoxM),[92] where it serves as the initial electron acceptor. These enzymes in which Cu_A occurs are members of an important group, as aerobic and anaerobic respiration enable living organisms to convert nutrients into stored energy. The proper assembly of Cu_A is essential to the important functions of the enzymes in which it occurs, as their catalytic centers are defunct without a reliable source of electrons on demand.

Due to its ability to generate hydroxyl radicals and replace nearly all other metal cofactors, copper inside the cell is carefully regulated, such that the free copper concentration is extremely low (estimated in the attomolar range).[171,172,175] The regulatory machinery responsible for keeping copper levels so low includes copper importers, exporters, and chaperones.[171-175]

Copper chaperones are proteins whose sole responsibility is to bind, transport and deliver copper to specific proteins that require copper as a cofactor. Such a chaperone has been proposed for Cu_A centers in C*c*Os, which is called Sco.[176] Whole cell studies have established firmly an important role for Sco in assembly of C*c*O subunit II, in which Cu_A is housed.[176] Many of these studies link the role of Sco to copper as well. However, direct metalation of Cu_A by Sco has not been demonstrated. Moreover, the structures of Sco proteins, which fall into the classification of thioredoxin/peroxiredoxin folds, suggests a redox regulatory function for this protein.[191-194] Knock out studies of a Sco protein associated with the N_2OR biogenesis cassette also demonstrated that this protein was not essential for Cu_A metalation in N_2OR.[197] The authors of this study proposed that either a Sco paralog fulfilled the chaperone role, or that metalation of N_2OR proceeded in an unmediated fashion, as unmediated metalation of N_2OR was known to occur *in vitro*. However, the *in vivo* mechanism of Cu_A metalation is still unknown in all enzymes that house this center. Some intriguing questions regarding the Cu_A center is how this valence-delocalized, [Cu(1.5)…Cu(1.5] site can form upon the addition of Cu(II) alone, and what structural features contribute to each of the intermediates. A comprehensive understanding of the kinetics of Cu(II) incorporation into an apo-Cu_A protein, including elucidation of a detailed mechanism, is important not only for establishing a firm evolutionary link between these types of cupredoxins, but also may illuminate features of the *in vivo* metallation of Cu_A sites.

Part of the difficulty in studying the metalation mechanism of Cu_A centers arises from their biological locations. The enzymes that house Cu_A centers all contain other metallocofactors,[5,88,89,91] which complicate spectral studies, and C*c*Os, NOR, and SoxM are all membrane-bound, multi-subunit enzyme complexes.[5,89,91] Thus, small, soluble Cu_A-containing enzymes, which consist either of truncated native Cu_A domains[60,91,96-104] or designed biosynthetic models,[105-108] have the potential to provide a wealth of information about the metalation of native Cu_A enzymes.

In one study of Cu biosynthetic Cu_A model, Cu_AAz, the metalation of the Cu_A center was followed by stopped-flow UV-Vis spectroscopy upon mixing with $CuSO_4$.[143] An intense absorption at ~385 nm formed rapidly ($k_{obs} \sim 1 \times 10^3\ s^{-1}$), characteristic of a T2 copper center with thiolate ligation. The T2 copper intermediate then decayed, converting to the final Cu_A center, as demonstrated by the presence of an isosbestic point shared with the 485 nm transition of Cu_A. Interestingly, although only Cu(II) was added, the [Cu(1.5)···Cu(1.5)] resting state of

Cu_A was formed as the final product. It was proposed that the active site thiolates of Cu_A provided the reducing equivalents required, yielding Cu(I) and disulfide-bonded Cys residues as the products. Since a disulfide bond in the Cu_A site would render it unable to form the Cu_A center, lowering the total yield of Cu_A centers, the increased yield of Cu_A centers upon addition of exogenous reductant or Cu(I) with the $CuSO_4$ supported this hypothesis. From this study, a mechanism was formulated in which a T2 copper complex initially forms, followed either by reduction to Cu(I) by the active site cysteines and incorporation of Cu(II), or incorporation of Cu(I) generated elsewhere by reduction from active site cysteines, to form the final Cu_A center (Scheme 2.1).

Scheme 2.1. Picture of copper incorporation into the Cu_A center of Cu_AAz based upon a previous study, in which a ten-fold molar excess of $CuSO_4$ was added at pH 5.

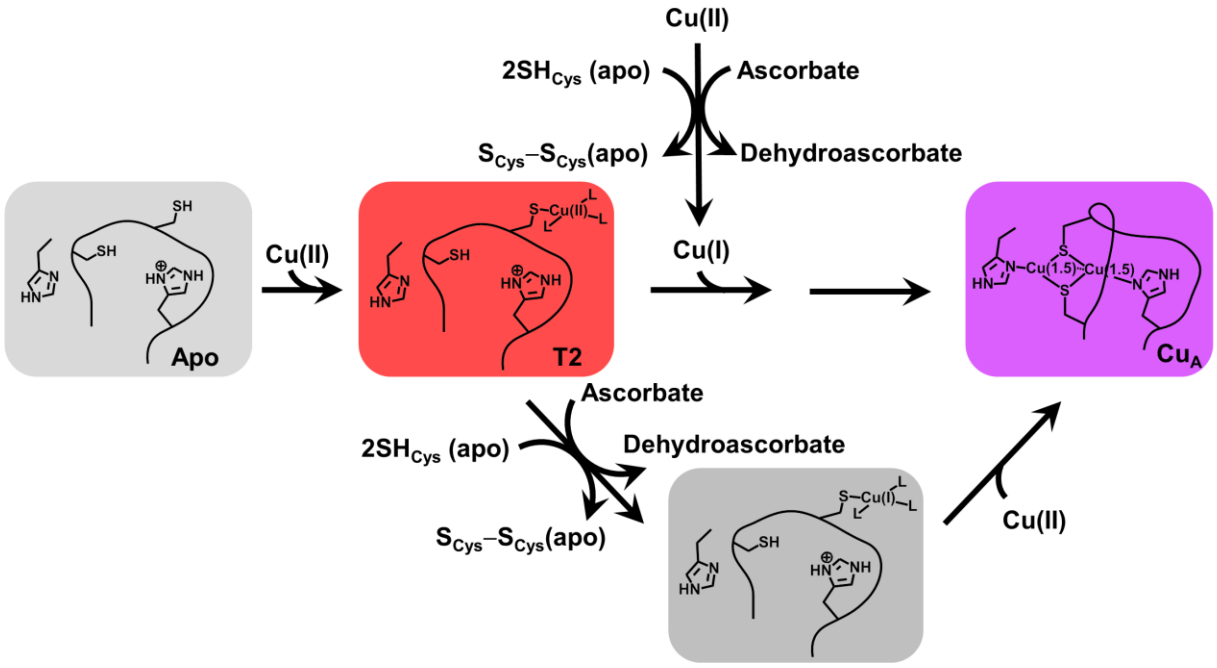

Given the observation of both T2 and T1 copper intermediates during the metalation of N_2OR,[207] the copper incorporation into Cu_AAz was revisited, to see if a T1 copper intermediate formed under conditions other than those explored previously. Detailed herein is a kinetics study of copper incorporation into Cu_AAz, upon mixing with a sub-equivalent addition of $CuSO_4$. A T1 copper intermediate was observed, in addition to the previously seen T2 copper intermediate, and

a new intermediate, which does not readily fall into a classification for known copper centers. Global analysis of the kinetics data permitted elucidation of a general mechanism for Cu(II) incorporation into the Cu_A center of Cu_AAz. These observations further strengthen the experimental evidence for an evolutionary link between these copper centers.

2.2. Materials and Methods

2.2.1. Materials and reagents

Bactotryptone and yeast extract were purchased from BD Biosciences. BL-21* (DE3) cells were purchased from Invitrogen. IPTG was purchased from Research Products International Corps or Gold Bio Technology Inc. All other reagents were purchased from Fisher, Sigma-Aldrich or Fluka. All water used was purified to 18.2 MΩcm by ultrafiltration with a Milli-Q Plus PF Ultra-Pure Water System. $CuSO_4$ solutions were prepared volumetrically in water that was incubated with Chelex prior to use. For pH dependent studies, a chelexed universal buffer (UB) containing 40 mM MES, MOPS, Tris, and CAPS, 50 mM NaOAc, and 100 mM $NaNO_3$ (to maintain relatively constant ionic strength) was utilized.

2.2.2. Protein expression, purification, and preparation for experiments

The engineered Cu_A azurin (Cu_AAz) was expressed and purified as previously reported.[107] Briefly, BL-21* (DE3) cells were transformed with pET-9a plasmid containing the DNA encoding Cu_AAz preceded by a periplasmic leader sequence from *Pseudomonas aeruginosa*. These cells were then grown in 2xYT media at 25 ºC and induced with IPTG at OD_{600} ~ 3. Cells were allowed to express protein periplasmically at 25°C for 4 hours. After harvesting the cells, lysis of the periplasmic membrane was achieved by osmotic shock. The supernatant after centrifugation was acidified to pH 4.1 with 500 mM sodium acetate, resulting in significant precipitation of contaminating biomolecules. After another round of centrifugation, the supernatant was applied to SP Sepharose cation exchange media, equilibrated with 50 mM ammonium acetate (NH_4OAc), pH 4.1. A step gradient was applied with 50 mM NH_4OAc, pH 6.35, as the elution buffer, resulting in elution of the desired protein over a broad range to near 100% purity, as determined by polyacrylamide gel electrophoresis. The nearly pure Cu_AAz was then applied to an additional Q-Sepharose HiTrap anion exchange column to remove a minor heme containing contaminant. At this stage, the pH of the protein solution was adjusted to within

the buffering range of NH_4OAc (typically pH 5.0-5.5), flash frozen, and stored at -80 °C until required for experiments. When needed for experiments, the appropriate amount of protein was thawed and exchanged into whichever buffer was to be employed for that experiment. Buffer exchanging was typically accomplished by application of the protein to a PD-10 desalting column (GE Healthcare), equilibrated with the buffer of interest. Alternatively, the protein was subjected to several cycles of concentration and dilution with the buffer of interest in a centrifugal filter unit with a 10 kDa molecular weight cutoff (Amicon Ultra from Millipore). The protein was then concentrated to the desired level for the experiment, and the concentration confirmed based on A_{280} using $\varepsilon_{280} = 8440\ cm^{-1}\,M^{-1}$.

2.2.3. Titrations of Cu_AAz with $CuSO_4$

For these experiments, electronic absorption spectra were collected on an Agilent Cary 5000 UV-Vis-NIR spectrophotometer with a mounted Peltier temperature-control unit. Titrations of apoCu_AAz with $CuSO_4$ to saturation (i.e. no further changes in the absorbance at 485 nm with further copper additions) were conducted in UB at 10 ºC. To 90 μL of ~ 0.25 mM protein in a 1 cm pathlength quartz cuvette, 3 μL additions of 1 mM $CuSO_4$ were made with mixing immediately after the addition by pipetting the mixture a few times. These additions were repeated until the absorptions due to Cu_A saturated. Once this point had been reached, the protein/copper mixture was covered to prevent evaporation and incubated at 10 ºC overnight, while monitoring the electronic absorption spectrum every 20 min. Actual protein concentrations were verified by the absorbance at 280 nm.

In a titration experiment designed to eliminate spectral differences due to kinetic processes (Fig. 2.4), increasing amounts of $CuSO_4$ were added to separate aliquots of protein, and the UV-Vis spectrum collected at 5 min and 18 hrs after $CuSO_4$ addition. To 10 separate microtubes, 90 μL of ~0.2 mM apoCu_AAz in UB was added. Incremented equivalents of $CuSO_4$ were added to these microtubes, from ~0.10 equivalents up to 1.0 equivalent, using a 2 mM $CuSO_4$ stock, so that 1 μL corresponded to ~0.1 equivalent. The difference between the cumulative volume of apoCu_AAz and $CuSO_4$ and 100 μL was made up with buffer, in order to avoid dilution effects. Immediately after making the $CuSO_4$ addition, the mixture was vortexed and a spectrum collected (i.e. the 5 min spectrum). These samples were then incubated overnight

in a 10 ºC water bath and a spectrum collected the following day (i.e. the 18 hr spectrum). Actual protein concentrations were verified by the absorbance at 280 nm.

2.2.4. Stopped-flow UV-Vis absorbance

Experiments were performed on an Applied Photophysics Ltd (Leatherhead, UK) SX18.MV stopped-flow spectrometer equipped with a 256 element photodiode array detector. Two-syringe mixing was employed to mix equal volumes of wt Cu_AAz with volumetrically prepared $CuSO_4$ solutions. All reported data sets originally consisted of 200 spectra collected over 50 s or 1000 s using logarithmic sampling. The integration period and minimum sampling period were both 1 ms. A water bath, connected to the syringe compartment and set to 15 ºC, provided temperature control. The actual temperature in the syringe compartment was measured to be between 16.3 and 16.5 ºC.

2.2.5. Sub-saturating $CuSO_4$ additions to Cu_AAz

Sub-saturating $CuSO_4$ additions were made to Cu_AAz and the resulting UV-Vis absorbance spectra monitored on an Agilent 8453 photodiode array spectrometer having a connected water bath for temperature control and water-propelled magnetic stirring. After blanking the instrument with a 1:1 mixture of UB:water in a 1cm x 1cm standard UV-Vis cuvette, 850 µL of 0.5 mM apoCu_AAz was added to the cuvette. The instrument was then set to collect a series of spectra over 900 s with 0.5 s scan time incremented by 5% after 45 s. After starting the data collection, and with constant magnetic stirring and temperature control set to 10 °C, an 850 µL aliquot of 0.2 mM $CuSO_4$ was quickly added to the stirring protein solution. The top of the cuvette was parafilmed once data collection was underway to reduce evaporation. Spectra were thenvcollected for an additional 14 hours, with 600 s scan time incremented by 1% after 3600 s.

2.2.6. Global analysis of stopped-flow UV-Vis absorbance kinetics data

As the kinetics obtained from stopped-flow and standard UV-Vis were generally complex, with multistep reactions and overlapping absorption bands, kinetic analyses were performed using a global analysis software called SpecFit/32 (Spectrum Software Associates, Inc), which employs singular value decomposition (SVD) and nonlinear regression modeling to

find kinetic parameters for the data. Briefly, models were determined through an iterative approach, where the starting point was the simplest conceivable set of reactions that could possibly explain the sequence of events observed in the spectra, while being consistent with other sources of data, and complexity was added as needed to improve the fit and consistency of the models. Fixed or known spectra were required in some cases for the fits to converge Table 2.1, Fig. 2.2). The quality of these fits was judged based on the size of the standard deviations for the observed rate constants (Table 2.1 and Table 2.2), the reasonableness of the resolved species spectra found by the software (Fig. 2.8), the size and trends of the residual spectra (Fig. 2.9), and the statistical measures calculated by the software for each fit (Table 2.1).

Table 2.1. Details of kinetics fits for Cu_AAz with a 0.4 equivalent addition of $CuSO_4$ at pH 6 over three timescales.

pH 6, 0.32 s	**Step in Model**	**k_{obs}**	**Species**	**Initial Conc. (μM)**	**Colored ?**	**Fixed ?**
	$CuSO_4 \rightarrow T2$	$40.6 \pm 2.9\ s^{-1}$	$CuSO_4$	100	No	No
			T2	0	Yes	No
	Convergence Statistics					
	Convergence Value	**Iterations Performed**	**Marquardt Parameter**	**Total Sum of Squares**	**Std. Deviation of Fit**	
	0.0	3	0.0	9.884×10^{-2}	3.980×10^{-3}	
pH 6, 370 s	**Step in Model**	**k_{obs}**	**Species**	**Initial Conc. (μM)**	**Colored ?**	**Fixed ?**
	$2\ T2 \rightarrow Cu_A$	$(3.39 \pm 0.11) \times 10^3\ M^{-1}s^{-1}$	T2	90	Yes	Yes
	$T2 \rightarrow I_X$	$0.241 \pm 0.007\ s^{-1}$	I_X	0	Yes	No
	$2\ I_X \rightarrow Cu(I)$	$25.6 \pm 1.0\ M^{-1}s^{-1}$	T1	0	Yes	Yes
	$I_X \rightarrow T1$	$(3.25 \pm 0.10) \times 10^{-3}\ s^{-1}$	Cu(I)	0	No	No
			Cu_A	0	Yes	Yes
	Convergence Statistics					
	Convergence Value	**Iterations Performed**	**Marquardt Parameter**	**Total Sum of Squares**	**Std. Deviation of Fit**	
	2.441×10^{-6}	3	0.0	0.7955	4.988×10^{-3}	
pH 6, 15 hr	**Step in Model**	**k_{obs}**	**Species**	**Initial Conc. (μM)**	**Colored ?**	**Fixed ?**
	$T1 + Cu(I) \rightarrow Cu_A$	$6.99 \pm 0.36\ M^{-1}s^{-1}$	T1	36	Yes	Yes
			Cu(I)	20	No	No
			Cu_A	22	Yes	Yes
	Convergence Statistics					
	Convergence Value	**Iterations Performed**	**Marquardt Parameter**	**Total Sum of Squares**	**Std. Deviation of Fit**	
	7.983×10^{-11}	3	0.0	0.3681	3.017×10^{-3}	

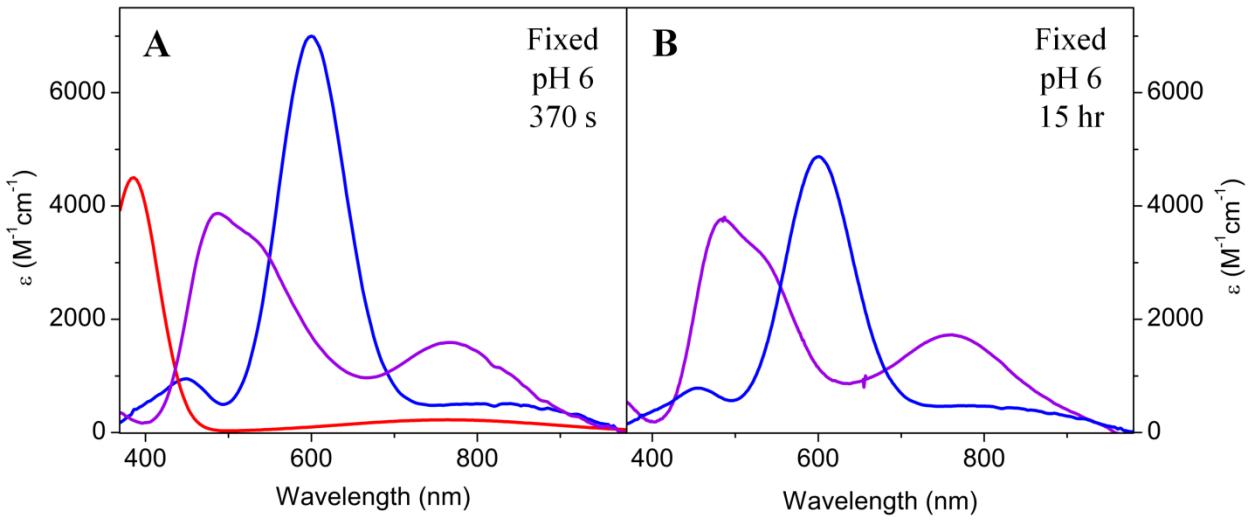

Fig. 2.2. Fixed T2 Cu (red), T1 Cu (blue) and Cu_A (purple) spectra used in the fitting of the kinetics for Cu_AAz with 0.4 equivalents $CuSO_4$ at pH 6 up to (A) 370 s and (B) 15 hr after $CuSO_4$ addition.

2.3. Results

2.3.1. Addition of $CuSO_4$ to apoCu_AAz under copper saturating or sub-saturating conditions

To probe the formation of intermediates during copper incorporation into the Cu_A site, Cu_AAz at pH 5, 6, and 7 was titrated in small increments with $CuSO_4$ in the same aliquot of the protein until no further absorbance increases were observed in the Cu_A absorption bands at 480, 530, and 760-800 nm, and the resulting spectra under these copper-saturating conditions were monitored over time (Fig. 2.3). At pH 5, only the absorptions due to Cu_A were observed. As the pH was raised from pH 5, new absorption bands at ~ 400 and 600 nm, assignable tentatively to T2 red Cu and T1 blue Cu species, respectively, were observed, with greater accumulation of these intermediates at lower equivalents of $CuSO_4$ and higher pH. These results are similar to those of native N_2OR,[207] except that isosbestic points between the T1 blue Cu species and Cu_A are not obvious. Therefore, other conditions were investigated, where the T1 blue Cu species might participate in final Cu_A site formation, including lower equivalents of $CuSO_4$. In order to eliminate spectral differences due to kinetic processes, titrations of Cu_AAz with $CuSO_4$ were repeated, where increasing equivalents of copper were added to separate aliquots of the protein and spectra were collected at the same interval after copper addition (Fig. 2.4). With Cu_A formation monitored at the major S → Cu charge transfer band (~480 nm), the process was

complete by ~0.5 molar equivalents of $CuSO_4$ at all pH values. This result was consistent with the hypothesis that, in the absence of external reductants, at least half of the proteins, assuming 100% efficiency, must serve as sacrificial reductants through formation of disulfide bonds between the two active site Cys residues, leaving only a fraction of the protein available for Cu_A formation. We further confirmed this hypothesis by repeating the same experiment as in Fig. 2.4 using an equimolar mixture of Cu(I) and Cu(II) (Fig. 2.5). Titration with the Cu(I):Cu(II) mixture resulted in greater Cu_A reconstitution at higher copper equivalents, based upon the absorbance at 480 nm, supporting that the active site thiols supply reducing equivalents when Cu(II) is added. Therefore, to avoid excess copper ions that could complicate the kinetics, we chose to add sub-saturating 0.4 equivalent amounts of $CuSO_4$ to apo-Cu_AAz in the subsequent experiments.

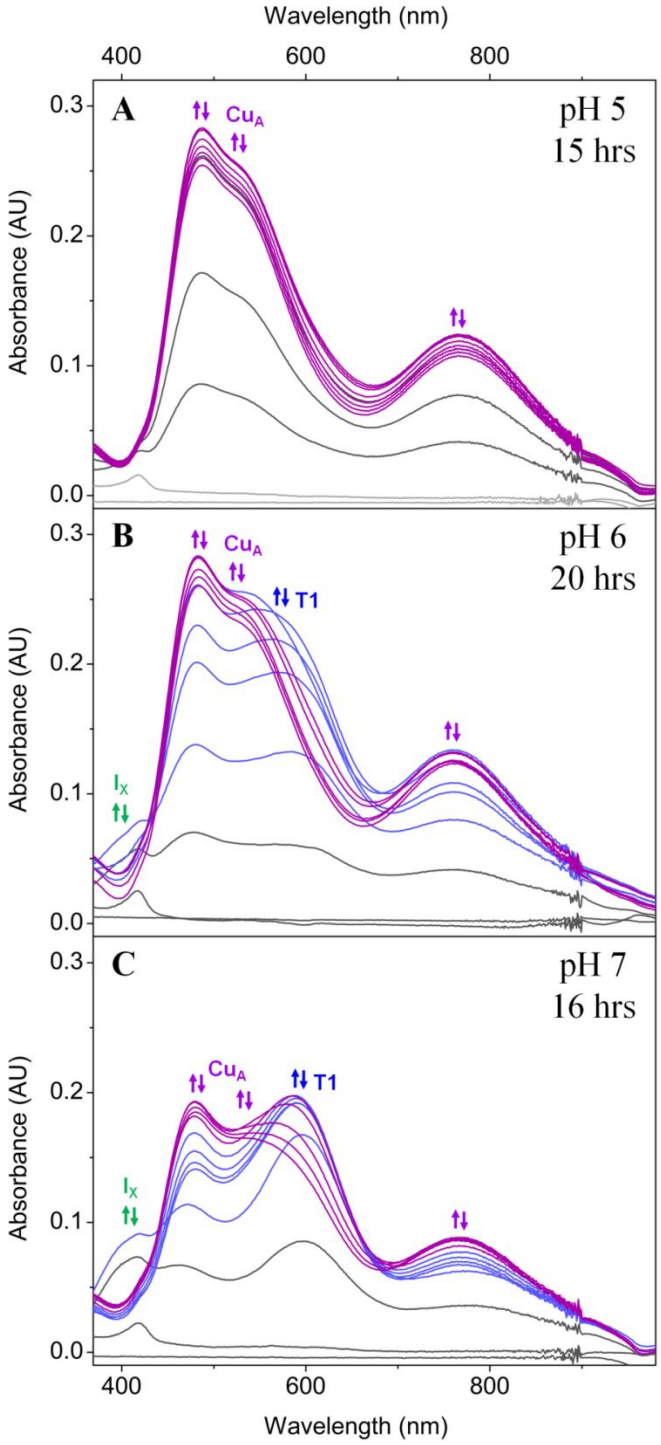

Fig. 2.3. Electronic absorption spectra of titrations to saturation (no further change in Abs(485nm) with further copper additions) of apoCu$_A$Az with $CuSO_4$ and subsequent overnight monitoring at (A) pH 5, (B) pH 6, and (C) pH 7. Early spectra are grey, while later spectra are colored according to the progression of species present in the mixture (grey to purple at pH 5, grey to blue to purple at pH 6 and 7). In all three data sets, the final spectrum is colored purple and is pure, or nearly pure, Cu$_A$. At pH 6 and 7, some I$_X$ and T1 Cu formation are observed.

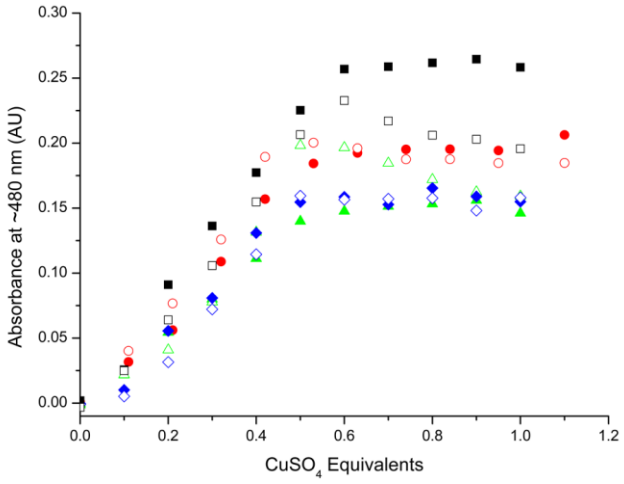

Fig. 2.4. Cu_AAz absorbance at the maximum around 475 nm as a function of $CuSO_4$ equivalents added. Filled shapes correspond to the UV-Vis measurements taken after 5 minutes of incubation, and open shapes to those taken after overnight incubation. Color/shape legend: black squares – pH 5, red circles – pH 6, green triangles – pH 7, and blue diamonds – pH 8.

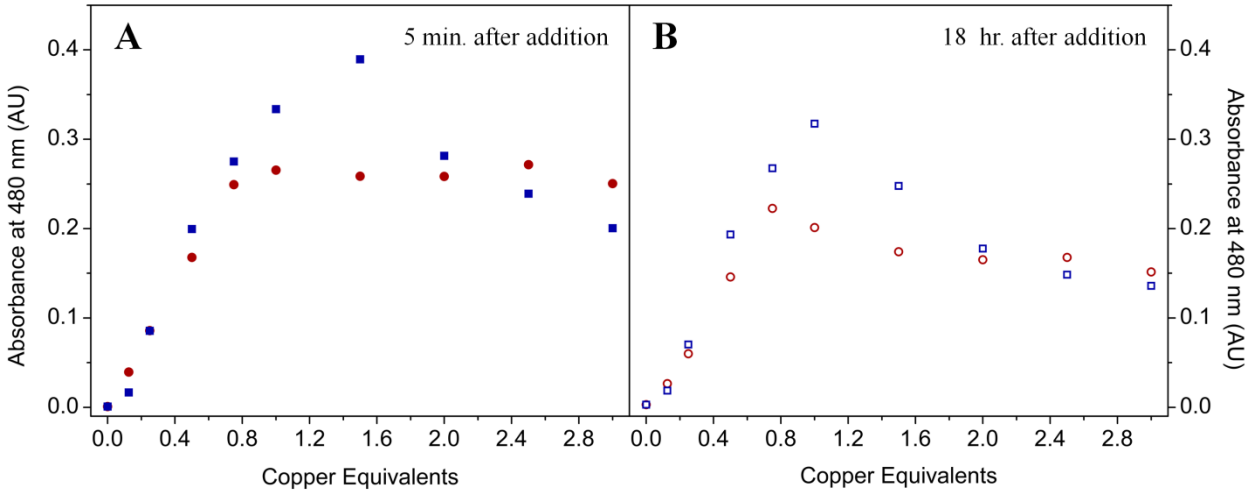

Fig. 2.5. Cu_AAz absorbance at 480 nm as a function of copper equivalents added, using $CuSO_4$ only (red circles) or an equimolar mixture of Cu(I):Cu(II) (blue squares) at (A) 5 minutes and (B) 18 hours after copper addition. Protein concentration was 0.16 mM in UB pH 5.

2.3.2. Kinetic data for copper incorporation into apo-Cu_AAz under sub-saturating copper conditions

Addition and rapid mixing of a sub-saturating 0.4 equivalents of $CuSO_4$ with 0.25 mM apo-Cu_AAz at pH 6 in the stopped-flow apparatus resulted in the ultraviolet-visible absorbance (UV-Vis) spectra in Fig. 2.6A over the following 0.33 s and the spectra in Fig. 2.6B over the next 360s. First, a spectrum with an intense absorbance maximum at ~385 nm, typical of a T2 red Cu center, appeared within 0.3 s (Fig. 2.6A). A spectrum very similar to this one was observed previously as an intermediate during formation of Cu_A at pH 5 with higher equivalents copper.[143] This initial $CuSO_4$ to T2 Cu step was too rapid to be captured in the same dataset as some of the slower processes (i.e. in the 370 s set of spectra), so this process is displayed separately, using a portion of a dataset collected over 50 s (Fig. 2.6A). In the present study, this ~385 nm peak subsequently decayed and shifted to ~410 nm, with absorption bands at 475, 625 and 760 nm growing in intensity over the same time period (Fig. 2.6B). This process completed in ~ 9.4 s after addition of copper, and the spectrum observed at its conclusion is associated with a new intermediate, called intermediate X (I_X) here, which is characterized by intense absorption maxima at ~ 410 and 760 nm. Over the next 370 s, the absorptions due to I_X decreased, while the shoulder at ~625 nm grew into a clearly defined peak at ~600 nm, suggesting accumulation of a T1 blue Cu intermediate. At longer time scales, the spectrum of T1 blue Cu decayed, while a spectrum with absorption maxima at ~480, 530 and 760 nm emerged (Fig. 2.6B inset); such a spectrum is typical of the Cu_A center in Cu_AAz.[107,142] This final process was accompanied by isosbestic points at 550 and 700 nm, strongly suggesting conversion of the T1 blue Cu center to Cu_A (see inset of Fig. 2.6B). The slower process in the inset of Fig. 2.6B was captured by standard UV-Vis spectroscopy, as the rapid kinetics obtained through stopped-flow were unnecessary to see this step.

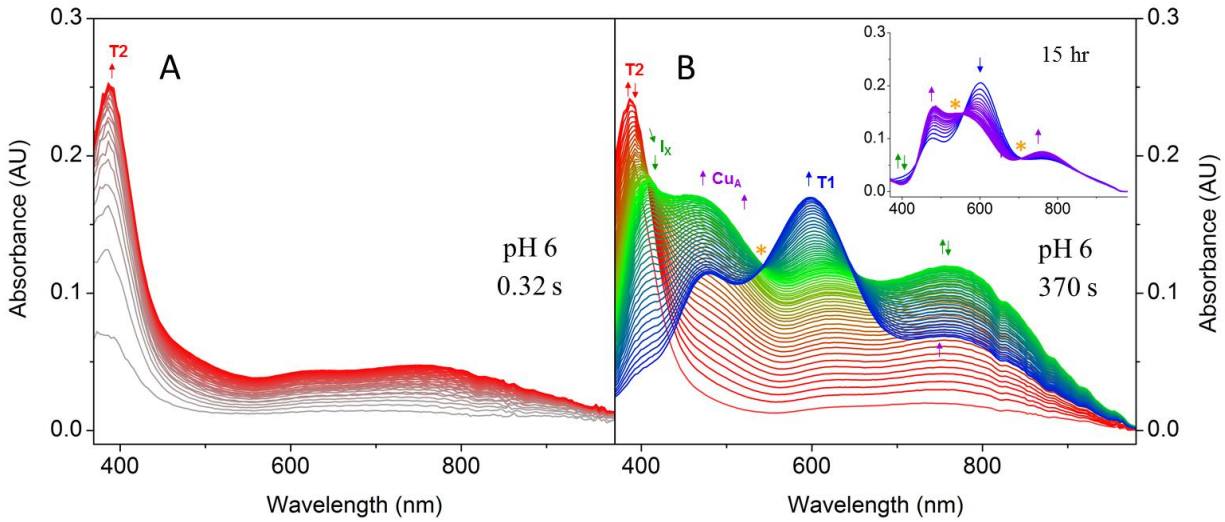

Fig. 2.6. Stopped-flow UV-vis absorbance spectra after mixing of a sub-saturating 0.4 equivalents of $CuSO_4$ with Cu_AAz at pH 6 over (A) 0.32 s, (B) 370s and (inset) 15 hours. Spectra are colored to indicate the species forming at that particular time. Arrows indicate direction of change in absorbance over course of experiment and are colored to correspond to the species giving rise to that peak. Golden asterisks indicate the positions of apparent isosbestic points. The final Cu_AAz concentration was 0.25 mM and $CuSO_4$ concentration was 0.1 mM. Stopped-flow spectra were collected with a logarithmic scale over (A) 50 s and (B) 1000 s and 200 total spectra. The first spectrum was collected at (A) 0.007 s and (B) 0.134 s. For the overnight UV-Vis data collection, spectra were collected initially with a 0.5 s scantime, which was incremented by 5% after 45 s over 900 s, to make sure that the initial portion of the data matched that collected on the stopped-flow instrument (data not shown). The spectra shown in the inset were collected with a 600 s scantime, which was incremented by 1% after 3600 s over 50400 s (14 hours).

2.3.3. Global analysis of the kinetic data for copper incorporation into Cu_AAz

As detailed in the Materials and Method section 2.2.6, the kinetic processes observed by stopped-flow and standard UV-Vis spectroscopies, displayed in Fig. 2.6, are quite complex, with a number of overlapping species and simultaneous processes. Therefore, these spectra were submitted to a global analysis software, called SpecFit/32 (Spectrum Software Associates, Inc). Using the protocol outlined in section 2.2.6, the model presented in Table 2.2 converged well. The observed rate constants found through global analysis using this model are provided in Table 2.2. The concentration profiles obtained for these kinetic data based on global analysis are shown in Fig. 2.7, and the molar absorptivity spectra of the pure species determined by the global analysis software are shown in Fig. 2.8. This model provided a high quality fit, as indicated by

the low standard deviations in the observed rate constants and the convergence statistics for the fits (Table 2.1), as well as the low intensity of the residual spectra shown in Fig. 2.9.

Table 2.2. Steps of the model that yielded a high quality fit for the data in Fig. 2.6 and corresponding observed rate constants found by global analysis.

Step in Model	Observed Rate Constant for Step
$CuSO_4 \rightarrow T2$	$40.6 \pm 2.9\ s^{-1}$
$2\ T2 \rightarrow Cu_A$	$(3.39 \pm 0.11)\times10^{3}\ M^{-1}s^{-1}$
$T2 \rightarrow I_X$	$0.241 \pm 0.007\ s^{-1}$
$2\ I_X \rightarrow Cu(I)$	$25.6 \pm 1.0\ M^{-1}s^{-1}$
$I_X \rightarrow T1$	$(3.25 \pm 0.10)\times10^{-3}\ s^{-1}$
$T1 + Cu(I) \rightarrow Cu_A$	$6.99 \pm 0.36\ M^{-1}s^{-1}$

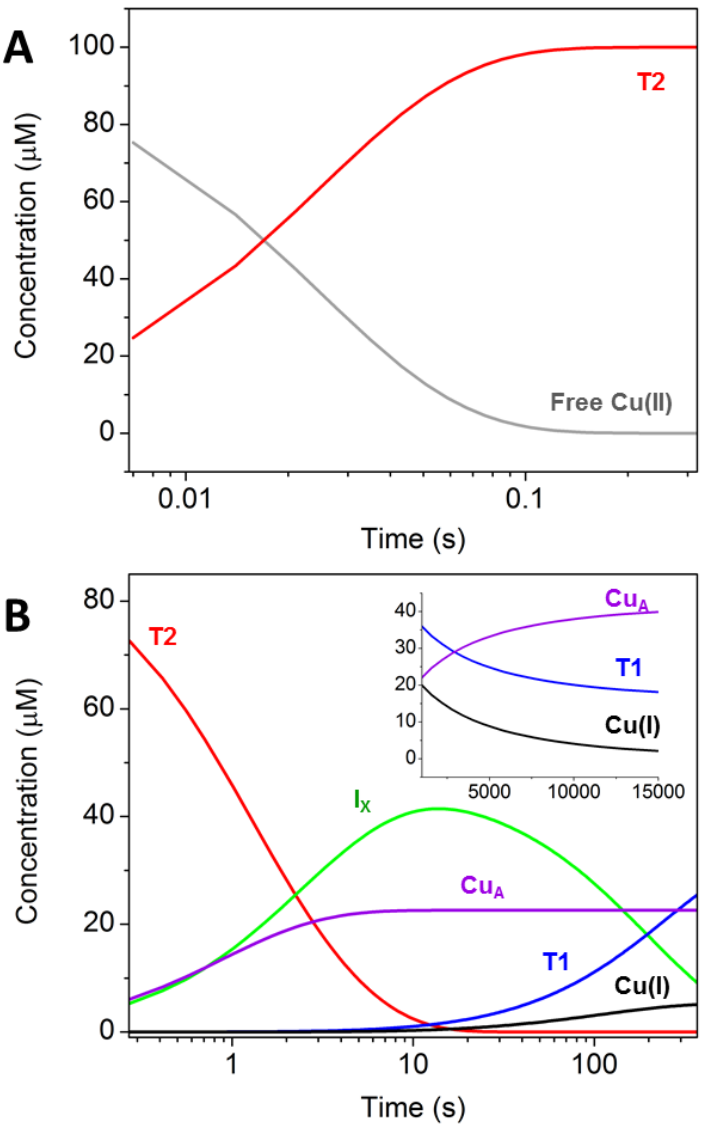

Fig. 2.7. Concentration profiles found by global analysis of the kinetics data in Fig. 2.6 over (A) 0.32 s, (B) 370 s and (inset) 15 hours. Concentration profiles are colored according to the species to which they correspond.

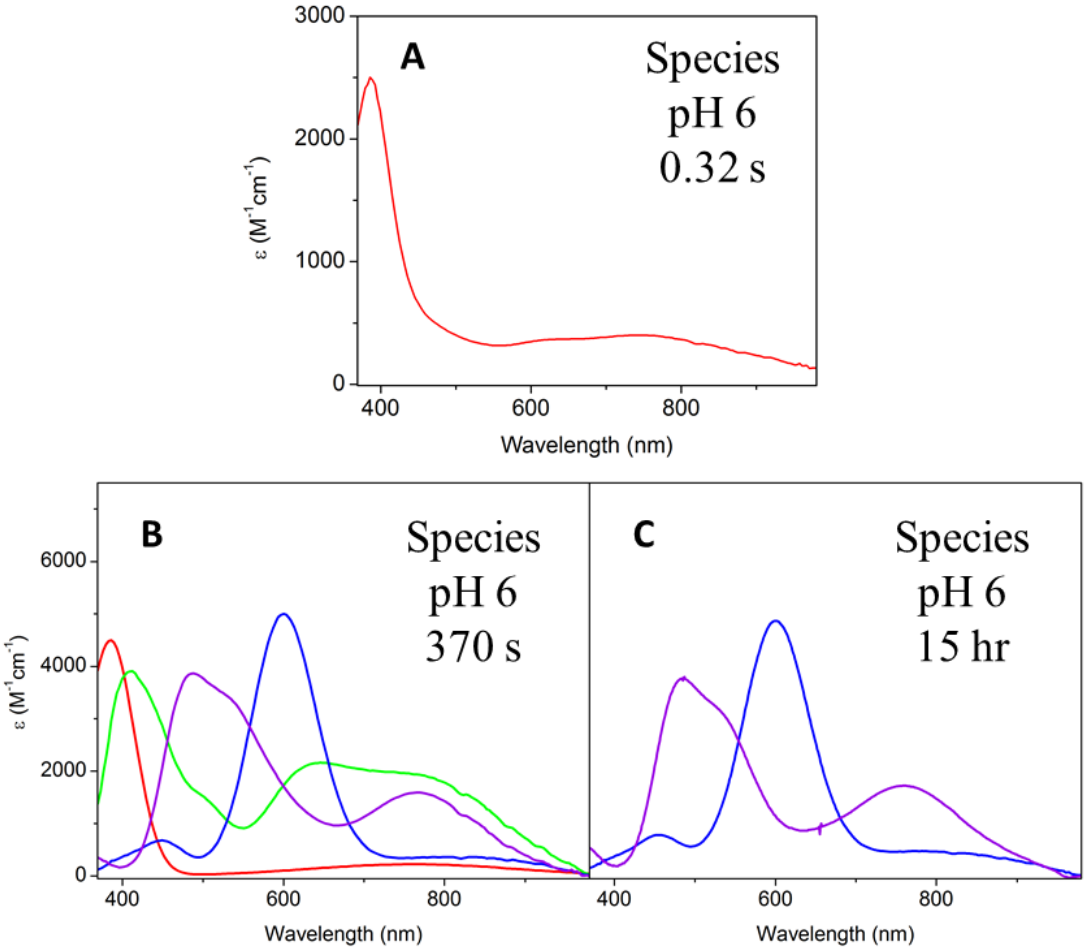

Fig. 2.8. Resolved species spectra for T2 Cu (red), I_X (green), T1 Cu (blue), and Cu_A (purple) calculated through the fitting of the kinetics for Cu_AAz with 0.4 equivalents $CuSO_4$ at pH 6 up to (A) 0.33 s, (B) 370 s and (C) 15 hrs after $CuSO_4$ addition.

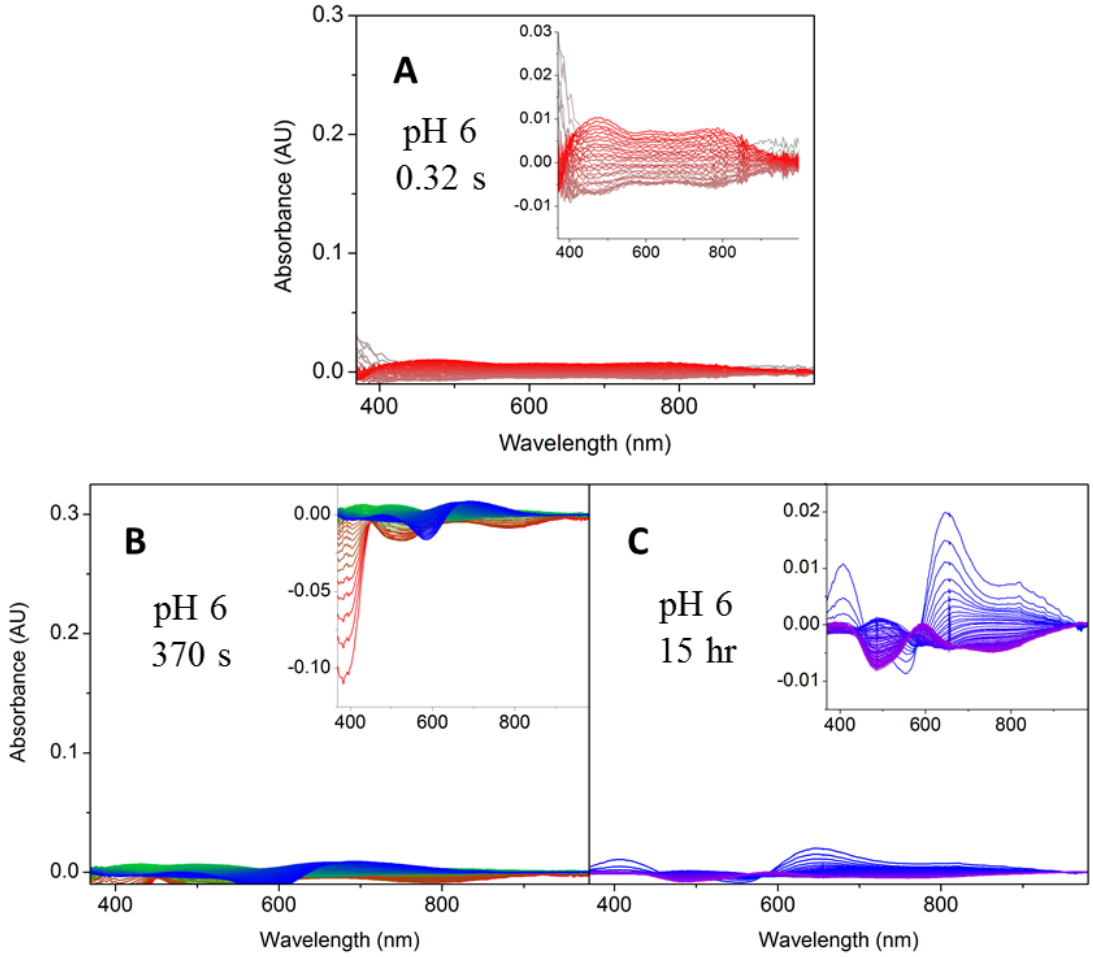

Fig. 2.9. Residual spectra from fitting process of the kinetics for Cu_AAz with 0.4 equivalents $CuSO_4$ at pH 6 up to (A) 0.32 s, (B) 370 s and (C) 15 hrs after $CuSO_4$ addition, plotted on the same scale as the original spectra for comparison. Inset: zoom in of residual spectra. Residual spectra are colored to correspond to spectra in original data.

2.4. Discussion

2.4.1. *Overall kinetics of copper incorporation into Cu_AAz: similarities to Cu_A in native N_2OR*

The Cu_AAz construct was designed as a biomimetic model of native Cu_A sites,[107] and several spectroscopic, X-ray crystallographic and electron transfer studies have established that Cu_AAz is a close structural and functional model of these Cu_A centers.[59,72,126,132,140,142,148,149] In a previous study of the native Cu_A center in N_2OR,[207] we discovered that formation of the purple Cu_A center went through T2 red and T1 blue Cu intermediates, characterized by peaks at ~385 nm and 640 nm, respectively. From Fig. 2.6 in this study, peaks at ~390 and 600 nm were

observed to appear after addition of copper to apo-Cu_AAz before the final spectrum of purple Cu_A formed. Given the intensity of these absorption bands and their positions, the ~390 nm peak can be assigned as a T2 copper site with thiolate coordination (i.e. a red copper site, by analogy to the native T2 copper protein), while the ~600 nm peak falls into the classification of T1 blue Cu sites.[35,65] Although the λ_{max} of this T1 blue Cu intermediate differs by ~40 nm from that in N_2OR, this degree of variation is found among native T1 blue Cu proteins, and, despite this variation, the primary coordination spheres of all of these T1 blue copper sites are remarkably similar.[23,209] Thus, the difference in λ_{max} of the T1 blue Cu intermediates between N_2OR and Cu_AAz is not surprising, and these values are still indicative of similar sites between the two proteins. Therefore, the engineered Cu_AAz is an excellent model of native Cu_A centers, as it not only displays almost identical structural and functional properties, but its kinetic copper incorporation also resembles that of the native Cu_A site of N_2OR. More importantly, the faster kinetics of copper incorporation into Cu_AAz relative to N_2OR allowed us to utilize lower copper equivalents, which mimics more closely the limited availability of copper ions in the cellular environment. These copper limiting conditions unveiled a pathway to copper incorporation involving a new intermediate (I_x).

2.4.2. Kinetics of copper incorporation in Cu_AAz under copper saturating vs. sub-saturating conditions: differences from Cu_A in N_2OR

In the titrations of Cu_AAz with a saturating amount of $CuSO_4$ at pH 5, 6, and 7,while the T2 red and T1 blue Cu intermediates were observed similarly to those in N_2OR,[207] the T1 blue Cu intermediate decayed without an obvious isosbestic point to indicate conversion to the Cu_A site formed in the end (Fig. 2.3). In contrast, when N_2OR was titrated with a similar saturating amount of $CuSO_4$, clear isosbestic points were observed between the T1 blue Cu intermediate and Cu_A.[207] However, when a sub-saturating amount of $CuSO_4$ was added to apo-Cu_AAz under otherwise identical conditions, isosbestic conversion of the T1 blue Cu species to Cu_A was unmistakable (Fig. 2.6). We attribute the differences between these proteins to the fact that N_2OR is a much larger protein with a total of ten cysteines residues, many of which are in close proximity to each other (PDB ID 1FWX),[61] and could serve as sacrificial reductants. In contrast, each molecule of Cu_AAz contains only four cysteine residues, two of which natively form a disulfide and the other two being Cys ligands in the Cu_A site (PDB ID 1CC3).[59] Since reducing

equivalents are required to form the mixed valent [Cu(1.5)…Cu(1.5)] Cu_A center from $CuSO_4$, the Cys thiols in these proteins likely serve as sacrificial reductants, as proposed in previous reports on the reconstitution of both Cu_AAz[143] and N_2OR.[207] The use of Cu(I) and Cu(II) in a titration of Cu_AAz here (Fig. 2.5) supports this use of the Cu_A center's Cys thiols as the source of reducing equivalents, as using Cu(I):Cu(II) increased the yield of Cu_A centers. Due to the excess of free Cys residues in N_2OR capable of forming disulfide bonds, the reducing capacity per molecule of N_2OR is much greater than that per molecule of Cu_AAz. Accordingly, if the Cu_A sites were saturated with Cu(II), N_2OR could still provide reducing equivalents at a ratio of copper to protein equal or greater than one, resulting in the formation of more Cu_A sites in N_2OR. In the case where the Cu_A site of Cu_AAz is saturated with Cu(II), all of the thiols are used up to form Cu_A, the various intermediates, or have already formed disulfide and Cu(I), and therefore are not available to provide further reducing equivalents. However, under sub-saturating $CuSO_4$ conditions, not all of the thiols in the Cu_A site of Cu_AAz are occupied or disulfide-bonded, so these additional sites are able to provide reducing equivalents, permitting conversion of the T1 blue Cu species to Cu_A. Another influence of sub-saturating $CuSO_4$ conditions that could lead to additional formation of Cu_A is that the excess apo-Cu_AAz likely stabilizes the Cu(I) produced *in situ*—which is unstable in aqueous solution in the absence of coordinating small molecules or proteins—by binding to the Cys residues in the Cu_A site.

2.4.3. Assignment of the intermediates formed in Cu_AAz under sub-equvalent copper conditions

The intermediates that form during copper incorporation into apo-Cu_AAz at pH 6 (Fig. 2.6) can be assigned to general types of copper centers, based upon the intense S $\rightarrow$ Cu charge transfer bands observed in the UV-Vis absorption spectra, as the energy and intensity of these bands are indicative of certain site geometries.[35,65,201] The intense ~385 nm band of the first intermediate (Fig. 2.6A) is characteristic of the S $\rightarrow$ Cu charge transfer bands displayed by T2 copper centers with thiolate ligations. T2 copper centers typically have tetragonal geometries, such as square planar, square pyramidal, and octahedral. Therefore, we can assign this first intermediate as a T2 copper complex with one of the two Cys residues in the Cu_A center.

Conversely, the intense ~600 nm band formed by the end of 370 s (Fig. 2.6B) is characteristic of a T1 copper center.[35,65,201] The primary coordination spheres of T1 copper centers always include a HisCysHis trigonal ligand set. Thus, we can assign this intermediate as

a T1 copper complex with coordination from one of the Cys residues in the Cu_A center, and likely from both of the His residues in the Cu_A center as well.

The third intermediate, I_X, presents more of a challenge, as far as assigning it to a particular type of copper center, as it is constantly present in a mixture of species, and its UV-Vis absorptions overlap to a large extent with those of other species (Fig. 2.6B). The molar absorptivity spectrum determined by the global analysis procedure gives an indication of the pure spectrum of I_X. In searching similar spectra to that of I_X from known Cu(II)-thiolate complexes, we found only one example, i.e., that of copper-substituted horse liver alcohol dehydrogenase (HLADH).[210] The electronic absorption spectra of copper-substituted HLADH in complex with exogenous ligands, including pyrazole and a coenzyme, modified nicotinamide adenine dinucleotide (H_2NADH), show similarly intense and broad transitions at low energy (690-720 nm versus ~710-740 nm for the I_X spectrum in Fig. 2.8), as well as intense transitions around 400 nm.[210,211] The copper center in these Cu(II)-HLADH complexes with exogenous ligands were then interpreted and later confirmed to be distorted (flattened) tetrahedral copper dithiolate sites, consisting of Cu(II)-S_2(Cys)N(His)L (L = exogenous ligand, e.g. water, pyrazole, imidazole, 2-mercaptoethanol, etc.).[210,211] Thus, I_X can tentatively be assigned as a copper-dithiolate complex formed with both of the Cys thiolates in the Cu_A center. However, further evidence for this assignment should be pursued.

2.4.4. Mechanism of Cu(II) Incorporation into the Cu_A Site

From all of these various data, a mechanistic picture begins to emerge (Scheme 2.2). Starting with apoCu_AAz and adding Cu(II), T2 red Cu formation occurs rapidly, as previously reported.[143] From the T2 red Cu intermediate, there are two pathways, both leading to purple Cu_A in the end. One pathway, reported in a prior study,[143] leads directly to purple Cu_A formation, presumably by the generation of Cu(I) ions *in situ* through the reaction of Cu(II) with an empty Cu_A site's thiolates to form a disulfide and Cu(I). In the presence of excess copper, this route is accelerated greatly and dominates the mechanism. This copper dependence suggests that the initial reductive event requires multiple coppers per Cu_A site, or multiple singly copper loaded proteins to interact and provide reducing equivalents, which is consistent with the 2 e^- reduction of thiols to disulfide. Conversely, the observed intermediates that form from I_X under sub-saturating copper conditions are a result of single copper occupation of the Cu_A site. On the

pathway that predominates at low copper concentration, the T2 red Cu center converts to I_X, possibly through a structural rearrangement involving ligation by the second Cys in the Cu_A site. After formation of I_X, it decays, converting isosbestically to the T1 blue Cu intermediate. Finally, isosbestic conversion of the T1 blue Cu intermediate to Cu_A occurs under sub-saturating $CuSO_4$ conditions. Based upon comparison to the native N_2OR system (*vide supra*), it is inferred that reducing equivalents, that is generation of Cu(I), are required to achieve this transformation. This scheme represents the understanding of how Cu(II) leads to the formation of Cu_A in Cu_AAz based on the UV-Vis kinetic data collected under sub-saturating copper conditions at pH 6.

Scheme 2.2. Picture of copper incorporation into the Cu_A center of Cu_AAz, based upon the kinetics ensuing from a sub-equivalent copper addition at pH 6. Residue numbers are omitted, since residue specific information is not available at this point.

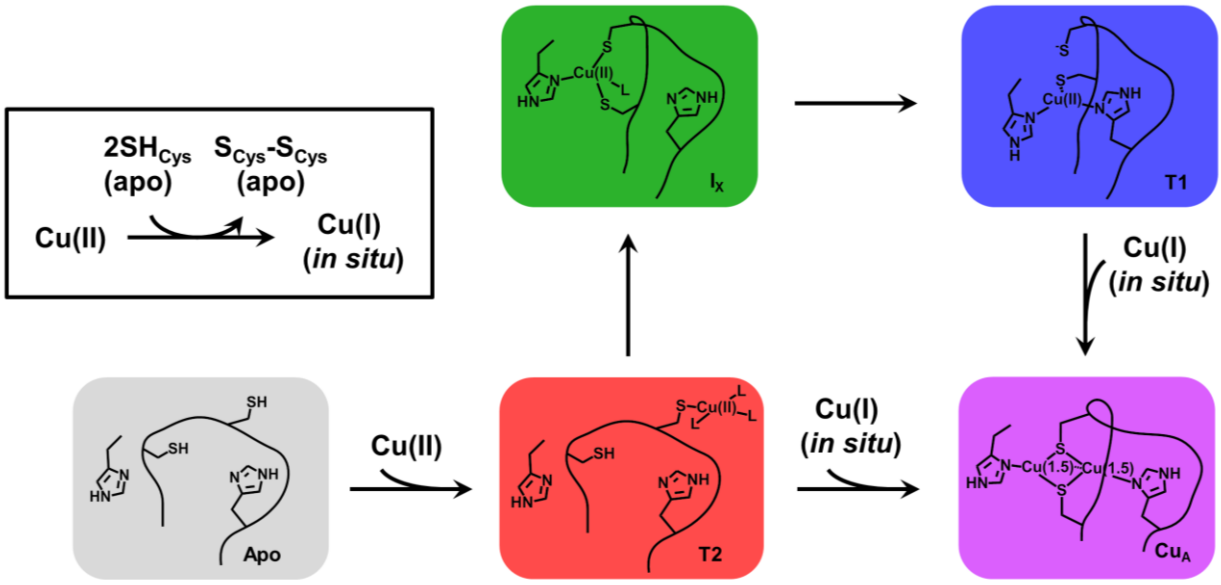

2.5. Conclusions

Detailed here was a stopped-flow and standard UV-Vis absorption study of copper incorporation into the Cu_A center of a biosynthetic Cu_A model, Cu_AAz. Whereas previously only a T2 Cu intermediate was observed during metalation of the Cu_A center in Cu_AAz, it was discovered here that the use of lower copper equivalents (sub-equivalent range) revealed a new pathway to Cu_A formation. In this new pathway, the same T2 Cu intermediate again served as the starting point, after addition of $CuSO_4$. However, the pathway to Cu_A formation diverged from the T2 Cu intermediate. In one pathway, Cu_A was formed directly from the T2 Cu intermediate,

which was observed previously. The other pathway proceeded through a new intermediate, I_X, whose unusual spectroscopic properties do not readily suggest any of the types of copper centers that occur naturally in cupredoxins. By comparison to copper centers reported in literature, one similar set of copper sites was found in copper-substituted horse liver alcohol dehydrogenase.[210,211] This set of copper sites is characterized by dithiolate ligation. Therefore, we tentatively assigned I_X as a copper dithiolate complex with the two Cys thiolates of the Cu_A center. I_X subsequently decayed, and was replaced by a T1 Cu intermediate, which also had not been previously observed as an intermediate in formation of Cu_A in Cu_AAz. Finally, the T1 Cu intermediate converted to the Cu_A center, presumably upon reaction with Cu(I) generated in solution. The observation of blue and red copper intermediates in the existing ligand set of now two Cu_A sites, both the native N_2OR protein[207] and biomimetic Cu_AAz model protein, suggests that the relationship among these three types of copper sites is universal and that the ligand loop is mainly responsible for the formation of the intermediates and final Cu_A center.

While the *in vivo* metallation of Cu_A sites is not completely understood, recent evidence suggests that the Cu(II) oxidation state is critical to the correct formation of this site in C*c*O.[195,196] Additionally, the Cu(II) state is stable in many environments in which Cu_A sites are found (e.g. bacterial C*c*Os[56,181,182] and N_2OR[183]).[172] Although copper chaperones have been proposed for the Cu_A center, and are surely required in eukaryotic organisms,[176] it has been suggested that Cu_A metalation of N_2OR may proceed in an unmediated fashion.[88] Therefore, studies of the *in vitro* reconstitution of Cu_A sites with Cu(II) may provide valuable insight into the practicality of Cu(II)-driven metallation of Cu_A sites *in vivo*. This study demonstrates that Cu(II) reconstitution of Cu_AAz occurs through a complex multistep reaction, resulting in Cu_A sites, but the overall yield of this process is rather low, saturating at ~30% of the total expected copper loading. Using a mixture of Cu(I) and Cu(II) yielded ~20% more Cu_A sites than when Cu(II) alone was added (Fig. 2.5). As the resting state of Cu_A requires a 1:1 ratio of Cu(I):Cu(II), and the reducing equivalents to generate Cu(I) are provided by the active site Cys thiols when Cu(II) alone is used, it is not surprising that including Cu(I) in the reconstitution mixture improved the yield of Cu_A sites. Taken altogether, it is unlikely that the *in vivo* metallation of Cu_A relies solely on Cu(II). Instead, the use of a mixture of Cu(II) and Cu(I) is more likely *in vivo*. However, nature does employ thiol:disulfide oxidoreductases to correct the oxidation state of a thiol-pair/disulfide.[212,213] Therefore, Cu(II)-driven, unmediated metalation of Cu_A may be

operational if a thiol:disulfide oxidoreductase is tasked with maintaining the correct oxidation state of Cu_A, i.e. the reduced thiol pair. Such a role has been verified *in vitro* for the Sco from *Thermus thermophilus*.[214]

CHAPTER 3: ELUCIDATION OF A DETAILED *IN VITRO* ASSEMBLY MECHANISM FOR CU_A IN AZURIN FROM SPECTROSCOPIC AND MUTATIONAL STUDIES[†]

Abstract

In this study, the kinetics of Cu(II) incorporation into the Cu_A site of a biosynthetic Cu_A model, Cu_A azurin (Cu_AAz) were examined under sub-equivalent copper concentrations. Under these conditions, a pathway was previously revealed at pH 6 in which type 2 (T2) and type 1 (T1) copper intermediates form, in addition to a new intermediate, called I_X. This copper incorporation process was discovered to be pH-dependent, with slower kinetics and greater accumulation of the intermediates as the pH is raised from 5.0 to 7.0. Time-dependent EPR spectra led to more detailed characterization of the intermediates. Spin quantification by EPR spectroscopy showed that I_X, which was proposed to be a Cu(II)-dithiolate, underwent reduction to Cu(I). Oxygen-dependence studies demonstrated that the T1 Cu species only formed in the presence of molecular oxygen, suggesting the T1 Cu intermediate is a one-electron oxidation product of a Cu(I) species. By studying Cu_AAz variants where the Cys and His ligands are mutated, we have identified the T2 Cu intermediate as a capture complex with Cys116 and the T1 Cu intermediate as a complex with Cys112 and His120. These characterizations resulted in a unified mechanism for copper incorporation into the Cu_A site, which may be relevant to native systems, provided they utilize a thiol:disulfide oxidoreductase to maintain the copper-binding Cys sidechains in the reduced state.

3.1. Introduction

Cu_A centers are unique, dinuclear copper sites that perform the function of electron transfer with great efficiency.[66,76-83] To date, Cu_A has only been found as the initial electron acceptor in cytochrome *c* oxidases (C*c*Os),[208] a nitric oxide reductase (NOR),[89,90] nitrous oxide reductases (N_2ORs)[183] and in a terminal oxidase from *Sulfolobus acidocaldarius* (SoxM).[92] Although Cu_A is utilized only in a handful of enzymes, these enzymes together occur in organisms across all domains of life, fulfilling critical roles in aerobic and anaerobic

[†] The work presented in this chapter is published under the following citation, and is reproduced here with permission from ACS Publications: Wilson, T. D.; Savelieff, M. G.; Nilges, M. J.; Marshall, N. M.; Lu, Y. *J. Am. Chem. Soc.* **2011**, *133*, 20778.

respiration.[5,88,92] Therefore, Cu_A centers are of broad interest, and have been studied intensively.[66,76-83] Much is now known about these centers, from many spectroscopic, structural, and functional studies. However, one aspect of these centers is still poorly understood: how they become metalated.

The unique structure of Cu_A centers confers them with the ability to transfer electrons very efficiently.[69,139] A salient feature of this structure is a rigid diamond core, consisting of two copper ions, bridged by two Cys thiolates, and a direct copper-copper bond (Fig. 3.1B).[56,57,62,63,67,68,126] Each copper ion also is coordinated equatorially by a His imidizolyl, generating a trigonal coordination environment. Finally, a weak axial ligand completes a distorted tetrahedral geometry for each copper ion, a Met thioether for one, and a backbone carbonyl for the other. The rigid diamond core of Cu_A cultivates an unusual mixed-valence, valence-delocalized resting state, in which the formally [Cu(I)-Cu(II)] oxidation state becomes [Cu(1.5)···Cu(1.5)], due to equal sharing of the 19th d-electron between the two copper ions.[67,70-75,109,198-200] Many of the functional advantages of Cu_A are attributed to this valence-delocalized resting state.[69,139]

Cu_A centers are housed in Greek-key β-barrel folds (Fig. 3.1A), which belong to a class called the cupredoxins.[35,65] Also included in this class are proteins containing mononuclear type 1 (T1) and type 2 (T2) copper centers (Fig. 3.1).[1,23,34,35,65,93-95] T1 copper centers, like Cu_A centers, perform electron transfer functions.[23,34,95] These T1 copper centers feature a copper ion coordinated approximately in a trigonal plane by two His imidizolyls and one Cys thiolate (Fig. 3.1B). One to two weak axial ligands may also coordinate the copper ion, usually a Met thioether for one, and, if present, the second is always a backbone carbonyl. Hence, the overall geometry of T1 copper sites can be distorted trigonal planar, tetrahedral, or trigonal bipyramidal.[23,34] Only one T2 copper protein, called nitrosocyanin, belongs to the cupredoxin class, and it is proposed to perform a catalytic function.[202,215,216] This T2 copper center displays an approximately square pyramidal geometry, with the copper ion coordinated in the plane by a Cys thiolate, two His imidizolyls, and a water, and apically coordinated by a Glu carboxylate (Fig. 3.1B). There are many structural similarities among the T1 copper, T2 copper, and Cu_A centers of cupredoxins, and indeed, an evolutionary relationship has been proposed for these proteins on the basis of sequence alignments and phylogenetic analyses.[205,206]

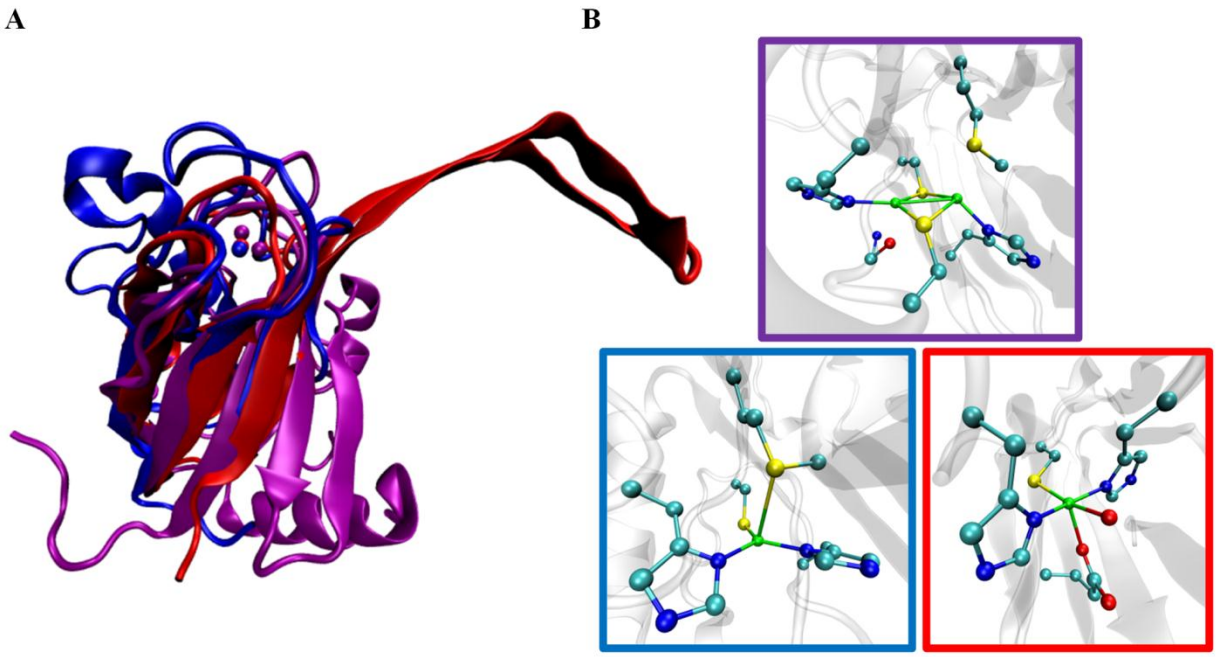

Fig. 3.1. (A) Overlay of the Greek-key β-barrel cupredoxin domains containing Cu_A (purple, *Paracoccus denitrificans* CcO, PDB ID code 3HB3), T1 blue Cu (blue, *Pseudomonas aeruginosa* azurin, PDB ID code 1AZU), and T2 red Cu (red, *Nitrosomonas europaea* nitrosocyanin, PDB ID code 1IBY), where copper ions are shown as VDW spheres in the same colors as the corresponding protein backbone. (B) Zoom in of associated active-site structures, with Cu_A shown in a purple box, T1 copper in a blue box and T2 copper in a red box. The copper sites are shown in ball-and-stick representation, and colors are assigned as follows: cyan for C, blue for N, red for O, yellow for S, and green for Cu. Figures were rendered using VMD software, and structural overlay performed in the MultiSeq extension of the VMD software.[203,204]

Experimental evidence for the proposed evolutionary relationship among cupredoxin proteins was lacking until the recent discovery of T1 and T2 copper intermediates that form in the native Cu_A ligand set of N_2OR.[207] In this study, it was found that the T1 and T2 copper intermediates formed initially, and then converted slowly to the final Cu_A center, as evidenced by isosbestic points between the UV-Vis transitions of these intermediates and the Cu_A center. Additionally, the formation of these intermediates was pH dependent, with greater intermediate formation, relative to Cu_A formation, and slower conversion to Cu_A at higher pH. This study constituted the first direct experimental evidence of the previously proposed evolutionary link among cupredoxin proteins.[205,206] Although a mechanism for metalation of the Cu_A center in N_2OR from these T1 and T2 copper intermediates was proposed in this study, a detailed mechanistic study has yet to confirm this mechanism.

The mechanism of Cu_A metallation *in vivo* is not fully understood. In bacteria, the crystal structures of C*c*O show that its Cu_A domain protrudes into the periplasmic or extracellular space,[56,181,182] while the entire N_2OR enzyme is known to be soluble in the periplasm.[183] These environments (periplasmic and extracellular space) are oxidizing relative to the cytoplasm, permitting the Cu(II) oxidation state to exist congruently with Cu(I). Moreover, Sco, a protein that plays some role in the biogenesis of Cu_A in C*c*O, was recently demonstrated to require the Cu(II) state for proper function in *Bacillus subtilis*.[196] Although Sco is the proposed copper chaperone to Cu_A in C*c*Os,[176] in *Thermus thermophilus*, it has been demonstrated that Sco does not deliver copper to Cu_A.[214] A Sco protein associated with an N_2OR maturation cassette also was shown to be dispensable for biogenesis of this enzyme, including an intact Cu_A center,[197] and another candidate copper chaperone to Cu_A has not been identified. It was proposed that the metalation of N_2OR may proceed unmediated by chaperones.[197] Therefore, *in vivo* metallation of Cu_A likely involves Cu(II), and in some cases may not be mediated by copper chaperones, rendering studies of *in vitro* Cu(II) incorporation into Cu_A sites important to understanding to the extent to which this oxidation state and unmediated copper insertion are relevant to *in vivo* assembly of Cu_A centers.

Mechanistic studies of Cu_A metalation in a biosynthetic Cu_A model, Cu_AAz, have represented the first such studies of Cu_A centers.[143,158] In the ealier study, the metalation of apo-Cu_AAz was probed by stopped-flow UV-Vis absorption spectroscopy upon the addition of a ten-fold excess of $CuSO_4$, which provided pseudo-first order kinetics.[143] It was found that Cu_A metalation under these conditions proceeded through a T2 copper intermediate. Since Cu(II) alone was provided, reducing equivalents had to be supplied from the system. The most likely candidate was determined to be the active site Cys thiolates, as Cu(II)-catalyzed oxidation of thiolates to disulfide was a well-known phenomenon.[178-180] Additional evidence for this proposal came from an increased yield of Cu_A centers when Cu(I) or ascorbate were added with the $CuSO_4$, as a disulfide formed between the Cys thiolates of Cu_A would render the site unable to accept copper.

The second study of Cu_A metalation in Cu_AAz was detailed in Chapter 2 of this thesis. It was discovered that, when the amount of $CuSO_4$ added to apo-Cu_AAz was reduced to sub-equivalent regimes, a complex, multistep metalation process was revealed, involving two more intermediates, a T1 copper species and a new intermediate, I_X, beyond the T2 copper

intermediate observed previously. This process was monitored by stopped-flow UV-Vis spectroscopy, and global analysis of the resulting data allowed deconvolution of the individual steps, and the species contributing to them, yielding a general mechanism for metalation of Cu_A in azurin under copper-limiting conditions (Scheme 3.1). These conditions are closer to those experienced by proteins in living organisms, as copper levels in the cell are carefully controlled.[171,172,175] However, atomistic detail about the intermediates involved in metalation of Cu_AAz, as well as the source(s) of reducing equivalents, have yet to be elucidated.

Scheme 3.1. Picture of copper incorporation into the Cu_A center of Cu_AAz, based upon the kinetics ensuing from a sub-equivalent copper addition at pH 6 (see Chapter 2). Residue numbers are omitted, since residue specific information is not available at this point.

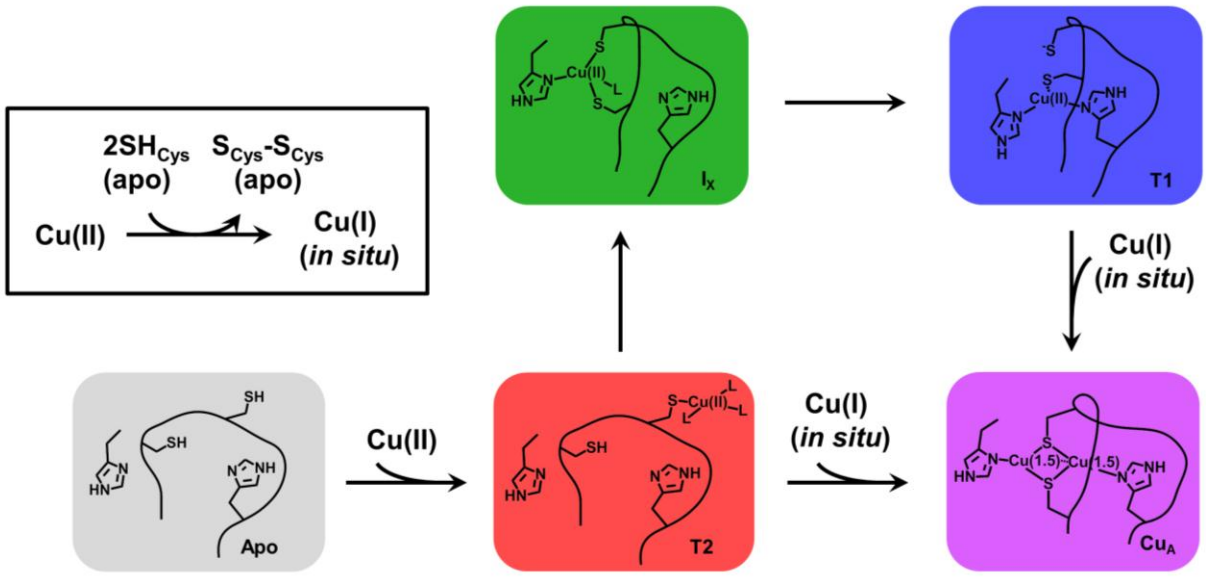

Herein, further studies of the metalation of Cu_A in azurin are described, which have allowed for greater elucidation of the mechanism detailed in Chapter 2. These studies include pH- and oxygen-dependent stopped-flow UV-Vis and time-dependent EPR spectroscopies, as well as mutagenesis of selected ligands to the Cu_A center. From these studies, important aspects of the copper incorporation into Cu_AAz are illuminated, including specific residues contributing to the intermediates, identification of a source of reducing equivalents, and a proposed identity for intermediate X (I_X).

3.2. Materials and Methods

3.2.1. Materials and reagents

Bactotryptone and yeast extract were purchased from BD Biosciences. BL-21* (DE3) cells were purchased from Invitrogen. IPTG was purchased from Research Products International Corps or Gold Bio Technology Inc. All other reagents were purchased from Fisher, Sigma-Aldrich or Fluka. All water used was purified to 18.2 MΩcm by ultrafiltration with a Milli-Q Plus PF Ultra-Pure Water System. $CuSO_4$ solutions were prepared volumetrically in water that was incubated with Chelex prior to use. For pH dependent studies, a chelexed universal buffer (UB) containing 40 mM MES, MOPS, Tris, and CAPS, 50 mM NaOAc, and 100 mM $NaNO_3$ (to maintain relatively constant ionic strength) was utilized. For EPR studies, a temperature independent pH (TIP) buffer, previously developed in our laboratory,[217] was used in order to avoid any pH changes upon cooling to 30 K.

3.2.2. Protein expression, purification, and preparation for experiments

The engineered Cu_A azurin (Cu_AAz) and its C116S and H120A mutants were expressed and purified as previously reported.[107,144,156] Briefly, BL-21* (DE3) cells were transformed with pET-9a plasmid containing the DNA encoding the protein of interest preceded by a periplasmic leader sequence from *Pseudomonas aeruginosa*. These cells were then grown in 2xYT media at 25 ºC and induced with IPTG at OD_{600} ~ 3. Cells were allowed to express protein periplasmically at 25°C for 4 hours. After harvesting the cells, lysis of the periplasmic membrane was achieved by osmotic shock. The supernatant after centrifugation was acidified to pH 4.1 with 500 mM sodium acetate, resulting in significant precipitation. After another round of centrifugation, the supernatant was applied to SP Sepharose cation exchange media, equilibrated with 50 mM ammonium acetate (NH_4OAc), pH 4.1. A step gradient was applied with 50 mM NH_4OAc, pH 6.35 as the elution buffer, resulting in elution of the desired protein over a broad range to near 100% purity, as determined by polyacrylamide gel electrophoresis. The nearly pure wt or mutant Cu_AAz was then applied to an additional Q-Sepharose HiTrap anion exchange column to remove a minor heme containing contaminant. At this stage, the pH of the protein solution was adjusted to within the buffering range of NH_4OAc (typically pH 5.0-5.5), flash frozen, and stored at -80 °C until required for experiments. When needed for experiments, the appropriate amount of protein was thawed and exchanged into whichever buffer was to be employed for that

experiment. Buffer exchanging was typically accomplished by application of the protein to a PD-10 desalting column (GE Healthcare), equilibrated with the buffer of interest. Alternatively, the protein was subjected to several cycles of concentration and dilution with the buffer of interest in a centrifugal filter unit with a 10 kDa molecular weight cutoff (Amicon Ultra from Millipore). The protein was then concentrated to the desired level for the experiment, and the concentration confirmed based on A_{280} using $\varepsilon_{280} = 8440\ cm^{-1}\,M^{-1}$.

3.2.3. Stopped-flow UV-Vis absorbance

Experiments were performed on an Applied Photophysics Ltd (Leatherhead, UK) SX18.MV stopped-flow spectrometer equipped with a 256 element photodiode array detector. Two-syringe mixing was employed to mix equal volumes of H120A or wt Cu_AAz with volumetrically prepared $CuSO_4$ solutions. All reported data sets originally consisted of 200 spectra collected over 50 s or 1000 s using logarithmic sampling. The integration period and minimum sampling period were both 1 ms. A water bath, connected to the syringe compartment and set to 15 ºC, provided temperature control. The actual temperature in the syringe compartment was measured to be between 16.3 and 16.5 ºC. The instrument was prepared for anaerobic stopped-flow by rinsing its lines out several times with buffer that had been degassed by bubbling argon gas through it. Special glass outer syringes fit with Teflon stoppers into which an argon line was run maintained an oxygen free environment. The protein was degassed on a Schlenk line using standard techniques. The copper solutions were degassed either on the Schlenk line or by bubbling with argon gas for 20 minutes in containers with only a small opening, to allow gases to escape. Oxygen-rich stopped-flow was accomplished by bubbling pure oxygen gas through the $CuSO_4$ solution for 20 minutes.

3.2.4. Sub-saturating $CuSO_4$ additions to Cu_AAz

Sub-saturating $CuSO_4$ additions were made to Cu_AAz and the resulting UV-Vis absorbance spectra monitored on an Agilent 8453 photodiode array spectrometer having a connected water bath for temperature control and water-propelled magnetic stirring. After blanking the instrument with a 1:1 mixture of UB:water in a 1cm x 1cm standard UV-Vis

cuvette, 850 µL of 0.5 mM apoCu_AAz was added to the cuvette. The instrument was then set to collect a series of spectra over 3600 s (pH 5) or 900 s (pH 6, 7, and 8) with 0.5 s scan time incremented by 5% after 45 s. After starting the data collection, and with constant magnetic stirring and temperature control set to 10 °C, an 850 µL aliquot of 0.2 mM $CuSO_4$ was quickly added to the stirring protein solution. The top of the cuvette was parafilmed once data collection was underway to reduce evaporation. For the pH 6, 7 and 8 experiments, spectra were collected for an additional 14 hours, with 600 s scan time incremented by 1% after 3600 s. The sets of data generated from this procedure are shown in their entirety in Fig. 3.2, but only a portion of this data is needed for analysis of the kinetic processes, as the steps occurring at shorter timepoints were analyzed by stopped-flow UV-Vis spectroscopy.

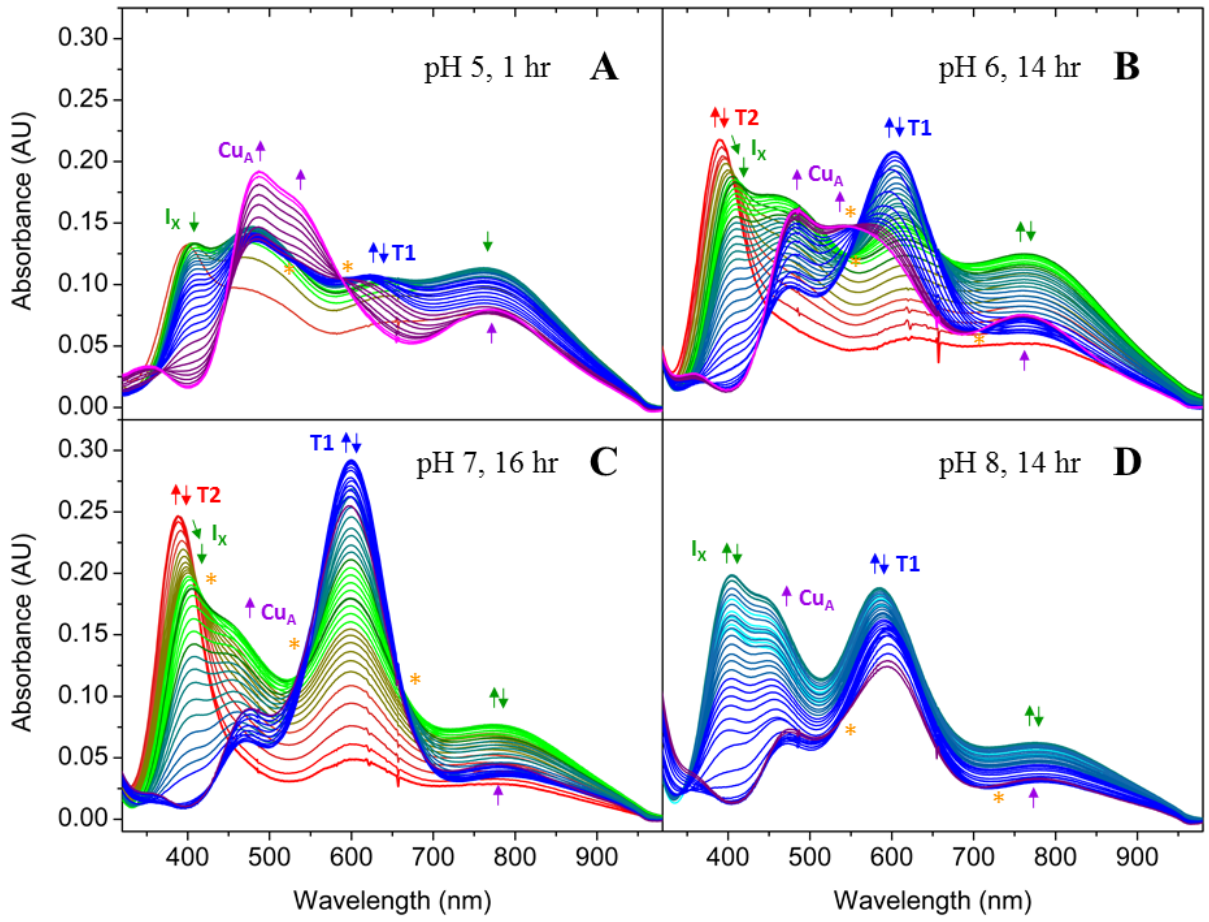

Fig. 3.2. Full electronic absorption kinetics experiments corresponding to the insets in Fig. 3.23. Spectra are colored to indicate the species forming at that particular time. Arrows indicate direction of change in absorbance over course of experiment and are colored to correspond to the

species giving rise to that peak. Golden asterisks indicate the positions of apparent isosbestic points. Final Cu_AAz concentrations were 0.25 mM.

3.2.5. Electron paramagnetic resonance (EPR) spectroscopy

EPR data collection was performed using an X-band Varian E-122 spectrometer at the Illinois EPR Research Center (IERC). The temperature was set to 30 K using liquid He and an Air Products Helitran cryostat. Frequencies were measured with an EIP frequency counter, and magnetic fields were calibrated with a Varian NMR gaussmeter.

Freeze quench samples were prepared by mixing a 6 mM apoCu_AAz solution in TIP buffer, pH 7 in a 2:1 volume ratio with a 1.2 mM $CuSO_4$ solution, containing 40% glycerol by volume, at room temperature, using an Update Instruments System 1000 equipped with a Wiskind Grid Mixer, a spraying nozzle, and a stirred isopentane bath, cooled by liquid nitrogen to approximately -130 ºC. The mixture was passed through a delay hose of appropriate length to give the desired quench time (for the 100 ms sample), or to yield enough overall sample with four injection/delay cycles (for the 1, 5, and 10 s samples). The sample was frozen by spraying into approximately -130 ºC spectrophotometric grade isopentane in a Pyrex collection funnel attached to the EPR tube. Using pre-cooled packing rods and long needles for breaking up improperly packed sample, the frozen sample was packed into the base of the EPR tube, while being maintained at -130 ºC. After packing, the samples were transferred to a dewar containing liquid nitrogen, and stored this way until collection of the EPR spectra.

The longer timeframe (30 s, 7 min, 15 min, 30 min, and 24 hr) Cu_AAz and C116S Cu_AAz in TIP buffer, pH 7 samples were prepared with 30% glycerol as a glassing agent. To achieve reasonably fast mixing for the Cu_AAz sample, 350 μL of the 4 mM apoCu_AAz /glycerol solution was added rapidly by syringe to ~20 μL of a 7.2 mM $CuSO_4$ solution in the bottom of an EPR tube, syringe mixed, and flash frozen in liquid N_2 in as short a time as possible.

EPR spectra were simulated with SIMPOW6.[218] As the 100 ms sample appeared to be homogeneous, it was simulated as a single species. The time dependent spectra were simulated

assuming the presence of four components which were simultaneously fit to minimize the total rms difference between the experimental and simulated spectra.

3.2.6. Global analysis of stopped-flow and standard UV-Vis absorbance kinetics data

As the kinetics resolved by stopped-flow and standard UV-Vis absorbance were generally complex, with multistep reactions and overlapping absorption bands, kinetic analyses were performed using a global analysis software called SpecFit/32 (Spectrum Software Associates, Inc), which employs singular value decomposition (SVD) and nonlinear regression modeling to find kinetic parameters for the data. Briefly, models were determined through an iterative approach, where the starting point was the simplest conceivable set of reactions that could possibly explain the sequence of events observed in the spectra, while being consistent with other sources of data, and complexity was added as needed to improve the fit and consistency of the models. Fixed or known spectra were required in some cases for the fits to converge (Table 3.1, Table 3.2, Fig. 3.3-Fig. 3.7). The quality of these fits was judged based on the size of the standard deviations for the observed rate constants (Table 3.1, Table 3.2), the reasonableness of the resolved species spectra found by the software (Fig. 3.8-Fig. 3.14), the convergence statistics calculated by the software for each fit (Table 3.1, Table 3.2) and the magnitude of the residual spectra (Fig. 3.15-Fig. 3.21).

Table 3.1. Details of kinetics fits for Cu_AAz with a 0.4 equivalent addition of $CuSO_4$ at various pH values and timescales.

pH 5, 0.32 s					
Step in Model	**k_{obs}**	**Species**	**Initial Conc. (μM)**	**Colored ?**	**Fixed?**
$CuSO_4 \rightarrow T2$	$11.7 \pm 1.2\ s^{-1}$	$CuSO_4$	100	No	No
		T2	0	Yes	No
Convergence Statistics					
Convergence Value	**Iterations Performed**	**Marquardt Parameter**	**Total Sum of Squares**	**Std. Deviation of Fit**	
6.117×10^{-16}	3	0.0	0.1361	4.746×10^{-3}	
pH 5, 1000 s					
Step in Model	**k_{obs}**	**Species**	**Initial Conc. (μM)**	**Colored ?**	**Fixed?**
$2\ T2 \rightarrow Cu_A$	$(1.29 \pm 0.05) \times 10^4\ M^{-1}s^{-1}$	T2	90	Yes	Yes
$T2 \rightarrow I_X$	$0.460 \pm 0.034\ s^{-1}$	I_X	0	Yes	No
$2\ I_X \rightarrow Cu(I)$	$82.2 \pm 11.9\ M^{-1}s^{-1}$	T1	0	Yes	Yes
$I_X \rightarrow T1$	$(7.93 \pm 0.40) \times 10^{-3}\ s^{-1}$	Cu(I)	0	No	No
$T1 \rightarrow Cu_A$	$(3.37 \pm 0.03) \times 10^{-2}\ s^{-1}$	Cu_A	0	Yes	No
Convergence Statistics					
Convergence Value	**Iterations Performed**	**Marquardt Parameter**	**Total Sum of Squares**	**Std. Deviation of Fit**	
2.011×10^{-5}	3	0.0	0.3688	3.091×10^{-3}	
pH 6, 0.32 s					
Step in Model	**k_{obs}**	**Species**	**Initial Conc. (μM)**	**Colored ?**	**Fixed?**
$CuSO_4 \rightarrow T2$	$40.6 \pm 2.9\ s^{-1}$	$CuSO_4$	100	No	No
		T2	0	Yes	No
Convergence Statistics					
Convergence Value	**Iterations Performed**	**Marquardt Parameter**	**Total Sum of Squares**	**Std. Deviation of Fit**	
0.0	3	0.0	9.884×10^{-2}	3.980×10^{-3}	
pH 6, 370 s					

Table 3.1, continued

Step in Model	k_{obs}	Species	Initial Conc. (μM)	Colored ?	Fixed?
2 T2 → Cu_A	$(3.39 \pm 0.11) \times 10^3$ $M^{-1}s^{-1}$	T2	90	Yes	Yes
T2 → I_X	0.241 ± 0.007 s^{-1}	I_X	0	Yes	No
2 I_X → Cu(I)	25.6 ± 1.0 $M^{-1}s^{-1}$	T1	0	Yes	Yes
I_X → T1	$(3.25 \pm 0.10) \times 10^{-3}$ s^{-1}	Cu(I)	0	No	No
		Cu_A	0	Yes	Yes

Convergence Statistics

Convergence Value	Iterations Performed	Marquardt Parameter	Total Sum of Squares	Std. Deviation of Fit
2.441×10^{-6}	3	0.0	0.7955	4.988×10^{-3}

pH 6, 15 hr

Step in Model	k_{obs}	Species	Initial Conc. (μM)	Colored ?	Fixed?
T1 + Cu(I) → Cu_A	6.99 ± 0.36 $M^{-1}s^{-1}$	T1	36	Yes	Yes
		Cu(I)	20	No	No
		Cu_A	22	Yes	Yes

Convergence Statistics

Convergence Value	Iterations Performed	Marquardt Parameter	Total Sum of Squares	Std. Deviation of Fit
7.983×10^{-11}	3	0.0	0.3681	3.017×10^{-3}

pH 7, 0.32 s

Step in Model	k_{obs}	Species	Initial Conc. (μM)	Colored ?	Fixed?
$CuSO_4$ → T2	56.3 ± 3.5 s^{-1}	$CuSO_4$	100	No	No
		T2	0	Yes	No

Convergence Statistics

Convergence Value	Iterations Performed	Marquardt Parameter	Total Sum of Squares	Std. Deviation of Fit
0.0	3	0.0	6.002×10^{-2}	3.102×10^{-3}

pH 7, 1000 s

Step in Model	k_{obs}	Species	Initial Conc. (μM)	Colored ?	Fixed?
2 T2 → Cu_A	$(9.48 \pm 0.47) \times 10^2$ $M^{-1}s^{-1}$	T2	90	Yes	Yes

Table 3.1, continued

$T2 \rightarrow I_X$	$0.182 \pm 0.006\ s^{-1}$	I_X	0	Yes	No
$T2 \rightarrow T1$	$(4.43 \pm 0.27) \times 10^{-2}\ s^{-1}$	T1	0	Yes	Yes
$2\ I_X \rightarrow T1 + Cu(I)$	$55.7 \pm 2.8\ M^{-1}s^{-1}$	Cu(I)	0	No	No
		Cu_A	0	Yes	Yes

Convergence Statistics

Convergence Value	Iterations Performed	Marquardt Parameter	Total Sum of Squares	Std. Deviation of Fit
2.104×10^{-12}	3	0.0	1.561	6.343×10^{-3}

pH 7, 15 hr

Step in Model	k_{obs}	Species	Initial Conc. (μM)	Colored ?	Fixed?
$T1 + Cu(I) \rightarrow Cu_A$	$0.521 \pm 0.023\ M^{-1}s^{-1}$	T1	42	Yes	Yes
$2\ Cu(I) \rightarrow A$	$1.60\ M^{-1}s^{-1}$ (fixed)	Cu(I)	40	No	No
		Cu_A	8	Yes	Yes
		A	0	No	No

Convergence Statistics

Convergence Value	Iterations Performed	Marquardt Parameter	Total Sum of Squares	Std. Deviation of Fit
1.446×10^{-8}	3	0.0	0.8562	4.875×10^{-3}

pH 8, 1000 s

Step in Model	k_{obs}	Species	Initial Conc. (μM)	Colored ?	Fixed?
$2\ T2 \rightarrow Cu_A$	$(1.79 \pm 0.06) \times 10^3\ M^{-1}s^{-1}$	T2	90	Yes	Yes
$T2 \rightarrow I_X$	$0.182 \pm 0.004\ s^{-1}$	I_X	0	Yes	No
$T2 \rightarrow T1$	$(5.51 \pm 0.14) \times 10^{-2}\ s^{-1}$	T1	0	Yes	Yes
$2\ I_X \rightarrow Cu(I)$	$60.1 \pm 2.4\ M^{-1}s^{-1}$	Cu(I)	0	No	No
		Cu_A	0	Yes	Yes

Convergence Statistics

Convergence Value	Iterations Performed	Marquardt Parameter	Total Sum of Squares	Std. Deviation of Fit

Table 3.1, continued

1.671×10^{-7}	3	0.0	0.7364	4.356×10^{-3}

pH 8, 15 hr					
Step in Model	**k_{obs}**	**Species**	**Initial Conc. (μM)**	**Colored ?**	**Fixed?**
T1 + Cu(I) → Cu_A	0.441 ± 0.017 $M^{-1}s^{-1}$	T1	22	Yes	Yes
2 T1 → E	0.1 $M^{-1}s^{-1}$ (fixed)	Cu(I)	20	No	No
		Cu_A	10	Yes	Yes
		E	0	No	No

Convergence Statistics				
Convergence Value	**Iterations Performed**	**Marquardt Parameter**	**Total Sum of Squares**	**Std. Deviation of Fit**
1.651×10^{-8}	3	0.0	0.1658	2.127×10^{-3}

Table 3.2. Details of kinetics fits for Cu_AAz with a 0.1 equivalent addition of $CuSO_4$ at pH 5, over 0.32 and 1000 s, under anaerobic, aerobic and oxygen-rich conditions.

Anaerobic, 0.32 s					
Step in Model	**k_{obs}**	**Species**	**Initial Conc. (μM)**	**Colored ?**	**Fixed?**
$CuSO_4$ → T2	15.1 ± 1.2 s^{-1}	$CuSO_4$	25	No	No
		T2	0	Yes	No

Convergence Statistics				
Convergence Value	**Iterations Performed**	**Marquardt Parameter**	**Total Sum of Squares**	**Std. Deviation of Fit**
0.0	3	0.0	8.409×10^{-3}	1.180×10^{-3}

Anaerobic, 1000 s					
Step in Model	**k_{obs}**	**Species**	**Initial Conc. (μM)**	**Colored ?**	**Fixed?**
2 T2 → Cu_A	$(1.72 \pm 0.05) \times 10^4$ $M^{-1}s^{-1}$	T2	25	Yes	Yes
T2 → I_X	0.854 ± 0.022 s^{-1}	I_x	0	Yes	Yes

Table 3.2, continued

$2\ I_X \rightarrow Cu(I)$	$48.5 \pm 0.9\ M^{-1}s^{-1}$	Cu(I)	0	No	No
$I_X + Cu(I) \rightarrow Cu_A$	$235 \pm 19\ M^{-1}s^{-1}$	Cu_A	0	Yes	Yes

Convergence Statistics

Convergence Value	Iterations Performed	Marquardt Parameter	Total Sum of Squares	Std. Deviation of Fit
7.405×10^{-7}	3	0.0	4.893×10^{-2}	1.129×10^{-3}

Aerobic, 0.32 s

Step in Model	k_{obs}	Species	Initial Conc. (μM)	Colored ?	Fixed?
$CuSO_4 \rightarrow T2$	$11.8 \pm 1.1\ s^{-1}$	$CuSO_4$	25	No	No
		T2	0	Yes	No

Convergence Statistics

Convergence Value	Iterations Performed	Marquardt Parameter	Total Sum of Squares	Std. Deviation of Fit
0.0	3	0.0	8.796×10^{-3}	1.206×10^{-3}

Aerobic, 1000 s

Step in Model	k_{obs}	Species	Initial Conc. (μM)	Colored ?	Fixed?
$2\ T2 \rightarrow Cu_A$	$(1.32 \pm 0.11) \times 10^4\ M^{-1}s^{-1}$	T2	25	Yes	Yes
$T2 \rightarrow I_X$	$0.831 \pm 0.031\ s^{-1}$	I_X	0	Yes	No
$2\ I_X \rightarrow Cu(I)$	$59.5 \pm 2.7\ M^{-1}s^{-1}$	T1	0	Yes	Yes
$I_X \rightarrow T1$	$(9.28 \pm 0.24) \times 10^{-4}\ s^{-1}$	Cu(I)	0	No	No
$T1 \rightarrow Cu_A$	$(1.63 \pm 0.11) \times 10^{-3}\ s^{-1}$	Cu_A	0	Yes	Yes

Convergence Statistics

Convergence Value	Iterations Performed	Marquardt Parameter	Total Sum of Squares	Std. Deviation of Fit
5.27×10^{-7}	3	0.0	5.512×10^{-2}	1.195×10^{-3}

Oxygen-rich, 0.32 s

Step in Model	k_{obs}	Species	Initial Conc. (μM)	Colored ?	Fixed?
$CuSO_4 \rightarrow T2$	$14.6 \pm 1.4\ s^{-1}$	$CuSO_4$	25	No	No
		T2	0	Yes	No

Convergence Statistics

Table 3.2, continued

Convergence Value	Iterations Performed	Marquardt Parameter	Total Sum of Squares	Std. Deviation of Fit
0.0	3	0.0	1.372×10^{-2}	1.506×10^{-3}

Oxygen-rich, 1000 s					
Step in Model	**k_{obs}**	**Species**	**Initial Conc. (μM)**	**Colored ?**	**Fixed?**
2 T2 → Cu_A	$(1.05 \pm 0.13) \times 10^4$ $M^{-1}s^{-1}$	T2	25	Yes	Yes
T2 → I_X	0.944 ± 0.038 s^{-1}	I_X	0	Yes	No
2 I_X → Cu(I)	60.4 ± 2.7 $M^{-1}s^{-1}$	T1	0	Yes	Yes
I_X → T1	$(9.28 \pm 0.24) \times 10^{-4}$ s^{-1}	Cu(I)	0	No	No
T1 → Cu_A	$(1.58 \pm 0.09) \times 10^{-3}$ s^{-1}	Cu_A	0	Yes	Yes

Convergence Statistics				
Convergence Value	**Iterations Performed**	**Marquardt Parameter**	**Total Sum of Squares**	**Std. Deviation of Fit**
3.24×10^{-7}	3	0.0	9.982×10^{-2}	1.608×10^{-3}

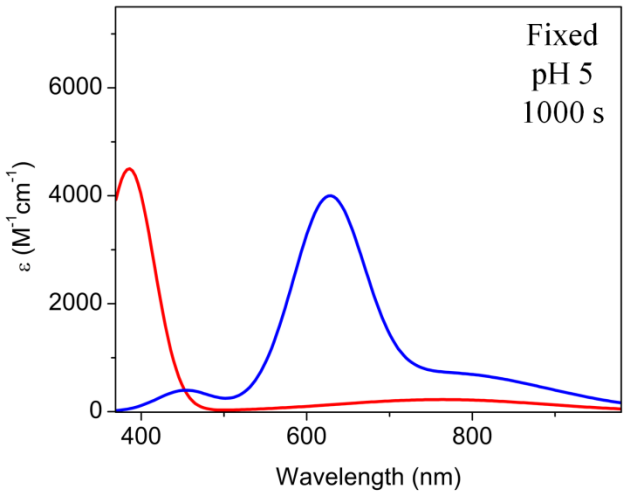

Fig. 3.3. Fixed T2 Cu (red) and T1 Cu (blue) spectra used in the fitting of the kinetics for Cu_AAz with 0.4 equivalents $CuSO_4$ at pH 5 over 1000s.

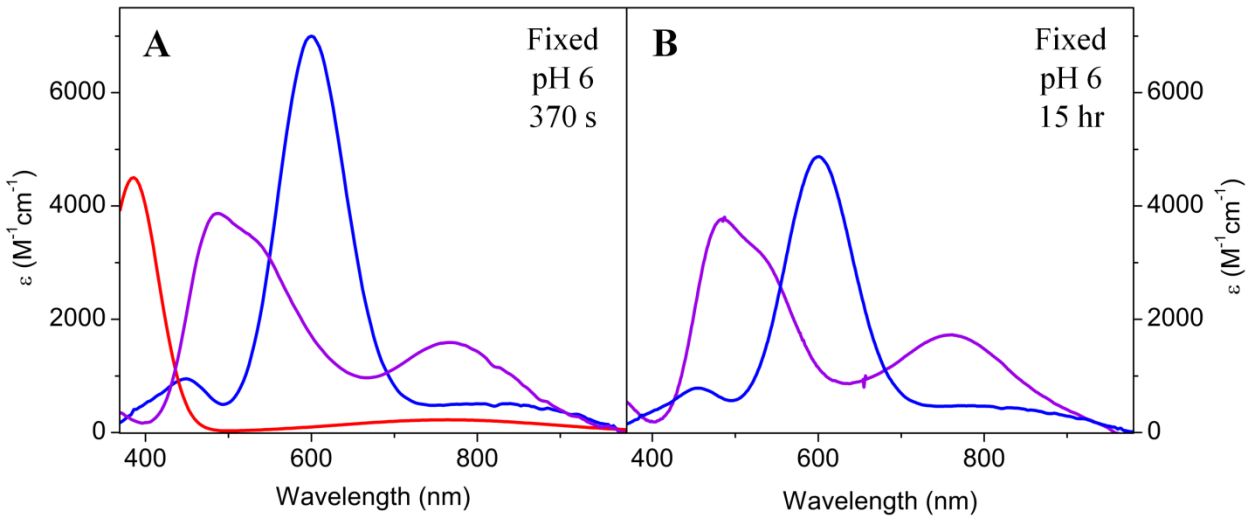

Fig. 3.4. Fixed T2 Cu (red), T1 Cu (blue) and Cu_A (purple) spectra used in the fitting of the kinetics for Cu_AAz with 0.4 equivalents $CuSO_4$ at pH 6 up to (A) 370 s and (B) 15 hr after $CuSO_4$ addition.

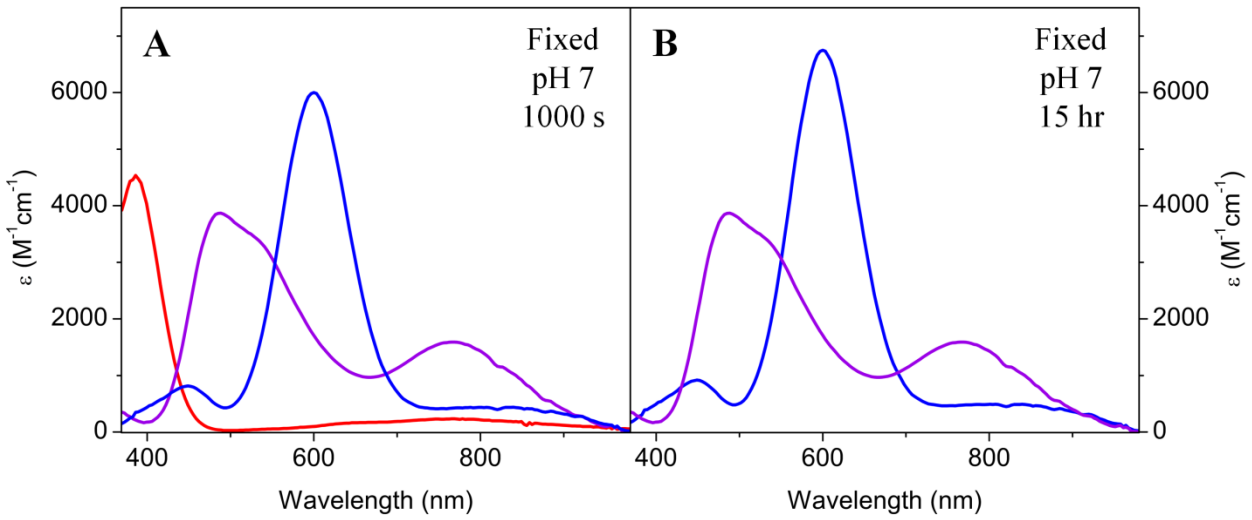

Fig. 3.5. Fixed T2 Cu (red), T1 Cu (blue) and Cu_A (purple) spectra used in the fitting of the kinetics for Cu_AAz with 0.4 equivalents $CuSO_4$ at pH 7 up to (A) 1000 s and (B) 15 hr after $CuSO_4$ addition.

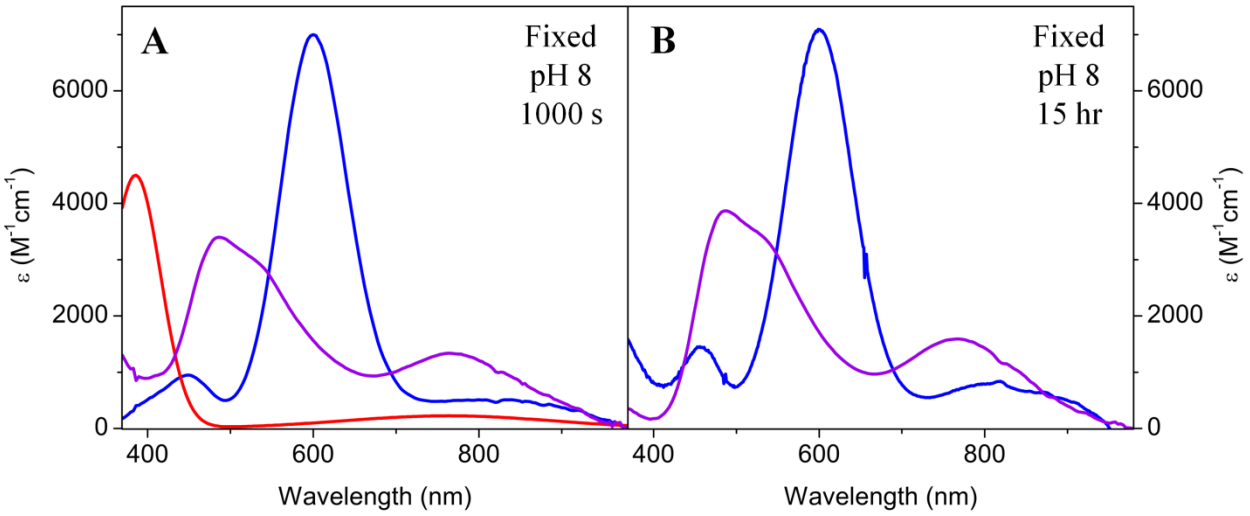

Fig. 3.6. Fixed T2 Cu (red), T1 Cu (blue) and Cu_A (purple) spectra used in the fitting of the kinetics for Cu_AAz with 0.4 equivalents $CuSO_4$ at pH 8 up to (A) 1000 s and (B) 15 hr after $CuSO_4$ addition.

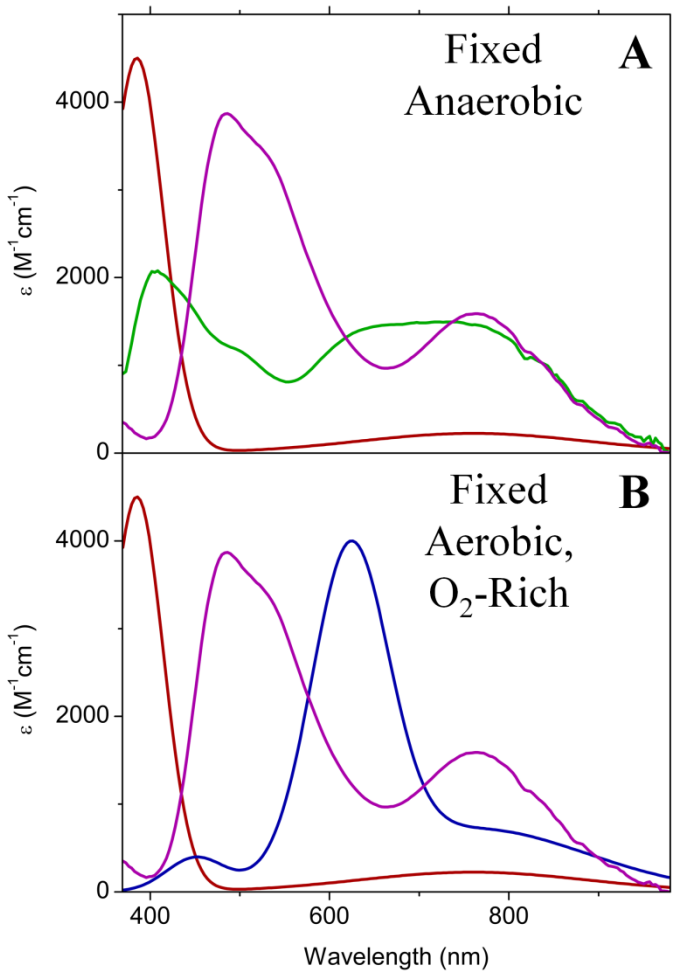

Fig. 3.7. Fixed T2 Cu (red), I_X (green), T1 Cu (blue) and Cu_A (purple) spectra used in the fitting of the kinetics for Cu_AAz with 0.1 equivalents $CuSO_4$ at pH 5, over 1000 s, under (A) anaerobic and (B) aerobic and oxygen-rich conditions.

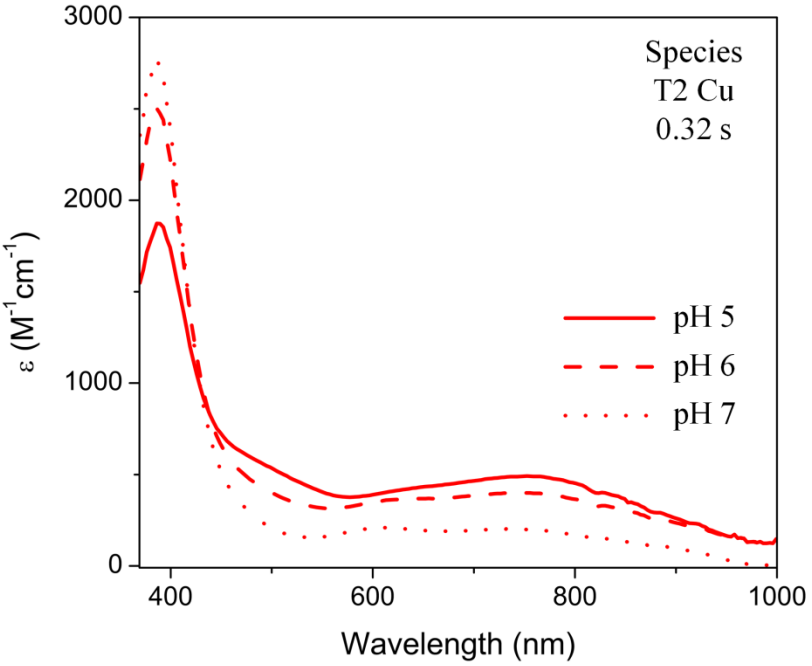

Fig. 3.8. Resolved species spectra for T2 Cu calculated through the fitting of the kinetics for Cu_AAz with 0.4 equivalents $CuSO_4$ at pH 5 (solid), pH 6 (dashed), and pH 7 (dotted) over 0.32 s.

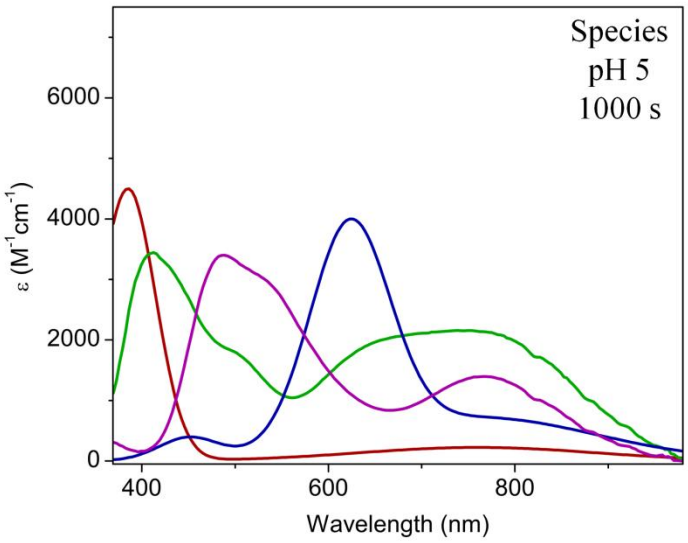

Fig. 3.9. Resolved species spectra for T2 Cu (red), I_X (green), T1 Cu (blue), and Cu_A (purple) calculated through the fitting of the kinetics for Cu_AAz with 0.4 equivalents $CuSO_4$ at pH 5 over 1000s.

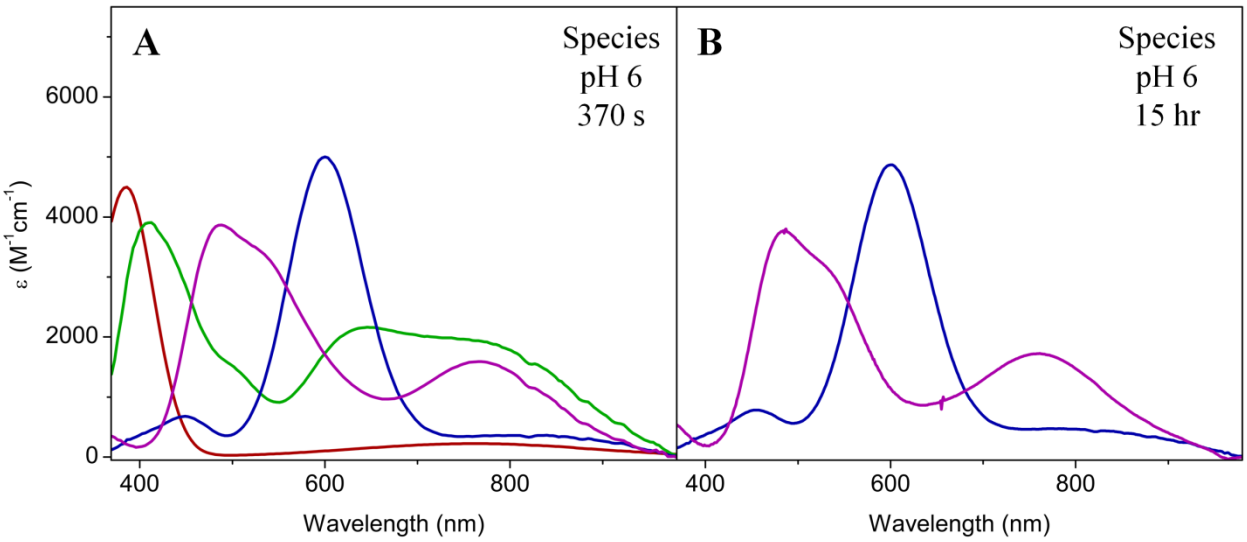

Fig. 3.10. Resolved species spectra for T2 Cu (red), I_X (green), T1 Cu (blue), and Cu_A (purple) calculated through the fitting of the kinetics for Cu_AAz with 0.4 equivalents $CuSO_4$ at pH 6 up to (A) 370 s and (B) 15 hrs after $CuSO_4$ addition.

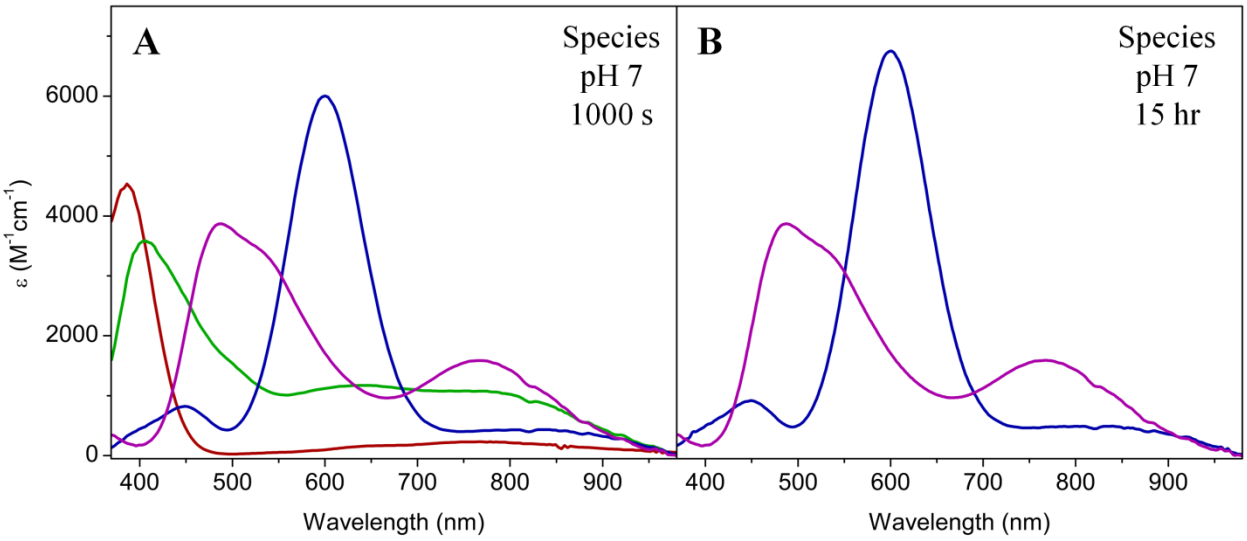

Fig. 3.11. Resolved species spectra for T2 Cu (red), I_X (green), T1 Cu (blue), and Cu_A (purple) calculated through the fitting of the kinetics for Cu_AAz with 0.4 equivalents $CuSO_4$ at pH 7 up to (A) 1000 s and (B) 15 hrs after $CuSO_4$ addition.

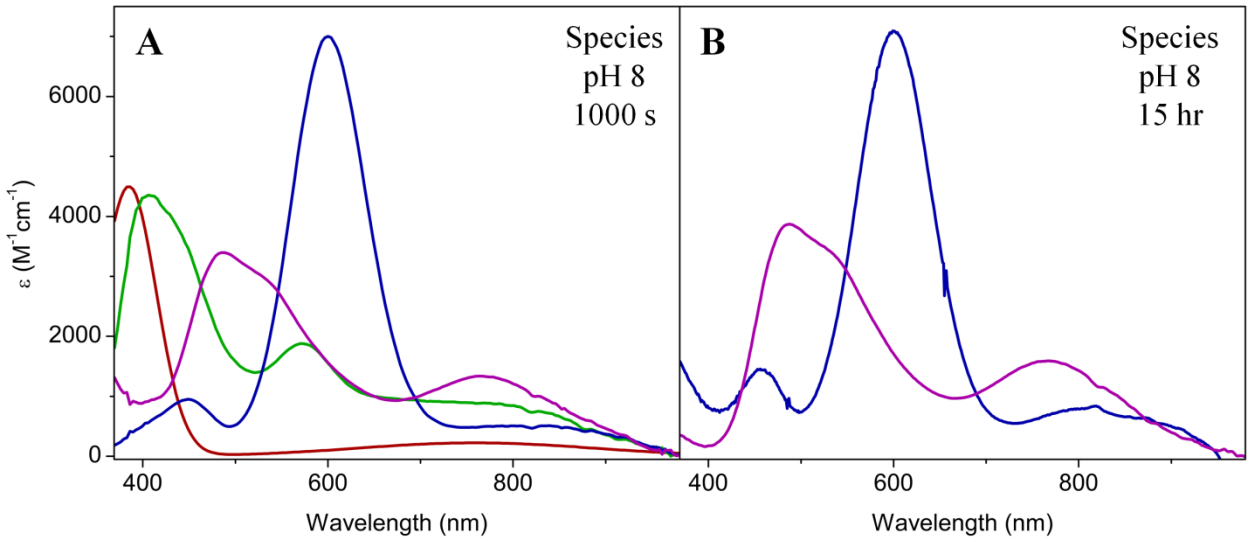

Fig. 3.12. Resolved species spectra for T2 Cu (red), I_X (green), T1 Cu (blue), and Cu_A (purple) calculated through the fitting of the kinetics for Cu_AAz with 0.4 equivalents $CuSO_4$ at pH 8 up to (A) 1000 s and (B) 15 hrs after $CuSO_4$ addition.

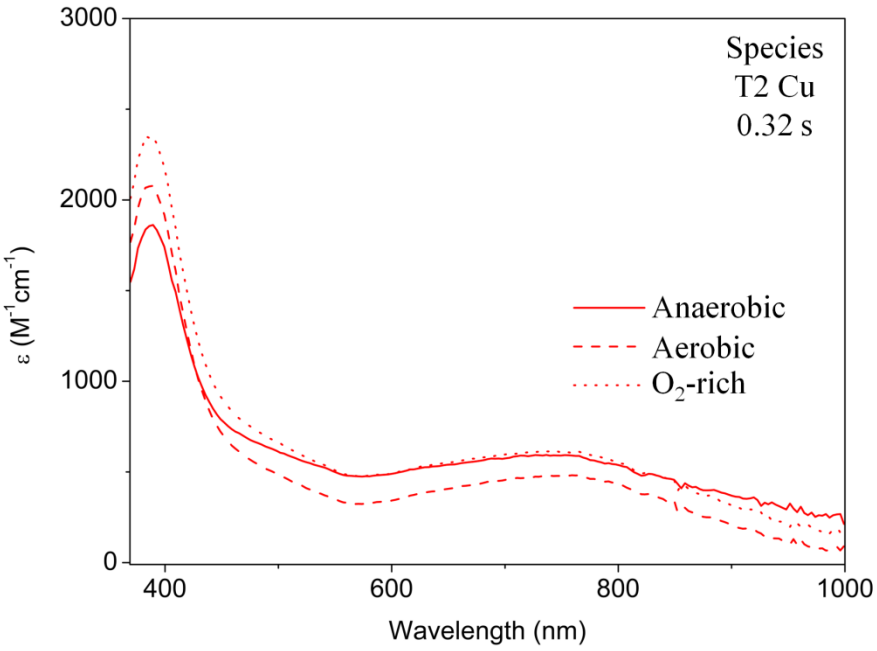

Fig. 3.13. Resolved species spectra for T2 Cu calculated through the fitting of the kinetics for Cu_AAz with 0.1 equivalents $CuSO_4$ at pH 5, over 0.32 s, under anaerobic (solid), aerobic (dashed), and oxygen-rich (dotted) conditions.

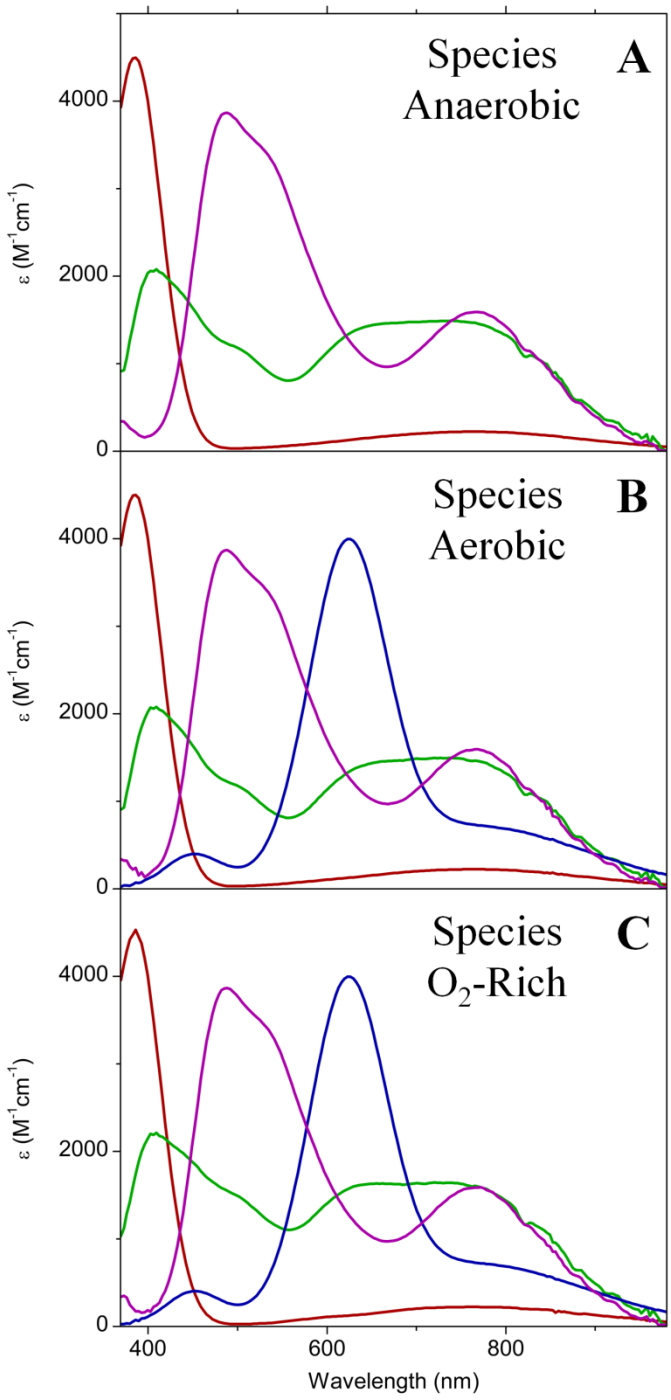

Fig. 3.14. Resolved species spectra for T2 Cu (red), I_X (green), T1 Cu (blue), and Cu_A (purple) calculated through the fitting of the kinetics for Cu_AAz with 0.1 equivalents $CuSO_4$ at pH 5, over 1000 s, under (A) anaerobic, (B) aerobic and (C) oxygen-rich conditions.

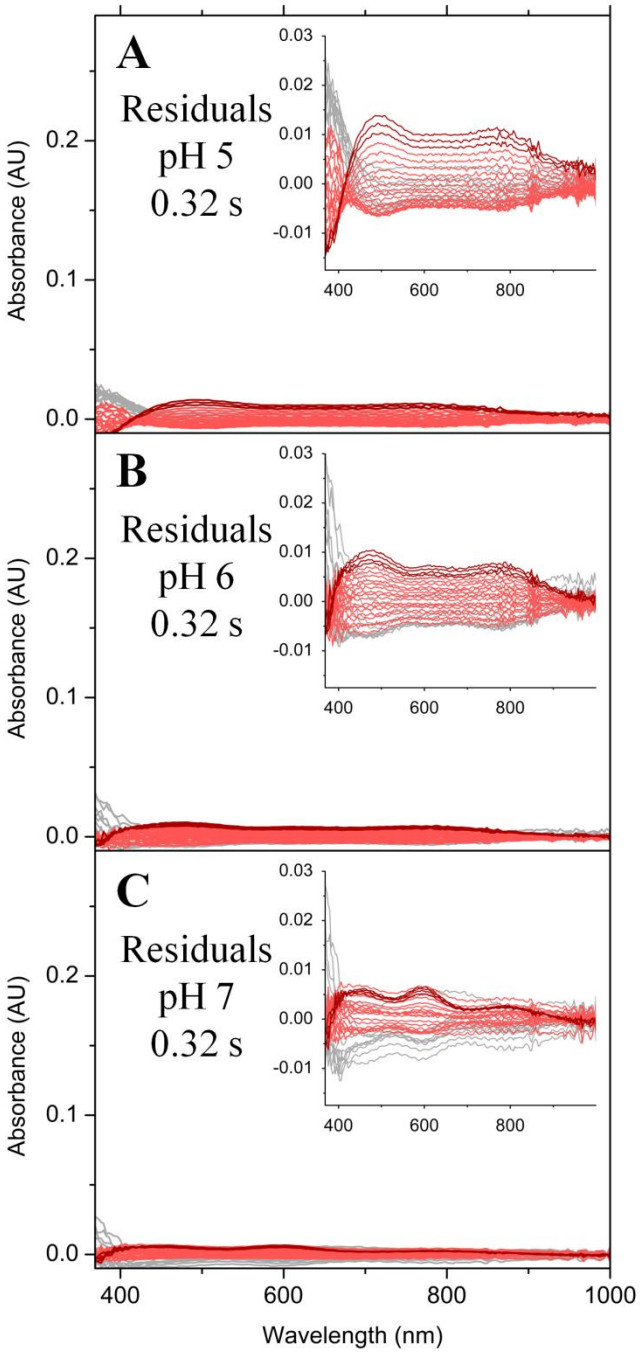

Fig. 3.15. Residual spectra from fitting process of the kinetics for Cu_AAz with 0.4 equivalents $CuSO_4$ over 0.32 s at (A) pH 5, (B) pH 6, and (C) pH 7, plotted on the same scale as the original spectra for comparison. Inset: zoom in of residual spectra.

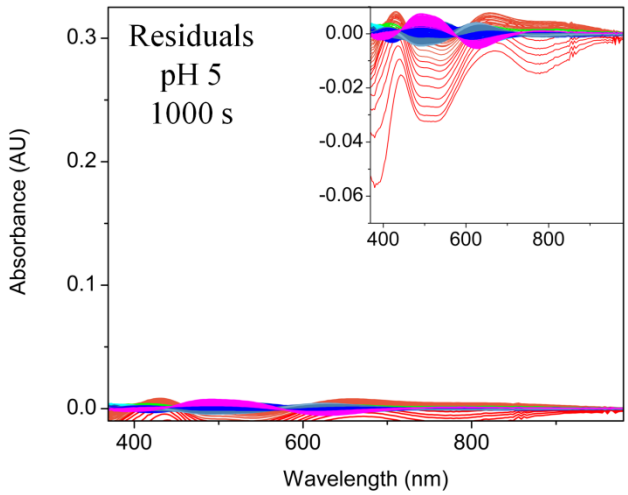

Fig. 3.16. Residual spectra from fitting process of the kinetics for Cu_AAz with 0.4 equivalents $CuSO_4$ at pH 5 over 1000 s, plotted on the same scale as the original spectra for comparison. Inset: zoom in of residual spectra. Residual spectra are colored to correspond to spectra in original data.

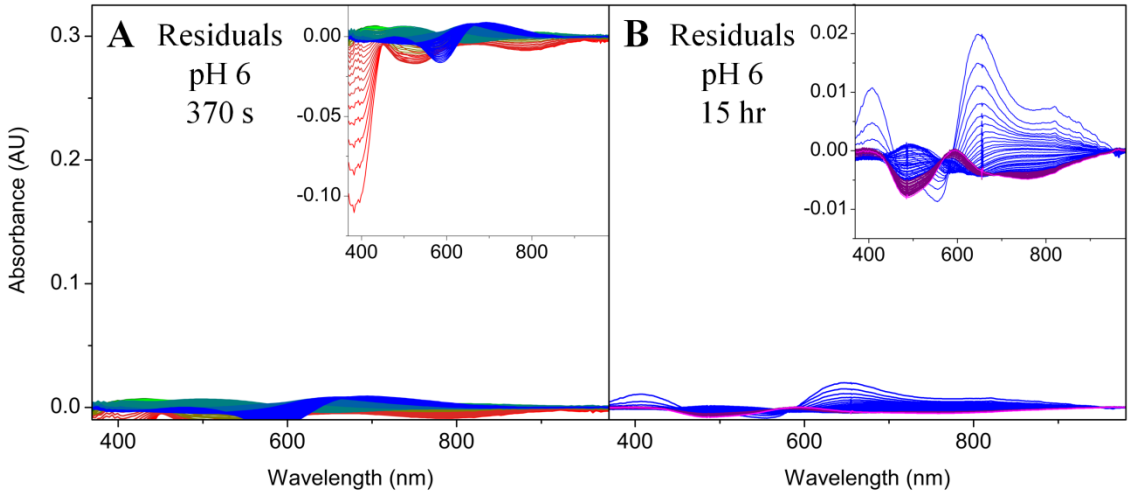

Fig. 3.17. Residual spectra from fitting process of the kinetics for Cu_AAz with 0.4 equivalents $CuSO_4$ at pH 6 up to (A) 370 s and (B) 15 hrs after $CuSO_4$ addition, plotted on the same scale as the original spectra for comparison. Inset: zoom in of residual spectra. Residual spectra are colored to correspond to spectra in original data.

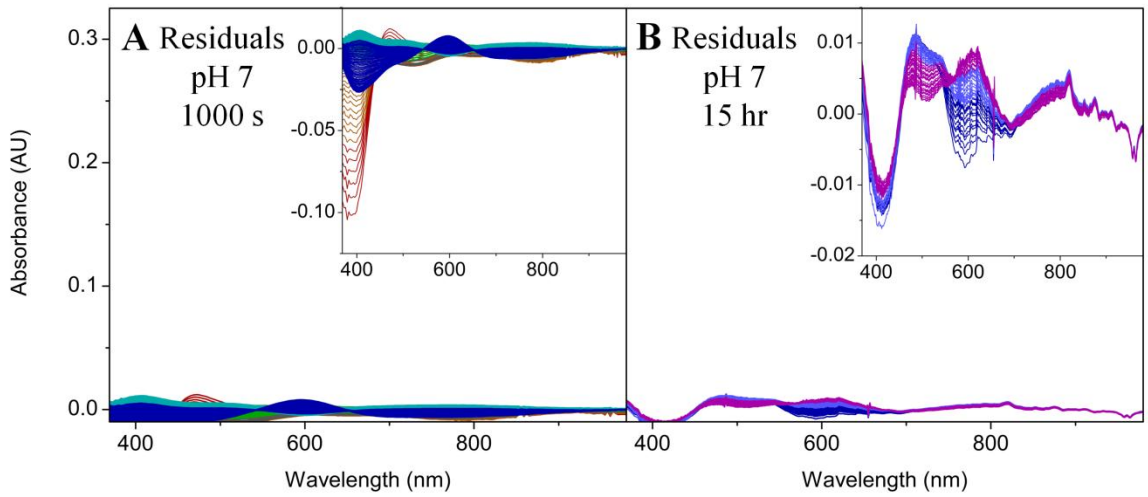

Fig. 3.18. Residual spectra from fitting process of the kinetics for Cu_AAz with 0.4 equivalents $CuSO_4$ at pH 7 up to (A) 1000 s and (B) 15 hrs after $CuSO_4$ addition, plotted on the same scale as the original spectra for comparison. Inset: zoom in of residual spectra. Residual spectra are colored to correspond to spectra in original data.

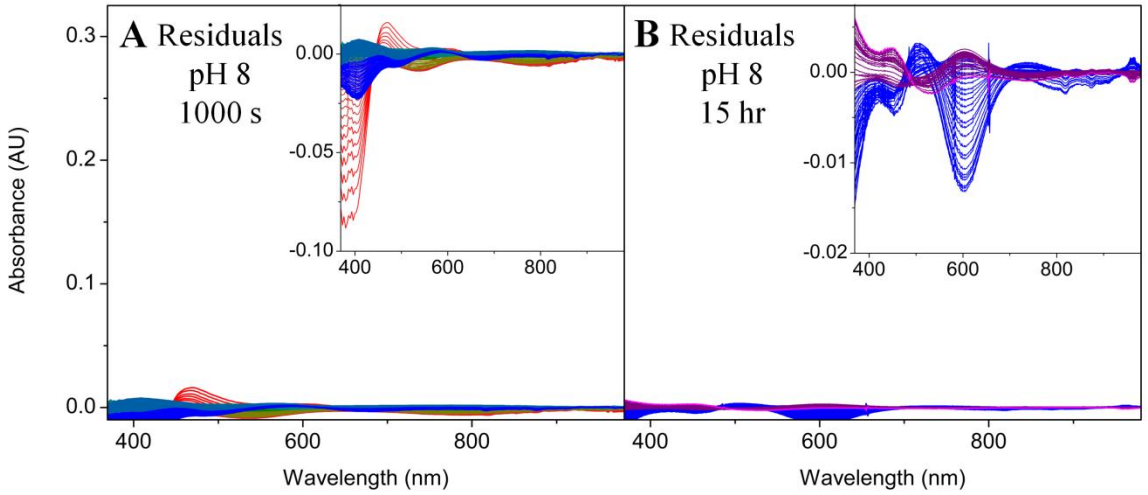

Fig. 3.19. Residual spectra from fitting process of the kinetics for Cu_AAz with 0.4 equivalents $CuSO_4$ at pH 8 up to (A) 1000 s and (B) 15 hrs after $CuSO_4$ addition, plotted on the same scale as the original spectra for comparison. Inset: zoom in of residual spectra. Residual spectra are colored to correspond to spectra in original data.

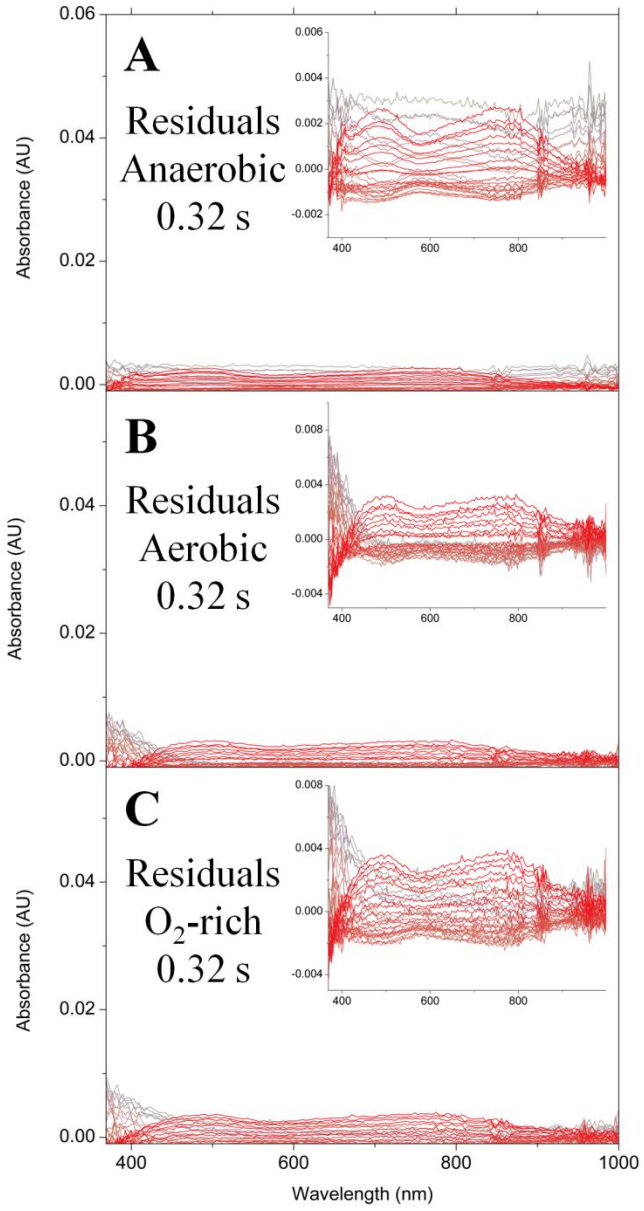

Fig. 3.20. Residual spectra from fitting process of the kinetics for Cu_AAz with 0.1 equivalents $CuSO_4$ over 0.32 s at pH 5, under (A) anaerobic, (B) aerobic, and (C) O_2-rich conditions, plotted on the same scale as the original spectra for comparison. Inset: zoom in of residual spectra. Residual spectra are colored to correspond to spectra in original data.

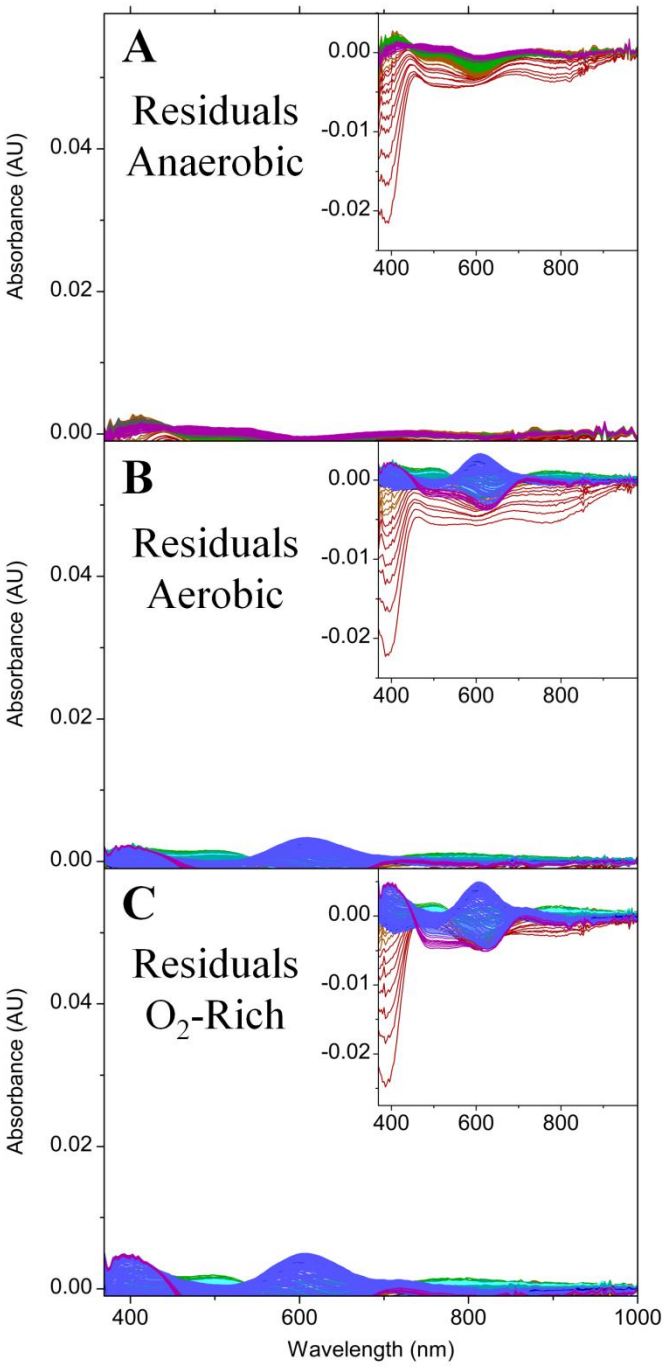

Fig. 3.21. Residual spectra from fitting process of the kinetics for Cu_AAz with 0.1 equivalents $CuSO_4$ at pH 5, over 1000 s, under (A) anaerobic, (B) aerobic and (C) oxygen-rich conditions. Spectra are plotted on the same scale as the original spectra for comparison. Inset: zoom in of residual spectra. Residual spectra are colored to correspond to spectra in original data.

3.3. Results

3.3.1. pH-dependent copper incorporation into apo-Cu_AAz

As the formation of intermediates during copper incorporation into the Cu_A center of N_2OR was pH-dependent, a similar investigation of pH-dependence during metalation of Cu_A in Cu_AAz was undertaken. Addition and rapid mixing of a sub-saturating 0.4 equivalents of $CuSO_4$ with 0.25 mM apo-Cu_AAz at pH 5 in the stopped-flow apparatus resulted in the ultraviolet-visible absorbance (UV-Vis) spectra in Fig. 3.22A and Fig. 3.23A over the following 0.32 s and 1000 s, respectively. The concentration profiles obtained for these kinetic data based on global analysis are shown in Fig. 3.22B and Fig. 3.23B. Spectra corresponding to each of the intermediates and Cu_A, as well as the kinetic models yielding optimal fits with associated observed rate constants, are summarized in Scheme 3.2. In general, the processes observed at pH 5 are similar to those observed at pH 6 (see Chapter 2 and Fig. 3.22C, DFig. 3.23C, D). First, a spectrum with an intense absorbance maximum at ~385 nm, typical of a T2 red Cu center, appeared within 0.3 s (Fig. 3.22A). A spectrum very similar to this one was observed previously as an intermediate during formation of Cu_A at pH 5 with higher equivalents copper.[143] This initial $CuSO_4$ to T2 Cu step was too rapid to be captured in the same dataset as some of the slower processes (i.e. in the 1000 s set of spectra in Fig. 3.23A), so this process was fit separately, using a portion of a dataset collected over 50 s (Fig. 3.22A). In the present study, this ~385 nm peak subsequently decayed and shifted to ~410 nm, with absorption bands at 475, 625 and 760 nm growing in intensity over the same time period. This process completed in ~ 3 s after addition of copper, and is equivalent to the T2 to intermediate X (I_X) process observed at pH 6. However, this process is faster at pH 5 than at pH 6 (complete in ~ 3 s vs. 9.4 s). Over the next 6.5 s, the absorptions due to I_X decreased, while the shoulder at ~625 nm intensified slightly and shifted to ~620 nm, suggesting moderate accumulation of a T1 blue Cu intermediate. This step too is faster at pH 5 than at pH 6, where the decay of I_X and formation of T1 blue Cu in not complete until ~370 s. Beyond 9.4 s, the absorption bands associated with I_X continued to decay, and the intensity of the shoulder at ~620 nm also diminished, while a spectrum with absorption maxima at ~480, 530 and 760 nm emerged, typical of the Cu_A center in Cu_AAz.[107,142] An isosbestic point at 580 nm was present between the spectrum of T1 blue Cu and that of Cu_A during this final timeframe, implying conversion of the T1 blue Cu intermediate to Cu_A.

The kinetic processes observed by stopped-flow and standard UV-Vis absorption spectroscopy are described in detail in Chapter 2, and are included here (Fig. 3.22C, D and Fig. 3.23C, D) only for comparison to the data collected at other pH values. The spectral changes and intermediate formation at pH 7 (Fig. 3.22E, F and Fig. 3.23E, F) were, like the pH 5 case, similar to those at pH 6, with some differences. First, the kinetics of the intermediate and final Cu_A product formation were slowed. Higher absorptions from the T2 Cu, I_X and T1 Cu intermediates were also observed, including a significant contribution of the T1 blue Cu intermediate in the final spectrum collected at 15 hours (Fig. 3.23E plus inset). As a result, clearer isosbestic points at 554 and 681 nm between the spectrum of I_X and that of T1 Cu were observed, suggesting a clean conversion of I_X to the T1 Cu center.

At pH 8, the initial processes are similar to those at the other pHs, including initial formation of a T2 red Cu intermediate and subsequent formation of I_X (Fig. 3.23G, H). However, the following step that occurs at pH 5-7, i.e. formation of a peak corresponding to a T1 blue Cu intermediate, is absent at pH 8. At both pH 7 and 8, a significant contribution of a T1 blue Cu peak is seen at the end of I_X formation. This peak is seen to be stable at pH 8 during I_X decay, suggesting that it actually corresponds to some T1 blue Cu formation. The same is likely true at pH 7, but the fate of that peak is unclear due to formation of T1 blue Cu from I_X. This small ~600 nm peak then decays slowly, while the transitions due to Cu_A increase (Fig. 3.23G, inset). Therefore, the overall set of processes at pH 8 appears to be similar to those at lower pH values, except that the I_X to T1 blue Cu step is missing.

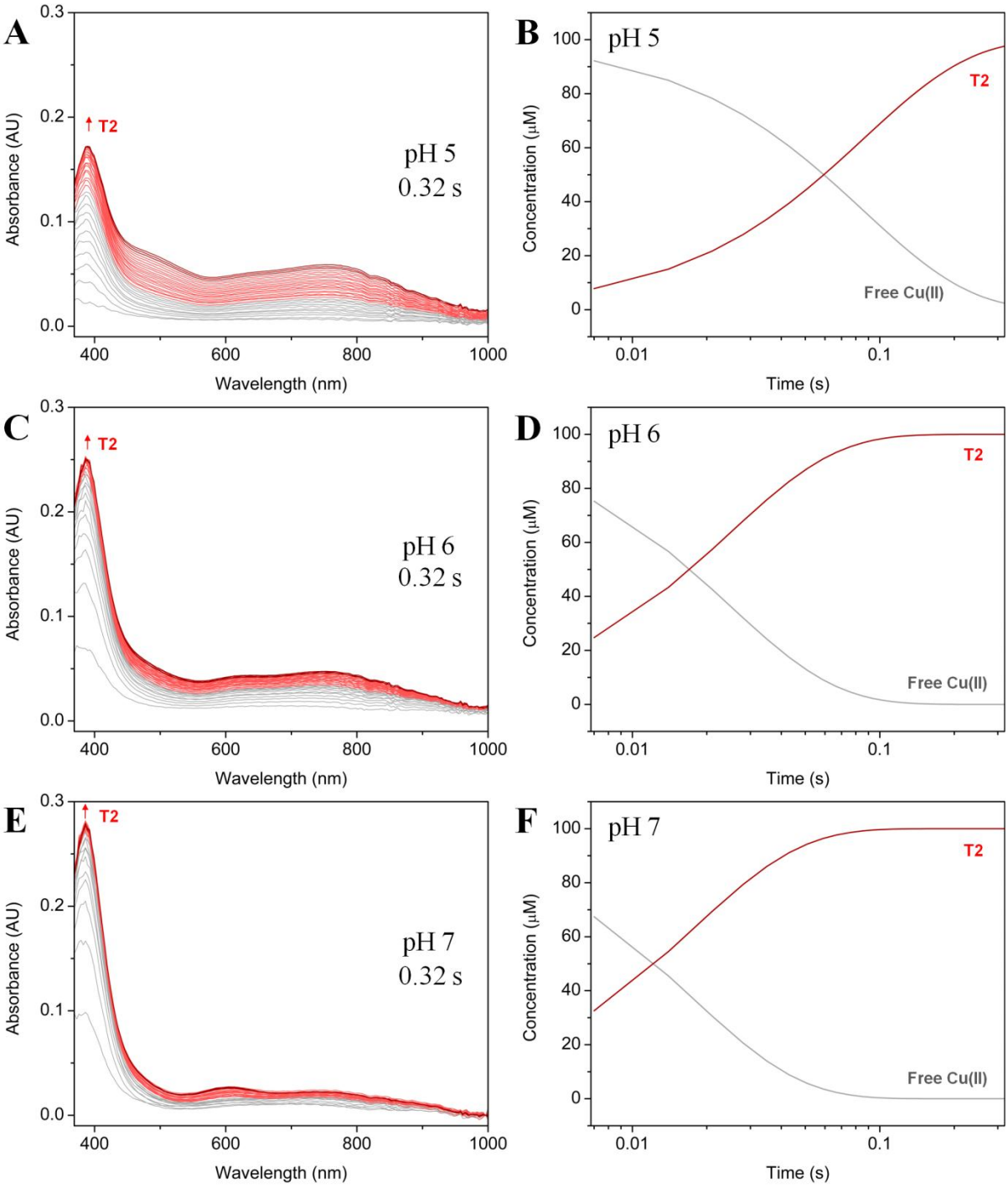

Fig. 3.22. Stopped-flow UV-vis absorbance spectra (A, C, E) and corresponding concentration profiles (B, D, F) after mixing of a sub-saturating 0.4 equivalents of $CuSO_4$ with Cu_AAz over 0.32 s at (A, B) pH 5, (C, D) pH 6, and (E, F) pH 7 in UB. (A, C, E) Spectra are colored to indicate the species forming at that particular time. Arrows indicate direction of change in absorbance over course of experiment and are colored to correspond to the species giving rise to that peak. Final Cu_AAz concentrations were 0.25 mM and $CuSO_4$ concentrations were 0.1 mM. Stopped-flow spectra were collected in each case with a logarithmic scale over 50 s and 200 total

spectra. The first spectrum was collected at 0.007 s, and the final spectrum displayed here is at 0.318 s (pH 5) or 0.334 s (pH 6 and 7). (B, D, F) Concentration profiles are those resulting from global analysis of the corresponding kinetics data. Further information about the global analysis process may be found in the experimental section about fitting of the kinetics data.

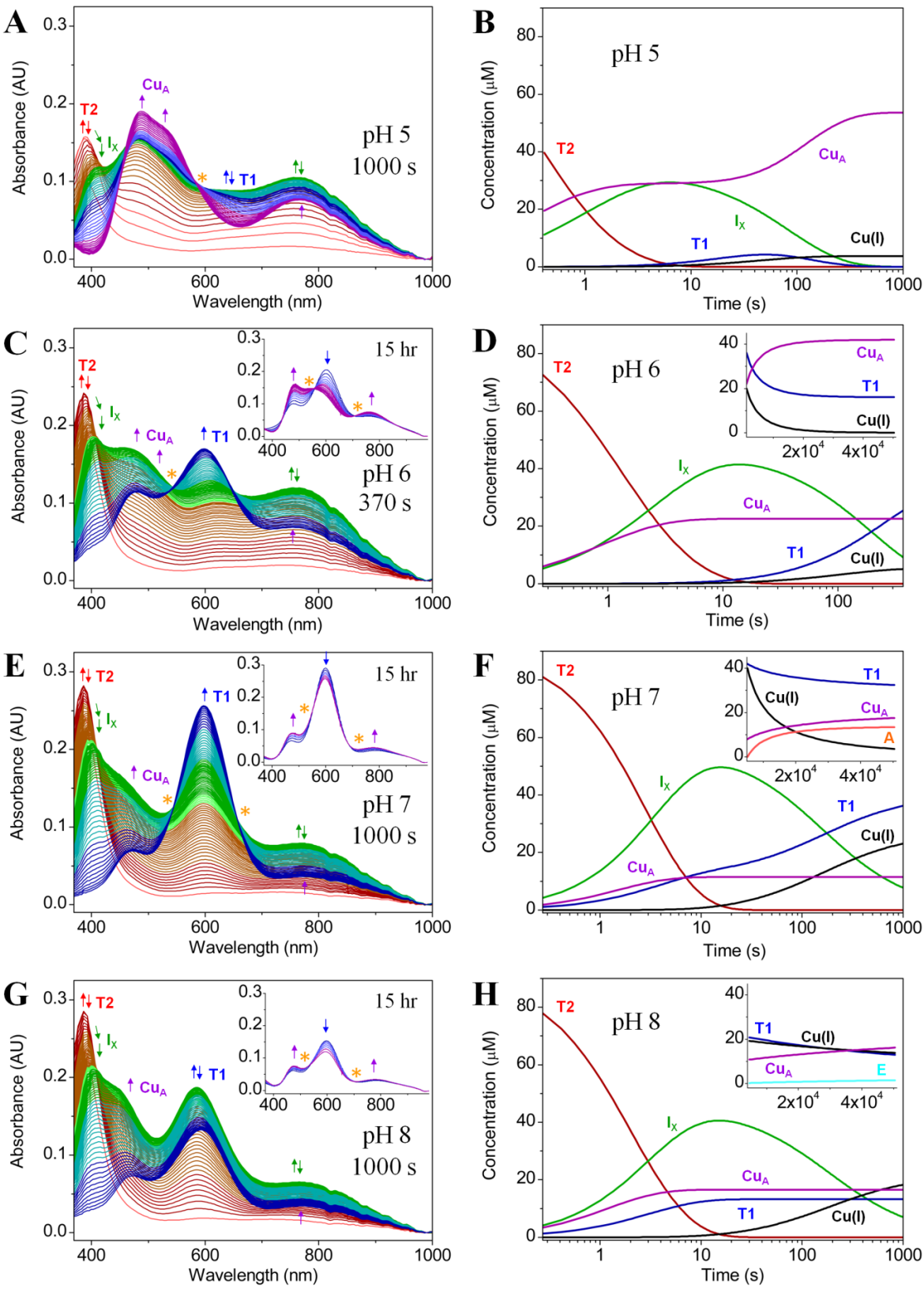

Fig. 3.23 (continued on next page)

Fig. 3.23. Stopped-flow UV-vis absorbance spectra (A, C, E) and corresponding concentration profiles (B, D, F) after mixing of a sub-saturating 0.4 equivalents of $CuSO_4$ with Cu_AAz over (A, B) 1000s at pH 5, (C, D) 370s at pH 6, (E, F) 1000 s at pH 7, and (G, H) 1000 s at pH 8 in UB. Insets: UV-Vis absorbance spectra (A, C, E, G) and corresponding concentration profiles (B, D, F, H) of subsequent overnight process (final timepoint: 15 hours from $CuSO_4$ addition). Full data sets corresponding to the overnight processes in the insets can be found in Fig. 3.2. (A, C, E, G) Spectra are colored to indicate the species forming at that particular time. Arrows indicate direction of change in absorbance over course of experiment and are colored to correspond to the species giving rise to that peak. Golden asterisks indicate the positions of apparent isosbestic points. Final Cu_AAz concentrations were 0.25 mM and $CuSO_4$ concentrations were 0.1 mM. Stopped-flow spectra were collected in each case with a logarithmic scale over 1000 s and 200 total spectra. The first spectrum was collected at 0.134 s. For the overnight UV-Vis data collection, spectra were collected initially with a 0.5 s scantime, which was incremented by 5% after 45 s over 900 s (pH 6, 7 and 8), to make sure that the initial portion of the data matched that collected on the stopped-flow instrument (Fig. 3.2). The spectra shown in the insets were collected with a 600 s scantime, which was incremented by 1% after 3600 s over 50400 s (14 hours). An additional two hours of spectra were collected at 600 s intervals in the case of the pH 7 set of data, to ensure that no further significant changes were occurring (data not shown). (B, D, F, H) Concentration profiles are those resulting from global analysis of the corresponding kinetics data. Further information about the global analysis process may be found in the experimental section about fitting of the kinetics data.

Scheme 3.2. Summary of species observed by UV-Vis absorption spectroscopy and models yielding optimal fits for the kinetics of pH-dependent, aerobic copper incorporation and oxygen-dependent, pH 5, copper incorporation into Cu_AAz. The representative UV-Vis spectra are those resolved by the global analysis of the data from Cu_AAz at pH 5, with addition of 0.4 equivalents $CuSO_4$.

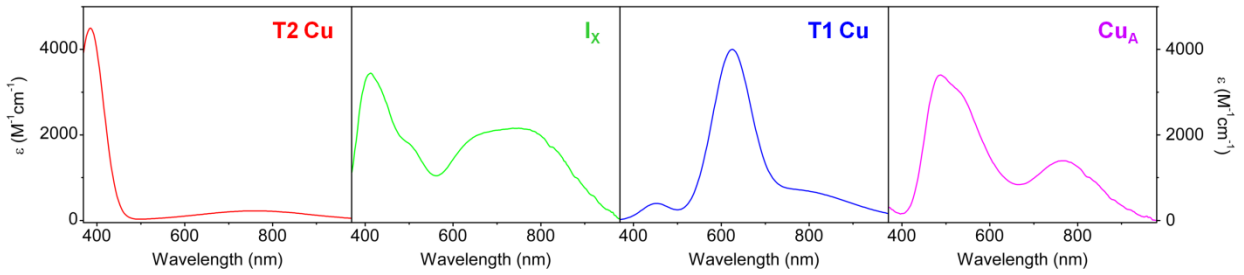

Summary of Models Yielding Optimal Fits for pH- and O_2-Dependent Kinetics of Cu_AAz upon Addition of $CuSO_4$

pH 5	$CuSO_4 \rightarrow$ T2	11.7 ± 1.2 s^{-1}	**Anaerobic**	$CuSO_4 \rightarrow$ T2	15.1 ± 1.2 s^{-1}
	2 T2 → Cu_A	(12.9 ± 0.52)×10^3 $M^{-1}s^{-1}$		2 T2 → Cu_A	(17.2 ± 0.5) × 10^3 $M^{-1}s^{-1}$
	T2 → I_X	0.460 ± 0.034 s^{-1}		T2 → I_X	0.854 ± 0.022 s^{-1}
	2 I_X → Cu(I)	82.2 ± 11.9 $M^{-1}s^{-1}$		2 I_X → Cu(I)	48.5 ± 0.9 $M^{-1}s^{-1}$
	I_X → T1	(7.93 ± 0.40)×10^{-3} s^{-1}		I_X + Cu(I) → Cu_A	235 ± 19 $M^{-1}s^{-1}$
	T1 → Cu_A	(3.37 ± 0.03)×10^{-2} s^{-1}			
pH 6	$CuSO_4 \rightarrow$ T2	40.6 ± 2.9 s^{-1}	**Aerobic**	$CuSO_4 \rightarrow$ T2	11.8 ± 1.1 s^{-1}
	2 T2 → Cu_A	(3.39 ± 0.11)×10^3 $M^{-1}s^{-1}$		2 T2 → Cu_A	(13.2 ± 1.1) × 10^3 $M^{-1}s^{-1}$
	T2 → I_X	0.241 ± 0.007 s^{-1}		T2 → I_X	0.831 ± 0.031 s^{-1}
	2 I_X → Cu(I)	25.6 ± 1.0 $M^{-1}s^{-1}$		2 I_X → Cu(I)	59.5 ± 2.7 $M^{-1}s^{-1}$
	I_X → T1	(3.25 ± 0.10)×10^{-3} s^{-1}		I_X → T1	(9.28 ± 0.24) × 10^{-4} s^{-1}
	T1 + Cu(I) → Cu_A	6.99 ± 0.36 $M^{-1}s^{-1}$		T1 → Cu_A	(1.63 ± 0.11) × 10^{-3} s^{-1}
pH 7	$CuSO_4 \rightarrow$ T2	56.3 ± 3.5 s^{-1}	**O_2-Rich**	$CuSO_4 \rightarrow$ T2	14.6 ± 1.4 s^{-1}
	2 T2 → Cu_A	(0.948 ± 0.047)×10^3 $M^{-1}s^{-1}$		2 T2 → Cu_A	(10.5 ± 1.3) × 10^3 $M^{-1}s^{-1}$
	T2 → T1	(4.43 ± 0.27)×10^{-2} s^{-1}		T2 → I_X	0.944 ± 0.038 s^{-1}
	T2 → I_X	0.182 ± 0.006 s^{-1}		2 I_X → Cu(I)	60.4 ± 2.7 $M^{-1}s^{-1}$
	2 I_X → T1 + Cu(I)	55.7 ± 2.8 $M^{-1}s^{-1}$		I_X → T1	(9.28 ± 0.24) × 10^{-4} s^{-1}
	T1 + Cu(I) → Cu_A	0.521 ± 0.023 $M^{-1}s^{-1}$		T1 → Cu_A	(1.58 ± 0.09) × 10^{-3} s^{-1}
	[a] 2 Cu(I) → A	1.60 (fixed) $M^{-1}s^{-1}$			

3.3.2. Time dependent EPR spectral studies of Cu_AAz after addition of a sub-saturating amount of $CuSO_4$

In order to further characterize the intermediates over the course of copper incorporation, EPR spectra were collected at various times after adding a sub-saturating amount of $CuSO_4$ (Fig. 3.24, Table 3.3). The pH 7 and 0.1 equivalents of $CuSO_4$ were chosen for this set of experiments, since the rates of conversion of the intermediates were slower and greater accumulation of the intermediates occurred under these conditions, which made capture of all of the intermediates by EPR more feasible. An EPR sample of Cu_AAz, 100 ms after mixing with 0.1 equivalents of $CuSO_4$, was prepared using a freeze quench apparatus, and the spectrum in Fig. 3.24A was

collected as a result. This spectrum was fit by a single species using EPR spectral simulation, and this species displayed A_z = |147| × 10^{-4} cm^{-1} (Table 3.3), typical of T2 Cu centers.[65] Stopped-flow UV-Vis spectra collected under the same conditions of ten-fold excess protein indicated that the initial T2 Cu intermediate is maximized by 100 ms (Fig. 3.25). Therefore, the species at 100 ms is assigned as the T2 Cu intermediate. Freeze quench samples prepared at 1, 5, and 10 s after $CuSO_4$ addition show the gradual decay of the T2 Cu species, and the growth of a new set of species, consistent with the timeframe for the decay of the T2 Cu intermediate, and the subsequent 30 s spectrum (Fig. 3.25 and Fig. 3.26).

Another sample of Cu_AAz was flash frozen 30 s after the addition of $CuSO_4$, and the EPR spectrum in Fig. 3.25B was collected. UV-Vis spectra collected for an identically prepared sample indicate that I_X and rapidly-formed Cu_A (Cu_A') were present in this sample at 30 s (Fig. 3.27). Thus, as expected, this early spectrum could not be assigned to a single Cu(II) species. EPR spectral simulation suggested the presence of one distinct species with a well-resolved axial spectrum, having small g_z = 2.200 and A_z = |47| × 10^{-4} cm^{-1} (Table 3.3). These parameters are similar to the published parameters for a mutant in which His120 is removed (H120A-Cu_AAz, Table 3.3),[140] leading to the assignment of this species as Cu_A', or fully reconstituted Cu_A lacking His120 coordination, formed rapidly from the T2 Cu intermediate. Due to the overlap of this rapidly formed Cu_A with other species, Cu_A' and normal Cu_A (i.e. with His120 coordination) cannot be distinguished in the corresponding UV-Vis spectrum.[154] For this reason, in the kinetic models of the UV-Vis absorbance data, both Cu_A' and Cu_A were treated as a single species (Cu_A). This treatment is valid because both species are Cu_A, just slightly different forms of it. As the changes in the absorptions of Cu_A upon protonation/deprotonation of His120 are minimal, any error introduced as a result of this treatment is minor. In the 30 s spectrum, a second species was also observed, which simulation showed to have features intermediate between a T1 and T2 Cu complex, with g_z = 2.234 and A_z = |115| × 10^{-4} cm^{-1} (see Table 3.3). This species was tentatively assigned to I_X, as all other intermediates identified by electronic absorption spectroscopy were assigned, and the population of this species correlated well with that of I_X from UV-Vis absorbance kinetics.

At 7 minutes after $CuSO_4$ addition, the signals that were dominant in the 30 s spectrum began to decay, and a species with g_z ~ 2.3 was observed, which gains intensity up to 30 min.

The UV-Vis spectra collected for an identically prepared sample show the absorbance band from the T1 blue Cu intermediate increases during this interval (Fig. 3.27). Simulation of the EPR spectra containing this species found relatively large *g*-values (g_x = 2.013, g_y = 2.063, and g_z = 2.307) and small (unresolved) hyperfine splittings along all directions (A_x = |24| × 10^{-4} cm^{-1}, A_y = A_z = |30| × 10^{-4} cm^{-1}), as compared to typical copper complexes. This spectrum, which we assigned to the T1 blue Cu intermediate based on the parameters and the corresponding UV-Vis spectra (Fig. 3.9, Fig. 3.12, Fig. 3.14), was strikingly similar to the previously reported EPR spectrum of C116S Cu_AAz.[156] To gather further support for the EPR spectral similarity of the T1 blue Cu to that of C116S Cu_AAz, an EPR spectrum of the C116S variant of Cu_AAz was also collected under the same condition for direct comparison. As expected, the EPR spectrum of this C116S variant is almost identical to that of the third species recognized in the EPR spectra of Cu_A.

Meanwhile, starting at 7 min and continually increasing throughout the rest of the experiment, yet another species, with three hyperfine peaks visible between *g* = 2.14 and 2.27 and distinct features in the perpendicular range, became visible. From the nearly pure spectrum of this species, collected at 24 hours after $CuSO_4$ addition, this species was readily identified as Cu_A, as its parameters (Table 3.3) and seven-line hyperfine splitting pattern are almost identical to previous spectra.[140,142,154] The timeframe for this process is also consistent with the UV-Vis data collected under these conditions (Fig. 3.27).

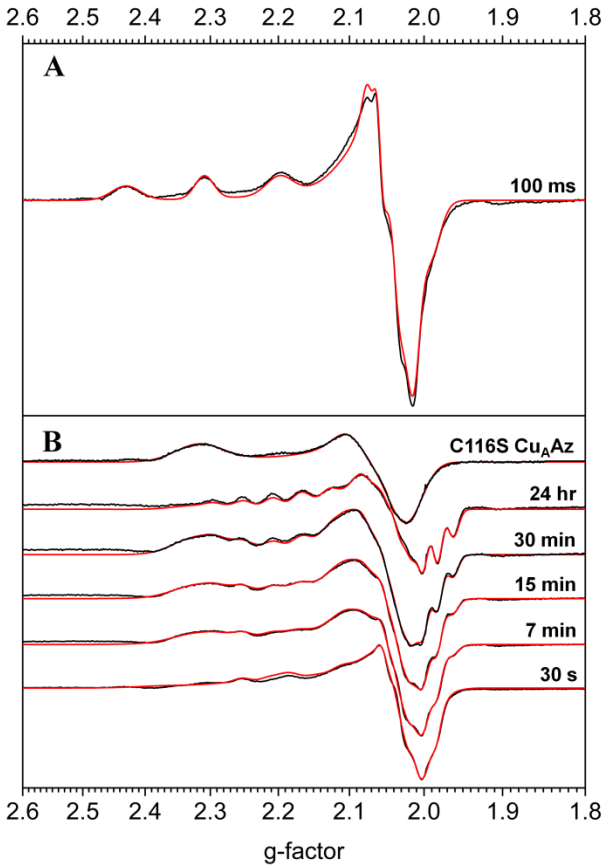

Fig. 3.24. EPR spectra of Cu_AAz, pH 7 in TIP buffer, (A) at 100 ms and (B) at 30 s, 7 min, 15 min, 30 min, and 24 hours after $CuSO_4$ addition, where the indicated times are incubation times at room temperature (20 °C, up to 30 min) or 4 °C (24 hr sample). An EPR spectrum of C116S Cu_AAz, pH 7 in TIP buffer is shown for direct comparison. Black spectra are the experimental data, whereas red spectra are the corresponding simulated data. Concentration of the Cu_AAz sample is 4 mM, while the $CuSO_4$ concentration is 0.4 mM. For the C116S Cu_AAz sample, protein concentration is 2 mM and the $CuSO_4$ concentration, 0.5 mM. Approximately 10% (100 ms) and 30% glycerol is present in the samples, as a glassing agent. X-band experimental conditions: microwave frequency, 9.05 GHz; power, 0.2 mW (C116S), 0.5 mW (30s, 24 hr), 1 mW (7, 15, and 30 min), 2 mW (100 ms); modulation amplitude, 2 G (C116S), 4 G (Cu_AAz); sweep time, 60s; gain, 6300 (30s, 24 hr), 10,000 (100 ms, 7, 15, 30 min, C116S); temperature, 33 K. The spike at g = 2.0 is an artifact of the EPR tubes used.

Table 3.3. EPR parameters of the species identified through simulation of spectra in Fig. 3.24 and the various percentages (± 5%) of these species as a function of time, as determined from EPR simulation.

	T2 Cu	Cu_A'	I_X[a]	T1 Cu	Cu_A	C116S Cu_AAz	H120A Cu_AAz[b]
Simulated Parameters of Species							
g_x	2.025	2.004	2.007	2.013	2.015	2.031	2.010

Table 3.3, continued

g_y	2.062	2.030	2.056	2.063	2.026	2.061	2.010
g_z	2.253	2.200	2.234	2.307	2.167	2.314	2.225
A_x (10^{-4} cm^{-1})	14	20	9	24	21 (Cu_1), 21 (Cu_2)	27	24 (Cu_1), 19 (Cu_2)
A_y (10^{-4} cm^{-1})	10	20	0.3	30	20 (Cu_1), 18 (Cu_2)	28	19 (Cu_1), 24 (Cu_2)
A_z (10^{-4} cm^{-1})	147	47	115	30	61 (Cu_1), 60 (Cu_2)	28	46 (Cu_1), 7 (Cu_2)
Population of Species (%) at Time							
100 ms	100	0	0	0	0	--	--
30 s	0	40	55	5	0	--	--
7 min	0	20	20	50	10	--	--
15 min	0	10	15	60	15	--	--
30 min	0	0	0	75	25	--	--
24 hr	0	0	0	30	75	--	--

[a] Tentative assignment. The percentage of this species correlates well with the kinetics of I_X in the electronic absorption spectra, and all other species have been identified. However, as a pure EPR spectrum of this intermediate has not yet been obtained, this assignment must remain tentative.
[b] From reference 64.

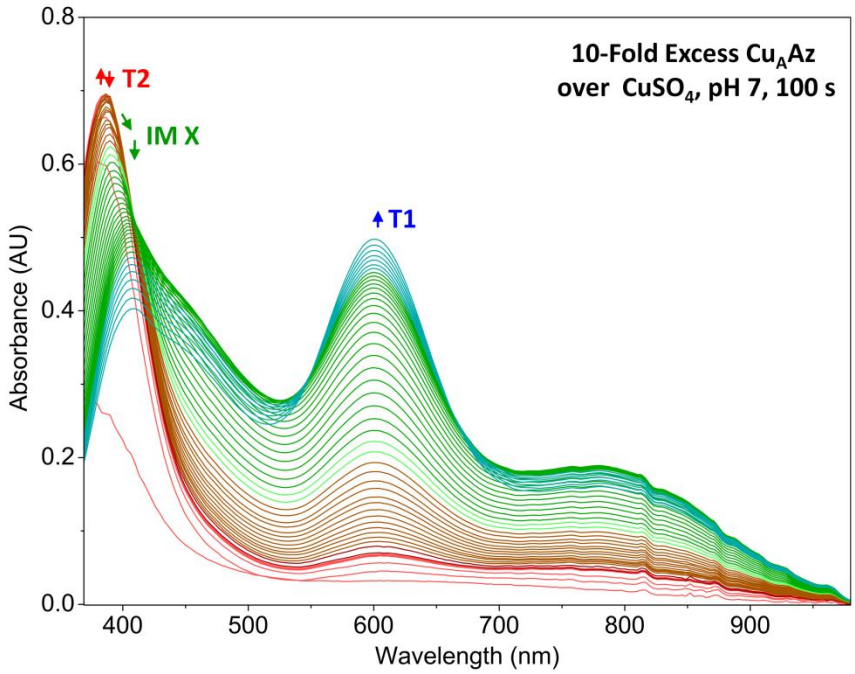

Fig. 3.25. Stopped-flow electronic absorption spectra of Cu_AAz after mixing with 0.1 equivalents $CuSO_4$ at pH 7 in UB over 100 s. Spectra are colored to indicate the species forming at that particular time. Arrows indicate direction of change in absorbance over course of experiment and are colored to correspond to the species giving rise to that peak. Final protein concentration was 3 mM, and $CuSO_4$ was 0.3 mM. Bolded red spectrum indicates the 100 ms timepoint, at which the T2 Cu formation is complete and maximized.

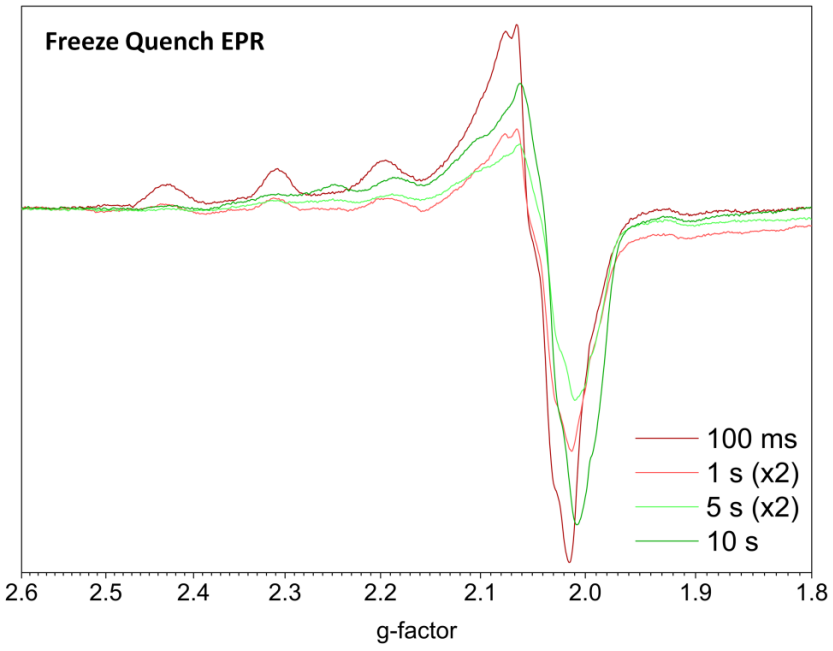

Fig. 3.26 (continued on next page)

Fig. 3.26. EPR spectra of samples prepared using freeze quench procedure, showing progression of species from 100 ms (dark red) to 1 s (pink), 5 s (pale green), and 10 s (dark green). The 1 s and 5 s spectra are displayed at twice the original intensity, to correct for the difference in gain between these spectra and the 100 ms spectrum. The 10 s spectrum was collected at a different power, so its intensity cannot be directly compared to the others. X-band experimental conditions: microwave frequency, 9.05 GHz; power, 1.5 mW (10 s), 2 mW (100 ms, 1 s, 5 s); modulation amplitude, 4 G; sweep time, 60s; gain, 5,000 (1 s, 5 s), 10,000 (100 ms), 12,500 (10 s); temperature, 33 K.

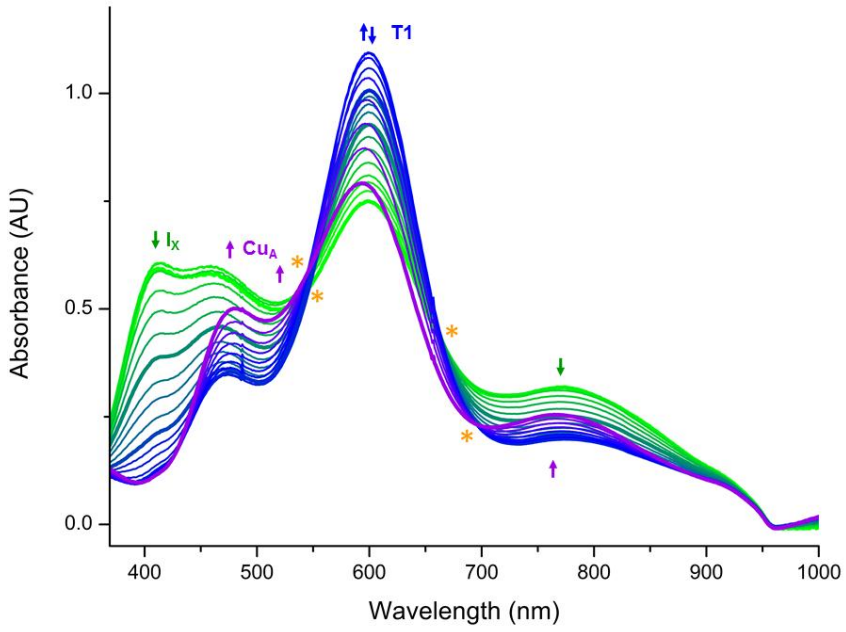

Fig. 3.27. Electronic absorption spectra of Cu_AAz, pH 7, prepared in the same way as the samples were for EPR collection in the main body of the paper. The first spectrum (bright green) was collected 60 s after the addition of 0.1 equivalents $CuSO_4$, and the final spectrum (purple) 13.65 hours after the addition. The first and last spectra, as well as the spectra at 7 and 30 min are bolded. Spectra are colored to indicate the species forming at that particular time. Arrows indicate direction of change in absorbance over course of experiment and are colored to correspond to the species giving rise to that peak. Temperature controller was set to 13 ºC.

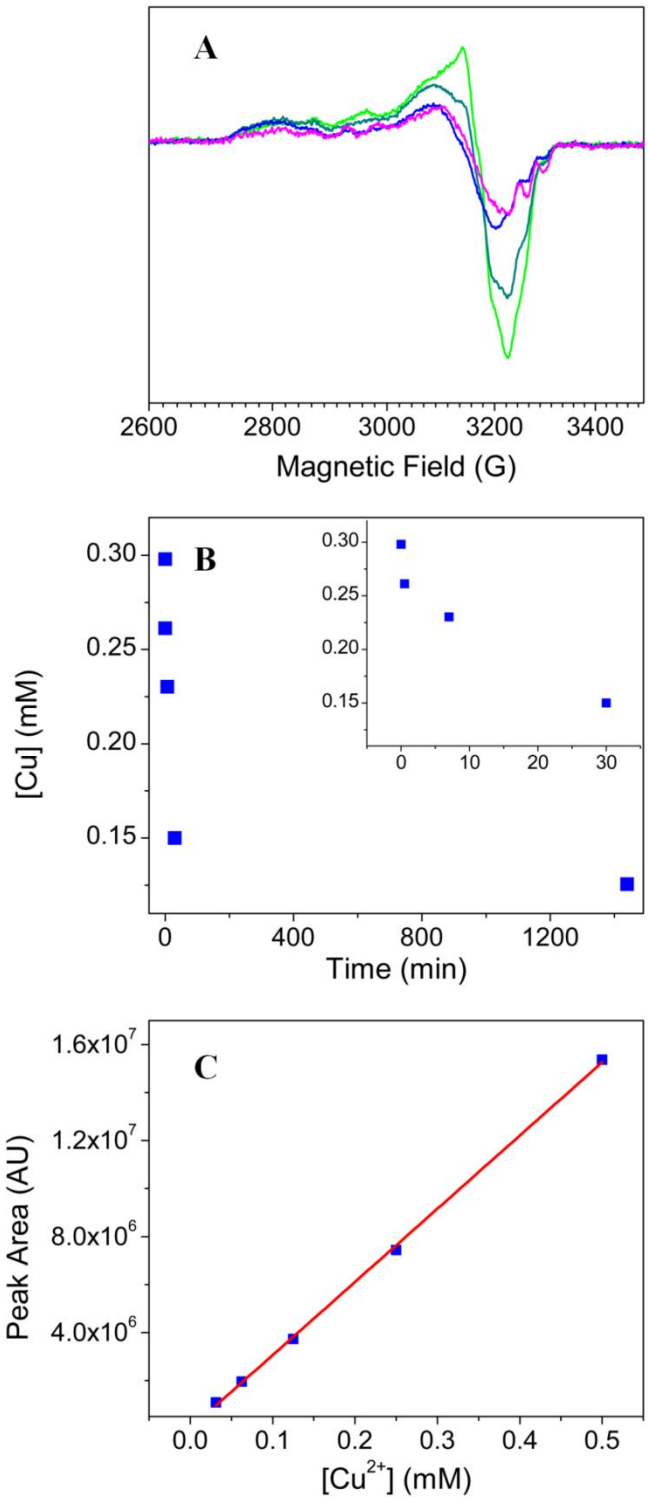

Fig. 3.28. EPR spin counting of Cu_AAz after addition of 0.1 eq $CuSO_4$. (A) EPR spectra of samples flash frozen at 30 s (green), 7 min (blue-green), 30 min (blue), and overnight (purple) after $CuSO_4$ addition. Final protein concentration was 0.3 mM. (B) Quantification of Cu(II)

content for spectra in (A) as a function of time. Inset: zoom in of time points up to 30 min. (C) Standard curve generated from aqueous $CuSO_4$ samples having theoretical concentrations of 0.5, 0.25, 0.125, 0.0625, and 0.03125 mM made through serial dilutions of a volumetrically prepared 0.5 mM stock. The $CuSO_4$ standards contained ~30% glycerol as a glassing agent.

3.3.3. Oxygen-dependent copper incorporation into apo-Cu_AAz

Due to the reported involvement of molecular oxygen in the copper-catalyzed formation of disulfide bonds from thiols,[178-180] stopped-flow absorption spectral studies of Cu_AAz with $CuSO_4$ under anaerobic, aerobic and oxygen-enriched conditions were conducted, to determine whether molecular oxygen played any role during the reconstitution of Cu_A. When Cu_AAz at pH 5 and a sub-saturating 0.1 equivalents of $CuSO_4$ were combined in the stopped-flow instrument under anaerobic, aerobic and oxygen-enriched conditions, the absorption spectra in Fig. 3.29 and Fig. 3.30 were observed over the subsequent 0.32 and 1000 s, respectively. Here, 0.1 equivalents instead of 0.4 equivalents of $CuSO_4$ were added, in order to further slow the kinetics and facilitate the observation of subtle differences in the formation of the intermediates. The initial $CuSO_4$ to T2 Cu step was too rapid to be characterized in the same set of data that was collected over 1000 s, so the kinetics of that step were fit separately, from the first several spectra of a data set collected over 50 s (Fig. 3.29). The appearance and decay of the intermediates shown in Fig. 3.29 and Fig. 3.30 and summarized in Scheme 3.2 was similar under all three conditions to what was observed in Fig. 3.22 and Fig. 3.23, with one key difference: the extent of formation of the ~620 nm peak, associated with the T1 blue Cu intermediate, correlates with the concentration of dissolved molecular oxygen.

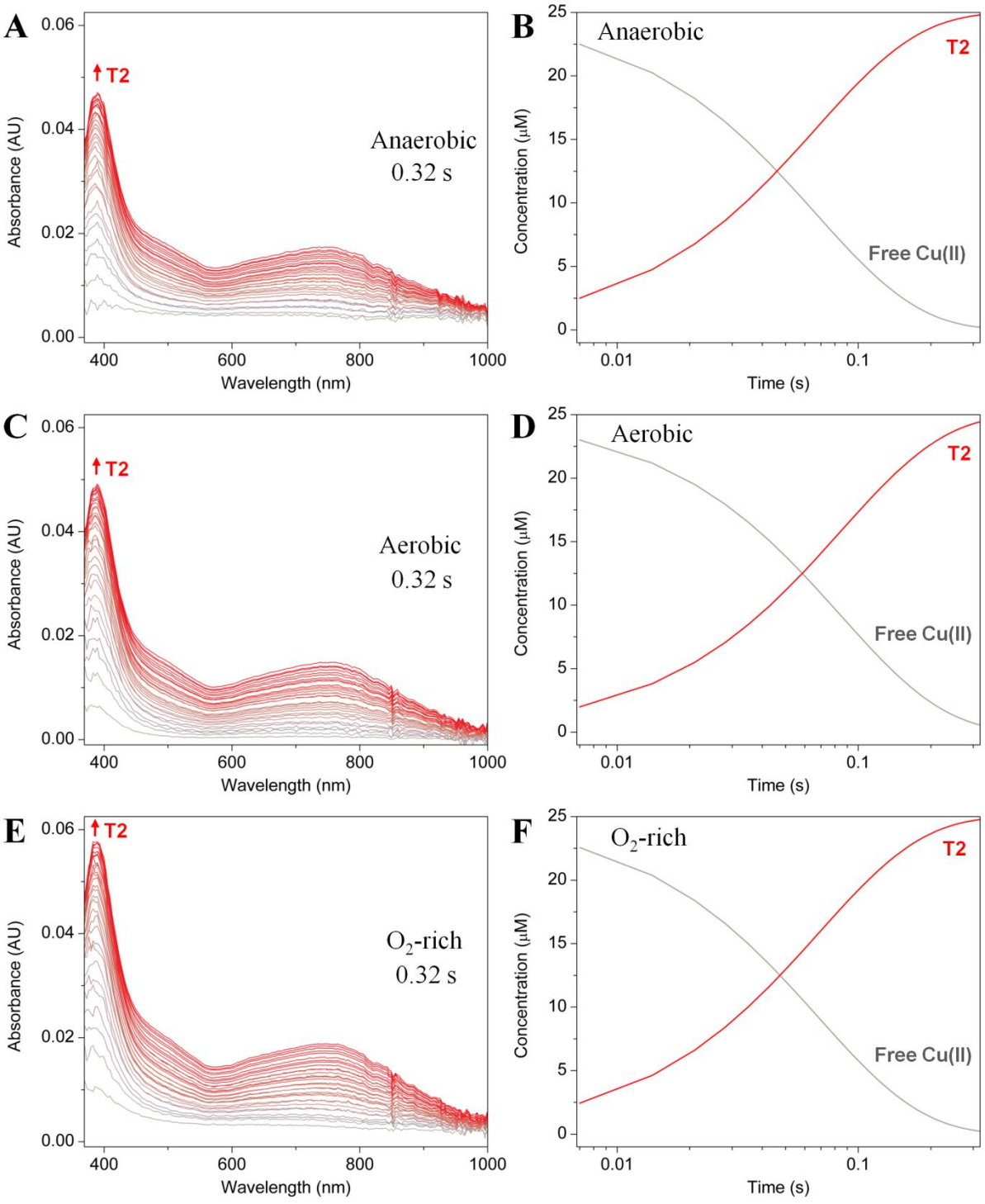

Fig. 3.29. Stopped-flow UV-vis absorbance spectra (A, C, E) and corresponding concentration profiles (B, D, F) after mixing of a sub-saturating 0.1 equivalents of $CuSO_4$ with Cu_AAz over 0.32 s at pH 5 under (A, B) anaerobic, (C, D) aerobic, and (E, F) oxygen-rich conditions. (A, C, E) Spectra are colored to indicate the species forming at that particular time. Arrows indicate direction of change in absorbance over course of experiment and are colored to correspond to the

species giving rise to that peak. Final protein concentration was 0.25 mM in 50 mM NaOAc, pH 5.0 ± 0.1, and $CuSO_4$, 0.025 mM. Stopped-flow spectra were collected in each case with a logarithmic scale over 50 s and 200 total spectra. The first spectrum was collected at 0.007 s, and the final spectrum displayed is at 0.318s. (B, D, F) Concentration profiles are those resulting from global analysis of the corresponding kinetics data. Further information about the global analysis process may be found in the experimental section about fitting of the kinetics data.

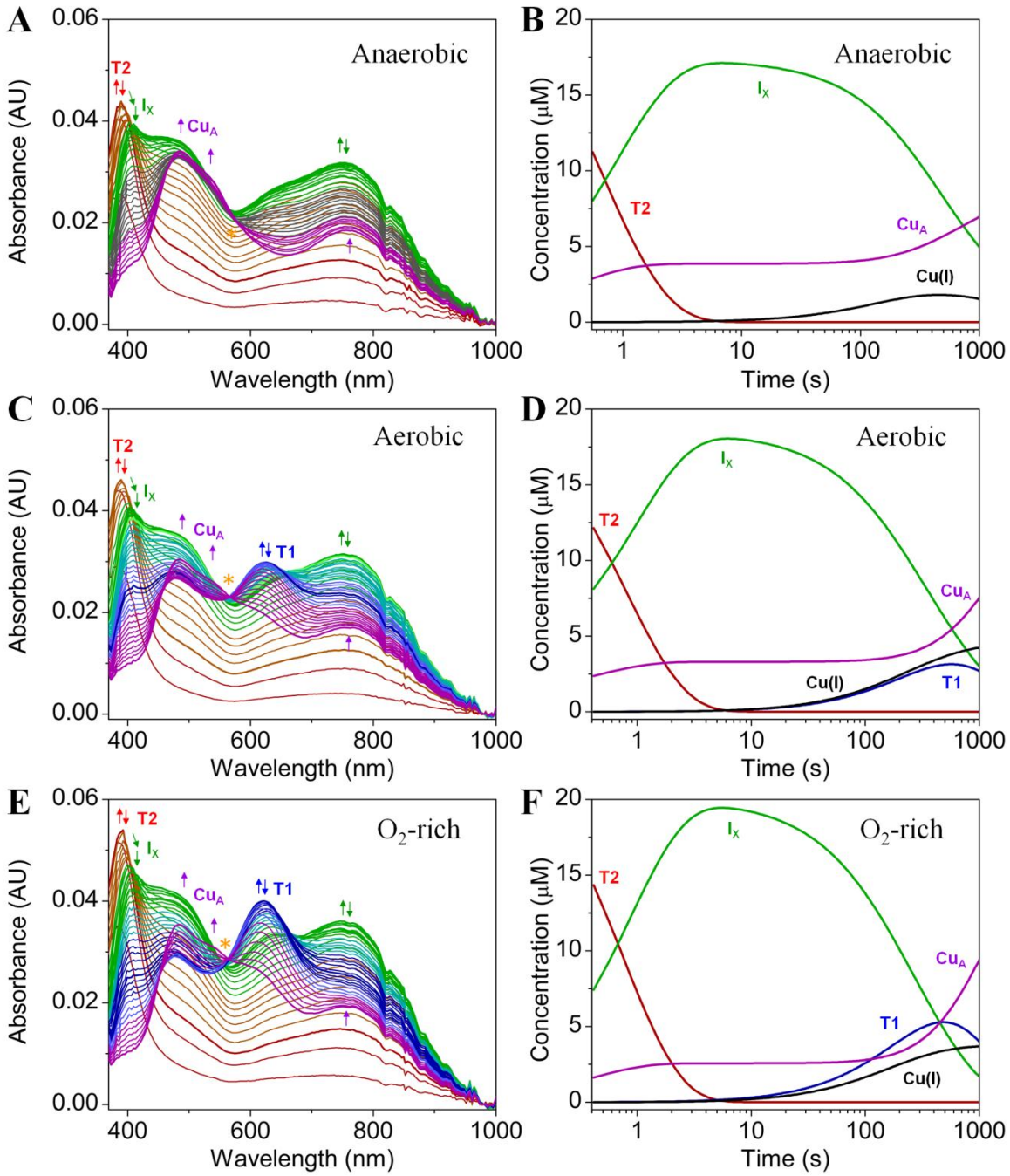

Fig. 3.30. Stopped-flow UV-vis absorption (A, C, E) and concentration profiles (B, D, F) of Cu_AAz in ten-fold excess over $CuSO_4$ at pH 5 under (A, B) anaerobic, (C, D) aerobic and (E, F) O_2-rich conditions. (A, C, E) Spectra are colored to indicate the species forming at that particular time. Arrows indicate direction of change in absorbance over course of experiment and are colored to correspond to the species giving rise to that peak. Golden asterisks indicate isosbestic points. Spectra (200 total) were collected in each case with logarithmic scale over 1000 s. Final protein concentration was 0.25 mM in 50 mM NaOAc, pH 5.0 ± 0.1, and $CuSO_4$, 0.025 mM. Average temperature was 16.1° C. (B, D, F) Concentration profiles are those resulting from global analysis of the corresponding kinetics data. Further information

about the global analysis process may be found in the experimental section about fitting of the kinetics data.

3.3.4. UV-vis absorption spectra of His120Ala Cu_AAz with sub-saturating amounts of $CuSO_4$

In order to search protonatable ligands responsible for the pH-dependent copper incorporation into apo-Cu_AAz, pH-dependent UV-vis absorption spectra of H120A-Cu_AAz after addition of 0.1 equivalents of $CuSO_4$ were collected (Fig. 3.31). Previous studies have shown that the H120A-Cu_AAz variant displays a UV-vis spectrum similar to that of original Cu_AAz, despite the lack of one His ligand.[140,144] As compared to the spectral changes of original Cu_AAz, two major differences were readily observable for the H120A-Cu_AAz variant: the ~385 nm peak that formed initially and the ~600 nm peak that formed later in original Cu_AAz were both missing from the spectral changes in H120A-Cu_AAz, indicating absence of the T2 red and T1 blue Cu intermediates (for the complete set of spectra at each pH, see Fig. 3.32). However, the ~400 and 750 nm bands of I_X still formed in H120A-Cu_AAz, and the shoulder at ~ 475 nm in the spectra of I_X appeared to correlate well with the amount of Cu_A formed under each condition (Fig. 3.31), again suggesting that some Cu_A is rapidly formed; this observation was also consistent with the kinetic models used to fit the data in Fig. 3.22, Fig. 3.23, Fig. 3.29, and Fig. 3.30. Another difference from original Cu_AAz is that little or no Cu_A appears to form after the initial, rapidly formed Cu_A. The presence of the rapidly formed Cu_A suggests that the T2 red Cu intermediate still forms in the H120A mutant, making Cu_A through the 2 T2 → Cu_A pathway, and that this T2 Cu intermediate formed too quickly to be observed (i.e. formation of the T2 Cu intermediate was no longer a rate determining step). This is reasonable, because His120 acts as a "gate" on the surface of the protein, excluding the Cu_A center from solvent.[140,154] The H120A mutation makes the site more accessible to copper, thus accelerating the T2 Cu and subsequent Cu_A formation. Additionally, these data demonstrated strong pH dependence for Cu_A site formation. At low pH (i.e. pH 5), substantial Cu_A formation was observed; however, as the pH was raised, the amount of Cu_A formed dropped off precipitously, with very little Cu_A formation seen at pH 7. Plotting the final absorbance at 485 nm against pH revealed a linear relationship between these parameters (Fig. 3.33).

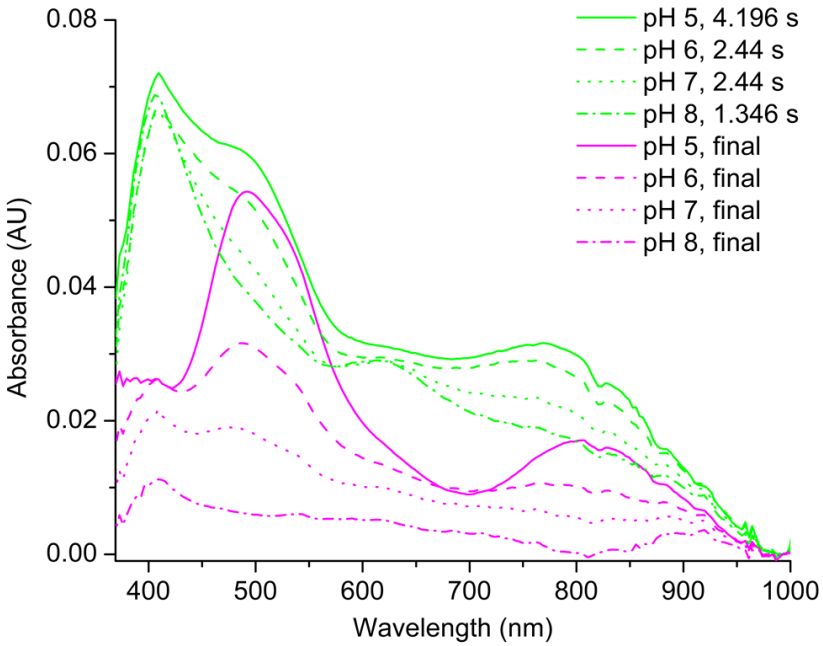

Fig. 3.31. Representative UV-vis absorbance spectra of H120A Cu_AAz mixed with 0.1 molar equivalents of $CuSO_4$, showing maximum I_X formation at 4.196 s for pH 5 and 2.44 s for pH 6 and 7. The final spectra after 1000 s are also shown for each pH. Final protein concentrations were 0.4 mM and $CuSO_4$ concentration was 0.035 mM. Average temperature was 16.3° C.

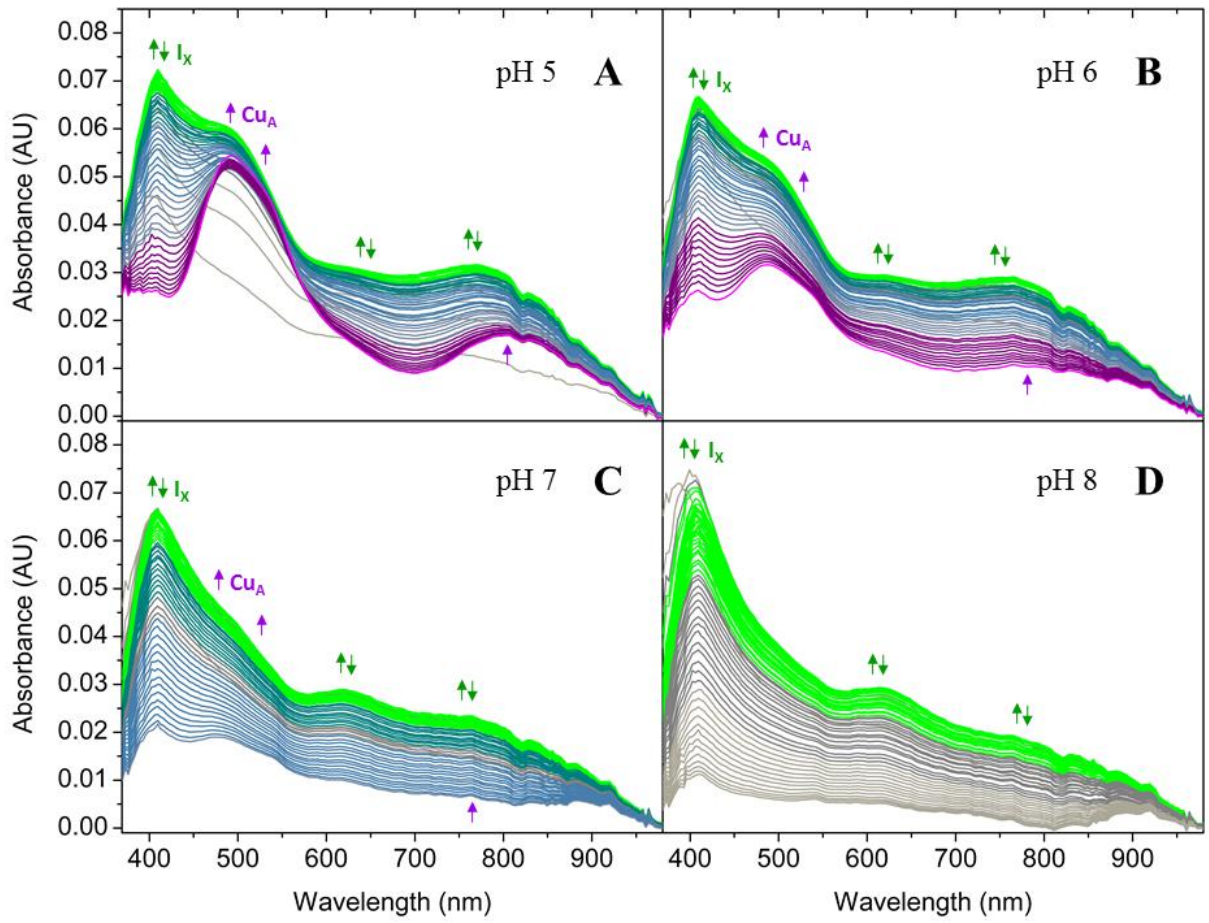

Fig. 3.32. Stopped-flow Vis of H120A Cu_AAz in ten-fold excess over $CuSO_4$ at pH (A) 5, (B) 6, (C) 7, and (D) 8 in UB Buffer. Spectra are colored to indicate the species forming at that particular time. I_X was assigned the color green, since its actual solution color is unknown. Arrows indicate direction of change in absorbance over course of experiment and are colored to correspond to the species giving rise to that peak. Spectra (200 total) were collected in each case with logarithmic scale over 1000 s. Final protein concentrations were 0.4 mM and $CuSO_4$ concentration was 0.035 mM. Average temperature was 16.3° C.

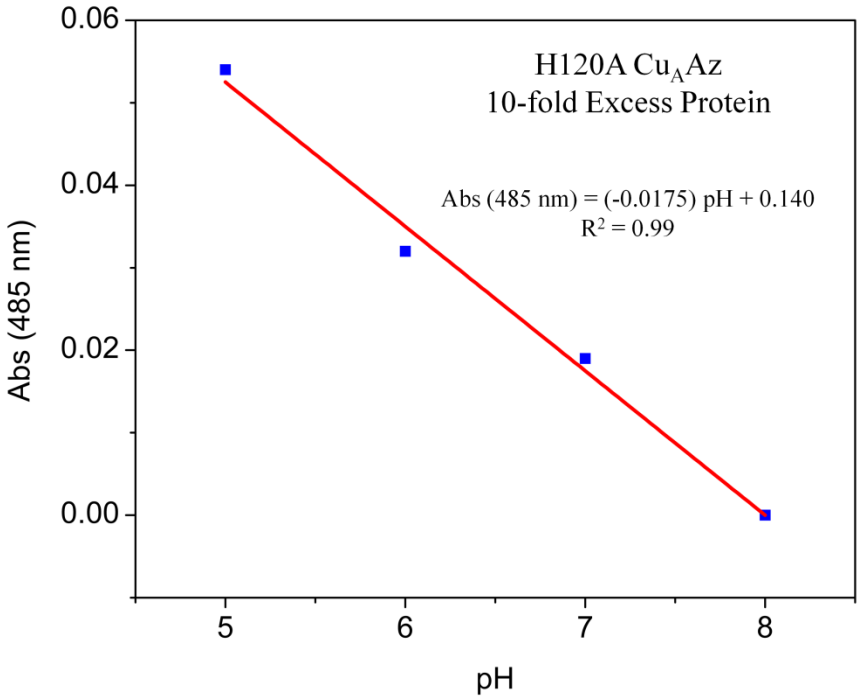

Fig. 3.33. Plot of the absorbance at 485 nm versus pH from the final spectrum of the H120A Cu_AAz kinetics data in Fig. 3.32. Linear regression analysis provided the linear curve and equation shown in the plot with an R^2 value of 0.99.

3.4. Discussion

3.4.1. *pH-dependence of copper incorporation in Cu_AAz: contributions from redox potential and His120*

From the spectra in Fig. 3.22 and Fig. 3.23 and the associated rates in Scheme 3.2, it can be seen that the copper incorporation into Cu_AAz is highly dependent on pH, with slower formation of the final Cu_A center and more accumulation of the intermediates as the pH is raised from pH 5 to 7. One factor contributing to this observation is the known ubiquitous dependence of reduction potential upon pH exhibited by the copper sites of cupredoxin proteins; the redox potential of the copper site of *Pseudomonas aeruginosa* Az decreases by ~60 mV as the pH is increased from 5.0 to 8.0.[219,220] This trend should generally apply to the copper intermediates observed here as well, since it was attributed to the protonation of two histidines, neither being copper ligands, and thus both intact in Cu_AAz. This trend was already demonstrated to apply to the Cu_A site in Cu_AAz.[154] At low pH, therefore, we expect the reduction potential of the copper

ion in the intermediates to be higher. Because reduction of Cu(II) to Cu(I) is an important step for the formation of the mixed valent [Cu(1.5)….Cu(1.5)] Cu_A site, the higher the driving force for the Cu(II)/Cu(I) redox couple, the faster the reduction may occur, increasing the availability of Cu(I) for forming the final product at low pH. As the pH is raised, the redox potential is lowered, making it more difficult to reduce Cu(II) to Cu(I), and decreasing the availability of Cu(I), which slows the final Cu_A formation and allows more accumulation of the intermediates.

Another factor contributing to the pH dependence of both intermediate and Cu_A formation in Cu_AAz is His120. H120A-Cu_AAz shows similar, but more drastic, pH dependence of Cu_A formation (Fig. 3.31) to original Cu_AAz, with Cu_A formation dropping off linearly with pH (Fig. 3.33). Therefore, an explanation for the observed pH-dependence of the rapidly formed Cu_A is that His120 is protonated and incapable of binding the copper at low pH. The EPR spectrum of Cu_AAz, pH 7, 30s after $CuSO_4$ addition and its simulated parameters (Fig. 3.24B, Table 3.3) provide support for this possibility. Here, the distinct species, Cu_A', identified through simulation has EPR parameters nearly identical to those previously reported for a species observed in low pH, His120-off holo-Cu_AAz and in holo-H120A Cu_AAz (Table 3.3).[140,154] Previous studies indicate that, when protonated, His120 in Cu_AAz swings away from the site, becoming more solvent exposed and creating an open coordination site.[140,154] Given that two coppers need to enter the site to form Cu_A, the loss of steric encumbrance from His120 may greatly expedite this process and thus yield faster rates of Cu_A formation at low pH. As the pH is raised, a greater portion of His120 is deprotonated in Cu_AAz, and therefore able to bind copper and slow down the Cu_A formation. Interestingly, no T2 Cu or T1 Cu intermediates were observed in the copper incorporation into the H120A-Cu_AAz (Fig. 3.31), suggesting that His120 is essential for formation of these intermediates (*vide infra*).

3.4.2. *Identity of the T2 red and T1 blue Cu intermediates: EPR and Cys-knockout mutants provide clues*

Due to the transient nature of the copper intermediates formed during reconstitution of Cu_AAz, and in many cases, their overlapping temporal existence, it is difficult to determine the characteristics of these copper sites. Fortunately, Cu(II) interactions with thiolate supply UV-Vis handles, through monitoring of the S(Cys) → Cu(II) ligand-to-metal charge transfer (LMCT) bands. The molar absorptivity and energy of these LMCT transitions are diagnostic of the type of

copper site involved.[35,65] The first species to appear, namely the ~385 nm peak, can be assigned to a tetragonal copper-thiolate center, similar to that found in the native T2 red Cu protein. The relatively large A_z of $|147| \times 10^{-4}$ cm^{-1} (Table 3.3) for this initial species is also consistent with its assignment as a T2 Cu intermediate. The species associated with the ~600 nm peak can be attributed to a distorted tetrahedral copper-thiolate center, analogous to those found in native T1 blue Cu proteins, where the EPR parameters of this species are also consistent with this assignment (Table 3.3).

An earlier study, in which each of the two active site Cys of Cu_AAz were, in turn, mutated to isostructural serine[156]—a residue that does not produce the same LMCT bands when interacting with copper—provided further insights into the makeup of these T2 red and T1 blue Cu intermediates. Notably, it was discovered that replacing Cys112 with Ser, leaving Cys116 intact to interact with Cu(II), resulted in a T2 red Cu complex with λ_{max} ~ 390 nm in its UV-Vis spectrum.[156] The UV-Vis spectrum of the copper-loaded C112S-Cu_AAz mutant is nearly identical to that observed for the T2 red Cu intermediate in original Cu_AAz observed in Fig. 3.22. Conversely, replacing Cys116 with Ser, which only leaves Cys112 to interact with Cu(II), yielded a T1 blue Cu complex.[156] The EPR and UV-vis spectra of both the T1 blue Cu intermediate observed here during Cu_A formation in original Cu_AAz and the T1 blue Cu site formed in C116S-Cu_AAz are markedly similar (Fig. 3.24B and Fig. 3.9-Fig. 3.12, Fig. 3.14).[156] Therefore, the evidence suggests that the T2 red Cu intermediate in Cu_AAz arises from a complex with Cys116, while the T1 blue Cu intermediate results from a complex with Cys112. This conclusion is supported by the difference in accessibility of Cys112 and Cys116 to exterior Cu(II) ions. From the crystal structure of Cu_AAz (PDB ID: 1CC3), Cys116 is revealed to be closer to the surface of the protein than Cys112, rendering it free to capture Cu(II) from solution and form the T2 Cu center first, which then undergoes conformational rearrangement, leading to I_X (*vide infra*). Unlike the native T2 red Cu protein, nitrosocyanin, no evidence of superhyperfine splitting from histidine coordination could be detected in the perpendicular region of the T2 Cu species' EPR spectrum (Fig. 3.24A), consistent with the hypothesis that this species is a capture complex with Cys116. Based upon the UV-Vis spectra of H120A-Cu_AAz in Fig. 3.31, removal of His120 changes this situation; instead of the T2 red Cu intermediate forming and then decaying to I_X and Cu_A', I_X and Cu_A' form directly. Thus, His120 may be forcing Cys116 sterically or through hydrogen bonding interactions to orient toward the exterior of the protein.

Because the T1 blue Cu intermediate forms from oxidation of the reduced copper product of I_X decay, its absence from the spectra of H120A Cu_AAz suggests that His120 is: 1) a required ligand in the T1 blue Cu species, 2) lowers the reduction potential of the Cu(I) precursor to the T1 Cu species, making this species more accessible to oxidation by O_2, or 3) required to protect the Cu(I) precursor to the T1 Cu species from bulk solution. While we have not eliminated the latter two possibilities, given the highly conserved, His-Cys-His primary coordination sphere of native T1 blue Cu sites, the first possibility is most likely. In support of His120 being a required ligand for the formation of the T1 Cu intermediate, the pH dependence of the T1 blue Cu intermediate formation in Cu_AAz (Fig. 3.23) falls into a similar range as the determined pK_a of His120.[154]

3.4.3. *Identity of I_X: Its Instability with Respect to Reduction and Unusual Spectral Properties*

A particularly interesting discovery of this study is that of I_X, having intense absorptions at 410 and 760 nm that are not immediately diagnostic of any known copper-thiolate binding site. Like the T1 blue Cu intermediate, I_X was not observed in the previous study of copper incorporation into the Cu_A site of Cu_AAz.[143] In the previous study, where ten-fold excess copper over protein conditions were used, the only process observed was the direct formation of Cu_A from the T2 red Cu intermediate.[143] This result makes sense from the observed rate constants and kinetics fits for copper incorporation in the present study, as the direct T2 to Cu_A pathway is bimolecular with respect to the T2 intermediate with a large observed rate constant (Scheme 3.2). Thus, at greater concentrations of copper, where more T2 red Cu intermediate forms, this step dominates the copper incorporation process.

In the present study, sub-saturating amounts of copper are used, and insufficient T2 Cu is formed to completely support the bimolecular direct T2 to Cu_A pathway. As a result, a slower step, where T2 is converted to I_X, competes for the initial pool of T2 Cu. The slower rate of the T2 to I_X step (Scheme 3.2) indicates that this step is accompanied by structural rearrangement of the T2 red Cu site, such as ligation of another residue from the protein to the copper. As discussed above, the T2 red Cu site is most likely a capture complex with a solvent-exposed Cys116. Thus, a picture emerges of the T2 red Cu capture complex swinging into the interior of the protein, perhaps being driven or accompanied by ligation of another residue (Scheme 3.3).

Once I_X is formed in Cu_AAz, it decays at a very similar rate regardless of changes to pH or O_2 content (Scheme 3.2). Likewise, the I_X that forms in H120A-Cu_AAz decays in the same timeframe (nearly complete 1000s after $CuSO_4$ addition). Under most conditions explored here, the decay of I_X is accompanied by formation of the T1 blue Cu intermediate (Fig. 3.23, Fig. 3.30). However, in the absence of molecular oxygen, although I_X decays at about the same rate (Fig. 3.30, Scheme 3.2), its decay does not appear to correspond to the production of any colored species, highlighting the possibility that I_X is generating Cu(I) in this system. This hypothesis was confirmed by spin-quantification EPR, performed under the same conditions as in Fig. 3.24B, which shows loss of spin from the system over the same timeframe that I_X is decaying (Fig. 3.28). Thus, the loss of the I_X signal is associated with production of Cu(I). Incorporating this knowledge into the models used for fitting the copper incorporation kinetics resulted in high quality fits (Scheme 3.2, Table 3.1, Table 3.2, Fig. 3.16-Fig. 3.19, Fig. 3.21).

Inferring the ligands and geometry of I_X is complicated by the fact that it is always present as one component in a mixture of several species. For this reason, the pure I_X UV-Vis absorbance and EPR spectra remain elusive. The resolved molar absorptivity spectra for I_X produced by the kinetics fitting procedure provide indications of the pure spectrum and thus the identity of I_X (Fig. 3.9-Fig. 3.12, Fig. 3.14), as do the EPR parameters assigned to I_X (Table 3.3). In searching similar spectra to that of I_X from known Cu(II)-thiolate complexes, we found only one example, i.e., that of copper-substituted horse liver alcohol dehydrogenase (HLADH).[210] The electronic absorption spectra of copper-substituted HLADH in complex with exogenous ligands, including pyrazole and a coenzyme, modified nicotinamide adenine dinucleotide (H_2NADH), show similarly intense and broad transitions at low energy (690-720 nm versus ~710-740 nm for I_X spectra in Fig. 3.9-Fig. 3.12, Fig. 3.14), as well as intense transitions around 400 nm.[210,211] The copper center in these Cu(II)-HLADH complexes with exogenous ligands were then interpreted and later confirmed to be distorted (flattened) tetrahedral copper dithiolate sites, consisting of Cu(II)-S_2(Cys)N(His)L (L = exogenous ligand, e.g. water, pyrazole, imidazole, 2-mercaptoethanol, etc.).[210,211] The tentatively-assigned A_z of $|115| \times 10^{-4}$ cm^{-1} for I_X falls into an intermediate range for those typical of T1 and T2 Cu sites. However, this A_z is identical to the that found for the binary complex of Cu(II)-HLADH with pyrazole,[221] and also similar to those of the complexes with imidazole and 2-mercaptoethanol.[222] Moreover, these complexes of Cu(II)-HLADH with pyrazole, imidazole, and 2-mercaptoethanol were metastable, bleaching

over time, which was attributed to intramolecular reduction of the active-site Cu(II) to Cu(I) by the coordinated cysteine thiolates, presumably accompanied by formation of a disulfide.[221,222] This process was also observed to be accelerated in the presence of oxygen. This instability with respect to autoreduction is consistent with the behavior of I_X, as demonstrated by spin quantification EPR (Fig. 3.28) Based on these results, we can deduce that I_X is formed from a rearrangement of the Cu(II)-Cys116 capture complex (i.e. T2 red Cu intermediate) into a Cu(II)-dithiolate complex, wherein Cys112 is the second thiolate ligand. Examples of other Cu(II)-dithiolate complexes for comparison to I_X are rare, as the thiol-ligands must have features that avoid the Cu(II)-catalyzed formation of disulfide from thiols.[178-180]

3.4.4. *Oxygen-dependence of the T1 blue Cu species: one-electron oxidation of the Cu(I) product of I_X decay*

When oxygen was excluded from the reconstitution of Cu_AAz at pH 5, the T1 blue Cu species no longer formed (Fig. 3.30). Conversely, when the reactant solution was enriched in O_2, more T1 blue Cu species formed than when the reactants were simply exposed to air (Fig. 3.30). Thus, the extent of T1 blue Cu species formed correlates positively with the concentration of dissolved molecular oxygen in the reaction mixture. Since the T1 blue Cu intermediate is primarily the product of I_X, the key to understanding this oxygen-dependence may lie in examination of I_X. As discussed above, EPR spin-counting experiments connected the decay of I_X with the formation of Cu(I). The O_2-dependent stopped-flow UV-Vis spectra are also consistent with this finding (Fig. 3.30 and Scheme 3.2). The rates for the steps prior to the decay of I_X are similar regardless of the O_2 concentration and whether or not the T1 blue Cu intermediate forms. The amount of I_X remaining at the end of the 1000 s experiments is also nearly identical between anaerobic, aerobic and O_2-rich conditions (Fig. 3.30). Since I_X decays at about the same rate, regardless of whether the T1 blue Cu intermediate forms afterward, it is likely that the product of I_X decay is the same whether or not the T1 blue Cu intermediate subsequently forms. By extension, the T1 blue Cu intermediate formed after I_X is actually the product of a Cu(I) species, generated by the decay of I_X. Given that molecular oxygen must be present for this Cu(I) → T1 Cu transformation to occur, oxygen is presumably acting as an oxidant to the Cu(I) species. Therefore, the most likely mechanism leading to the observed oxygen-dependent formation of the T1 blue Cu intermediate is the formation of a reduced T1

blue Cu site, which then undergoes a one-electron oxidation to the T1 blue Cu intermediate, with oxygen serving as the oxidant.

3.4.5. *Mechanism of Cu(II) Incorporation into the Cu_A Site*

From all of these various data, a mechanistic picture begins to emerge (Scheme 3.3), which is similar to the mechanism formulated from the pH 6 UV-Vis kinetic data (Chapter 2 and Scheme 3.1), but with much more detailed information. Starting with apoCu_AAz and adding Cu(II), T2 red Cu formation occurs rapidly, as previously reported.[143] The available evidence does not allow us to distinguish whether His120 is bound in the T2 Cu intermediate. The lack of T2 Cu formation in H120A-Cu_AAz suggests that His120 may be a required ligand for T2 Cu formation. However, due to the direct formation of I_X in this mutant, we propose instead that Cys116 is able to rapidly adopt a conformation more internal to the protein, thus eliminating the barrier for conformational rearrangement to form I_X. From the T2 red Cu intermediate, there are three pathways, all leading to purple Cu_A in the end. One pathway, reported in a prior study,[143] leads directly to purple Cu_A formation, presumably by the generation of Cu(I) ions *in situ* through the reaction of Cu(II) with an empty Cu_A site's thiolates to form a disulfide and Cu(I). In the presence of excess copper, this route is accelerated greatly and dominates the mechanism. This copper dependence suggests that the initial reductive event requires multiple coppers per Cu_A site, or multiple singly copper loaded proteins to interact and provide reducing equivalents, which is consistent with the 2 e^- reduction of thiols to disulfide. Conversely, the observed intermediates that form from I_X under sub-saturating copper conditions are a result of single copper occupation of the Cu_A site. On the pathway that predominates at low copper concentration, the T2 red Cu center converts to I_X, likely through a structural rearrangement to a dithiolate complex. After formation of I_X, it decays, due to reduction of the copper to Cu(I) by the active site cysteine thiolates. Given the highly thiophilic nature of Cu(I), the Cu(I) generated likely binds to the free cysteines of another equivalent of apo-Cu_AAz, which is in strong excess. Some portion of this Cu(I) likely forms the reduced version of the Cu_A site, which can then be oxidized to the purple, [Cu(1.5)…Cu(1.5] state either by another Cu(II) site or by molecular oxygen.

All of the wtCu_AAz electronic absorption studies (Fig. 3.23, Fig. 3.30) indicate that the next step is formation of the T1 blue Cu species. Because no T1 blue Cu intermediate was

observed in the UV-Vis spectra of H120A-Cu_AAz (see Fig. 3.31, Fig. 3.32), His120 is required to form the T1 blue Cu species. Moreover, the pH-dependent UV-Vis spectra (Fig. 3.23) indicated that more T1 blue Cu species formed at higher pH. Given these observations and the fact that the His-Cys-His primary coordination sphere is completely conserved among T1 blue Cu sites, we can infer that deprotonation and coordination of His120 is a necessary step to formation of the T1 blue Cu intermediate. The other pathway from the T2 red Cu species supports this deprotonation step as well; in this pathway the T1 blue Cu intermediate is formed directly from T2 Cu at high pH, where we would expect His120 to be deprotonated (see Fig. 3.23E-H). Anaerobic and oxygen-rich stopped-flow data of Cu_AAz with $CuSO_4$ (Fig. 3.30) also reveal that formation of the T1 blue Cu intermediate is dependent upon the concentration of molecular oxygen in solution, strongly suggesting one-electron oxidation of a Cu(I) precursor. Finally, isosbestic conversion of the T1 blue Cu intermediate to Cu_A occurs under sub-saturating $CuSO_4$ conditions. Based upon comparison to the native N_2OR system (*vide supra*), it is inferred that reducing equivalents, that is generation of Cu(I), are required to achieve this transformation. This scheme represents our current understanding of how Cu(II) leads to the formation of Cu_A in Cu_AAz under sub-saturating copper conditions.

Scheme 3.3. Current picture of how Cu(II) is incorporated into the Cu_A site. Interior and exterior labels are used to indicate the inside versus the outside of the protein.

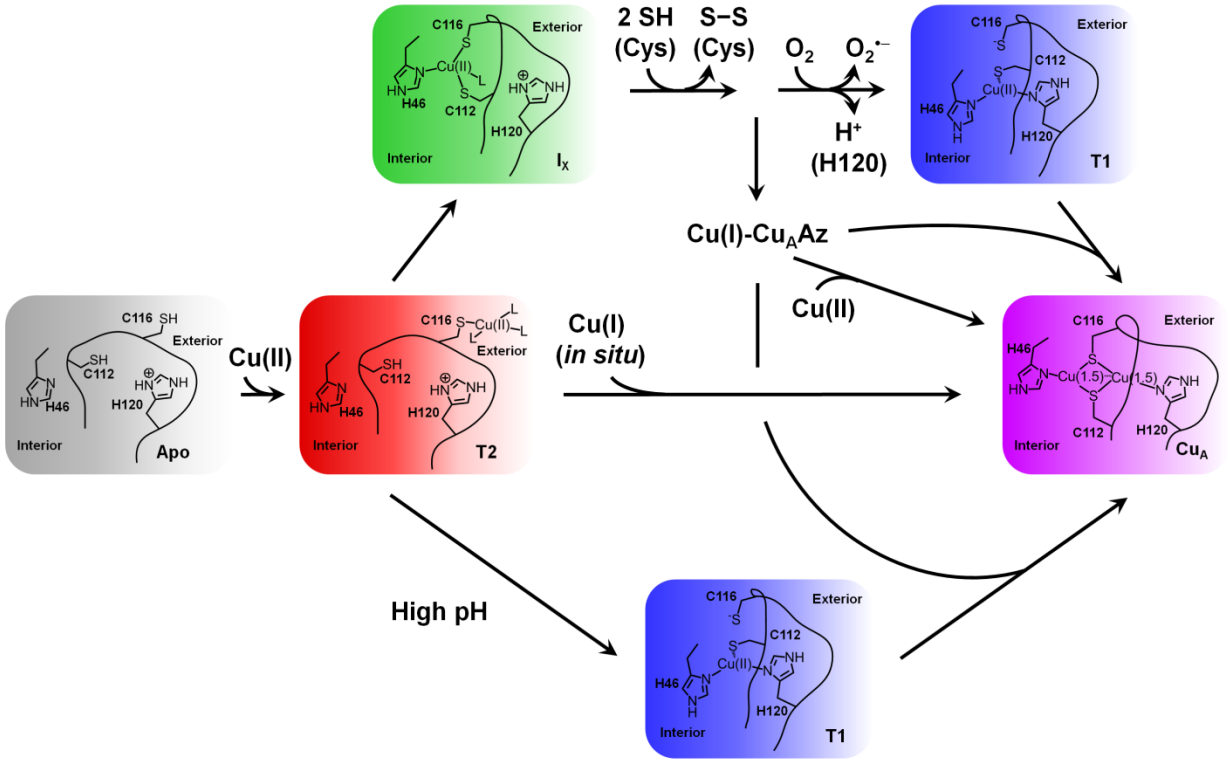

3.5. Conclusions

In this study, the kinetics of copper incorporation into the Cu_A site of an engineered structural and functional Cu_A model protein, Cu_AAz, have been characterized extensively by electronic absorption and electron paramagnetic resonance spectroscopies. These characterizations have provided new insight into the mechanism of Cu_A formation. Global analysis of the UV-Vis absorbance kinetics at pH 6 under sub-equivalent copper additions had revealed a second pathway proceeding from the T2 Cu intermediate (Chapter 2). The investigations reported here, of pH- and O_2-dependence stopped-flow UV-Vis spectroscopy, time-dependent EPR spectroscopy, and mutations to copper-binding residues, have revealed molecular level detail of the copper incorporation mechanism (Scheme 3.3). From the T2 red Cu intermediate, conversion occurs to an intermediate, I_X, with unusual electronic absorption and EPR spectra, similar to those of a Cu(II)-dithiolate center.[210,211,221,222] I_X then decays to a Cu(I) species, where this step can be attributed to the Cu(II)-catalyzed formation of a disulfide bond between the cysteine thiols in the Cu_A site. Depending upon the protonation state, and resulting

ability to coordinate copper, of one of the active site histidines, molecular oxygen can then oxidize a Cu(I) site to a T1 blue Cu intermediate. Gradually, this T1 blue Cu intermediate isosbestically converts to the final purple Cu_A center.

This study, together with the previous investigation of copper incorporation into Cu_AAz, under ten-fold excess copper conditions, represent the only mechanistic studies of *in vitro* Cu(II) incorporation into Cu_A centers. Given that the *in vivo* mechanism of Cu_A site assembly is still poorly understood, studies such as these may facilitate understanding of this *in vivo* mechanism. From the present study, it is apparent that Cu_A centers can assemble, even from unmediated Cu(II) addition to the apo-site. While this method of Cu_A assembly may not the represent most efficient method conceivable, even the inefficiencies in the Cu_A assembly from unmediated incorporation of Cu(II) are not insurmountable barriers for native systems to overcome. As discussed in Chapter 2, the primary problem encountered in this unmediated incorporation of Cu(II) into the Cu_A site is the use of the copper-binding Cys residues as reducing equivalents, which renders these sites unable to form Cu_A. However, nature has evolved proteins that maintain a thiol-pair/disulfide in the proper oxidation state. Therefore, the mechanism presented here may be relevant to Cu_A domains in organisms where the Cu_A is in the periplasm or extracellular space, which are environments where the +2 oxidation state of copper is stable.

CHAPTER 4: TOWARD A BIOSYNTHETIC COPPER CHAPERONE MIMIC FOR PROTEIN-DIRECTED CU_A ASSEMBLY

Abstract

Copper is a widely utilized and versatile cofactor for many enzymes in organisms across all domains of life. Free copper, however, is potentially dangerous to the cell, as it can produce hydroxyl radicals and replace native metal cofactors in non-copper containing enzymes. Hence, copper chaperones have evolved to shuttle copper to its intracellular targets, while sequestering it from solution. The proposed copper chaperone to the Cu_A center in cytochrome *c* oxidases (C*c*Os) is called Sco. However, the function of Sco has not yet been definitively shown. Other redox regulatory functions have been proposed for this protein. Sco is known to bind both Cu(I) and Cu(II). Although Cu(I) is the dominant oxidation state for copper chaperones, the Cu(II) state is essential for Sco's function in the maturation of Cu_A. Yet, no structure of Cu(II)-bound Sco exists. Described here is the progress toward designing a mimic of the copper-binding site in Sco proteins, through a mutant of the type 1 copper protein azurin (Az), His46Cys/Cys112His Az. This mutant binds Cu(II) in a site similar to a Sco mutant, as demonstrated by UV-Vis and EPR spectroscopies. Structural elucidation of this Az mutant may shed light on the nature and importance of the Cu(II) center in Sco proteins. Additionally, future redesigns of this Az mutant may yield a full mimic of the copper centers in Sco, allowing deconvolution of the copper center's function from that of the protein fold.

4.1. Introduction

Copper is an essential trace element for the majority of organisms across all domains of life.[163-165] Copper centers in enzymes activate oxygen, performing important roles in such biological processes as activation of peptide hormones, melanin pigment biosynthesis, iron homeostasis and methane oxidation.[223] In addition to these oxygen-activation roles, copper centers in proteins catalyze remarkably efficient electron transfer reactions between a large diversity of donors and acceptors (see Chapter 1).[1] However, the very same properties of copper ions that render them such useful cofactors for enzymes—their suitable reduction potentials for oxygen activation and stable Cu(I) and Cu(II) oxidation states—also pose a danger to the cellular environments in which these ions are utilized. Aqueous copper and many small copper

complexes react through Fenton and Haber-Weiss chemistry to generate destructive hydroxyl radicals, which would damage or destroy cellular components.[169] Moreover, copper's superior affinity for most ligand sets, as demonstrated by its position at the top of the Irving-Williams series, could lead to displacement of native metal cofactors in non-copper containing metalloenzymes, if copper were free in the cellular environment.[224] For these reasons, much cellular machinery has evolved to manage copper, ensuring that this essential element is provided to the enzymes that use it, while free copper levels are kept at a minimum.[170-174] This cellular machinery includes copper importers, exporters, and chaperones. The copper chaperones are proteins that bind copper ions, thus preventing them from generating hydroxyl radicals or replacing other metal ions, and deliver these ions to their cellular targets.[170-175] Such copper chaperones have been identified for a number of copper enzymes.

Cu_A is a unique, dinuclear copper center, the unusual properties of which make this center particularly well-suited for its function: electron transfer under the low driving forces at the end of electron transport chains (see Chapter 1).[66] The properties of Cu_A centers that render them so effective in their biological roles also present distinct challenges for their assembly. The primary feature of Cu_A centers that gives them an advantage over the more common and simpler type 1 (T1) copper electron transfer centers is their mixed-valence, valence-delocalized resting state.[69,139] Essential to this electronic structure in the resting state of Cu_A is the rigid diamond core of the center, in which the two copper ions form a metal-metal bond and are bridged by two Cys thiolates.[69] While the bridging Cys ligands are indispensable in the formation of this rigid diamond core,[84,156] two thiolates in such close proximity can present difficulties for incorporating metals into the center, as the formation of a disulfide bond between such thiolates is generally favorable. Copper is also a well-known catalyst for the formation of disulfide bonds between free thiolates.[178-180] Therefore, in addition to delivering copper ions to Cu_A, the assembly cofactor(s) for this center must either avoid or address the propensity for copper-catalyzed disulfide formation between the active site thiolates of Cu_A. Another factor to consider in metalation of the Cu_A center is the oxidation state of the entering copper ions. The resting state of the center is formally Cu(II)-Cu(I), so metal reconstitution should either occur entirely through Cu(I), or through a mixture of Cu(II) and Cu(I). Thus far, the Cu(II)-Cu(II) state of Cu_A centers has not been reported, so metalation is unlikely to occur only through Cu(II) ions, without the presence of some form of reductant.

A protein called Sco has been proposed to act as copper chaperone to the Cu_A center in cytochrome *c* oxidases (C*c*Os).[176] This proposed function was primarily based upon a study in yeast, where overexpression of Sco rescued a respiratory deficiency caused by deletion of an upstream copper chaperone, Cox17.[185] Providing support for this copper chaperone role, Sco proteins associated with C*c*O bind copper tightly, through a highly conserved CXXXCP motif and His residue (Fig. 4.1A) .[186-190] However, direct metalation of a Cu_A center by a Sco protein has not been demonstrated. Furthermore, the global folds of Sco proteins fall into the classification of thioredoxin/peroxiredoxin-like, which suggests a redox regulatory or signaling role for these proteins.[191-194] Indeed, an *in vitro* study of Sco from *Thermus thermophilus* demonstrated that Sco did not deliver copper to the Cu_A domain, but did reduce a disulfide formed in the apo Cu_A site, while another protein, PCu_AC, metalated the Cu_A center.[214] However, a protein equivalent to PCu_AC is not found in all organisms containing C*c*O, so this protein cannot act as universal copper chaperone to Cu_A.[176,225] As a result, while it is widely accepted that Sco plays an important role in the biogenesis of the Cu_A subunit in C*c*Os, the exact role it plays is still a point of contention.[176]

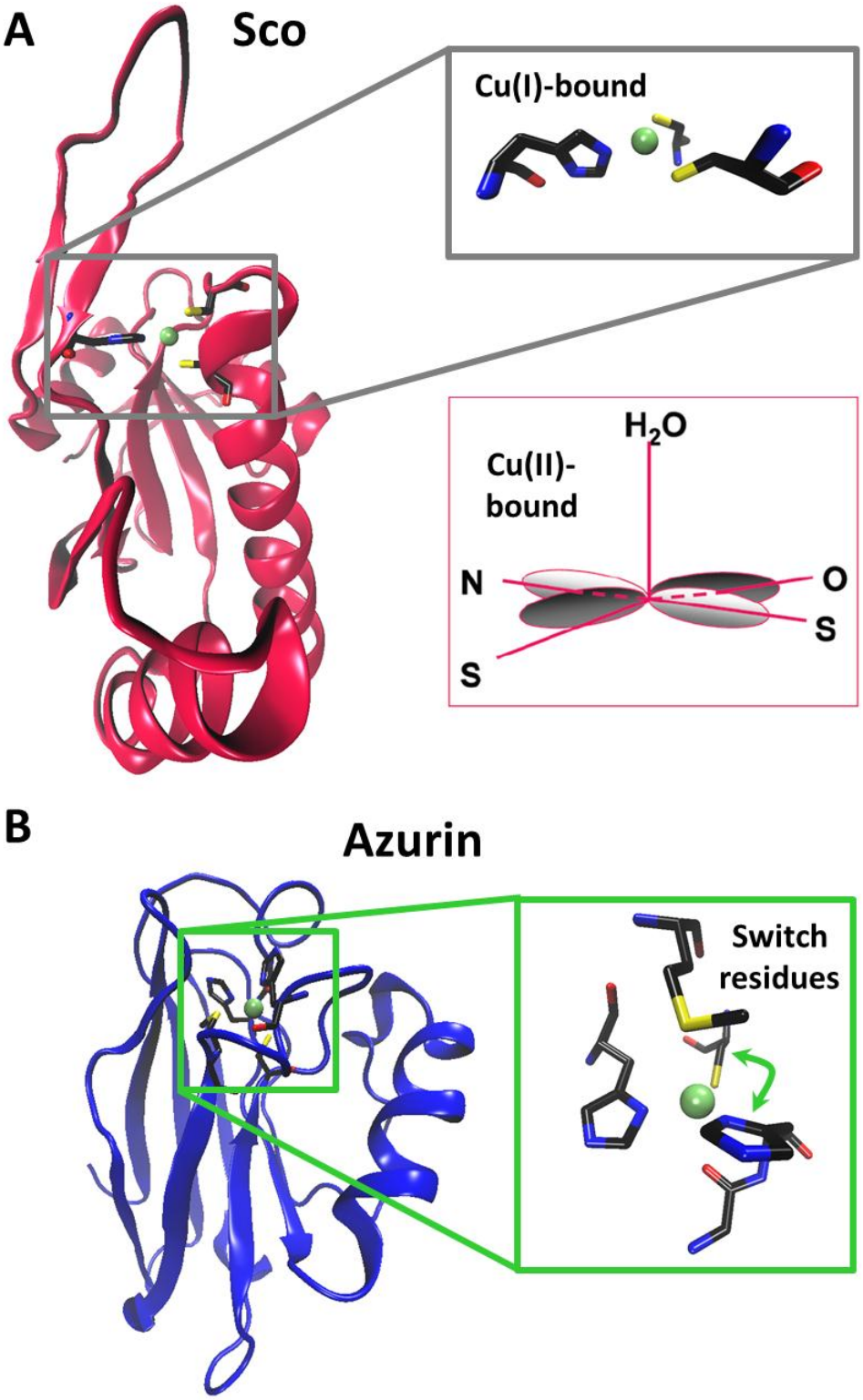

Fig. 4.1. Structures of Cu(I)-Sco (A) and Cu(II)-Azurin (B), with copper-binding sites shown to the right. (A) The solution structure of Cu(I)-bound human Sco (PDB ID 2GT6), showing a zoom-in of the Cu(I) center (top-right), as well as the proposed structure of the Cu(II)-bound Sco, based on EPR and XAS studies (bottom-right; from ref 226). (B) The crystal structure of

Cu(II)-bound azurin from *Pseudomonas aeruginosa* (PDB ID 4AZU), showing a zoom-in of the Cu(II) center (right). The two residues whose positions are interchanged in this study are indicated by a double-sided arrow. Individual amino acids are shown as sticks, while the copper ions are spheres. Coloring scheme: carbon is black, nitrogen is blue, oxygen is red, sulfur is yellow, and copper is green.

One interesting facet of Sco proteins is that they bind Cu(II) very stably,[187,190] and this oxidation state has been demonstrated to be essential for their function.[195,196] All confirmed copper chaperones discovered to date bind and transport copper in the +1 oxidation state.[170-175] Again, this stable Cu(II) state may suggest a redox role for Sco. However, it is tempting to envision Sco delivering both Cu(II) and Cu(I) ions to the Cu_A center, forming the site in its resting state. The Cu(I)-bound Sco structure has been well characterized by NMR (Fig. 4.1A).[193] Attempts to crystallize the Cu(II)-bound Sco, on the other hand, have been unsuccessful, and paramagnetic broadening from the Cu(II) ion renders NMR useless for this purpose. EPR and XAS studies have suggested a structure (Fig. 4.1A),[188] but one of the residues/ligands that contribute to this structure is not known. A Cu(II)-bound Sco structure may provide insight into the function of this center.

A mutant of the T1 copper protein, azurin (Az), was discovered that formed a center similar to a variant of Cu(II)-bound Sco, based upon its UV-Vis and EPR spectra. In this mutant, the positions of the copper-binding Cys (residue 112) and one of the His (residue 46) are interchanged, giving His46Cys/Cys112His Az (Fig. 4.1B). The Sco variant that this Az mutant models is one in which a copper-binding Cys is mutated to Ala, C45A Sco,[226] which is consistent with the available ligand sidechains in H46C/C112H Az. A model of the copper site of Sco in a different protein fold could allow deconvolution of the copper center's function from the function of the protein fold. In particular, Az does not adopt a thioredoxin/peroxiredoxin fold, so the associated thiol/disulfide oxidoreductase function of this class of proteins should be absent. Additionally, mutants of Az have been generally amenable to crystallization, so H46C/C112H Az may lead to a structure for a Cu(II)-Sco-like site, which could be related back to Sco proteins and their functions.

4.2. Materials and Methods

4.2.1. Materials and Reagents

Bactotryptone and yeast extract were purchased from BD Biosciences. XL-1 Blue and BL-21* (DE3) cells were purchased from Invitrogen. *Pfu* DNA polymerase and *Dpn1* were purchased from Stratagene. DNA primers were purchased with standard desalting from IDT Technologies, and were used without further purification. IPTG was purchased from Research Products International Corps or Gold Bio Technology Inc. $^{63}CuSO_4$ was prepared previously by Dr. Masha G. Savelieff, by recrystallizing isotopically pure ^{63}Cu metal, from Daniella Goldfarb (Weizmann Institute Chemical Physics), which had been dissolved in H_2SO_4/HNO_3. All other reagents were purchased from Fisher, Sigma-Aldrich or Fluka. All water used was purified to 18.2 MΩcm by ultrafiltration with a Milli-Q Plus PF Ultra-Pure Water System. $CuSO_4$ solutions were prepared volumetrically in water that was incubated with Chelex prior to use. EDTA solutions were prepared volumetrically. For pH dependent studies, a chelexed universal buffer (UB) containing 40 mM MES, MOPS, CAPS, and either Tris (UB) or Hepes (UB_{HEPES}), 50 mM NaOAc, and 100 mM $NaNO_3$ (to maintain relatively constant ionic strength) was utilized. For copper/EDTA titrations, a temperature independent buffer at pH 7 (TIP7), previously developed in our laboratory,[217] was used, as this buffer has low ionic strength and is in the middle of the pH window explored.

4.2.2. Mutagenesis, Expression and Purification of H46C/C112H Az

The mutant H46C/C112H Az was created on the wild type Az template from *Pseudomonas aeruginosa* using the Stratagene quick change mutagenesis kit. First, the H46C mutation was introduced with the primers 5'-GAACGTTATGGGTTGCAACTGGGTTCTG-3' (forward) and 5'-CAGAACCCAGTTGCAACCCATAACGTTC-3' (reverse). After verification by DNA sequencing that the resulting plasmid contained the H46C mutation and no others, the C112H mutation was introduced with the primers 5'-GTACATGTTCTTCCACACTTTCCCGGG-3' (forward) and 5'-CCCGGGAAAGTGTGGAAGAACATGTAC-3' (reverse). The sequence of this final H46C/C112H Az plasmid was verified by DNA sequencing.

The H46C/C112H Az mutant was expressed and purified as previously reported for Az mutants,[227,228] with minor changes. Briefly, BL-21* (DE3) cells were transformed with pET-9a plasmid containing the H46C/C112H Az gene preceded by a periplasmic leader sequence. These cells were then grown in 2xYT media at 25 ºC and induced with IPTG at OD_{600} ~ 3. Cells were

allowed to express protein and export it to the periplasm at 25°C for 4 hours. After harvesting the cells, lysis of the periplasmic membrane was achieved by osmotic shock. The supernatant after centrifugation was acidified to pH 4.1 with 500 mM sodium acetate, resulting in significant precipitation. After another round of centrifugation, the supernatant was applied to SP Sepharose cation exchange media, equilibrated with 50 mM ammonium acetate (NH_4OAc), pH 4.1. A step gradient was applied with 50 mM NH_4OAc, pH 6.35 as the elution buffer, resulting in elution of the desired protein over a broad range. The H46C/C112H Az protein from the SP Sepharose column was then applied to an additional Q-Sepharose HiTrap anion exchange column to remove a minor heme containing contaminant. The protein eluted from the Q-Sepharose column was concentrated to < 12 mL volume, using a Millipore Amicon Bioseparations Stirred Cell, and applied to a size exclusion chromatography (SEC) column, packed with Sephacryl S-100 HR media (GE Healthcare). This SEC column removed a ribose-binding contaminant, which binds and elutes in the same place as H46C/C112H Az on the cation and anion exchange columns. Five peaks elute from the SEC column. When these peaks were subjected to ESI-MS, it was found that the fourth and largest peak contains only the mass corresponding to H46C/C112H Az. Therefore, the fractions corresponding to this fourth peak were collected and used for experiments.

At this stage, the protein solution was divided into aliquots, flash frozen, and stored at -80 °C until required for experiments. When needed for experiments, the appropriate amount of protein was thawed and exchanged into whichever buffer was to be employed for that experiment. Buffer exchanging was typically accomplished by application of the protein to a standard desalting column (PD-10, GE Healthcare), equilibrated with the buffer of interest. Alternatively, the protein was subjected to several cycles of concentration and dilution with the buffer of interest in a centrifugal filter unit with a 10 kDa molecular weight cutoff (Amicon Ultra from Millipore). The protein was then concentrated to the desired level for the experiment, and the concentration confirmed based on A_{280} using $\varepsilon_{280} = 9800\ cm^{-1}\ M^{-1}$.

4.2.3. Expression and Purification of Cu_AAz

Cu_AAz was expressed and purified as described in Chapters 2 and 3.

4.2.4. Expression and Purification of N_2OR

N_2OR was expressed and purified as previously described.[207] Briefly, the BL-21* (DE3) cells were transformed with the N_2OR plasmid (gene from *Paracoccus denitrificans*), which were then grown in LB media supplemented with 100 mg/L ampicillin at 37 °C to an OD_{600} ~ 0.6, at which time the cells were induced with 1 mM IPTG. Induction was allowed to occur over 5 hours at 25 °C before harvesting cells. Cell pellets were lysed by sonication in a lysis buffer consisting of 100 mM Tris•HCl, pH 8, with 1 mM each PMSF and EDTA. The lysate was applied to a DEAE CL-6B column equilibrated with 50 mM Tris•HCl/100 mM NaCl, pH 8, and eluted with a linear gradient up to 1 M NaCl. The protein-containing fractions were then applied to a Phenyl Sepharose 6 FF (low sub) column, equilibrated against 25% $(NH_4)_2SO_4$/100 mM Tris•HCl, pH 8, and eluted with a linear gradient up to 100 mM Tris•HCl, pH 8. Fractions rich in N_2OR were then applied to a second DEAE CL-6B column, equilibrated against 50 mM MOPS, pH 7, and eluted with a linear gradient up to 650 mM NaCl. The pure N_2OR protein was then dialyzed against 25 mM Tris•HCl/10 mM EDTA, pH 8, followed by 25 mM Tris•HCl/100 mM NaCl, pH 8. N_2OR purified by this method is very pure.[207] This protein was divided into aliquots, flash frozen, and stored at -80 °C for future experiments.

4.2.5. $CuSO_4$ and EDTA Titrations of H46C/C112H Az

$CuSO_4$ titrations of H46C/C112H Az were performed in a standard 1cm x 1cm cuvette, with stirring. Small aliquots of the $CuSO_4$ solution were added slowly (over several seconds) using a pipetman. The titrations were monitored by UV-Vis absorption spectroscopy, and $CuSO_4$ was added until the visible absorptions no longer increased with each $CuSO_4$ addition.

Weakly bound copper was removed by a similar titration procedure. After titrating the protein sample with $CuSO_4$, small aliquots of EDTA were added to the protein solution with stirring to remove lower-affinity bound copper. At pH 4 and 7, this removal of low-affinity copper could be monitored by UV-Vis absorption spectroscopy, as a decrease in the S $\rightarrow$ Cu charge transfer band, and the EDTA additions were stopped once this band stopped decreasing (for an example, see Fig. 4.2).

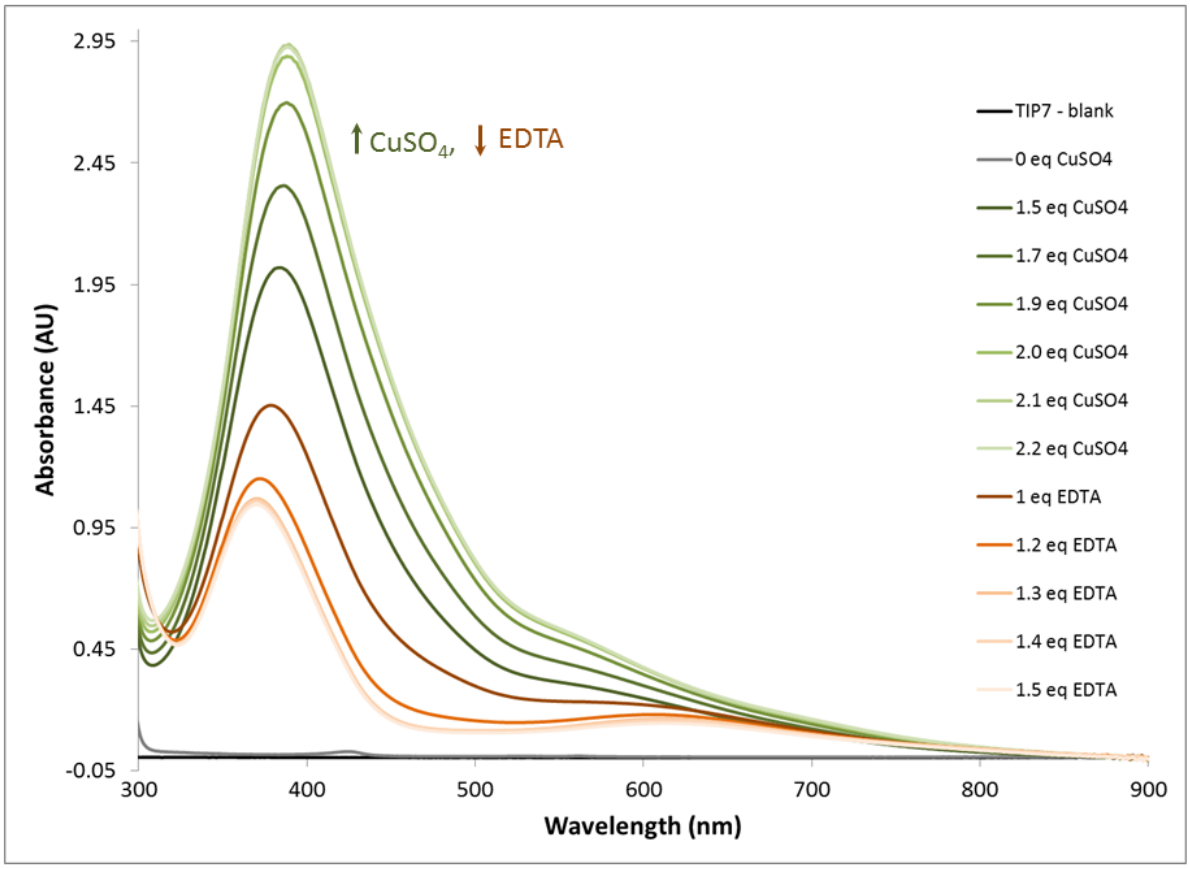

Fig. 4.2. UV-Vis absorption spectra collected during titration of H46C/C112H Az, pH 7 in TIP buffer, first with $CuSO_4$ then with EDTA. The initial $CuSO_4$ addition was large (1.5 eq), as it was known that H46C/C112H Az binds ~ 2 eq $CuSO_4$ at this pH. Likewise, the initial EDTA was large (1 eq), because H46C/C112H was known to require at least this amount to remove loosely bound copper.

4.2.6. UV-Vis Absorption Spectroscopy

UV-Vis absorption spectra were collected on one of three instruments: an HP (now Agilent) 8453 photodiode array, a Varian (now Agilent) Cary 3E dual monochromator, or a Varian (now Agilent) Cary 5000 dual monochromator. For the HP 8453, the wavelength range was set to 190-1100 nm, integration time to 0.5 s, and interval to 1 nm. For the Cary 3E and 5000, the scan controls were set to a 0.10 s average time, a 1.0 nm data interval, and 600 nm/min scan rate. Temperature control was achieved on the HP 8453 and Cary 3E by a water bath connected to the cuvette holder, while a mounted Peltier temperature control unit provided temperature control for the Cary 5000 instrument. A baseline was collected for experiments

conducted on the Cary instruments, in which both the reference and sample cuvettes were filled with the same buffer used for the protein sample.

Monitoring of the kinetic process upon addition of $CuSO_4$ to H46C/C112H Az was performed by setting up a cycle mode on either the Cary 3E or Cary 5000, in which regular scans were collected by specifying a cycle time. Although these instruments cannot collect rapid kinetic data over the full wavelength range, the kinetic process in H46C/C112H Az is quite slow, so this did not present a problem. The same cycle mode procedure was used to monitor copper transfer from Cu(II)-H46C/C112H Az to Cu_AAz or N_2OR.

4.2.7. Electron Paramagnetic Resonance (EPR) Spectroscopy

EPR data collection was performed using an X-band Varian E-122 spectrometer at the Illinois EPR Research Center (IERC). The temperature was set to 30 K using liquid He and an Air Products Helitran cryostat. Frequencies were measured with an EIP frequency counter, and magnetic fields were calibrated with a Varian NMR gaussmeter. At least 30% glycerol was added to all samples, as a glassing agent. Prepared samples were flash frozen in liquid nitrogen and stored this way until collection of the EPR data. The EPR spectrum of ^{63}Cu-H46C/C112H Az in UB, pH 9 was simulated with SIMPOW6.[218]

4.2.8. Syringe-Pump Electrospray Ionization Mass Spectrometry (ESI-MS)

Syringe-pump ESI-MS data were collected using a Quattro II MS instrument. The sample was first exchanged thoroughly into 50 NH_4OAc buffer, pH 4.1. Data collection was performed in positive ion mode, over a scan range of 500 to 4000 m/z. Fourier transformation of the data was performed to within 3 Da.

4.2.9. pH-Dependent EPR Spectroscopy

Copper bound H46C/C112H Az was prepared by titration with $CuSO_4$ until saturation of the ~385 nm band of the UV-Vis spectrum in TIP7, followed by removal of excess copper or weakly bound copper with EDTA. The sample was divided into 6 parts and was then exchanged into each of UB, pH 4, 5, 6, 7, 8, or 9. Buffer exchange was accomplished using a PD-10 column and standard techniques, in order to simultaneously exchange the buffer and remove the excess Cu(II)/EDTA.

4.2.10. Time-Dependent UV-Vis and EPR Spectroscopy at pH 9

For the time-dependent UV-Vis and EPR spectra metal-free H46C/C112H Az was exchanged into UB pH 9 using a PD-10 column. For the 0.9 eq $CuSO_4$ addition, the protein was concentrated to 0.1 mM, and 1.6 mL was added to a standard 1 cm x 1 cm cuvette, to which 0.9 eq $CuSO_4$ was added slowly, while stirring. The ensuing changes were monitored by UV-Vis spectroscopy over 16.5 hours.

For the 5 eq $CuSO_4$ addition, the protein was concentrated to 10 mL of 0.2 mM, and 5 eq of $CuSO_4$ was added while stirring at room temperature. At 5 min, 2.5 mL of this sample was applied to a PD-10 column, to effectively quench the reaction by removal of excess $CuSO_4$. Also at 5 min, 2.5 mL of this sample was transferred to the Cary 3E spectrophotometer to begin monitoring of the UV-Vis absorbance changes. Samples were quenched in the same way as the 5 min sample using the remaining 2.5 mL aliquots, at 75 min, 185 min, and 21 hours (final sample at 21 hours was the same sample for which the UV-Vis absorbance changes were monitored). The quenched samples were frozen in liquid nitrogen to stop any further changes with time, until the EPR samples were prepared. To prepare the EPR samples, the quenched samples were thawed, concentrated down to 125 μL, mixed thoroughly with 125 μL glycerol, and then flash frozen in EPR tubes.

4.2.11. Preparation of ^{63}Cu-H46C/C112H Az for EPR Spectroscopy

^{63}Cu-H46C/C112H Az sample was prepared by adding 0.9 equivalents of $^{63}CuSO_4$ to the metal-free H46C/C112H Az in UB, pH 9 slowly and while stirring. The buffer was then exchanged to remove any free copper by several concentration/dilution cycles in an Amicon Ultra centricon (Millipore). To 125 μL of the protein sample, 125 μL of glycerol was added with thorough mixing. The final protein concentration was 2 mM. This sample was transferred to an EPR tube and flash frozen in liquid nitrogen.

4.2.12. Test of Copper-Transfer Ability from H46C/C112H Az to Cu_A Centers

In order to probe the ability of H46C/C112H Az to transfer Cu(II) to metal-free Cu_A centers, equal volumes of Cu(II)-H46C/C112H Az and either Cu_AAz or N_2OR were mixed, and the subsequent processes were monitored by UV-Vis absorbance spectroscopy. The Cu(II)-

H46C/C112H Az was prepared by titrating the apo protein with $CuSO_4$, followed by EDTA to remove weakly bound copper, either in TIP7 buffer (for the experiment with Cu_AAz) or UB pH 9 (for the experiment with N_2OR). The excess Cu(II)/EDTA was removed using a PD-10 column equilibrated with the same buffer as used in the titration and standard techniques. Metal-free Cu_AAz or N_2OR were exchanged into the appropriate buffer using a PD-10 column and standard techniques, and then their concentrations were adjusted to the appropriate value using Amicon Ultra centricons (Millipore). To a standard 1cm x 1cm cuvette, 900 μL of the Cu(II)-H46C/C112H Az was added. After collecting a spectrum of this sample, 900 μL of metal-free Cu_AAz or N_2OR was added, with thorough mixing accomplished either by pipetting several times or by stirring. The cuvette was covered to prevent concentration of the sample due to evaporation. Scans were collected at regular intervals (see section 4.2.6).

4.2.13. Crystallography

Crystals of H46C/C112H Az were obtained by the hanging drop method. The conditions which yielded the best crystals were 3 μL of apo-H46C/C112H Az, 1.5 mM mixed with 3 μL of the crystallization buffer. The crystallization buffer used was one reported to give crystals previously for Az mutants. It consisted of 100 mM Tris•HCl, 100 mM $LiNO_3$, and 10 mM $CuSO_4$, pH 8, with 17.5% PEG 4000 as the precipitant. Crystals grew within one week at 4 °C, with the wells unsealed. One of the crystals was mounted, which diffracted to 2.9 Å. This structure is currently being refined.

4.3. Results

4.3.1. Initial UV-Vis Absorption and EPR Spectroscopic Characterizations of H46C/C112H Az

H46C/C112H Az was expressed and purified as previously reported for Az and its mutants,[227,228] with some minor modifications (see section 4.2.2). These mutations were originally made to probe the proposed electron transfer pathways in azurin. However, upon titration of the purified, metal-free H46C/C112H Az with ~2 molar equivalents of $CuSO_4$, the solution color turned yellow, reflecting an intense band centered at ~375 nm in the electron absorption spectrum (Fig. 4.3). Intense absorptions in the range of 360-400 nm are characteristic of the S $\rightarrow$ Cu charge transfer (CT) bands of type 2 (T2) copper centers with thiolate ligation.[65,201] In order to study the proposed electron transfer pathway in Az, a site very similar to

the original T1 copper center would be necessary, which would exhibit an intense S → Cu CT band centered near 620 nm. To better characterize this site as a T2 copper site, EPR spectroscopy was collected. In the interim between collection of the original UV-Vis and of the EPR spectrum, the UV-Vis absorptions of the protein changed, such that the color was grey instead of yellow (Fig. 4.3). The EPR spectrum of this grey Az displayed a rhombic spectrum (Fig. 4.4), with wide parallel hyperfine splittings and superhyperfine structure in the perpendicular region. The overall appearance and estimated g_z (~2.18) and A_z (~175 G) of the EPR spectrum were very similar to that of Cu(II)-bound Sco proteins.[187-189,226] Thus, further study of this Az mutant was undertaken, to explore whether it could be a structural and/or functional mimic of Cu(II) centers in Sco proteins.

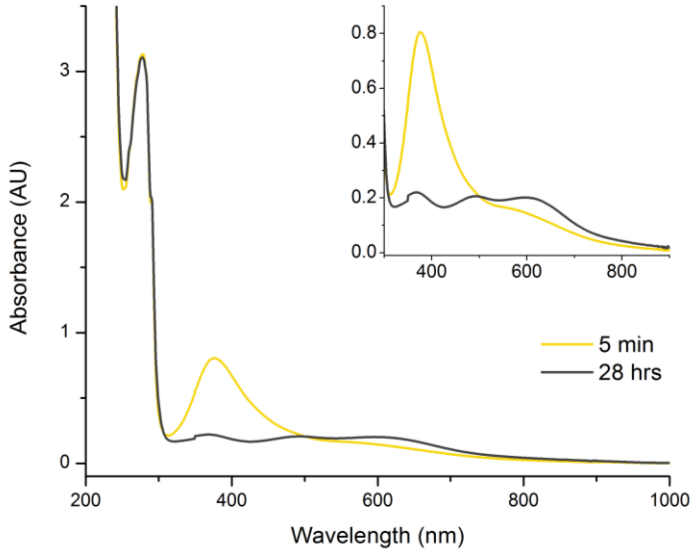

Fig. 4.3. Electronic absorption spectrum of 3.5 mM H46C/C112H Az, 5 min (yellow) and 28 hrs (grey) after addition of 0.9 eq $CuSO_4$, in 50 mM NH_4OAc, pH 4.1, 15 ºC. Cuvette path-length is 1 mm.

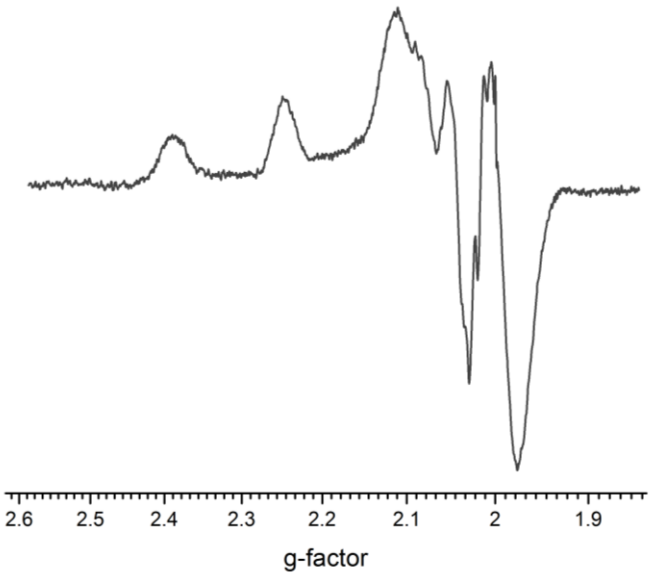

Fig. 4.4. EPR spectrum of Cu(II)-H46C/C112H Az, pH 4 in UB_{HEPES} (grey form). The protein concentration was 2.4 mM. X-band experimental conditions: microwave frequency, 9.05 GHz; power, 0.2 mW; modulation amplitude, 2 G; sweep time, 60 s; gain, 16000; temperature, 35 K.

4.3.2. Syringe-pump ESI-MS of H46C/C112H Az and Removal of Low-Affinity Copper

Syringe-pump ESI-MS, in which the mass spectra of the protein are collected under non-denaturing conditions in buffer, was performed. Whereas normal ESI-MS would remove metals from the copper binding site of Az, collection of the mass spectra under these conditions enables the detection of metal-bound to proteins. When this experiment was performed under similar conditions to those used to collect the EPR spectrum at pH 4, peaks corresponding to protein containing both one- and two-coppers bound were observed (Fig. 4.5). This was initially very puzzling, as the EPR spectrum appeared to be a single species. However, subsequent titrations of copper-bound H46C/C112H Az with EDTA showed bleaching of the ~385 nm band in the electronic absorption spectrum, up to ~1 eq of EDTA, suggesting that there was a second, lower-affinity copper bound to the protein. The EPR spectrum of the protein with the lower affinity copper removed revealed a loss of resolution for the superhyperfine structure in the perpendicular region (Fig. 4.6). As this superhyperfine structure is a major feature of Cu(II)-bound Sco, other conditions were explored to see if this structure could be resolved.

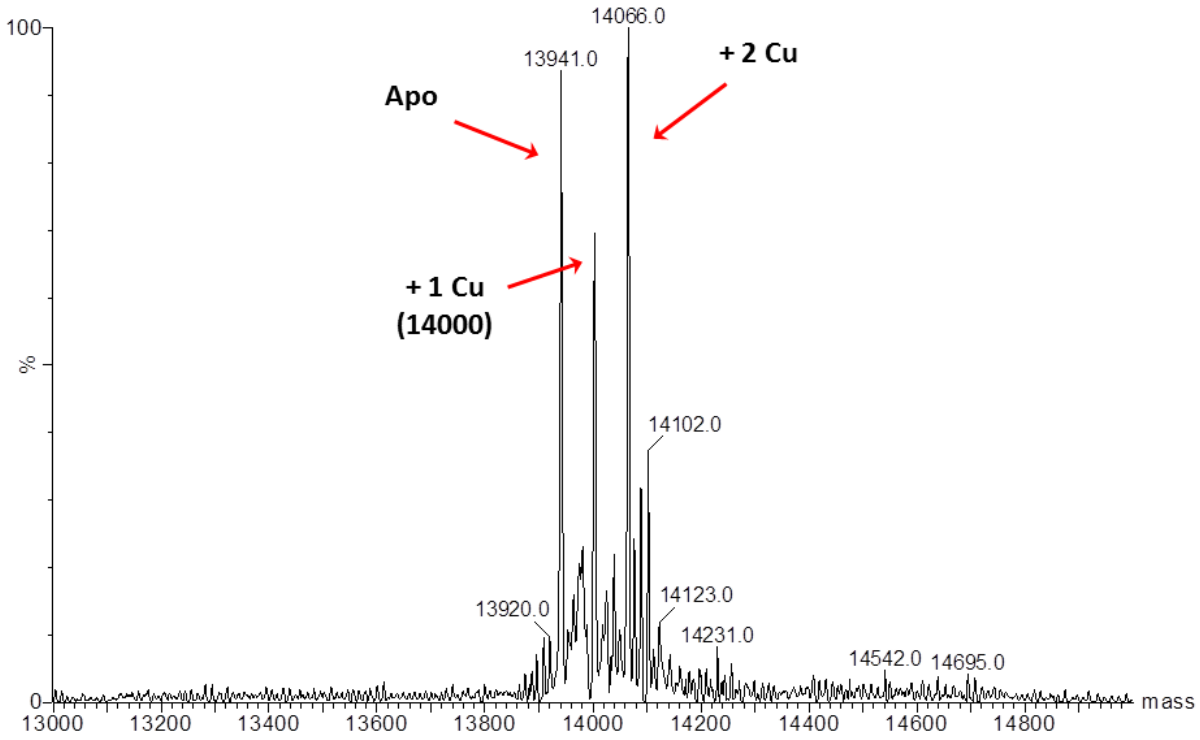

Fig. 4.5. Syringe-pump ESI-MS of Cu(II)-H46C/C112H Az, pH 4.1 in 50 mM NH_4OAc.

4.3.3. pH-dependent EPR Spectroscopy

Much of the superhyperfine structure present in the perpendicular region of Sco proteins arises from strong interaction with a His nitrogen.[188] As His residues may be protonated at low pH, the pH-dependence of the EPR spectra for H46C/C112H Az was explored, to see if superhyperfine structure from His coordination would appear at higher pH. EPR spectra of Cu(II)-H46C/C112H Az were collected from pH 4-9, in one pH unit increments (Fig. 4.6). These pH-dependent EPR spectra exhibit a mixture of species from pH 5 to 7, eliminating these pH values as being suitable for further study. At pH 8 and 9, however, the spectrum appears to be primarily a single species, with resolved superhyperfine splittings in the perpendicular region. Therefore, additional studies were conducted at pH 9, as this pH provided the cleanest EPR spectrum.

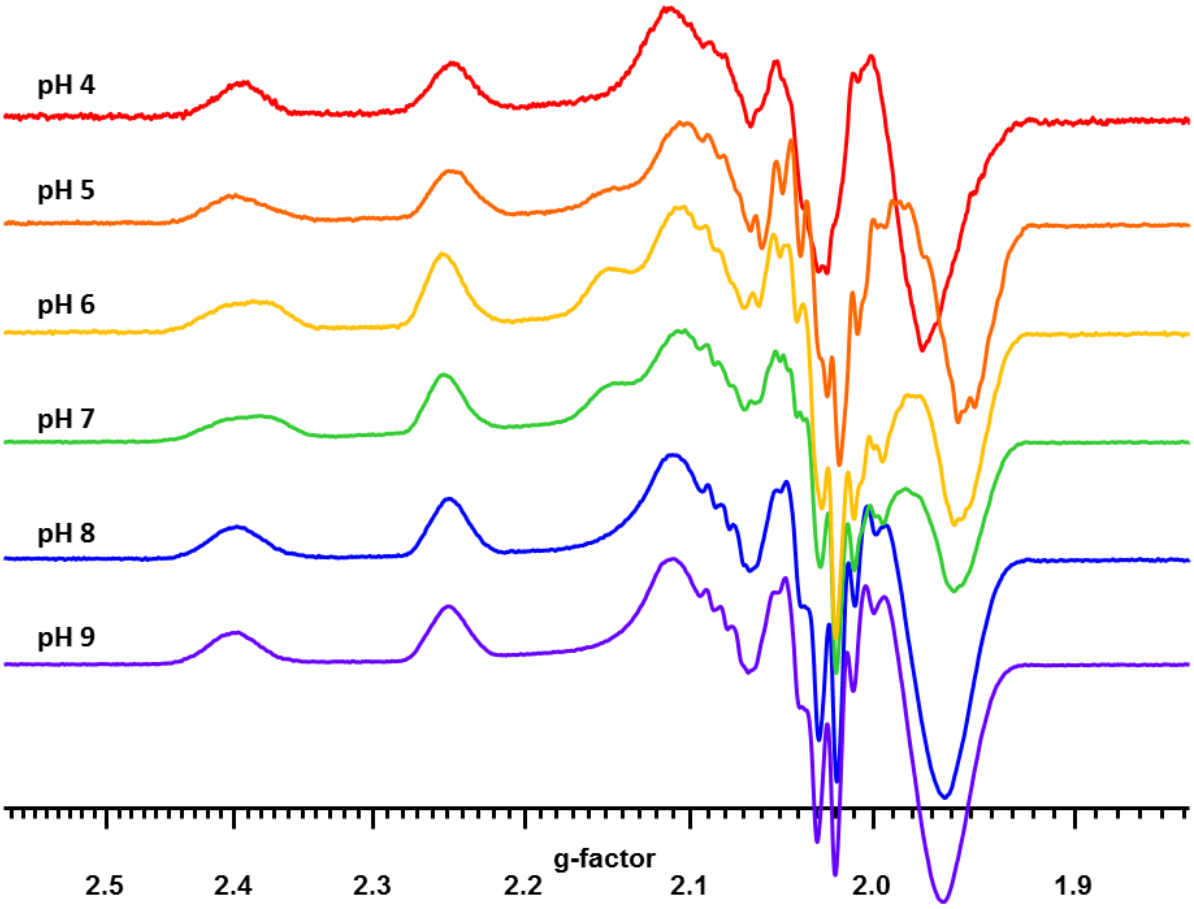

Fig. 4.6. pH-dependent EPR of Cu(II)-H46C/C112H Az in UB, which has been cleaned with EDTA, to remove low-affinity copper ions. Protein concentration for all samples is 2 mM. Glycerol concentration is ~30% vol/vol. X-band experimental conditions: microwave frequency, 9.05 GHz; power, 0.2 mW; modulation amplitude, 2 G; sweep time, 60s; gain, 5000; temperature, 35 K.

4.3.4. Detailed Characterization at pH 9 by Electronic Absorption and EPR Spectroscopy

The electronic absorption spectrum of H46C/C112H Az at pH 9 features an intense S → Cu CT band at 367 nm, slightly blue-shifted from the pH 4.1 case, as well as a less intense, broad transition at ~570 nm (Fig. 4.7). To further resolve the superhyperfine splittings in the EPR, an EPR spectrum of $^{63}CuSO_4$ metalated H46C/C112H Az was collected (Fig. 4.8). This EPR spectrum was simulated as a single species (Table 4.1). The superhyperfine splittings were also well simulated by two nitrogens (here, "a" and "b"), with parameters of A_x = 33 (a), 28 (b) cm^{-1}, A_y = 42 (a), 42 (b) cm^{-1}, and A_z = 36 (a), 31 (b) cm^{-1}. These electronic absorption and EPR

spectra provided a basis for comparison of H46C/C112H Az with Cu(II)-bound Scos and Sco mutants.

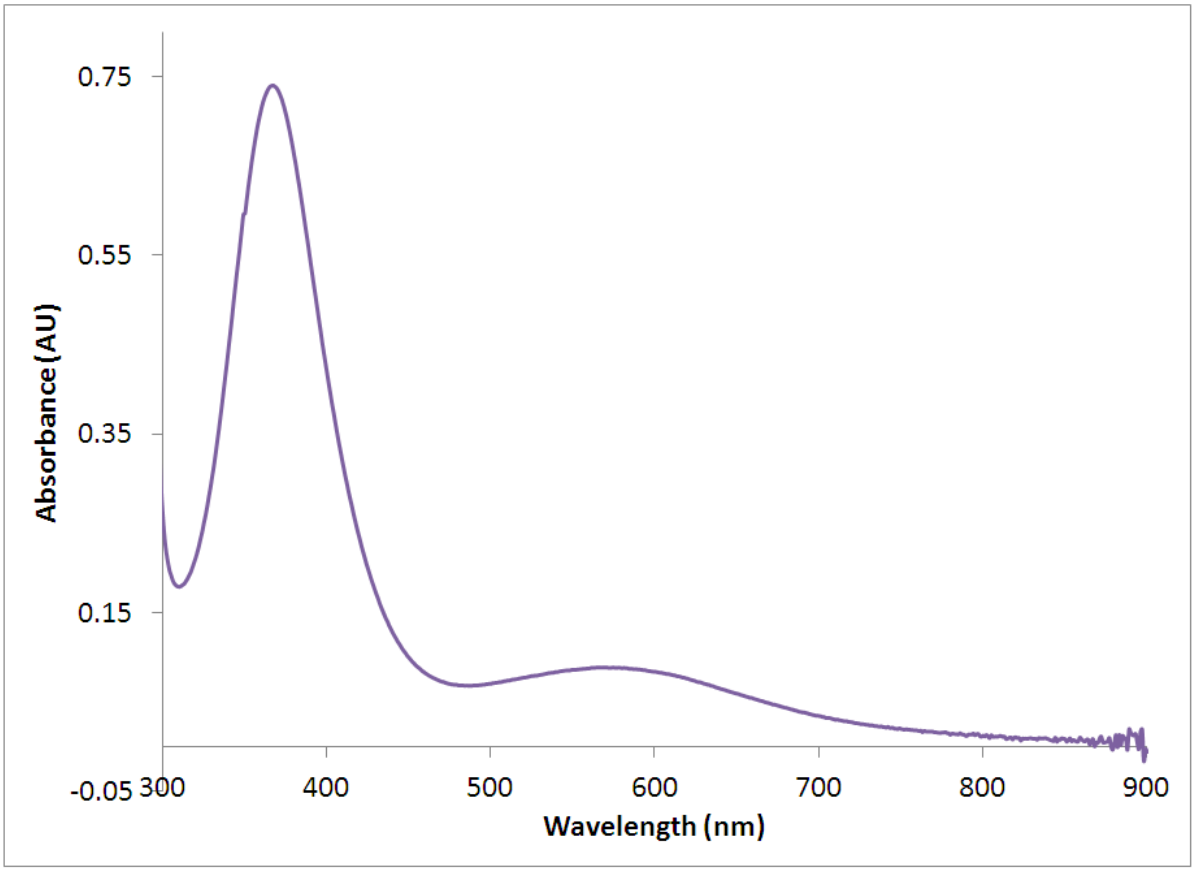

Fig. 4.7. UV-Vis absorption spectrum of Cu(II)-H46C/C112H Az, pH 9 in UB. Protein concentration is 0.2 mM. Cu(II)-H46C/C112H Az was prepared by titration with $CuSO_4$, followed by EDTA to remove low-affinity copper, and removal of excess Cu/EDTA by PD-10 column.

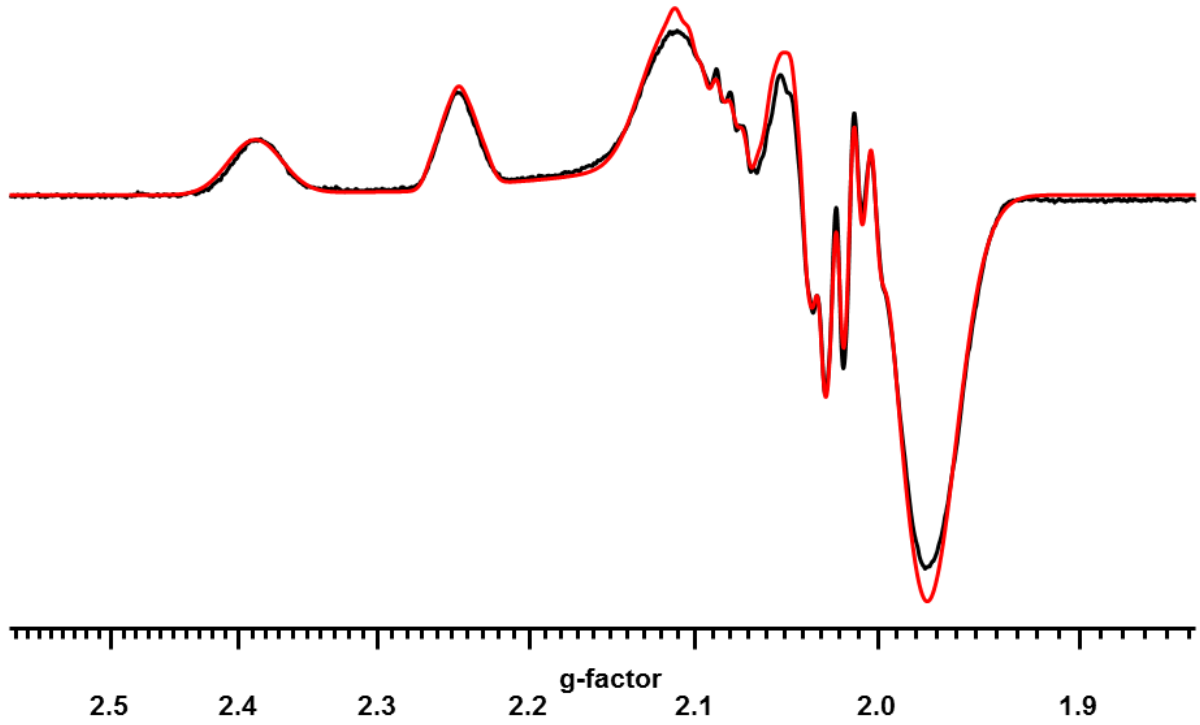

Fig. 4.8. EPR spectrum of ^{63}Cu-H46C/C112H Az, pH 9 in UB (black trace) and the simulated spectrum (red trace). Protein concentration is 2 mM. Glycerol concentration is ~50% vol/vol. X-band experimental conditions: microwave frequency, 9.05 GHz; power, 0.2 mW; modulation amplitude, 2 G; sweep time, 60s; gain, 5000; temperature, 35 K.

Table 4.1. EPR parameters of the ^{63}Cu-H46C/C112H Az identified through simulation of the spectrum in Fig. 4.8 and comparison to the Cu(II)-bound C45A-Sco parameters.[a]

	^{63}Cu(II)-H46C/C112H Az	^{63}Cu(II)-C45A Sco[b]
g_x	2.05	2.05
g_y	2.02	2.03
g_z	2.18	2.19
A_x	37	33
A_y	4 (unresolved)	22 (unresolved)
A_z	175	171
N1 (A_x)	11	9

Table 4.1, continued

N1 (A_y)	14	12
N1 (A_z)	12	11
N2 (A_x)	9	8
N2 (A_y)	14	11
N2 (A_z)	10	9

[a] Hyperfine principle values are reported in units of 10^{-4} cm^{-1}
[b] From ref. 226

4.3.5. Kinetic Yellow to Grey Transformation at pH 9

Some variation in color of H46C/C112H Az was observed while working with the protein at pH 9. In order to systematically probe this variation, the kinetics ensuing from addition of a sub-equivalent and excess amount of copper were monitored by visible absorption spectroscopy. Fig. 4.9 shows the changes that take place over 16.5 hours after the addition of 0.9 molar equivalents of $CuSO_4$, and over 21 hours after the addition of 5 molar equivalents, to H46C/C112H Az. In both samples, the absorption band at 367 nm decays gradually, while absorptions at ~500 and 600 nm increase, accompanied by an isosbestic point at ~450 nm, suggesting conversion of the species responsible for the 367 nm peak to the final product. This process appears to be copper-dependent, as the kinetics are much faster for the sample to which 5 eq $CuSO_4$ were added, seeming to be complete within 6 hours. Past 6 hours with 5 equivalents of $CuSO_4$, all of the visible bands decay. This may be due to reduction of the copper, loss or re-arrangement of copper away from the thiolate ligand, or denaturation of the protein. Time-dependent EPR spectra were also collected for the sample to which 5 eq $CuSO_4$ were added (Fig. 4.10). In general, the intensity of the EPR signal decreases over time, suggesting either antiferromagnetic coupling between two copper ions, precipitation of the protein, loss of copper from the protein, or reduction of copper ions. The latter option is not considered to be likely, since an isosbestic point is present in the electron absorption spectrum up to 6 hours, with loss of signal intensity in the EPR spectrum over this period; Cu(I) species are d^{10}, and therefore colorless, such that their formation could not give rise to an isosbestic point. The same is true for precipitation of the protein. If there were enough precipitation to affect the EPR spectrum so dramatically, an isosbestic point would not be present in the electronic absorption spectrum. Some reduction of copper or precipitation may be in effect past 6 hours, but these processes do

not account for the EPR signal loss up to 6 hours. Loss of copper from the protein is also not considered a likely possibility, as it is not consistent with the acceleration in the rate of this process with increasing copper equivalents. Therefore, the most likely possibility is that an antiferromagnetically coupled dicopper site is forming, leading to decreased signal intensity in the EPR spectrum. This behavior has not been reported for Sco proteins, and therefore, was not pursued further in the context of modeling native Sco centers using H46C/C112H Az.

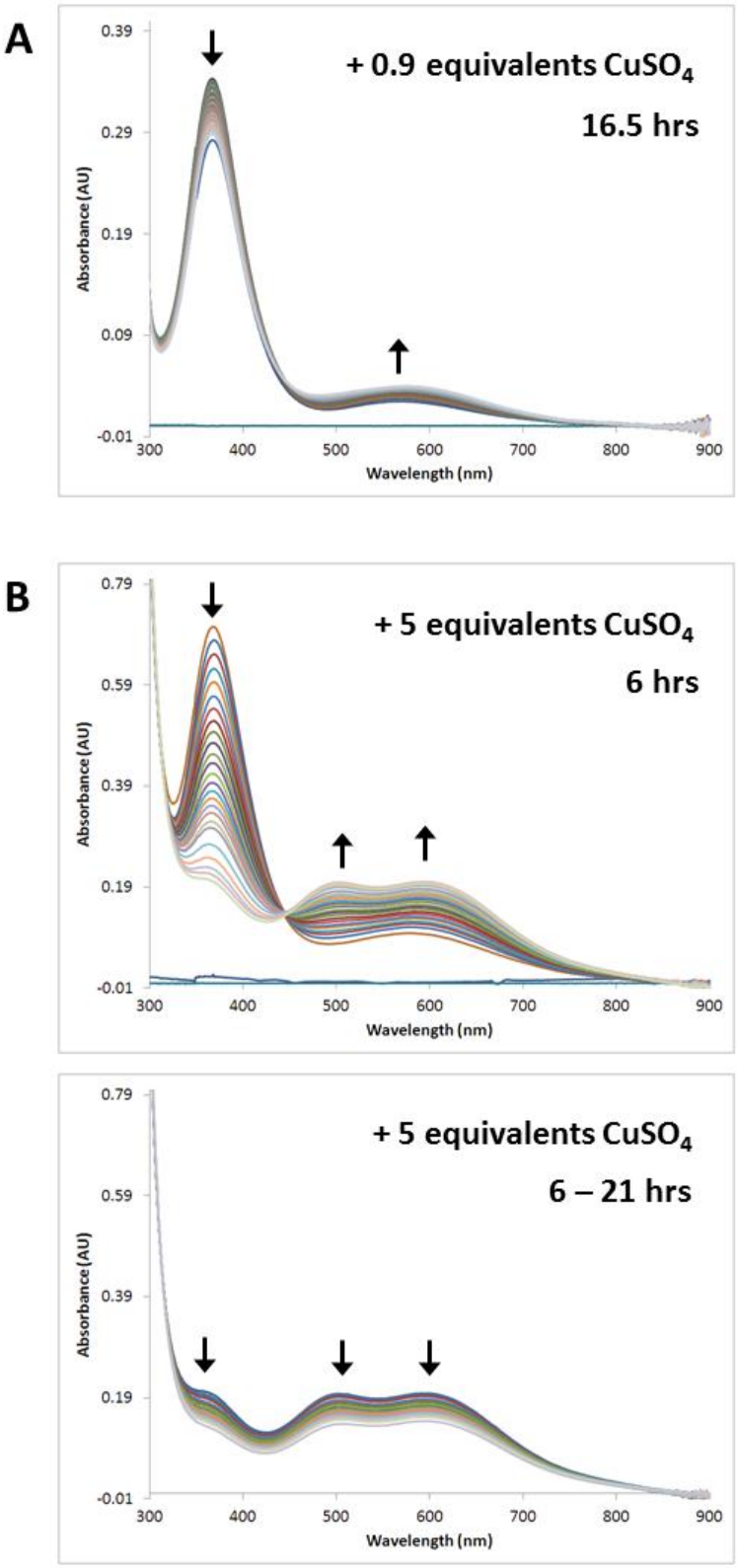

Fig. 4.9. Kinetic process observed in H46C/C112H Az after addition of (A) 0.9 equivalents of $CuSO_4$ and (B) 5 equivalents of $CuSO_4$, 20 °C. The process with 0.9 equivalents of $CuSO_4$ (A) is

very slow, with only ~20% change in the absorbance at 367 nm over 16.5 hrs. Protein concentration was 0.1 mM. Initial scans are at 5, 10, 15, 20, and 27 min after $CuSO_4$ addition. Starting at 27 min, spectra were collected every 30 min over the following 16 hours. When the $CuSO_4$ equivalents are increased to 5 (B), the process is greatly accelerated, appearing to complete within 6 hours. Past 6 hours, all of the visible bands decrease. Protein concentration was 0.2 mM. Scans from 5 min to 3 hours were collected every 10 min. Starting at 3.3 hours, scans were collected every 30 min up to 21 hours.

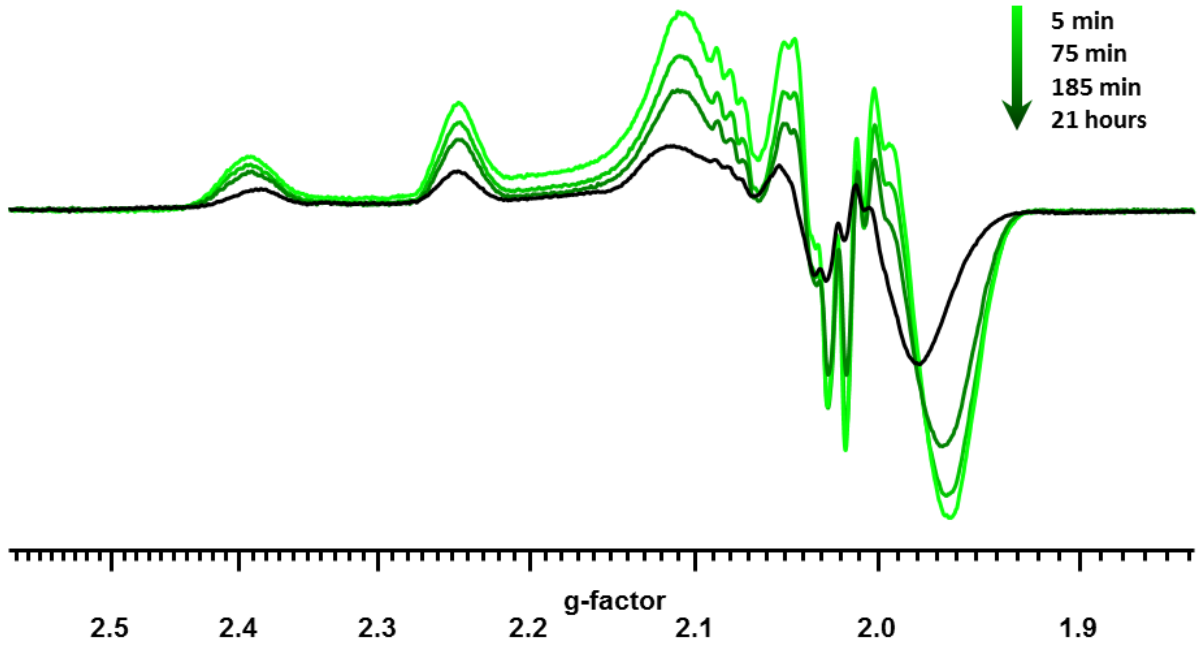

Fig. 4.10. Time-dependent EPR spectra of H46C/C112H Az, pH 9, after the addition of 5 equivalents of $CuSO_4$. Protein concentration was 2 mM. Glycerol concentration is ~50% vol/vol. X-band experimental conditions: microwave frequency, 9.05 GHz; power, 0.2 mW; modulation amplitude, 2 G; sweep time, 60s; gain, 5000; temperature, 35 K.

4.3.6. Test of H46C/C112H Az's Ability to Perform as a Cu(II) Chaperone to Cu_A

The ability of Cu(II)-H46C/C112H Az to perform as a copper chaperone to Cu_A was tested by incubating this protein with either the biosynthetic Cu_A model in Az (Cu_AAz) or nitrous oxide reductase (N_2OR) and monitoring the results by visible absorption spectroscopy. This experiment was performed with metal-free Cu_AAz, at pH 7, in a 1:1 mixture of Cu_AAz to Cu(II)-H46C/C112H Az and showed very slow copper transfer (change shown over 12 hrs) to a T1 copper intermediate (Fig. 4.11). Likewise, the same experiment performed with metal-free N_2OR at pH 9 revealed very slow (change shown over 22 hrs) copper transfer to a T1 copper

intermediate (Fig. 4.12). Both T1 copper intermediates were previously observed for Cu_A Az and N_2OR when Cu(II) was used to reconstitute them.[158,207]

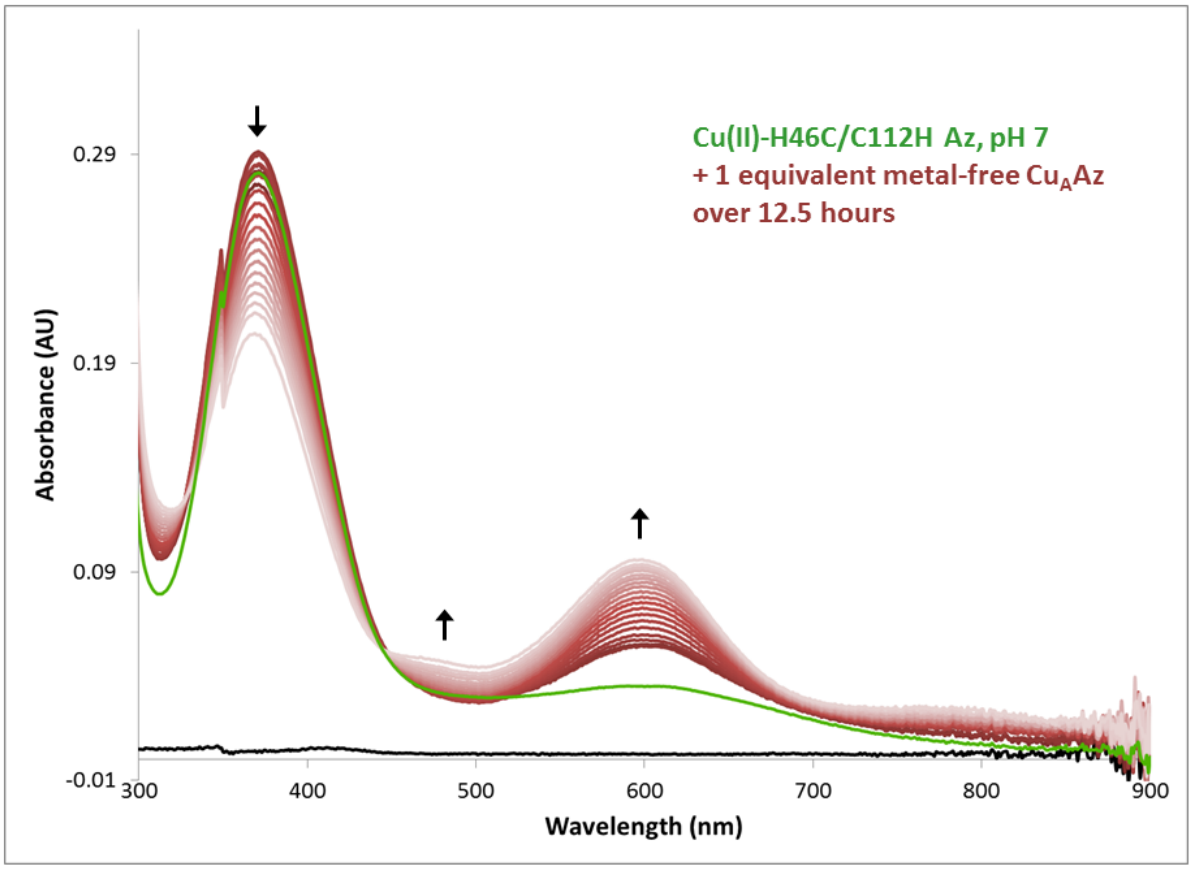

Fig. 4.11. Test of Cu(II) transfer ability from H46C/C112H Az to metal-free Cu_AAz at pH 7 in TIP buffer, 10 °C. The green trace corresponds to Cu(II)-H46C/C112H Az before the addition of Cu_AAz (corrected for dilution by dividing by 2). The series of red traces correspond to the kinetic process following the addition of an equal volume and concentration of Cu_AAz, with a smooth transition of dark to light color as time elapses. First several spectra were collected at 0.5, 5.5, 10.5, 15.5, 20.5, and 35 min after mixing. From 35 min after mixing, subsequent spectra were collected at 20 min intervals over 12 hours. The scan range is 200-1100 nm. Baseline correction was applied to the spectra at 928 nm. Final concentration of both proteins was 0.1 mM.

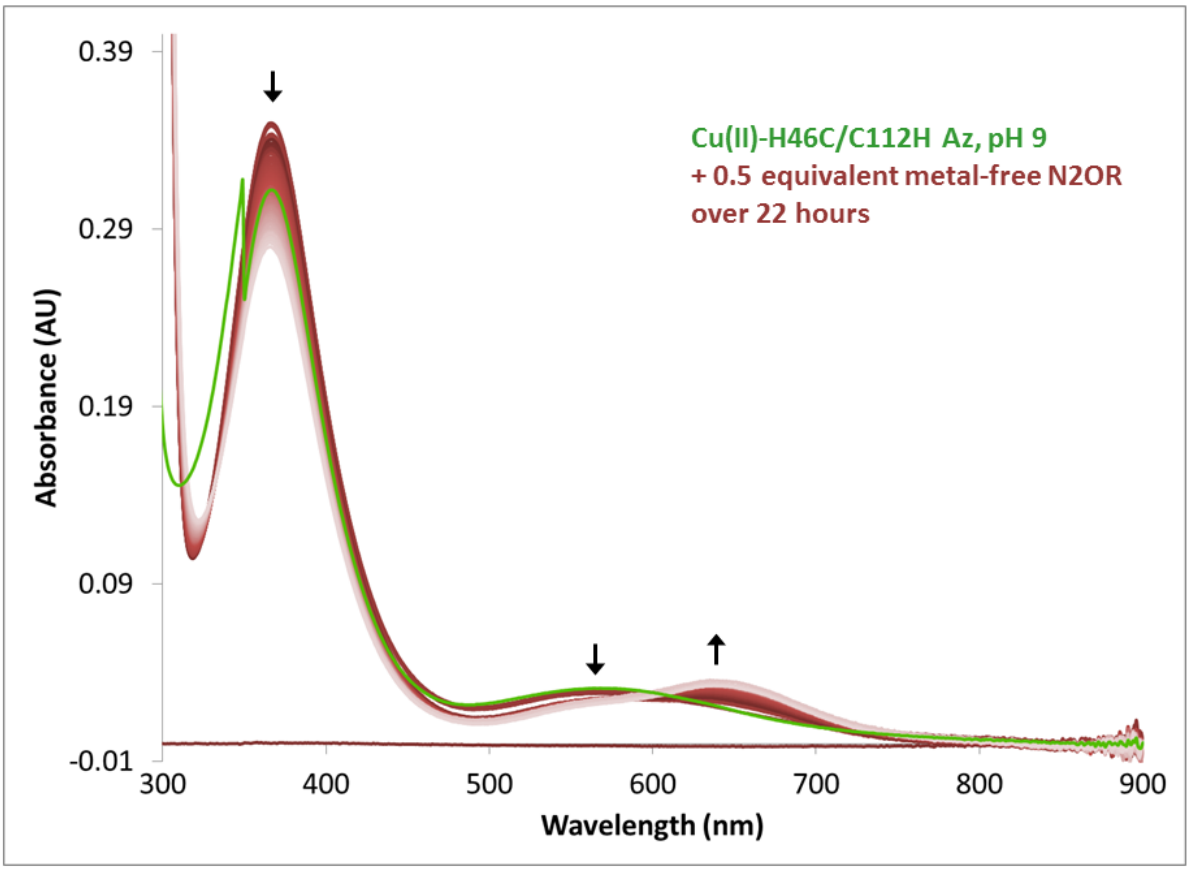

Fig. 4.12. Test of Cu(II) transfer ability from H46C/C112H Az to metal-free N_2OR at pH 9 in UB, 10 °C. The green trace corresponds to Cu(II)-H46C/C112H Az before the addition of N_2OR (corrected for dilution by dividing by 2). The series of red traces correspond to the kinetic process following the addition of 1 equivalent of N_2OR, with a smooth transition of dark to light color as time elapses. The first several spectra are collected at 5, 7.5, 10, and 15 min after mixing. Starting at 15 min after mixing, spectra were collected every 30 min over 22 hours. The Scan range was 200-1200 nm. Spectra were baseline corrected to 915 nm. The final concentration of both proteins was 0.1 mM.

4.3.7. X-ray Crystallography

Since a Cu(II)-bound structure of native Sco proteins has not yet been reported, a crystal structure of the Cu(II) center in H46C/C112H Az may be able to provide insight into native Sco structure and function. A variety of conditions for crystallization of this Az mutant have been explored. Recently, conditions where crystals form have been found (see Materials and Methods section 4.2.13). A diffraction pattern for one such crystal has been collected at Brookhaven National Laboratory, but the structure is still being refined, as locating the copper ion(s) in the structure has not been straightforward.

4.4. Discussion

4.4.1. Similarity of H46C/C112H Az to the C45A Mutant of Sco

The single species electronic absorption and EPR spectra (Table 4.1) of Cu(II)-H46C/C112H Az at pH 9 show a high degree of similarity to a mutant of Sco from *Bacillus subtilis*, in which one of the copper binding Cys residues, Cys45, is mutated to an Ala.[226] H46C/C112H Az displays absorption maxima at 367 nm ($\varepsilon \sim 3100\ M^{-1}\ cm^{-1}$) and 570 nm ($\varepsilon \sim 400\ M^{-1}\ cm^{-1}$) in its UV-Vis absorption spectrum (Fig. 4.7), compared to 370 nm ($\varepsilon \sim 2700\ M^{-1}\ cm^{-1}$), 455 nm ($\varepsilon \sim 400\ M^{-1}\ cm^{-1}$), and 600 nm ($\varepsilon \sim 400\ M^{-1}\ cm^{-1}$) for C45A Sco.[226] The EPR spectra of H46C/C112H Az and C45A Sco are also highly similar (Table 4.1), including superhyperfine splittings from two nitrogens. Thus, on the basis of electronic absorption and EPR spectroscopic parameters, H46C/C112H Az closely mimics the structural and electronic properties of C45A Sco.

Whole cell studies of bacterial, yeast, and human cells, in which the two copper-binding Cys residues of Sco were mutated to Ala or Ser, have shown that these Cys residues are essential for the function of Sco.[186,187,229] From these studies, however, it was unknown whether these mutations completely abrogated copper binding to Sco, or simply altered it. A study by Blackburn and coworkers, in which they individually mutated the Cys residues to Ala, showed that these Sco mutants still bound copper, but in modified sites.[226] The C49A mutation in Sco led to Cu(II) binding that was unstable with respect to autoreduction, forming a linear Cu(I) species as a result. Conversely, C45A Sco displayed more stable Cu(II) binding, although still ~35% of the Cu(II) added to this mutant became autoreduced to Cu(I). Therefore, the redox balance of the copper center, as well as its coordination set, is modified in each of these Cys to Ala mutants, but they both still bind copper. The ability of Sco to modulate the redox state of another pair of thiolates, such as those in the Cu_A site, would also be lost with these Cys to Ala mutants. Hence, the origin of the negative effects that Cys to Ala substitutions have upon the function of Sco proteins is presently unknown, and could be attributed to one or more of multiple changes induced by these mutations.

Studies of the H46C/C112H Az copper-binding center may help in deconvoluting the multiple effects of Cys to Ala mutation in Sco. Structural elucidation of Cu(II)-H46C/C112H Az is at hand, and the resulting picture would represent the first for Cu(II)-Sco-like centers. This

structure may allow some rationalization of the C45A-Sco Cu(II) structure, and the effects of this mutation on native Sco function. Furthermore, if H46C/C112H Az can be redesigned, based on its three-dimensional structure, to include the second Cys residue present in native Sco Cu(II) centers, then comparisons between this redesigned Sco-mimic in Az and H46C/C112H Az could provide a full picture of Cu(II)-Sco, independent of its thioredoxin-like fold.

4.4.2. pH Dependence of H46C/C112H Az

The Cu(II)-binding properties of H46C/C112H Az appear to vary with pH, based upon pH-dependent EPR spectra (Fig. 4.6). In the pH range of 5-7, a species with smaller A_z appears, in addition to the original species with larger A_z. This smaller A_z species is not expected to be the result of a second copper binding site, but rather, an alteration to the original copper site, the reason being that the Cu(II)-H46C/C112H Az used for this pH-dependent study was cleaned with EDTA, to remove the second, weakly-bound copper. The nature of the alterations to the copper site, however, is unknown. It could be the result of the deprotonation of an amino acid sidechain. However, if this were the case, one would expect a smooth transition from the protonated/unligated to the deprotonated/ligated form, as the pH is increased. This type of behavior is not observed here, as the second, smaller A_z species appears during a specific pH window, and then disappears as the pH is raised further. Another possibility is that an exogenous ligand is bound to Cu(II)-H46C/C112H Az, and that the second, smaller A_z species is the result of a change in this exogenous ligand binding, which then changes again at higher pH. A third possibility is that this pH-dependent behavior is a combination of amino acid side chain and exogenous ligand changes across the pH window of 4-9. As this pH-dependent behavior is not currently known to have any relevance to native Sco centers, which have all been studied in the range of pH 7-8, it was not investigated further.

4.4.3. Kinetic Alteration to the Copper Site of H46C/C112H Az

In addition to pH-dependent variations to the Cu(II)-binding of H46C/C112H Az, a dynamic process also leads to changes in the Cu(II) site over time. This dynamic process was observed both at pH 4 and pH 9, resulting in a similar grey-colored product, with three approximately equal intensity absorption maxima at ~ 370, 500, and 600 nm in the UV-Vis absorption spectra (Fig. 4.3 and Fig. 4.9). A more detailed investigation at pH 9 showed that this

dynamic process is accelerated by higher copper equivalents, suggesting that it may correspond to binding of a second copper (Fig. 4.9). An isosbestic point is also present in the UV-Vis absorption spectrum at ~450 nm, indicating clean conversion of the species giving rise to the 367 nm peak into the final product. Assuming this process corresponds to binding of a second copper ion, the fact that this event perturbs the original Cu(II) site further suggests that a dinuclear copper center may be forming. With 5 equivalents of $CuSO_4$ (Fig. 4.9), all of the visible bands begin to bleach past 6 hours. This is likely the result of excess copper, which typically destabilizes proteins. Time-dependent EPR spectra show an overall loss of spin from the system over the course of this process (Fig. 4.10), which may be due to reduction of Cu(II) to Cu(I), loss of copper from the protein, precipitation of the protein and/or antiferromagnetic coupling between two bound copper ions. Reduction of the copper ions and precipitation of the protein are eliminated from this list of possibilities, as neither of these processes would permit the observation of an isosbestic point in the UV-Vis absorption spectrum. Loss of copper from the protein is also unlikely, because it would contradict the observed acceleration of the kinetic process with increasing equivalents of copper. Hence, the dynamic process observed in Cu(II)-H46C/C112H Az most likely arises from formation of a dinuclear copper complex, in which the copper ions are close enough to each other to be antiferromagnetically coupled. While it is unlikely to be related to the copper center of Sco proteins, due to the fact that these centers are mononuclear, the nature of this putative dinuclear site is currently under investigation.

4.4.4. Copper Transfer Ability of H46C/C112H Az

To investigate the ability of Cu(II)-H46C/C112H Az to perform as a copper chaperone, it was incubated with two Cu_A-forming proteins, Cu_AAz and N_2OR, in their metal free forms. In both cases, the transfer of copper to these proteins is very slow, suggesting that Cu(II)-H46C/C112H Az does not perform well as a copper chaperone. As the mutant of Sco, C45A, that H46C/C112H Az most closely mimics is not functional in its role for C*c*O biogenesis, this poor copper chaperone activity of H46C/C112H Az is consistent with this most similar Sco variant. However, it also does not confirm a copper chaperone function for Scos.

4.5. Conclusions

A mutant of the type 1 copper protein Az, H46C/C112H Az, was shown to bind Cu(II) in a site very similar to a C45A mutant of Sco, as evidenced by its comparable UV-Vis and EPR spectral parameters. This Az variant also displays interesting pH- and time-dependent processes. Conditions have been found where H46C/C112H Az crystallizes, and a structure of its Cu(II)-bound form is expected soon. From this three-dimensional information, properties of the C45A Sco mutant may be inferred. Moreover, a three-dimensional structure of H46C/C112H Az should allow for redesign of this Az mutant into a close structural mimic of native Sco Cu(II) sites. From this redesigned Sco-mimic in Az, many useful insights into Sco structure and function may be gleaned. Since Az is highly amenable to crystallization, a structural model of Sco Cu(II) centers in Az may yield the first three-dimensional structure of a Sco-like Cu(II)-binding site. Moreover, Az adopts a distinct fold from that of Sco proteins, which would enable separation of the Cu(II) site's properties from those of the protein fold. Separating these two aspects of Sco proteins could shed light on the enigmatic function of these proteins. Specifically, a thioredoxin-type function has been proposed for Sco proteins, in maintaining the Cu_A-site Cys thiols in their reduced form, on the basis of the thioredoxin-like folds adopted by Sco proteins. Such a function is not associated with the cupredoxin fold adopted by Az, so the properties of a Sco-like copper-binding site in Az and their relationship to Cu_A formation could be investigated free of this possible function.

CHAPTER 5: REFERENCES

1. Solomon, E. I.; Randall, D. W.; Glaser, T. Electronic structures of active sites in electron transfer metalloproteins: contributions to reactivity. *Coord. Chem. Rev.* **2000**, *200-202*, 595.
2. Kaim, W.; Rall, J. Copper - a Modern Bioelement. *Angew. Chem. Int. Ed.* **1996**, *35*, 43.
3. Crichton, R. R.; Pierre, J. L. Old iron, young copper: from Mars to Venus. *BioMetals* **2001**, *14*, 99.
4. Sykes, A. G. Plastocyanin and the blue copper proteins. *Struct. Bond.* **1991**, *75*, 175.
5. Brzezinski, P.; Gennis, R. B. Cytochrome c oxidase: exciting progress and remaining mysteries. *J. Bioenerg. Biomembr.* **2008**, *40*, 521.
6. Muh, F.; Zouni, A. Light-induced water oxidation in photosystem II. *Front. Biosci., Landmark Ed.* **2011**, *16*, 3072.
7. Hakemian, A. S.; Rosenzweig, A. C. The biochemistry of methane oxidation. *Annu. Rev. Biochem.* **2007**, *76*, 223.
8. Nanda, V.; Koder, R. L. Designing artificial enzymes by intuition and computation. *Nat. Chem.* **2010**, *2*, 15.
9. Holm, R. H.; Solomon, E. I. Preface: Biomimetic Inorganic Chemistry. *Chem. Rev.* **2004**, *104*, 347.
10. Varadarajan, R.; Zewert, T. E.; Gray, H. B.; Boxer, S. G. Effects of buried ionizable amino acids on the reduction potential of recombinant myoglobin. *Science* **1989**, *243*, 69.
11. Backes, G.; Mino, Y.; Loehr, T. M.; Meyer, T. E.; Cusanovich, M. A.; Sweeney, W. V.; Adman, E. T.; Sanders-Loehr, J. The environment of Fe_4S_4 clusters in ferredoxins and high-potential iron proteins. New information from x-ray crystallography and resonance Raman spectroscopy. *J. Am. Chem. Soc.* **1991**, *113*, 2055-2064.
12. Stephens, P. J.; Jollie, D. R.; Warshel, A. Protein Control of Redox Potentials of Iron-Sulfur Proteins. *Chem. Rev.* **1996**, *96*, 2491.
13. Swartz, P. D.; Beck, B. W.; Ichiye, T. Structural origins of redox potentials in Fe-S proteins: electrostatic potentials of crystal structures. *Biophys. J.* **1996**, *71*, 2958.
14. Swartz, P. D.; Ichiye, T. Protein contributions to redox potentials of homologous rubredoxins: an energy minimization study. *Biophys. J.* **1997**, *73*, 2733.

15. Battistuzzi, G.; Borsari, M.; Loschi, L.; Sola, M. Redox thermodynamics, acid-base equilibria and salt-induced effects for the cucumber basic protein. General implications for blue-copper proteins. *J. Biol. Inorg. Chem.* **1997**, *2*, 350.
16. Gunner, M. R.; Alexov, E.; Torres, E.; Lipovaca, S. The importance of the protein in controlling the electrochemistry of heme metalloproteins: methods of calculation and analysis. *J. Biol. Inorg. Chem.* **1997**, *2*, 126.
17. Battistuzzi, G.; Borsari, M.; Loschi, L.; Sola, M. Redox properties of the basic blue protein (plantacyanin) from spinach. *J. Inorg. Biochem.* **1998**, *69*, 97.
18. Benini, S.; Borsari, M.; Ciurli, S.; Dikiy, A.; Lamborghini, M. Modulation of Bacillus pasteurii cytochrome c553 reduction potential by structural and solution parameters. *J. Biol. Inorg. Chem.* **1998**, *3*, 371.
19. Battistuzzi, G.; Borsari, M.; Cowan, J. A.; Eicken, C.; Loschi, L.; Sola, M. Redox chemistry and acid-base equilibria of mitochondrial plant cytochromes c. *Biochemistry* **1999**, *38*, 5553.
20. Battistuzzi, G.; Borsari, M.; Loschi, L.; Righi, F.; Sola, M. Redox thermodynamics of blue copper proteins. *J. Am. Chem. Soc.* **1999**, *121*, 501.
21. Battistuzzi, G.; Loschi, L.; Borsari, M.; Sola, M. Effects of nonspecific ion-protein interactions on the redox chemistry of cytochrome c. *J. Biol. Inorg. Chem.* **1999**, *4*, 601.
22. Eidsness, M. K.; Burden, A. E.; Richie, K. A.; Kurtz, D. M., Jr.; Scott, R. A.; Smith, E. T.; Ichiye, T.; Beard, B.; Min, T.; Kang, C. Modulation of the Redox Potential of the Fe(SCys)4 Site in Rubredoxin by the Orientation of a Peptide Dipole. *Biochemistry* **1999**, *38*, 14803.
23. Gray, H. B.; Malmström, B. G.; Williams, R. J. P. Copper coordination in blue proteins. *J. Biol. Inorg. Chem.* **2000**, *5*, 551.
24. Battistuzzi, G.; Borsari, M.; Loschi, L.; Menziani, M. C.; De Rienzo, F.; Sola, M. Control of Metalloprotein Reduction Potential: The Role of Electrostatic and Solvation Effects Probed on Plastocyanin Mutants. *Biochemistry* **2001**, *40*, 6422.
25. Battistuzzi, G.; Borsari, M.; Loschi, L.; Ranieri, A.; Sola, M.; Mondovi, B.; Marchesini, A. Redox properties and acid-base equilibria of zucchini mavicyanin. *J. Inorg. Biochem.* **2001**, *83*, 223.

26. Battistuzzi, G.; Borsari, M.; Canters, G. W.; de Waal, E.; Loschi, L.; Warmerdam, G.; Sola, M. Enthalpic and Entropic Contributions to the Mutational Changes in the Reduction Potential of Azurin. *Biochemistry* **2001**, *40*, 6707.
27. Donaire, A.; Jimenez, B.; Moratal, J.-M.; Hall, J. F.; Hasnain, S. S. Electronic Characterization of the Oxidized State of the Blue Copper Protein Rusticyanin by 1H NMR: Is the Axial Methionine the Dominant Influence for the High Redox Potential? *Biochemistry* **2001**, *40*, 837.
28. Machczynski, M. C.; Gray, H. B.; Richards, J. H. An outer-sphere hydrogen-bond network constrains copper coordination in blue proteins. *J. Inorg. Biochem.* **2002**, *88*, 375.
29. Olsson, M. H. M.; Hong, G.; Warshel, A. Frozen Density Functional Free Energy Simulations of Redox Proteins: Computational Studies of the Reduction Potential of Plastocyanin and Rusticyanin. *J. Am. Chem. Soc.* **2003**, *125*, 5025.
30. Battistuzzi, G.; Bellei, M.; Borsari, M.; Canters, G. W.; de Waal, E.; Jeuken, L. J. C.; Ranieri, A.; Sola, M. Control of Metalloprotein Reduction Potential: Compensation Phenomena in the Reduction Thermodynamics of Blue Copper Proteins. *Biochemistry* **2003**, *42*, 9214.
31. Fernandez, C. O.; Niizeki, T.; Kohzuma, T.; Vila, A. J. Metal-ligand interactions in perturbed blue copper sites: a paramagnetic 1H NMR study of Co(II)-pseudoazurin. *J. Biol. Inorg. Chem.* **2003**, *8*, 75.
32. Yanagisawa, S.; Sato, K.; Kikuchi, M.; Kohzuma, T.; Dennison, C. Introduction of a Ï□â^'Ï□ Interaction at the Active Site of a Cupredoxin: Characterization of the Met16Phe Pseudoazurin Mutantâ€ *Biochemistry* **2003**, *42*, 6853.
33. Battistuzzi, G.; Borsari, M.; Di Rocco, G.; Ranieri, A.; Sola, M. Enthalpy/entropy compensation phenomena in the reduction thermodynamics of electron transport metalloproteins. *J. Biol. Inorg. Chem.* **2004**, *9*, 23.
34. Solomon, E. I.; Szilagyi, R. K.; DeBeer George, S.; Basumallick, L. Electronic Structures of Metal Sites in Proteins and Models: Contributions to Function in Blue Copper Proteins. *Chemical reviews* **2004**, *104*, 419.
35. Dennison, C. Investigating the structure and function of cupredoxins. *Coord. Chem. Rev.* **2005**, *249*, 3025.

36. Marshall, N. M.; Garner, D. K.; Wilson, T. D.; Gao, Y.-G.; Robinson, H.; Nilges, M. J.; Lu, Y. Rationally tuning the reduction potential of a single cupredoxin beyond the natural range. *Nature* **2009**, *462*, 113.
37. Berry, S. M.; Baker, M. H.; Reardon, N. J. Reduction potential variations in azurin through secondary coordination sphere phenylalanine incorporations. *J. Inorg. Biochem.* **2010**, *104*, 1071.
38. Zheng, P.; Takayama, S.-i. J.; Mauk, A. G.; Li, H. Hydrogen bond strength modulates the mechanical strength of ferric-thiolate bonds in rubredoxin. *J. Am. Chem. Soc.* **2012**, *134*, 4124.
39. Borovik, A. S. Bioinspired Hydrogen Bond Motifs in Ligand Design: The Role of Noncovalent Interactions in Metal Ion Mediated Activation of Dioxygen. *Acc. Chem. Res.* **2005**, *38*, 54.
40. Rivas, J. C. M. Cooperation of metals and hydrogen bonding groups in metal-promoted reactions. *Curr. Org. Chem.* **2007**, *11*, 1434.
41. Shook, R. L.; Borovik, A. S. The effects of hydrogen bonds on metal-mediated O2 activation and related processes. *Chem. Commun.* **2008**, 6095.
42. Liu, Y.-C.; Tu, L.-K.; Yen, T.-H.; Lee, G.-H.; Yang, S.-T.; Chiang, M.-H. Secondary Coordination Sphere Interactions within the Biomimetic Iron Azadithiolate Complexes Related to Fe-Only Hydrogenase: Dynamic Measure of Electron Density about the Fe Sites. *Inorg. Chem.* **2010**, *49*, 6409.
43. Shook, R. L.; Borovik, A. S. Role of the Secondary Coordination Sphere in Metal-Mediated Dioxygen Activation. *Inorg. Chem.* **2010**, *49*, 3646.
44. Lu, Y.; Berry, S. M.; Pfister, T. D. Engineering novel metalloproteins: Design of metal-binding sites into native protein scaffolds. *Chemical Reviews (Washington, D.C.)* **2001**, *101*, 3047.
45. Lu, Y. Design and engineering of metalloproteins containing unnatural amino acids or non-native metal-containing cofactors. *Curr. Opin. Chem. Biol.* **2005**, *9*, 118.
46. Lu, Y. Biosynthethic inorganic chemistry. *Angew. Chem. Int. Ed.* **2006**, *45*, 5588.
47. Lu, Y.; Yeung, N.; Sieracki, N.; Marshall, N. M. Design of functional metalloproteins. *Nature* **2009**, *460*, 855.

48. Marshall, N. M.; Miner, K. D.; Wilson, T. D.; Lu, Y. In *Coordination Chemistry in Protein Cages*; Ueno, T., Watanabe, Y., Eds.; John Wiley & Sons Inc: Hoboken, NJ, 2012, p In Press.
49. Ghosh, D.; Pecoraro, V. L. Understanding Metalloprotein Folding Using a de Novo Design Strategy. *Inorg. Chem.* **2004**, *43*, 7902.
50. Calhoun, J. R.; Nastri, F.; Maglio, O.; Pavone, V.; Lombardi, A.; DeGrado, W. F. Artificial diiron proteins: From structure to function. *Biopolymers* **2005**, *80*, 264.
51. Ghosh, D.; Pecoraro, V. L. Probing metal-protein interactions using a de novo design approach. *Curr. Opin. Chem. Biol.* **2005**, *9*, 97.
52. Maglio, O.; Nastri, F.; Martin de Rosales, R. T.; Faiella, M.; Pavone, V.; DeGrado, W. F.; Lombardi, A. Diiron-containing metalloproteins: Developing functional models. *C. R. Chim.* **2007**, *10*, 703.
53. Peacock, A. F. A.; Iranzo, O.; Pecoraro, V. L. Harnessing natures ability to control metal ion coordination geometry using de novo designed peptides. *Dalton Trans.* **2009**, 2271.
54. Rosati, F.; Roelfes, G. Artificial Metalloenzymes. *ChemCatChem* **2010**, *2*, 916.
55. Zastrow, M. L.; Peacock, A. F. A.; Stuckey, J. A.; Pecoraro, V. L. Hydrolytic catalysis and structural stabilization in a designed metalloprotein. *Nat. Chem.* **2012**, *4*, 118.
56. Iwata, S.; Ostermeier, C.; Ludwig, B.; Michel, H. Structure at 2.8A resolution of cytochrome c oxidase from Paracoccus denitrificans. *Nature* **1995**, *376*, 660.
57. Tsukihara, T.; Aoyama, H.; Yamashita, E.; Tomizaki, T.; Yamaguchi, H.; Shinzawa-Itoh, K.; Nakashima, R.; Yaono, R.; Yoshikawa, S. Structures Of metal sites Of oxidized bovine heart cytochrome c oxidase at 2.8 Angstrom. *Science* **1995**, *269*, 1069.
58. Tsukihara, T.; Aoyama, H.; Yamashita, E.; Tomizaki, T.; Yamaguchi, H.; Shinzawa-Itoh, K.; Nakashima, R.; Yaono, R.; Yoshikawa, S. The whole structure of the 13-subunit oxidized cytochrome c oxidase at 2.8 Angstrom. *Science* **1996**, *272*, 1136.
59. Robinson, H.; Ang, M. C.; Gao, Y.-G.; Hay, M. T.; Lu, Y.; Wang, A. H. J. Structural Basis of Electron Transfer Modulation in the Purple CuA Center. *Biochemistry* **1999**, *38*, 5677.
60. Williams, P. A.; Blackburn, N. J.; Sanders, D.; Bellamy, H.; Stura, E. A.; Fee, J. A.; McRee, D. E. The CuA domain of Thermus thermophilus ba3-type cytochrome c oxidase at 1.6 Å resolution. *Nat. Struct. Biol.* **1999**, *6*, 509.

61. Brown, K.; Djinovic-Carugo, K.; Haltia, T.; Cabrito, I.; Saraste, M.; Moura, J. J. G.; Moura, I.; Tegoni, M.; Cambillau, C. Revisiting the catalytic CuZ cluster of nitrous oxide (N2O) reductase. Evidence of a bridging inorganic sulfur. *J. Biol. Chem.* **2000**, *275*, 41133.

62. Brown, K.; Tegoni, M.; Prudencio, M.; Pereira, A. S.; Besson, S.; Moura, J. J.; Moura, I.; Cambillau, C. A novel type of catalytic copper cluster in nitrous oxide reductase. *Nat. Struct. Biol.* **2000**, *7*, 191-195.

63. Haltia, T.; Brown, K.; Tegoni, M.; Cambillau, C.; Saraste, M.; Mattila, K.; Djinovic-Carugo, K. Crystal structure of nitrous oxide reductase from Paracoccus denitrificans at 1.6 Å resolution. *Biochemical Journal* **2003**, *369*, 77.

64. Paraskevopoulos, K.; Antonyuk, S. V.; Sawers, R. G.; Eady, R. R.; Hasnain, S. S. Insight into Catalysis of Nitrous Oxide Reductase from High-resolution Structures of Resting and Inhibitor-bound Enzyme from Achromobacter cycloclastes. *J. Mol. Biol.* **2006**, *362*, 55.

65. Lu, Y. In *Biocoordination Chemistry*; Que, J. L., Tolman, W. B., Eds.; Elsevier: Oxford, UK, 2004; Vol. 8; 8, p 91.

66. Savelieff, M. G.; Lu, Y. Cu_A centers and their biosynthetic models in azurin. *J. Biol. Inorg. Chem.* **2010**, *15*, 461-483.

67. Blackburn, N. J.; Barr, M. E.; Woodruff, W. H.; van der Oost, J.; de Vries, S. Metal-Metal Bonding In Biology: EXAFS Evidence for a 2.5A Copper-Copper Bond in the CuA Center Of Cytochrome Oxidase. *Biochemistry* **1994**, *33*, 10401-10407.

68. Henkel, G.; Müller, A.; Weissgräber, S.; Buse, G.; Soulimane, T.; Steffens, G. C. M.; Nolting, H. F. The Active Sites of the Native Cytochrome-c-Oxidase from Bovine Heart Mitochondria: EXAFS-Spectroscopic Characterization of a Novel Homobinuclear Copper Center (CuA) and of the Heterobinuclear Fea3-CuB Center. *Angew. Chem. Int. Ed.* **1995**, *34*, 1488.

69. Solomon, E. I.; Xie, X.; Dey, A. Mixed valent sites in biological electron transfer. *Chem. Soc. Rev.* **2008**, *37*, 623.

70. Antholine, W. E.; Kastrau, D. H. W.; Steffens, G. C. M.; Buse, G.; Zumft, W. G.; Kroneck, P. M. H. A comparative EPR investigation of the multicopper proteins nitrous-oxide reductase and cytochrome c oxidase. *Eur. J. Biochem.* **1992**, *209*, 875.

71. Farrar, J. A.; Neese, F.; Lappalainen, P.; Kroneck, P. M. H.; Saraste, M.; Zumft, W. G.; Thomson, A. J. The electronic structure of CuA: A novel mixed-valence dinuclear copper electron transfer center. *J. Am. Chem. Soc.* **1996**, *118*, 11501.

72. Gamelin, D. R.; Randall, D. W.; Hay, M. T.; Houser, R. P.; Mulder, T. C.; Canters, G. W.; de Vries, S.; Tolman, W. B.; Lu, Y.; Solomon, E. I. Spectroscopy of Mixed-Valence CuA-Type Centers: Ligand-Field Control of Ground-State Properties Related to Electron Transfer. *J. Am. Chem. Soc.* **1998**, *120*, 5246.

73. Kroneck, P. M. H.; Antholine, W. E.; Koteich, H.; Kastrau, D. H. W.; Neese, F.; Zumft, W. G. The EPR-detectable copper of nitrous oxide reductase as a model for CuA in cytochrome c oxidase: A multifrequency electron paramagnetic resonance investigation. *Bioinorg. Chem. Copper* **1993**, 419.

74. Neese, F.; Zumft, W. G.; Antholine, W. E.; Kroneck, P. M. H. The Purple Mixed-Valence CuA Center in Nitrous-oxide Reductase: EPR of the Copper-63-, Copper-65-, and Both Copper-65- and 15N Histidine-Enriched Enzyme and a Molecular Orbital Interpretation. *J. Am. Chem. Soc.* **1996**, *118*, 8692.

75. Olsson, M. H. M.; Ryde, U. Geometry, Reduction Potential, and Reorganization Energy of the Binuclear CuA Site, Studied by Density Functional Theory. *J. Am. Chem. Soc.* **2001**, *123*, 7866.

76. Malmström, B. G.; Aasa, R. The Nature Of the CuA Center In Cytochrome-C-Oxidase. *FEBS Lett.* **1993**, *325*, 49.

77. Lappalainen, P.; Saraste, M. The Binuclear CuA Center of Cytochrome-Oxidase. *Biochim. Biophys. Acta* **1994**, *1187*, 222.

78. Bertagnolli, H.; Kaim, W. The Dinuclear CuA Center in Cytochrome c Oxidase and N2O Reductase-A Metal-Metal Bond in Biology? *Angew. Chem. Int. Ed.* **1995**, *34*, 771.

79. Dennison, C.; Canters, G. W. The CuA site of cytochrome c oxidase. *Recl. Trav. Chim. Pays-Bas* **1996**, *115*, 345.

80. Beinert, H. Copper A of Cytochrome c Oxidase, a Novel, Long-Embattled, Biological Electron-Transfer Site. *Eur. J. Biochem.* **1997**, *245*, 521-532.

81. Randall, D. W.; Gamelin, D. R.; LaCroix, L. B.; Solomon, E. I. Electronic structure contributions to electron transfer in blue Cu and CuA. *J. Biol. Inorg. Chem.* **2000**, *5*, 16.

82. Sanders-Loehr, J. In *Physical Methods in Bioinorganic Chemistry*; Que, L., Jr., Ed.; University Science Books: Sausalito, CA, 2000, p 505.
83. Kroneck, P. M. H. In *Handbook of Metalloproteins*; Messerschmidt, A., Huber, R., Poulos, T., Wieghardt, K., Eds.; Wiley: Chichester, 2001; Vol. 2; 2, p 1333.
84. Savelieff, M. G.; Lu, Y. pH dependent copper binding properties of a Cu_A azurin variant with both bridging cysteines replaced with serines. *Inorg. Chem. Acta* **2008**, *361*, 1087.
85. Richter, O. M. H.; Ludwig, B. Cytochrome c oxidase - structure, function, and physiology of a redox-driven molecular machine. *Rev. Physiol. Biochem. Pharmacol.* **2003**, *147*, 47.
86. Wikstrom, M. Cytochrome c oxidase: 25 years of the elusive proton pump. *Biochim. Biophys. Acta* **2004**, *1655*, 241.
87. Brunori, M.; Giuffre, A.; Sarti, P. Cytochrome c oxidase, ligands and electrons. *J. Inorg. Biochem.* **2005**, *99*, 324.
88. Zumft, W. G.; Kroneck, P. M. H. Respiratory transformation of nitrous oxide (N_2O) to dinitrogen by Bacteria and Archaea. *Adv. Microb. Physiol.* **2007**, *52*, 107-227.
89. Suharti, M. J. F. S.; Schroeder, I.; de Vries, S. A Novel Copper A Containing Menaquinol NO Reductase from Bacillus azotoformans. *Biochemistry* **2001**, *40*, 2632.
90. Suharti, H. A. H.; de Vries, S. NO reductase from Bacillus azotoformans is a bifunctional enzyme accepting electrons from menaquinol and a specific endogenous membrane-bound cytochrome c551. *Biochemistry* **2004**, *43*, 13487.
91. Komorowski, L.; Anemuller, S.; Schafer, G. First expression and characterization of a recombinant CuA-containing subunit II from an archaeal terminal oxidase complex. *J. Bioenerg. Biomembr.* **2001**, *33*, 27.
92. Komorowski, L.; Verheyen, W.; Schafer, G. The archaeal respiratory supercomplex SoxM from S. acidocaldarius combines features of quinole and cytochrome c oxidases. *Biol. Chem.* **2002**, *383*, 1791.
93. Adman, E. T. Copper Protein Structures. *Adv. Protein Chem.* **1991**, *42*, 145-197.
94. Vila, A. J.; Fernández, C. O. In *Handbook on Metalloproteins*; Bertini, I., Sigel, A., Sigel, H., Eds.; Marcel Dekker: New York, NY, 2001, p 813.
95. Farver, O.; Pecht, I. Elucidation of electron-transfer pathways in copper and iron proteins by pulse radiolysis experiments. *Prog. Inorg. Chem.* **2007**, *55*, 1.

96. Lappalainen, P.; Aasa, R.; Malmström, B. G.; Saraste, M. Soluble CuA-Binding Domain from the Paracoccus Cytochrome c Oxidase. *J. Biol. Chem.* **1993**, *268*, 26416.

97. von Wachenfeldt, C.; de Vries, S.; van der Oost, J. The CuA site of the caa3-type oxidase of Bacillus subtilis is a mixed-valence binuclear copper centre. *FEBS Lett.* **1994**, *340*, 109.

98. Farrar, J. A.; Lappalainen, P.; Zumft, W. G.; Saraste, M.; Thomson, A. J. Spectroscopic and mutagenesis studies on the CuA centre from the cytochrome-c oxidase complex of Paracoccus denitrificans. *Eur. J. Biochem.* **1995**, *232*, 294.

99. Lappalainen, P.; Watmough, N. J.; Greenwood, C.; Saraste, M. Electron Transfer Between Cytochrome c and the Isolated CuA Domain: Identification Of Substrate-Binding Residues in Cytochrome c Oxidase. *Biochemistry* **1995**, *34*, 5824.

100. Slutter, C. E.; Langen, R.; Sanders, D.; Lawrence, S. M.; Wittung, P.; Di Bilio, A. J.; Hill, M. G.; Fee, J. A.; Richards, J. H.; Winkler, J. R.; Malmström, B. G. Electron-transfer studies with the CuA domain of Thermus thermophilus cytochrome ba3. *Inorg. Chim. Acta* **1996**, *243*, 141.

101. Slutter, C. E.; Sanders, D.; Wittung, P.; Malmström, B. G.; Aasa, R.; Richards, J. H.; Gray, H. B.; Fee, J. A. Water-soluble, recombinant CuA-domain of the cytochrome ba3 subunit II from Thermus thermophilus. *Biochemistry* **1996**, *35*, 3387.

102. Song, A.-X.; Li, L.-Z.; Yu, T.; Chen, S.-M.; Huang, Z.-X. Role of tryptophan 121 in the soluble CuA domain of cytochrome c oxidase: structure and electron transfer studies. *Protein Eng.* **2003**, *16*, 435.

103. Maneg, O.; Ludwig, B.; Malatesta, F. Different Interaction Modes of Two Cytochrome-c Oxidase Soluble CuA Fragments with Their Substrates. *J. Biol. Chem.* **2003**, *278*, 46734.

104. Paumann, M.; Lubura, B.; Regelsberger, G.; Feichtinger, M.; Koellensberger, G.; Jakopitsch, C.; Furtmueller, P. G.; Peschek, G. A.; Obinger, C. Soluble CuA Domain of Cyanobacterial Cytochrome c Oxidase. *J. Biol. Chem.* **2004**, *279*, 10293.

105. van der Oost, J.; Lappalainen, P.; Musacchio, A.; Warne, A.; Lemieux, L.; Rumbley, J.; Gennis, R. B.; Aasa, R.; Pascher, T.; Malmström, B. G.; Saraste, M. Restoration of a lost metal-binding site: construction of two different copper sites into a subunit of the E. coli cytochrome o quinol oxidase complex. *The EMBO journal* **1992**, *11*, 3209.

106. Dennison, C.; Vijgenboom, E.; de Vries, S.; van der Oost, J.; Canters, G. W. Introduction of a CuA site into the blue copper protein amicyanin from Thiobacillus versutus. *FEBS Lett.* **1995**, *365*, 92.

107. Hay, M.; Richards, J. H.; Lu, Y. Construction and characterization of an azurin analog for the purple copper site in cytochrome c oxidase. *Proc. Natl. Acad. Sci. U.S.A.* **1996**, *93*, 461.

108. Jones, L. H.; Liu, A.; Davidson, V. L. An Engineered CuA Amicyanin Capable of Intermolecular Electron Transfer Reactions. *J. Biol. Chem.* **2003**, *278*, 47269.

109. Immoos, C.; Hill, M. G.; Sanders, D.; Fee, J. A.; Slutter, C. E.; Richards, J. H.; Gray, H. B. Electrochemistry of the CuA domain of Thermus thermophilus cytochrome ba3. *J. Biol. Inorg. Chem.* **1996**, *1*, 529.

110. Fujita, K.; Nakamura, N.; Ohno, H.; Leigh, B. S.; Niki, K.; Gray, H. B.; Richards, J. H. Mimicking Protein-Protein Electron Transfer: Voltammetry of Pseudomonas aeruginosa Azurin and the Thermus thermophilus CuA Domain at w-Derivatized Self-Assembled-Monolayer Gold Electrodes. *J. Am. Chem. Soc.* **2004**, *126*, 13954.

111. Ledesma, G. N.; Murgida, D. H.; Ly, H. K.; Wackerbarth, H.; Ulstrup, J.; Costa-Filho, A. J.; Vila, A. J. The Met Axial Ligand Determines the Redox Potential in CuA Sites. *J. Am. Chem. Soc.* **2007**, *129*, 11884.

112. Riester, J.; Zumft, W. G.; Kroneck, P. M. H. Nitrous oxide reductase from Pseudomonas stutzeri. Redox properties and spectroscopic characterization of different forms of the multicopper enzyme. *Eur. J. Biochem.* **1989**, *178*, 751.

113. Hulse, C. L.; Averill, B. A. Isolation of a high specific activity pink, monomeric nitrous oxide reductase from Achromobacter cycloclastes. *Biochem. Biophys. Res. Commun.* **1990**, *166*, 729.

114. Froncisz, W.; Scholes, C. P.; Hyde, J. S.; Wei, Y.-H.; King, T. E.; Shaw, R. W.; Beinert, H. Hyperfine structure resolved by 2 to 4 GHz EPR of cytochrome c oxidase. *J. Biol. Chem.* **1979**, *254*, 7482.

115. Hoffman, B. M.; Roberts, J. E.; Swanson, M.; Speck, S. H.; Margoliash, E. Copper electron-nuclear double resonance of cytochrome c oxidase. *Proc. Natl. Acad. Sci. U.S.A.* **1980**, *77*, 1452.

116. Slutter, C. E.; Gromov, I.; Richards, J. H.; Pecht, I.; Goldfarb, D. Mutations of the Weak Axial Ligand in the Thermus CuA Center Modulates Its Electronic Structure. *J. Am. Chem. Soc.* **1999**, *121*, 5077.

117. Greenwood, C.; Hill, B. C.; Barber, D.; Eglinton, D. G.; Thomson, A. J. The Optical-Properties Of Cua In Bovine Cytochrome-C Oxidase Determined By Low-Temperature Magnetic-Circular-Dichroism Spectroscopy. *Biochemical Journal* **1983**, *215*, 303.

118. Thomson, A. J.; Greenwood, C.; Peterson, J.; Barrett, C. P. Determination of the optical properties of copperA(II) in bovine cytochrome c oxidase using magnetic circular dichroism as an optical detector of paramagnetic resonance. *J. Inorg. Biochem.* **1986**, *28*, 195.

119. Greenwood, C.; Thomson, A. J.; Barrett, C. P.; Peterson, J.; George, G. N.; Fee, J. A.; Reichardt, J. Some spectroscopic views of the copperA site in cytochrome c oxidase preparations. *Ann. N. Y. Acad. Sci.* **1988**, *550*, 47.

120. Dooley, D. M.; McGuirl, M. A.; Rosenzweig, A. C.; Landin, J. A.; Scott, R. A.; Zumft, W. G.; Devlin, F.; Stephens, P. J. Spectroscopic Studies Of the Copper Sites In Wild-Type Pseudomonas-Stutzeri N2o Reductase and In an Inactive Protein Isolated From a Mutant Deficient In Copper-Site Biosynthesis. *Inorg. Chem.* **1991**, *30*, 3006.

121. Larsson, S.; KÃ¤llebring, B.; Wittung, P.; MalmstrÃ¶m, B. G. The Cu A center of cytochrome-c oxidase: Electronic structure and spectra of models compared to the properties of CuA domains. *Proc. Natl. Acad. Sci. U.S.A.* **1995**, *92*, 7167.

122. Farrar, J. A.; Zumft, W. G.; Thomson, A. J. CuA and CuZ are variants of the electron transfer center in nitrous oxide reductase. *Proc. Natl. Acad. Sci. U.S.A.* **1998**, *95*, 9891.

123. Dooley, D. M.; Moog, R. S.; Zumft, W. G. Characterization of the copper sites in Pseudomonas perfectomarina nitrous oxide reductase by resonance Raman spectroscopy. *J. Am. Chem. Soc.* **1987**, *109*, 6730.

124. Takahashi, S.; Ogura, T.; Shinzawa-Itoh, K.; Yoshikawa, S.; Kitagawa, T. Resonance Raman Studies on the CuA site of Cytochrome c Oxidase Using a Multichannel Scanning Raman Spectrometer with a CCD Detector. *Biochemistry* **1993**, *32*, 3664.

125. Andrew, C. R.; Han, J.; de Vries, S.; van der Oost, J.; Averill, B. A.; Loehr, T. M.; Sanders-Loehr, J. CuA of Cytochrome c Oxidase and the A Site Of N2O Reductase Are Tetrahedrally Distorted Type 1 Cu Cysteinates. *J. Am. Chem. Soc.* **1994**, *116*, 10805.

126. Andrew, C. R.; Lappalainen, P.; Saraste, M.; Hay, M. T.; Lu, Y.; Dennison, C.; Canters, G. W.; Fee, J. A.; Slutter, C. E.; Nakamura, N.; Sanders-Loehr, J. Engineered Cupredoxins and Bacterial Cytochrome c Oxidases Have Similar CuA Sites: Evidence from Resonance Raman Spectroscopy. *J. Am. Chem. Soc.* **1995**, *117*, 10759-10760.

127. Andrew, C. R.; Fraczkiewicz, R.; Czernuszewicz, R. S.; Lappalainen, P.; Saraste, M.; Sanders-Loehr, J. Identification and Description of Copper-Thiolate Vibrations in the Dinuclear CuA Site of Cytochrome c Oxidase. *J. Am. Chem. Soc.* **1996**, *118*, 10436-10445.

128. Scott, R. A.; Schwartz, J. R.; Cramer, S. P. Structural aspects of the copper sites in cytochrome c oxidase. An x-ray absorption spectroscopic investigation of the resting-state enzyme. *Biochemistry* **1986**, *25*, 5546.

129. Scott, R. A. X-Ray Absorption Spectroscopic Investigations of Cytochrome c Oxidase Structure and Function. *Annu. Rev. Biophys. Biophys. Chem.* **1989**, *18*, 137.

130. Blackburn, N. J.; de Vries, S.; Barr, M. E.; Houser, R. P.; Tolman, W. B.; Sanders, D.; Fee, J. A. X-ray Absorption Studies on the Mixed-Valence and Fully Reduced Forms of the Soluble CuA Domains of Cytochrome c Oxidase. *J. Am. Chem. Soc.* **1997**, *119*, 6135-6143.

131. Blackburn, N. J.; Ralle, M.; Sanders, D.; Fee, J. A.; de Vries, S.; Houser, R. P.; Tolman, W. B.; Hay, M. T.; Lu, Y. In *Spectroscopic Methods in Bioinorganic Chemistry*; Solomon, E. I., Hodgson, K. O., Eds.; ACS: Washington, DC, 1998; Vol. 692, p 241-261.

132. DeBeer George, S.; Metz, M.; Szilagyi, R. K.; Wang, H.; Cramer, S. P.; Lu, Y.; Tolman, W. B.; Hedman, B.; Hodgson, K. O.; Solomon, E. I. A Quantitative Description of the Ground-State Wave Function of CuA by X-ray Absorption Spectroscopy: Comparison to Plastocyanin and Relevance to Electron Transfer. *J. Am. Chem. Soc.* **2001**, *123*, 5757.

133. Williams, K. R.; Gamelin, D. R.; LaCroix, L. B.; Houser, R. P.; Tolman, W. B.; Mulder, T. C.; de Vries, S.; Hedman, B.; Hodgson, K. O.; Solomon, E. I. Influence of Copper-Sulfur Covalency and Copper-Copper Bonding on Valence Delocalization and Electron Transfer in the CuA Site of Cytochrome c Oxidase. *J. Am. Chem. Soc.* **1997**, *119*, 613.

134. Di Bilio, A. J.; Hill, M. G.; Bonander, N.; Karlsson, B. G.; Villahermosa, R. M.; MalmstrÃ¶m, B. G.; Winkler, J. R.; Gray, H. B. Reorganization Energy of Blue Copper:

Effects of Temperature and Driving Force on the Rates of Electron Transfer in Ruthenium- and Osmium-Modified Azurins. *J. Am. Chem. Soc.* **1997**, *119*, 9921.

135. Sigfridsson, K.; Ejdeback, M.; Sundahl, M.; Hansson, O. Electron transfer in ruthenium-modified spinach plastocyanin mutants. *Arch. Biochem. Biophys.* **1998**, *351*, 197.
136. Skov, L. K.; Pascher, T.; Winkler, J. R.; Gray, H. B. Rates of Intramolecular Electron Transfer in Ru(Bpy)2(Im)(His83)-Modified Azurin Increase below 220 K. *J. Am. Chem. Soc.* **1998**, *120*, 1102.
137. Shadle, S. E.; Penner-Hahn, J. E.; Schugar, H. J.; Hedman, B.; Hodgson, K. O.; Solomon, E. I. X-ray absorption spectroscopic studies of the blue copper site: metal and ligand K-edge studies to probe the origin of the EPR hyperfine splitting in plastocyanin. *J. Am. Chem. Soc.* **1993**, *115*, 767.
138. Lowery, M. D.; Guckert, J. A.; Gebhard, M. S.; Solomon, E. I. Active-site electronic structure contributions to electron-transfer pathways in rubredoxin and plastocyanin: direct versus superexchange. *J. Am. Chem. Soc.* **1993**, *115*, 3012.
139. Farver, O.; Lu, Y.; Ang, M. C.; Pecht, I. Enhanced Rate of Intramolecular Electron Transfer in an Engineered Purple CuA Azurin. *Proc. Natl. Acad. Sci. U.S.A.* **1999**, *96*, 899.
140. Xie, X.; Gorelsky, S. I.; Sarangi, R.; Garner, D. K.; Hwang, H. J.; Hodgson, K. O.; Hedman, B.; Lu, Y.; Solomon, E. I. Perturbations to the Geometric and Electronic Structure of the CuA Site: Factors that Influence Delocalization and Their Contributions to Electron Transfer. *J. Am. Chem. Soc.* **2008**, *130*, 5194.
141. Hay, M. T.; Milberg, R. M.; Lu, Y. Preparation and Characterization of Mercury and Silver Derivatives of an Engineered Purple Copper Center in Azurin. *J. Am. Chem. Soc.* **1996**, *118*, 11976.
142. Hay, M. T.; Ang, M. C.; Gamelin, D. R.; Solomon, E. I.; Antholine, W. E.; Ralle, M.; Blackburn, N. J.; Massey, P. D.; Wang, X.; Kwon, A. H.; Lu, Y. Spectroscopic characterization of an engineered purple CuA center in azurin. *Inorg. Chem.* **1998**, *37*, 191.
143. Wang, X.; Ang, M. C.; Lu, Y. Kinetics of Copper Incorporation into an Engineered Purple Azurin. *J. Am. Chem. Soc.* **1999**, *121*, 2947-2948.

144. Wang, X.; Berry, S. M.; Xia, Y.; Lu, Y. The Role of Histidine Ligands in the Structure of Purple CuA Azurin. *J. Am. Chem. Soc.* **1999**, *121*, 7449.

145. Berry, S. M.; Wang, X.; Lu, Y. Ligand replacement study at the His 120 site of purple CuA azurin. *J. Inorg. Biochem.* **2000**, *78*, 89-95.

146. Hay, M. T.; Lu, Y. Metal-binding properties of an engineered purple CuA center in azurin. *J. Biol. Inorg. Chem.* **2000**, *5*, 699.

147. Berry, S. M.; Gieselman, M. D.; Nilges, M. J.; Van der Donk, W. A.; Lu, Y. An Engineered Azurin Variant Containing a Selenocysteine Copper Ligand. *J. Am. Chem. Soc.* **2002**, *124*, 2084-2085.

148. Lukoyanov, D.; Berry, S. M.; Lu, Y.; Antholine, W. E.; Scholes, C. P. Role of the coordinating histidine in altering the mixed valency of CuA: An electron nuclear double resonance-electron paramagnetic resonance investigation. *Biophys. J.* **2002**, *82*, 2758.

149. Epel, B.; Slutter, C. S.; Neese, F.; Kroneck, P. M. H.; Zumft, W. G.; Pecht, I.; Farver, O.; Lu, Y.; Goldfarb, D. Electron-Mediating CuA Centers in Proteins: A Comparative High Field 1H ENDOR Study. *J. Am. Chem. Soc.* **2002**, *124*, 8152.

150. Berry, S. M.; Ralle, M.; Low, D. W.; Blackburn, N. J.; Lu, Y. Probing the Role of Axial Methionine in the Blue Copper Center of Azurin with Unnatural Amino Acids. *J. Am. Chem. Soc.* **2003**, *125*, 8760-8768.

151. Hwang, H. J.; Lu, Y. Spectroscopic evidence for interactions between hexacyanoiron(II/III) and an engineered purple CuA azurin. *J. Inorg. Biochem.* **2004**, *98*, 797.

152. Ralle, M.; Berry, S. M.; Nilges, M. J.; Gieselman, M. D.; Van der Donk, W. A.; Lu, Y.; Blackburn, N. J. The Selenocysteine-Substituted Blue Copper Center: Spectroscopic Investigations of Cys112SeCys Pseudomonas aeruginosa Azurin. *J. Am. Chem. Soc.* **2004**, *126*, 7244.

153. Hwang, H. J.; Ang, M. C.; Lu, Y. Determination of reduction potential of an engineered CuA azurin by cyclic voltammetry and spectrochemical titrations. *J. Biol. Inorg. Chem.* **2004**, *9*, 489.

154. Hwang, H. J.; Lu, Y. pH-dependent transition between delocalized and trapped valence states of a CuA center and its possible role in proton-coupled electron transfer. *Proc. Natl. Acad. Sci. U.S.A.* **2004**, *101*, 12842.

155. Hwang, H. J.; Berry, S. M.; Nilges, M. J.; Lu, Y. Axial Methionine Has Much Less Influence on Reduction Potentials in a CuA Center than in a Blue Copper Center. *J. Am. Chem. Soc.* **2005**, *127*, 7274.

156. Hwang, H. J.; Nagraj, N.; Lu, Y. Spectroscopic Characterizations of Bridging Cysteine Ligand Variants of an Engineered $Cu_2(S_{Cys})_2$ Cu_A Azurin. *Inorg. Chem.* **2006**, *45*, 102-107.

157. Farver, O.; Hwang, H. J.; Lu, Y.; Pecht, I. Reorganization Energy of the CuA Center in Purple Azurin: Impact of the Mixed Valence-to-Trapped Valence State Transition. *J. Phys. Chem. B* **2007**, *111*, 6690.

158. Wilson, T. D.; Savelieff, M. G.; Nilges, M. J.; Marshall, N. M.; Lu, Y. Kinetics of Copper Incorporation into a Biosynthetic Purple CuA Azurin: Characterization of Red, Blue, and a New Intermediate Species. *J. Am. Chem. Soc.* **2011**, *133*, 20778-20792.

159. Garner, D. K.; Vaughan, M. D.; Hwang, H. J.; Savelieff, M. G.; Berry, S. M.; Honek, J. F.; Lu, Y. Reduction Potential Tuning of the Blue Copper Center in Pseudomonas aeruginosa Azurin by the Axial Methionine as Probed by Unnatural Amino Acids. *J. Am. Chem. Soc.* **2006**, *128*, 15608.

160. MacPherson, I.; Murphy, M. Type-2 copper-containing enzymes. *Cell. Mol. Life Sci.* **2007**, *64*, 2887.

161. Wang, K.; Geren, L.; Zhen, Y.; Ma, L.; Ferguson-Miller, S.; Durham, B.; Millett, F. Mutants of the CuA site in cytochrome c oxidase of Rhodobacter sphaeroides: II. Rapid kinetic analysis of electron transfer. *Biochemistry* **2002**, *41*, 2298.

162. Zhen, Y.; Schmidt, B.; Kang, U. G.; Antholine, W.; Ferguson-Miller, S. Mutants of the CuA site in cytochrome c oxidase of Rhodobacter sphaeroides: I. Spectral and functional properties. *Biochemistry* **2002**, *41*, 2288.

163. Andreini, C.; Banci, L.; Bertini, I.; Rosato, A. Occurrence of copper proteins through the three domains of life: A bioinformatic approach. *J. Proteome Res.* **2008**, *7*, 209.

164. Zhang, Y.; Gladyshev, V. N. General Trends in Trace Element Utilization Revealed by Comparative Genomic Analyses of Co, Cu, Mo, Ni, and Se. *J. Biol. Chem.* **2010**, *285*, 3393.

165. Zhang, Y.; Gladyshev, V. N. Comparative Genomics of Trace Element Dependence in Biology. *J. Biol. Chem.* **2011**, *286*, 23623.

166. McCord, J. M.; Fridovich, I. Superoxide dismutase. Enzymic function for erythrocuprein (hemocuprein). *J. Biol. Chem.* **1969**, *244*, 6049.

167. Hellman, N. E.; Gitlin, J. D. Ceruloplasmin metabolism and function. *Annu. Rev. Nutr.* **2002**, *22*, 439.

168. Klinman, J. P. The Copper-Enzyme Family of Dopamine b-Monooxygenase and Peptidylglycine a-Hydroxylating Monooxygenase: Resolving the Chemical Pathway for Substrate Hydroxylation. *J. Biol. Chem.* **2006**, *281*, 3013.

169. Halliwell, B.; Gutteridge, J. M. C. Oxygen toxicity, oxygen radicals, transition metals and disease. *Biochem. J.* **1984**, *219*, 1.

170. Kim, B.-E.; Nevitt, T.; Thiele, D. J. Mechanisms for copper acquisition, distribution and regulation. *Nat. Chem. Biol.* **2008**, *4*, 176.

171. Boal, A. K.; Rosenzweig, A. C. Structural Biology of Copper Trafficking. *Chem. Rev.* **2009**, *109*, 4760.

172. Banci, L.; Bertini, I.; McGreevy, K. S.; Rosato, A. Molecular recognition in copper trafficking. *Nat. Prod. Rep.* **2010**, *27*, 695.

173. Banci, L.; Bertini, I.; Cantini, F.; Ciofi-Baffoni, S. Cellular copper distribution: a mechanistic systems biology approach. *Cell. Mol. Life Sci.* **2010**, *67*, 2563.

174. Bertini, I.; Cavallaro, G.; McGreevy, K. S. Cellular copper management-a draft user's guide. *Coord. Chem. Rev.* **2010**, *254*, 506.

175. Robinson, N. J.; Winge, D. R. Copper Metallochaperones. *Annu. Rev. Biochem.* **2010**, *79*, 537.

176. Banci, L.; Bertini, I.; Cavallaro, G.; Ciofi-Baffoni, S. Seeking the determinants of the elusive functions of Sco proteins. *FEBS J.* **2011**, *278*, 2244-2262.

177. Neuba, A.; Haase, R.; Meyer-Klaucke, W.; Floerke, U.; Henkel, G. A Halide-Induced Copper(I) Disulfide/Copper(II) Thiolate Interconversion. *Angew. Chem. Int. Ed.* **2012**, *51*, 1714.

178. Cavallini, D.; De Marco, C.; Dupre, S. Luminol chemiluminescence studies of the oxidation of cysteine and other thiols to disulfides. *Arch. Biochem. Biophys.* **1968**, *124*, 18.

179. Cavallini, D.; De Marco, C.; Dupre, S.; Rotilio, G. Copper-catalyzed oxidation of cysteine to cystine. *Arch. Biochem. Biophys.* **1969**, *130*, 354.

180. Pecci, L.; Montefoschi, G.; Musci, G.; Cavallini, D. Novel findings on the copper-catalyzed oxidation of cysteine. *Amino Acids* **1997**, *13*, 355.

181. Ostermeier, C.; Iwata, S.; Ludwig, B.; Michel, H. Fv fragment-mediated crystallization of the membrane protein bacterial cytochrome c oxidase. *Nat. Struct. Biol.* **1995**, *2*, 842.

182. Soulimane, T.; Buse, G.; Bourenkov, G. P.; Bartunik, H. D.; Huber, R.; Than, M. E. Structure and mechanism of the aberrant ba3-cytochrome c oxidase from Thermus thermophilus. *EMBO J.* **2000**, *19*, 1766.

183. Zumft, W. G. Cell biology and molecular basis of denitrification. *Microbiol. Mol. Biol. Rev.* **1997**, *61*, 533.

184. Schulze, M.; Roedel, G. SCO1, a yeast nuclear gene essential for accumulation of mitochondrial cytochrome c oxidase subunit II. *Mol. Gen. Genet.* **1988**, *211*, 492.

185. Glerum, D. M.; Shtanko, A.; Tzagoloff, A. SCO1 and SCO2 act as high copy suppressors of a mitochondrial copper recruitment defect in Saccharomyces cerevisiae. *J. Biol. Chem.* **1996**, *271*, 20531.

186. Nittis, T.; George, G. N.; Winge, D. R. Yeast Sco1, a protein essential for cytochrome c oxidase function is a Cu(I)-binding protein. *J. Biol. Chem.* **2001**, *276*, 42520.

187. Horng, Y.-C.; Leary, S. C.; Cobine, P. A.; Young, F. B. J.; George, G. N.; Shoubridge, E. A.; Winge, D. R. Human Sco1 and Sco2 Function as Copper-binding Proteins. *J. Biol. Chem.* **2005**, *280*, 34113.

188. Andruzzi, L.; Nakano, M.; Nilges, M. J.; Blackburn, N. J. Spectroscopic Studies of Metal Binding and Metal Selectivity in Bacillus subtilis BSco, a Homologue of the Yeast Mitochondrial Protein Sco1p. *J. Am. Chem. Soc.* **2005**, *127*, 16548.

189. Imriskova-Sosova, I.; Andrews, D.; Yam, K.; Davidson, D.; Yachnin, B.; Hill, B. C. Characterization of the Redox and Metal Binding Activity of BsSco, a Protein Implicated in the Assembly of Cytochrome c Oxidase. *Biochemistry* **2005**, *44*, 16949.

190. Davidson, D. E.; Hill, B. C. Stability of oxidized, reduced and copper bound forms of Bacillus subtilis Sco. *Biochim. Biophys. Acta* **2009**, *1794*, 275.

191. Martin, J. L. Thioredoxin-a fold for all reasons. *Structure* **1995**, *3*, 245.

192. Williams, J. C.; Sue, C.; Banting, G. S.; Yang, H.; Glerum, D. M.; Hendrickson, W. A.; Schon, E. A. Crystal Structure of Human SCO1: Implications for redox signaling by a

mitochondrial cytochrome c oxidase "assembly" protein. *J. Biol. Chem.* **2005**, *280*, 15202.

193. Banci, L.; Bertini, I.; Calderone, V.; Ciofi-Baffoni, S.; Mangani, S.; Martinelli, M.; Palumaa, P.; Wang, S. A hint for the function of human Sco1 from different structures. *Proc. Natl. Acad. Sci. U.S.A.* **2006**, *103*, 8595.
194. Banci, L.; Bertini, I.; Ciofi-Baffoni, S.; Gerothanassis, I. P.; Leontari, I.; Martinelli, M.; Wang, S. A Structural Characterization of Human SCO2. *Structure* **2007**, *15*, 1132.
195. Siluvai, G. S.; Nakano, M. M.; Mayfield, M.; Nilges, M. J.; Blackburn, N. J. H135A Controls the Redox Activity of the Sco Copper Center: Kinetic and Spectroscopic Studies of the His135Ala Variant of Bacillus subtilis Sco. *Biochemistry* **2009**, *48*, 12133.
196. Siluvai, G. S.; Nakano, M.; Mayfield, M.; Blackburn, N. J. The essential role of the Cu(II) state of Sco in the maturation of the CuA center of cytochrome oxidase: evidence from H135Met and H135SeM variants of the Bacillus subtilis Sco. *J. Biol. Inorg. Chem.* **2011**, *16*, 285.
197. Wunsch, P.; Herb, M.; Wieland, H.; Schiek, U. M.; Zumft, W. G. Requirements for Cu_A and Cu-S center assembly of nitrous oxide reductase deduced from complete periplasmic enzyme maturation in the nondenitrifier Pseudomonas putida. *J. Bacteriol.* **2003**, *185*, 887-896.
198. Bertini, I.; Bren, K. L.; Clemente, A.; Fee, J. A.; Gray, H. B.; Luchinat, C.; Malmström, B. G.; Richards, J. H.; Sanders, D.; Slutter, C. E. The CuA Center of a Soluble Domain from Thermus Cytochrome ba3. An NMR Investigation of the Paramagnetic Protein. *J. Am. Chem. Soc.* **1996**, *118*, 11658.
199. Dennison, C.; Berg, A.; de Vries, S.; Canters, G. W. 1H NMR studies of the paramagnetic CuA center of cytochrome oxidase. *FEBS Lett.* **1996**, *394*, 340.
200. Abriata, L. A.; Ledesma, G. N.; Pierattelli, R.; Vila, A. J. Electronic Structure of the Ground and Excited States of the CuA Site by NMR Spectroscopy. *J. Am. Chem. Soc.* **2009**, *131*, 1939-1946.
201. Solomon, E. I. Spectroscopic Methods in Bioinorganic Chemistry: Blue to Green to Red Copper Sites. *Inorg. Chem.* **2006**, *45*, 8012.
202. Lieberman, R. L.; Arciero, D. M.; Hooper, A. B.; Rosenzweig, A. C. Crystal Structure of a Novel Red Copper Protein from Nitrosomonas europaea. *Biochemistry* **2001**, *40*, 5674.

203. Humphrey, W.; Dalke, A.; Schulten, K. VMD: Visual molecular dynamics. *J. Mol. Graph.* **1996**, *14*, 33.

204. Roberts, E.; Eargle, J.; Wright, D.; Luthey-Schulten, Z. MultiSeq: unifying sequence and structure data for evolutionary analysis. *BMC Bioinformatics* **2006**, *7*, 382.

205. Ryden, L. G.; Hunt, L. T. Evolution of protein complexity: the blue copper-containing oxidases and related proteins. *J. Mol. Evol.* **1993**, *36*, 41.

206. Abolmaali, B.; Taylor, H. V.; Weser, U. Evolutionary aspects of copper binding centers in copper proteins. *Struct. Bond.* **1998**, *91*, 91.

207. Savelieff, M. G.; Wilson, T. D.; Elias, Y.; Nilges, M. J.; Garner, D. K.; Lu, Y. Experimental evidence for a link among cupredoxins: red, blue, and purple copper transformations in nitrous oxide reductase. *Proc. Natl. Acad. Sci. U.S.A.* **2008**, *105*, 7919-7924.

208. Ostermeier, C.; Michel, H. Cytochrome c oxidase - the key enzyme of aerobic respiration. *Transition Met. Microb. Metab.* **1997**, 311.

209. Solomon, E. I.; Baldwin, M. J.; Lowery, M. D. Electronic Structures of Active Sites in Copper Proteins: Contributions to Reactivity. *Chem. Rev.* **1992**, *92*, 521.

210. Maret, W.; Kozlowski, H. Electronic absorption and EPR spectroscopy of copper alcohol dehydrogenase: pink, violet and green forms of a type 1 copper center analog. *Biochim. Biophys. Acta* **1987**, *912*, 329.

211. Farrar, J. A.; Formicka, G.; Zeppezauer, M.; Thomson, A. J. Magnetic and optical properties of copper-substituted alcohol dehydrogenase: a bisthiolate copper(II) complex. *Biochemical Journal* **1996**, *317*, 447.

212. Holmgren, A. Thioredoxin and glutaredoxin systems. *J. Biol. Chem.* **1989**, *264*, 13963.

213. Nordberg, J.; Arner, E. S. J. Reactive oxygen species, antioxidants, and the mammalian thioredoxin system. *Free Radical Biol. Med.* **2001**, *31*, 1287.

214. Abriata, L. A.; Banci, L.; Bertini, I.; Ciofi-Baffoni, S.; Gkazonis, P.; Spyroulias, G. A.; Vila, A. J.; Wang, S. Mechanism of CuA assembly. *Nature Chemical Biology* **2008**, *4*, 599.

215. Arciero, D. M.; Pierce, B. S.; Hendrich, M. P.; Hooper, A. B. Nitrosocyanin, a red cupredoxin-like protein from Nitrosomonas europaea. *Biochemistry* **2002**, *41*, 1703.

216. Basumallick, L.; Sarangi, R.; DeBeer George, S.; Elmore, B.; Hooper, A. B.; Hedman, B.; Hodgson, K. O.; Solomon, E. I. Spectroscopic and Density Functional Studies of the Red Copper Site in Nitrosocyanin: Role of the Protein in Determining Active Site Geometric and Electronic Structure. *J. Am. Chem. Soc.* **2005**, *127*, 3531.

217. Sieracki, N. A.; Hwang, H. J.; Lee, M. K.; Garner, D. K.; Lu, Y. A temperature independent pH (TIP) buffer for biomedical biophysical applications at low temperatures. *Chem. Commun.* **2008**, 823.

218. Nilges, M. J.; Matteson, K.; Belford, R. L. In *ESR Spectroscopy in Membrane Biophysics*; Hemminga, M. A., Berliner, L., Eds.; Springer: New York, 2006; Vol. 27, p 394.

219. St. Clair, C. S.; Ellis, W. R., Jr.; Gray, H. B. Spectroelectrochemistry of blue copper proteins: pH and temperature dependences of the reduction potentials of five azurins. *Inorg. Chim. Acta* **1992**, *191*, 149.

220. Van de Kamp, M.; Canters, G. W.; Andrew, C. R.; Sanders-Loehr, J.; Bender, C. J.; Peisach, J. Effect of lysine ionization on the structure and electrochemical behavior of the Met44Â®Lys mutant of the blue-copper-protein azurin from Pseudomonas aeruginosa. *Eur. J. Biochem.* **1993**, *218*, 229.

221. Maret, W.; Dietrich, H.; Ruf, H. H.; Zeppezauer, M. Active site-specific reconstituted copper(II) horse liver alcohol dehydrogenase: a biological model for type 1 copper(2+) and its changes upon ligand binding and conformational transitions. *J. Inorg. Biochem.* **1980**, *12*, 241.

222. Maret, W.; Zeppezauer, M.; Desideri, A.; Morpurgo, L.; Rotilio, G. Ligand binding to the blue copper center of horse liver alcohol dehydrogenase. *FEBS Lett.* **1981**, *136*, 72.

223. Rosenzweig, A. C.; Sazinsky, M. H. Structural insights into dioxygen-activating copper enzymes. *Curr. Opin. Struct. Biol.* **2006**, *16*, 729.

224. Tottey, S.; Patterson, C. J.; Banci, L.; Bertini, I.; Felli, I. C.; Pavelkova, A.; Dainty, S. J.; Pernil, R.; Waldron, K. J.; Foster, A. W.; Robinson, N. J. Cyanobacterial metallochaperone inhibits deleterious side reactions of copper. *Proc. Natl. Acad. Sci. U.S.A.* **2012**, *109*, 95.

225. Andreini, C.; Bertini, I.; Cavallaro, G.; Decaria, L.; Rosato, A. A simple protocol for the comparative analysis of the structure and occurrence of biochemical pathways across superkingdoms. *J. Chem. Inf. Model.* **2011**, *51*, 730.

226. Siluvai, G. S.; Mayfield, M.; Nilges, M. J.; De Beer George, S.; Blackburn, N. J. Anatomy of a Red Copper Center: Spectroscopic Identification and Reactivity of the Copper Centers of Bacillus subtilis Sco and Its Cys-to-Ala Variants. *J. Am. Chem. Soc.* **2010**, *132*, 5215-5226.

227. Chang, T. K.; Iverson, S. A.; Rodrigues, C. G.; Kiser, C. N.; Lew, A. Y. C.; Germanas, J. P.; Richards, J. H. Gene Synthesis, Expression, and Mutagenesis Of the Blue Copper Proteins Azurin and Plastocyanin. *Proc. Natl. Acad. Sci. U.S.A.* **1991**, *88*, 1325-1329.

228. Mizoguchi, T. J.; Di Bilio, A. J.; Gray, H. B.; Richards, J. H. Blue to Type 2 Binding. Copper(II) and Cobalt(II) Derivatives Of a Cys112Asp Mutant Of Pseudomonas aeruginosa Azurin. *J. Am. Chem. Soc.* **1992**, *114*, 10076.

229. Mattatall, N. R.; Jazairi, J.; Hill, B. C. Characterization of YpmQ, an accessory protein required for the expression of cytochrome c oxidase in Bacillus subtilis. *J. Biol. Chem.* **2000**, *275*, 28802.